ONE-PEDAL-DRIVE AND REGENERATIVE BRAKING STRATEGY

ONE-PEDAL-DRIVE AND REGENERATIVE BRAKING STRATEGY: STUDY ON VEHICLE DRIVABILITY AND ENERGY EFFICIENCY

BY

DANIEL GORETTI LEPORATE BARROSO, B. Eng. Mechanical

A THESIS

SUBMITTED TO THE DEPARTMENT OF MECHANICAL ENGINEERING AND THE SCHOOL OF GRADUATE STUDIES OF MCMASTER UNIVERSITY IN PARTIAL FULFILMENT OF THE REQUIREMENTS FOR THE DEGREE OF DOCTOR OF PHILOSOPHY OF APPLIED SCIENCE

Ph.D. of Applied Science (2024)	McMaster University
(Mechanical Engineering)	Hamilton, Ontario, Canada

TITLE:	One-pedal-drive and regenerative braking strategy: study on vehicle drivability and energy efficiency.
AUTHOR:	Daniel Goretti Leporate Barroso B. Eng. Mechanical
SUPERVISOR:	Dr. Ali Emadi
NUMBER OF PAGES:	xx, 344

To my family

In memory of Tio Julio and Tio Walmir

Abstract

The shift towards electric transportation on a global scale is being primarily driven by regulatory requirements and market demand. The impact of the COVID-19 pandemic on air pollution, energy demand, and CO2 emissions has further accelerated this transition. This transformation necessitates the development of efficient electric propulsion systems, particularly for commercial vehicles. These systems not only have a positive environmental impact but also offer significant financial advantages to fleet owners due to lower overall costs.

One of the major challenges in this transition is the design and calibration of regenerative braking strategies, especially for commercial vehicles that exhibit significant variations in weight. This weight difference between curb and gross vehicle weight is a common scenario in the commercial vehicle sector. This thesis introduces the Adaptive One-Pedal Drive (A-OPD) strategy, which is specifically tailored for electric commercial vehicles with varying weight profiles and lacking advanced drive-by-wire braking systems.

The thesis focuses on the development and accurate assessment of a model-centric approach for electrified propulsion systems. This approach establishes a strong correlation between the model and physical data, demonstrating its reliability in estimating critical variables such as battery state-of-charge, battery terminal voltage, system high-voltage DC, and wheel torque, even under diverse driving conditions. This model-centric approach serves as a valuable tool for optimizing

design and conducting tradeoff analyses, enabling efficient evaluation of energy efficiency and drivability.

Selecting the most suitable electrified propulsion system architecture is a crucial decision. The thesis categorizes electrified propulsion system architectures based on their impact on vehicle performance, energy consumption, and total cost of ownership. This selection process involves a multidisciplinary approach that takes into account both technical and business requirements.

The central research focus of this thesis centers on regenerative braking systems. It compares series and parallel configurations, traditional one-pedal-drive (OPD), and introduces an innovative Adaptive One-Pedal Drive (A-OPD). The A-OPD relies on vehicle running mass identification using the Recursive Least Square Filter (RLS) and weight classification. This A-OPD strategy significantly enhances energy efficiency in urban traffic scenarios, even when vehicles are partially loaded. It outperforms parallel regenerative braking systems by up to 50% while maintaining performance levels similar to the series regenerative braking strategy. This innovation represents a significant leap in energy efficiency for electric commercial vehicles without the need for complex electronic braking systems.

In summary, this thesis advances our understanding of optimizing the performance of electric commercial vehicles. The A-OPD strategy proves to be a practical and valuable tool for enhancing energy efficiency, particularly in dense urban traffic, and it outperforms parallel regenerative braking systems. Utilizing model-in-the-loop and driver-in-the-loop simulations, this thesis offers a comprehensive framework for designing efficient electrified propulsion system architectures.

Acknowledgement

I would like to dedicate this thesis to my father, Ivan, and my mother, Josefina. Without them, I would never have become the person I am today. They sacrificed everything to provide education for me and my sister, leading by example to instill the values of life beyond just work. They emphasized the importance of family, dreams, and taking risks, instilling in me the confidence that everything will fall into place.

This thesis is dedicated to my wife, whom I love unconditionally, Camila. She serves as my pillar, offering emotional and mental stability. I consider myself fortunate to have someone by my side, ready to embark on any adventure I propose. Camila gave up her own dreams to support my pursuit of developing electrification. Additionally, I dedicate this thesis to my three-year-old daughter, Giulia, who, at a young age, questions whether cars emit pollution and consistently expresses a desire for us to own an electric car.

This thesis signifies the conclusion of a significant chapter in my life. Electrification has been my goal from the inception of my academic and professional journey. I have had the opportunity to contribute to the development of numerous electrified propulsion products and make my mark in the automotive industry. None of this would have been possible without the collaboration of dedicated team members and the invaluable support and guidance of industry

legends such as Mike Duhaime, Michael Vincent, Bob Lee, and Aldo Marangoni. I will forever be grateful for the privilege of working with these industry leaders.

In pursuit of my dream to develop electrified vehicles, I have sacrificed time with my family, my health, and my relationships with loved ones. This thesis marks the end of an era. For my family, it heralds the beginning of a new one, where they will have a better father, a better husband, a better son, and a better brother. It is now time for Camila and Giulia to pursue and live their dreams.

This thesis is also offered in memory of my Tio Julio, and Tio Walmir. They have passed during this journey. I wish I had had the chance to tell them how important they were in my life and how much I love them.

Nomenclature

ABS	Anti-Lock Braking System
AC	Alternate Current
AMT	Automatized Manual Transmission
A-OPD	Adaptative One-Pedal-Drive
APM	Auxiliary Power Module
AT	Automatic Transmission
AVG	Average
AWD	All wheel drive
BAS	Belt Alternator Starters
BMS	Battery Management System
CAN	Controller Area Network
CONAMA	Conselho Nacional de Meio Ambiente
CVT	Continuous Variable Transmission
CW	Curb Weight
DC	Direct Current
DCT	Dual-Clucht Transmission
DiL	Driver-in-the-Loop
EBS	Electronic Brake System
ECU	Electronic Control Unit
EM	Electric Machine
EPA	Environmental Protection Agency
ESP	Eletronic Stability Control
EU	European Union

EU	European Union
EVs	Electric Vehicles
FEAD	Front Engine Accessory Drive
FTP 75	Federal Test Procedure 75
FWD	Front Wheel Drive
Gan	Gallium Nitride
GDP	Gross Domestic Product
GHG	Green House Gas
GM	Generator Mode
GVW	Gross Vehicle Weight
HEV	Hybrid Electric Vehicle
HiL	Hardware-in-the-Loop
HV	High Voltage
ICCT	International Council on Clean Transportation
ICE	Internal Combustion Engine
IEA	International Energy Agency
IGBT	Insulated-gate bipolar transistor
IM	Induction Machines
IPCC	Intergovernmental Panel on Climate Change
IRR	Internal Rate of Return
ISG	Integrated Starter Generator
LA92	Los Angeles 92
LCV	Light-Commercial Vehicles
LIN	Local Interconnected Network
LPE	Limited Pure Electric
MBDE	Model-Based Design Engineering

MG	Motor Generator
mHEV	Micro Hybrid Electric Vehicle
MHEV	Mild Hybrid Electric Vehicle
MiL	Model-in-the-Loop
MMA	Multi Electric Machine Architecture
NCM	Nickel Cobalt Manganese
NEDC	New European Drive Cycle
NiMH	Nickel Metal Hydride
NVH	Noise, vibration, and harshness
NY_City	New York City
OBCM	On-Board Charger Module
OCV	Open Circuit Voltage
OCV-R	Open Circuit Voltage - Resistance
OEM	automotive original equipment manufacturer
OPD	One-pedal-drive
PB	Pay Back
PDC	Power Distribution Center
PE	Pure Electric
PEV	Pure Electric Vehicle
PHEV	Plug-in Hybrid Vehicle
PID	Proportional-Integral-Derivative
PiL	Processor-in-the-Loop
PIM	Power Inverter Module
PM2.5	Particulate Matter 2.5
PM	Permanent Magnet
PV	Passenger Vehicles

PWM	Pulse Width Modulation
RB	Regenerative Braking
REEV	Range Extender Electric Vehicle
RLS	Recursive Least Square
RMSE	Root Mean Square Error
ROI	Return on Investment
RWD	Rear wheel drive
SARS	Severe Acute Respiratory Syndrome
SHEV	Series Hybrid Electric Vehicle
SiC	Silicon Carbide
SI-EVT	single-input electronic variable transaxle
SiL	Software-in-the-Loop
SMA	Single Motor Architectures
SOC	State of Charge
SRM	Switch Reluctance Machines
SS	Stop-Start
TA	Torque Assist
TCO	Total Cost of Ownership
US06	United States 06
USA	United States of America
WHO	World Health Organization
WLTP	Worldwide Harmonised Light Vehicle Test Procedure
WWII	World War Two

Content

List of Figures

List of Tables

Chapter 1

Introduction

1.1 Background and Motivation

Some estimations predict that the number of motorized vehicles used for transportation can surpass more than 1 billion cars [1]. The number of new vehicles on the roads in 2018 reached about 80 million units, with a growth rate of about 10% compared with the number of produced cars by 2015 [2].

The United States is known as a country on wheels, and the vehicle market has mostly plateaued. More than 280 million vehicles are on the road in the USA, and about 35% are light passenger vehicles – at least four wheels, no more than eight seats, and a maximum GVW of 8500 lbs [3]. The International Council on Clean Transportation (ICCT) estimates that transportation causes 23% of global emissions. About 60% of the emission is from commercial vehicles [4]. The Environmental Protection Agency (EPA) estimates that in the United States, the level of Global Carbon emission caused by fossil fuels rose about 90% when compared with the status of the 1970s, and 28% of the total gas emission comes from the transportation system [5].

The CO_2 emission regulations are prevalent in major automotive markets. The ICCT presents the perspectives of the regulatory landscape for the most important automotive markets in the world regarding the target CO_2 emission, parametrized for the same test procedure, the New European Drive Cycle (NEDC).

European Union is leading many efforts to establish the metrics to reduce harmful gas emissions. The average CO_2 emission by cars in the European region has decreased from 185 g/km in 1995 to 118 g/km in 2018. The European target for 2020 was to meet, on average, 95 g/km of CO_2 and about 80 g/km by 2025 [4]. The mandatory average reduction of CO_2 emission is about 40% in the United States and Canada from the 2012 level by 2025, and the regions that comprehend the most important automotive markets in the world will have a target to meet an average CO_2 emission of about 100 g/km [4].

During the COVID-19 "Great Lockdown," at its most critical point, in April 2020, the economic contraction resulted in a 17% CO_2 emission reduction compared to the same period in 2019. The ground transportation and aviation sectors accounted for more than 50% of total CO_2 emissions reduction [6]. This data shows that reducing mobility or replacing ICE vehicles with non-pollutant vehicles powered by renewable energy effectively reduces air pollution and limits greenhouse gas emissions.

The adoption of the electrification of the propulsion system is hence mandatory to meet the CO_2 emission targets. The wide range of road vehicles includes buses, trucks, light commercial vehicles, and passenger vehicles, each with distinct segments and performance needs [7].

Various electrified propulsion system architecture configurations, electrification degrees, and electric machine quantities are possible. Vehicle performance and energy efficiency rely on the collaboration of multiple subsystems and the architecture of the electrified propulsion system. The vehicle's capabilities hinge on the number of driving axles, electric motors, battery energy and power, and the coordination of power electronics for synchronizing multiple power units simultaneously. Consequently, electrified vehicles are highly intricate systems [8], [9].

Electric vehicles don't only bring environmental benefits but are also a smart financial move for fleet owners. Research shows that owning an electric vehicle can cost up to 80% less than a traditional car with a gas engine. The economic benefits depend on how many miles the vehicle runs a year and how efficient the whole system is.

In 2022, a slight but notable shift occurred in the transportation landscape. Electric buses and trucks began to carve out their space, representing 4.5% and 1.2% of total sales, respectively. Interestingly, 90% of these electric trucks were of the box truck variety, boasting a maximum weight limit of 10,000 lbs, classifying these vehicles as light commercial vehicles.

By 2035, half of all newly acquired commercial vehicles are expected to be electric. By 2040, the shift towards cleaner, eco-friendly transportation options is set to continue, with a projected 40% of commercial vehicles worldwide being fully electric.

1.2 Problem Statement

Architecture selection and regenerative braking play a pivotal role in increasing the propulsion system efficiency of EVs. The benefits, however, depend on the specific propulsion system architecture selected, the brake subsystem architecture, and control calibration.

Advanced regenerative braking architectures offer substantial energy efficiency benefits. Still, it requires a complex braking control module that integrates electronic and anti-lock braking systems with a brake-by-wire pedal. This complexity makes its development expensive and less common in commercial vehicles typically produced in low volumes. The option to avoid series regenerative braking is called parallel regenerative braking. However, depending on the driving cycle, parallel regenerative braking can be up to 50% less efficient than series regenerative braking for applications where the gross vehicle weight is significantly larger than the curb weight [10].

The one-pedal drive (OPD) strategy becomes crucial, allowing commercial vehicles to efficiently recover energy during deceleration by enabling the driver to control the car using just the accelerator pedal and, as a consequence, only using the e-machines to slowdown the vehicle. However, the OPD effectively improves energy efficiency in commercial vehicles when vehicles are not loaded. The efficiency problem is still relevant when the commercial vehicle is loaded.

In this context, there is a need for a regenerative braking system that allows commercial vehicles to adopt a simple brake subsystem architecture; simultaneously, it optimizes the opportunity for energy recovery during decelerations at any vehicle weight. This thesis aims to bridge this gap by presenting an adaptative one-pedal drive (A-OPD), which changes the OPD calibration as a function of the running vehicle weight.

1.3 Thesis Scope

This thesis proposal centers around three key chapters addressing distinct aspects of electric commercial vehicle efficiency and performance. The primary focus is on the Adaptive One-Pedal Drive (A-OPD) strategy, propulsion system model correlation, and brake pedal-based energy recovery strategies.

The A-OPD strategy forms the cornerstone of this research. It leverages the flexibility of one-pedal drive, enabling drivers to control launching, acceleration, braking, parking, and stopping using only the accelerator pedal. However, it recognizes the challenge posed by calibration, where efficiency depends on variables such as vehicle mass and applied braking torque. This challenge is particularly evident when dealing with vehicles of varying loads, highlighting the necessity for nuanced calibration to ensure safety and comfort under diverse load conditions.

The A-OPD strategy is presented as a solution to optimize this calibration, addressing the complex issue of commercial vehicles with significant disparities between curb and gross vehicle weight (GVW). Through an algorithmic approach that estimates running mass using a Recursive Least Squares filter (RLS), the A-OPD strategy offers a dynamic solution. It classifies and selects from pre-calibrated A-OPD regenerative torque maps, promoting uniform driving experiences irrespective of the vehicle's weight. The goal is to enhance energy efficiency while maintaining driveability, performance, and safety.

In summary, this thesis proposal embarks on a multifaceted exploration of electric commercial vehicle optimization. It introduces the A-OPD strategy to enhance driveability, performance, and safety while delving into the complexities of designing efficient commercial vehicles and evaluating regenerative braking strategies. This research aims to contribute valuable insights into the evolving landscape of electric commercial vehicles, offering practical solutions for enhancing their efficiency, performance, and economic viability.

1.4 Research Contributions

The research presented in this study addresses the issue of CO_2 in the transportation sector, particularly in the context of the increasing global demand for commercial vehicles, especially box trucks.

The central problem addressed in this research is optimizing propulsion system efficiency in electric commercial vehicles, focusing on the regenerative braking system. While advanced regenerative braking offers energy efficiency benefits, it is complex and expensive to implement, particularly in commercial vehicles produced in low volumes. The study introduces an Adaptive One-Pedal Drive (A-OPD) strategy that aims to simplify the brake subsystem architecture while optimizing energy recovery during deceleration, even with varying vehicle loads. The A-OPD strategy utilizes an algorithm to estimate running mass, enabling the selection of pre-calibrated regenerative torque maps for consistent and efficient operation.

The peripherical problems this thesis addresses involve using model-based engineering to develop propulsion systems and perform multiple study cases and what-if analyses. This paper also demonstrates how to migrate from a model-in-the-loop to a driver-in-the-loop approach to evaluate the driveability and safety aspects of the design in the early stages of the product development process by using a driving simulator. This paper also addresses the importance of considering the financial facets of the product cost and product operation while designing a system.

In summary, this research significantly contributes to electric commercial vehicles by proposing a practical A-OPD strategy to enhance energy efficiency, performance, and safety while addressing the challenge of variable vehicle loads. It also contributes by showing the importance of virtual engineering and its innovative application using a driving simulator. This work aligns with the global effort to reduce CO2 emissions from the transportation sector; at the same time, it addresses the need for financial benefits. The combination of environmental and economic benefits are the drivers that support the growing transition towards cleaner and more sustainable transportation options.

1.5 Thesis Outline

This thesis presents its content in six main chapters beyond the Introduction and Conclusion chapters.

Chapter 2 delves into Air Pollution and CO2 emission amid the COVID-19 pandemic, recognizing it as a major health crisis and economic disruptor. The "Great Lockdown" period, called "The Experiment," offers insights into electrifying transportation and boosting renewable energy in electricity generation. This chapter shows the potential to cut CO2 emissions and air pollution by electrifying 40% of surface transportation powered by renewable electricity.

Chapter 3 comprehensively explores electrified propulsion systems, defining subsystems, degrees of electrification, and potential architectures combining electric motors. It also categorizes operational modes into primary and secondary ones for clarity. The chapter also proposed a workflow for propulsion system architecture design.

Chapter 4 reviews a model-based engineering approach for electric vehicles. It evaluates an electric vehicle model's correlation with physical results, ensuring dynamic responsiveness for reliable design choices, energy efficiency assessment, software, and control calibration while referencing data from [11]. This chapter equips the thesis with the background to rely on the energy consumption and performance simulation results.

Chapter 5 of this thesis delves into electric commercial vehicles. It analyzes four distinct electric vehicle propulsion configurations. This investigation goes beyond energy efficiency assessment, examining acquisition costs and Total Cost of Ownership (TCO) considerations. The objective is to scrutinize the financial viability of electrified commercial vehicles as a profitable investment opportunity for fleet owners. Metrics like the internal rate of return (IRR), payback period (PB), and return on investment (ROI) are analyzed to provide a comprehensive financial perspective.

Chapter 6 focuses on regenerative braking strategies for light commercial electric vehicles (up to 10,000 lbs GVW). It investigates and compares two methods, series and parallel, regarding their energy efficiency and drivability. Energy efficiency assessments simulate different regenerative braking strategies in five distinct driving cycles. Furthermore, the study uses a static driving simulator to evaluate drivability during deceleration maneuvers through a driver-in-the-loop simulation. The chapter introduces an innovative integrated Model-in-the-Loop (MiL) and Driver-in-the-Loop (DiL) approach to assess the interactions between propulsion and braking systems using a driving simulator. This approach enables objective and subjective evaluations of energy efficiency and drivability performance, utilizing metrics such as pedal travel, longitudinal acceleration, and acceleration ratio for comprehensive comparisons. The chapter also presents the energy efficiency problem when not using optimum brake subsystem architecture.

Chapter 7 introduces the Adaptive One-Pedal Drive (A-OPD) as a solution to optimize one-pedal drive (OPD) systems for electric commercial vehicles, particularly addressing the challenge posed by significant variations between curb weight and gross vehicle weight (GVW). The A-OPD strategy incorporates an algorithm utilizing a Recursive Least Square (RLS) filter for accurate mass estimation. It classifies and selects from pre-calibrated A-OPD regenerative torque maps, ensuring consistent and efficient vehicle operation, regardless of load conditions. This approach aims to enhance energy efficiency in real-world driving scenarios while maintaining driveability, performance, and safety.

The study cases presented in **Chater 5**, **Chapter 6**, and **Chapter 7** all use the exact base commercial vehicle and technical specifications.

Chapter 2

Transportation System Electrification

The World Health Organization defines a Pandemic as "the worldwide spread of a new disease." Until a pandemic is declared, the new disease's progress through different contagion phases is analyzed. Stage 6 marks the pandemic announcement stage when community outbreaks occur in at least two countries. The pandemic is over when the spread of the disease ceases or is controlled to acceptable levels, similar to the flu [12]–[14].

During the COVID-19 Pandemic, social distancing measures have been implemented to contain the spread of the Coronavirus. Most of the restriction measures were eased, and a complete return to normal, including international travel, happened when vaccines were widely available globally to developed and developing countries, limiting the surge of new variants [15].

Due to social distancing, a significant reduction in economic activities led to a global economic downturn. GDP growth for most of the G-20 economies was negative in 2020 [16], and a significant decrease in CO_2 emissions and air pollution in urban areas was observed, caused mainly by the drastic reduction in mobility and electricity demand [17].

Air pollution and CO_2 emissions have grown exponentially since the first industrial revolution. During this time, periods of crises have demonstrated a correlation of economic downturns with a temporary reduction in the levels of CO_2 emitted by the combustion of fossil fuels.

Structural changes implemented in the energy system during the energy crisis of the 1970s and the implementation of policies and regulations to limit air pollution and emissions were demonstrated as effective ways to reduce the carbon intensity of the global economy.

However, the measures implemented globally have failed to reduce the global average temperatures, and the increasing concentration of CO_2 in the atmosphere remains a significant environmental threat. It is the driver of climate change and many global environmental disasters [18], [19].

Reduced air quality in populated areas is also associated with disastrous consequences to population health. In many cities, the concentration of harmful gases and particulate matter is far beyond what the World Health Organization (WHO) indicates. Air pollution in big cities is associated with the cause of premature deaths and reduced life expectancy [20]–[25]. The WHO estimates that 4.2 million premature deaths yearly are due to air pollution [26]. Air pollution is a global problem; cities in almost every country and continent face issues due to climate change and air pollution [27].

Air pollution is defined as the contamination of the atmosphere with a harmful substance that causes a risk to the health of human beings or any other living form [28]. In this thesis, the term "Air Pollution" will be used for gases and particulates that are harmful to human health, such as particulate matter 2.5 and NO_x. The gases that cause climate change are defined as Greenhouse gases (GHG), of which CO2 is the most harmful for the transportation sector.

For a long time, the World has suffered from air pollution and excessive CO2 emissions as if it were a global disease, weakening its ecosystem and dimming the future of humanity. It is possible to draw a parallel between the COVID-19 pandemic and an ongoing global "Air Pollution Pandemic." However, while the former has monopolized headlines since the beginning of 2020, the latter receives much less attention, although the implications in both cases are comparable in many ways. In March 2019, David R. Boyd, UN Special Rapporteur on Human Rights and the Environment, made a statement in which he called air pollution a pandemic: "Yet, this pandemic receives inadequate attention as these deaths are not as dramatic as those caused by other disasters or epidemics […] Every hour, 800 people are dying, many after years of suffering, from cancer, respiratory illness or heart disease directly caused by breathing polluted air". [29] The global "Air Pollution Pandemic" also takes a back position concerning global warming, a related but distinct problem.

Living in a world under the conditions of confinement seen during the COVID-19 crisis is not sustainable, as economic activities and social relationships are part of our current social structure. The economy and social interactions returned to their previous levels, including air pollution, which returned to business as usual when the economy reopened.

Many impacted countries provided economic stimulus to keep the structural integrity of their economies intact and to help create the conditions for economic recovery and confidence during the post-crisis. These incentives were usually presented as financial packages, embodying a collection of monetary and fiscal policies, e.g., lower interest rates and provision of subsidies [30].

Putting aside all the terrible consequences of COVID-19, we could view the 2020 "shutdown" crisis as a large-scale experiment designed to observe how extreme public measures would impact the environment and humanity's health by drastically reducing the power generation and transportation intensity.

This "experiment" could provide insights and motivation for new government policies, including more extensive adoption of alternative energy sources and vehicle technologies, e.g., electric vehicles and renewables. Some governments have already announced investments in this direction: for example, in May 2020, France announced an injection of approximately €8 billion into the automotive sector, with a significant portion of that investment earmarked to boost the market for electric and hybrid vehicles. These incentives, in the form of purchase bonuses, will stay in place until July 2020 [31]. In November 2021, the USA announced an incentive investment package in the form of a $2 trillion climate plan. $174 billion was earmarked to boost the electric car market [32].

Economies around the World are recovering, but the consequences of the economic crisis generated by the pandemic could last much longer. Therefore, if, to a certain degree, the introduction of "healthier technologies" can not only be combined with more conventional fiscal and monetary government stimulus measures but also – shared with countries that will suffer longer, economically, and socially with the pandemic – this would not only mitigate the economic downturn but, at the same time, improve the health of a large portion of the global population while alleviating the problem of climate change.

Examples of such "healthier technologies" could include: (1) the introduction of incentives to reduce commuting, such as providing stimulus for more remote working; (2) the introduction of greener technologies, such as introducing completely electrified propulsion systems for surface transportation and aviation; (3) the systematic replacement at different scales of fossil-fuel-powered electricity generation by renewables sources, e.g., solar, wind, hydro; and (4) introducing stimulus for the usage of clean public transportation, and micro-mobility.

2.1 Emissions and Air Pollution as a Pandemic

2.1.1 Air Pollution and Health

There are many sources of air pollution and CO2 emissions, including outdoor and household air pollution. The use of fossil fuels significantly contributes to ambient air pollution. The correlation of air pollution with disease and premature death is a well-established field of study. Many publications are available on the topic [33], [34], and Air Pollution is directly associated with increasing the risk of cardiovascular and respiratory problems [35]–[39].

Research undertaken during the SARS epidemic [40] noted an associated increase of 86-100% chance of death in highly polluted areas when compared with geographic regions with a lower level of air pollution. Amid the COVID-19 Pandemic, researchers are identifying a spatial association of air pollution with increased mortality rate [41], [42]. A US study found a direct correlation between high deaths due to COVID-19 in areas with long-term exposure to PM2.5 [43]. Another study, considering data from France, Germany, Italy, Spain, Netherlands, and England, confirmed a pattern of increased mortality rates due to COVID-19 in areas with long-term exposure to PM2.5 and NO2 [44].

Another investigation [45] found a correlation between outdoor air pollution and premature deaths on a global scale. This study noted that 2010 saw a peak of deaths related to air pollution of about 4.8 million worldwide, predominantly in Asia. It also showed a significant geographical difference in the associated causes of pollution and premature deaths. For example, in the U.S. and Germany, 36% of premature deaths related to air pollution are attributable to surface transportation. In comparison, power generation and residential energy count respectively for 19% and 12% in the U.S. and 10% and 19% in Germany. In China, land traffic and power generation were responsible for 7% and 2% of the premature deaths associated with air pollution, while residential energy was responsible for 76% due to coal and wood fire used for heating and cooking. In the same study, the researcher predicts that the fatalities will double by 2050.

A 2015 study found air pollution was correlated with 8.8 million deaths annually and a reduced life expectancy of 2.9 years [46]. From the total associated deaths by air pollution, the authors indicated that 35% were concentrated in East Asia, 32% in South Asia, 11% in Africa, and 9% in Europe. East Asia represents a death rate of 196 deaths per 100k inhabitants: for Europe, 133 deaths per 100k inhabitants.

Conversely, the study forecasts an increase of 1.1 years in life expectancy and an avoidance of 3.6 million deaths by eliminating air pollution caused by fossil fuel combustion.

2.1.2 Economic Implications of Air Pollution and Climate Change

Air pollution and the concentration of CO2 in the atmosphere impact human health but are also a potential threat to the global economy. There are several economic implications for mitigating the health problems associated with air pollution and the consequences of climate change.

A 2018 study [47] estimated the cost of treating air pollution-related diseases in England at approximately $6 billion annually. The WHO estimated the global cost in 2014 was $3.5 trillion [48]. For reference, in 2014, the global GDP was $79.3 trillion. The implication is that healthcare spending to treat diseases associated with air pollution represented approximately 4.5% of global GDP in 2014 [49]. In 2020, research [50] estimated the cost of $5.3 billion per million COVID-19 patients. According to [51], in 2020, 84 million people were infected with the new Coronavirus. Using these data to make an approximation, the global cost of health care to treat COVID-19 could be estimated at $450 billion, without considering the investment in equipment to increase the healthcare system's capacity to meet the high demand.

In the latest Carbon Budget report, published by the Intergovernmental Panel on Climate Change (IPCC), the accumulated amount of CO2 emissions from 2018 to 2030, to limit the earth's average temperature increase to $1.5^{o}C$ in 2030, is calculated at 770 GtCO2. Even if the pace of emissions remains constant with the 2019 levels, the budget will be exceeded in 2030 [52], [53]. Per [54], the accumulated economic losses by 2050 due to climate change can reach up to $10 trillion if business is as usual.

2.2 Pollution Reduction Learnings from the COVID-19 Pandemic Lockdown

The measures to limit the spread of the Coronavirus led to the closure of all non-essential activities in many jurisdictions. The outbreak of COVID-19 and its associated confinement strategies resulted in restrictions on people's movement and the temporary closure of businesses and commercial activities, with a significant reduction in economic activity [55], [56]. Therefore, there was an impact on the demand for energy and a temporary decrease in CO2 emissions and air pollution in urban areas [57][42].

In a series of studies published by the International Energy Association, global energy demand was identified to be temporarily reduced by approximately 3.8%

during the first half of 2020 due to the confinement measures implemented to control the spread of the new Coronavirus. Oil and coal demand decreased by 5% and 8% compared to the same period in 2019. Surface transportation decreased by 50%, while aviation decreased by 60%. In this period, the share of renewables increased in the USA, China, and India. In Europe, it grew, but from February to July 2020, the percentage of renewables in the mix exceeded that of fossil fuels. At the end of 2020, with the easing of confinement measures, the weekly demand for electricity returned to 2019 levels, and in China averaged 6.5% higher than 2019 levels [58][59].

In April 2020, the anticipated global GDP growth 2020 was estimated at -3%. However, the first calculations of real 2020 global GDP growth are in the range of -4%. [16]. Poverty grew most of all in developing countries – specifically in Latin America, the Caribbean, the Middle East, North Africa, and Sub-Saharan Africa – adding approximately 100 million people below the extreme poverty line. In Europe, East Asia, and North America, the trend of poverty reduction over time has remained constant [60]. In the developed world, despite a significant spike in 2020, unemployment rates are now near normal levels [61], [62].

The total annual energy demand drop in 2020 was 6%, seven times more than the reduction during the global financial crisis of 2008/2009 and equivalent to double all the crises between WWII and the global financial crisis combined [58].

In [58], the IEA listed the significant impacts on the energy sector due to the COVID-19 outbreak. Approximately 4.2 billion people were under some level of confinement in April 2020. This represents about 54% of the global population and is linked to around 60% of the worldwide GDP. Countries under complete lockdown experienced a reduction of about 25% in energy demand, while for countries under partial lockdown, it was approximately 18%. That is the most significant drop since WWII, and it is six times bigger than the decline seen during the global financial crisis of 2008/2009.

In [6], CO2 emission reduction was presented as a function of the confinement index (which is calculated in terms of length and the level of confinement). The authors noted that by mid-March 2020, approximately 85% of global emissions were emitted from quarantined areas. In April, the peak reached 90%.

At its lowest point, the economic contraction resulted in a 17% CO2 emission reduction compared to the same period in 2019. The annual decrease is estimated in the interval of 4% to 7.5%, depending on the confinement index. Table 2.1 shows the contribution of each sector to the daily emissions reduction during the "Great Lockdown" [6].

Table 2.1 Daily CO2 Emission Reductions per Economic Sector.

	AVG Daily Reduction [MtCO2]
Electricity Power	-3.3
Industrial	-4.3
Transportation	-7.5
Public Sector	-0.9
Residential	0.2
Aviation	-1.7
TOTAL	-17

The ground transportation and aviation sectors accounted for more than 50% of total CO2 emissions reduction, followed by the power generation and industrial sectors. Figure 2.1 shows the contribution of economic sectors to the temporary global CO2 emission reduction. Figure 2.2 shows the temporary effect of CO2 emission within each analyzed economy sector, compared with the same period in 2019 [6].

COVID-19 is the worst health crisis since the 1918 Pandemic and has resulted in an economic downturn that dramatically impacted energy demand. "The Experiment," during the COVID-19 "Great Lockdown," gives us a perspective of how measures to electrify the transportation system and drastically increase the share of renewable sources in electricity production can reduce CO2 emissions and air pollution. An estimated electrification of 40% of the surface transportation fleet, powered by renewable electricity, is an effective way to meet the Paris Agreement targets.

The transition to Transportation 2.0 could help to save millions of lives. The needed structural changes in the energy and transportation sectors are highly capital-intensive. Governments should also work to strengthen air pollution and CO2 emission regulations and to remove incentives to the fossil fuel industry. The transition should start with the electrification of surface transportation, investments in developing technologies to reduce reliance on rare earth materials, and electrification costs. Also, there is a strong need to expand the charging infrastructure system and generate electricity from renewable sources. Massive investments in innovation and research are still necessary to make the electrification of the aviation sector economically feasible. However, the electrification of this sector can cause a paradigm shift in its entire business model. A transition of the aviation supply chain is also necessary, and incentives are essential to change the mobility industry.

The impact of the COVID-19 "Great Lockdown" and the "return to normal" effect on the CO2 emission and pollution footprint is an excellent example of how a major sector of the economy impacts the global CO2 emission and air pollution profiles. We have also seen where and by how much measures to reduce the pollution of economic sectors could simultaneously help limit global warming.

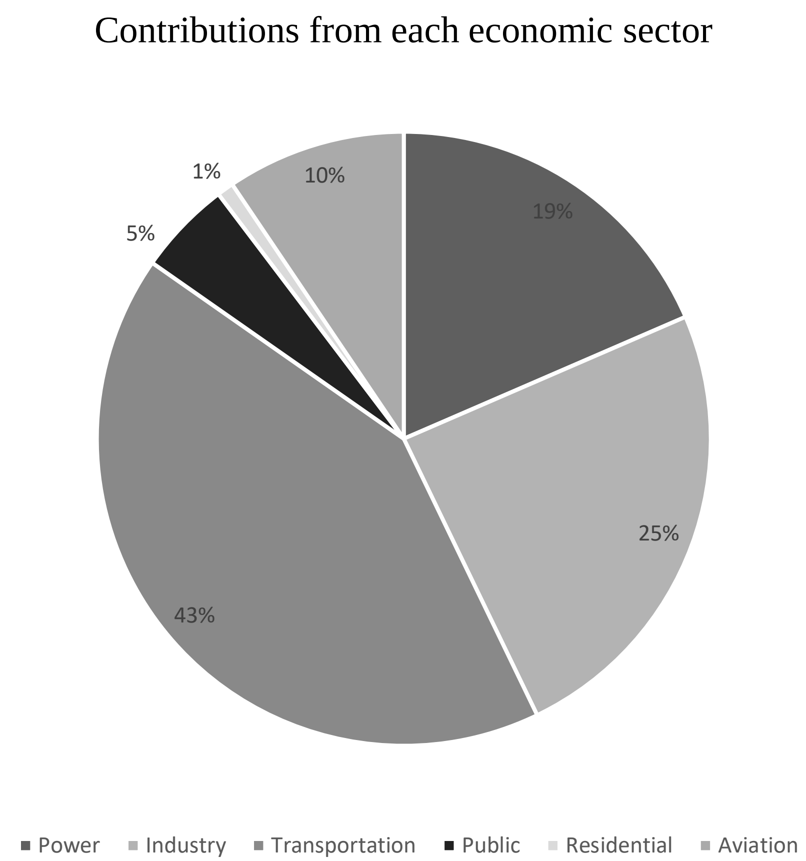

Figure 2.1 Contribution to Temporary Co2 Emission Reduction During the COVID-19 "Great Lockdown".

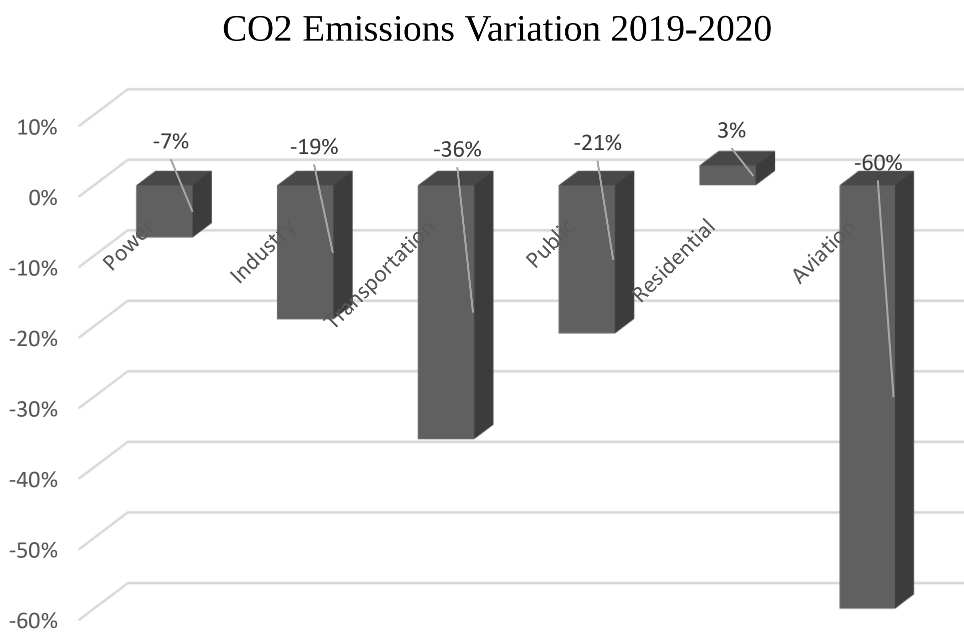

Figure 2.2: Percentage decrease in CO2 emissions comparing the same period of 2019 and 2020.

To keep global warming under 1.5C, an annual linear CO2 emission reduction of approximately 1-2GtCO2 is necessary. That is equivalent to a daily CO2 emission reduction of roughly 2.8-5.6MtCO2 [63]. A drop of this magnitude has only happened a handful of times in the modern era: globally during the Great Depression and WWII; regionally, with the collapse of the Soviet Union; and in 2020, with the COVID-19 "Great Lockdown" [64].

Figure 2.3 shows the changes in the concentration of particulate matter (PM2.5) in nine global cities. The comparison is based on data measured during three weeks of lockdown in 2020 and then compared to the same period in 2019 and the average of the air pollution data of the prior four years [65]. The changes in PM2.5 concentration were measured in high-density urban areas with heavy traffic.

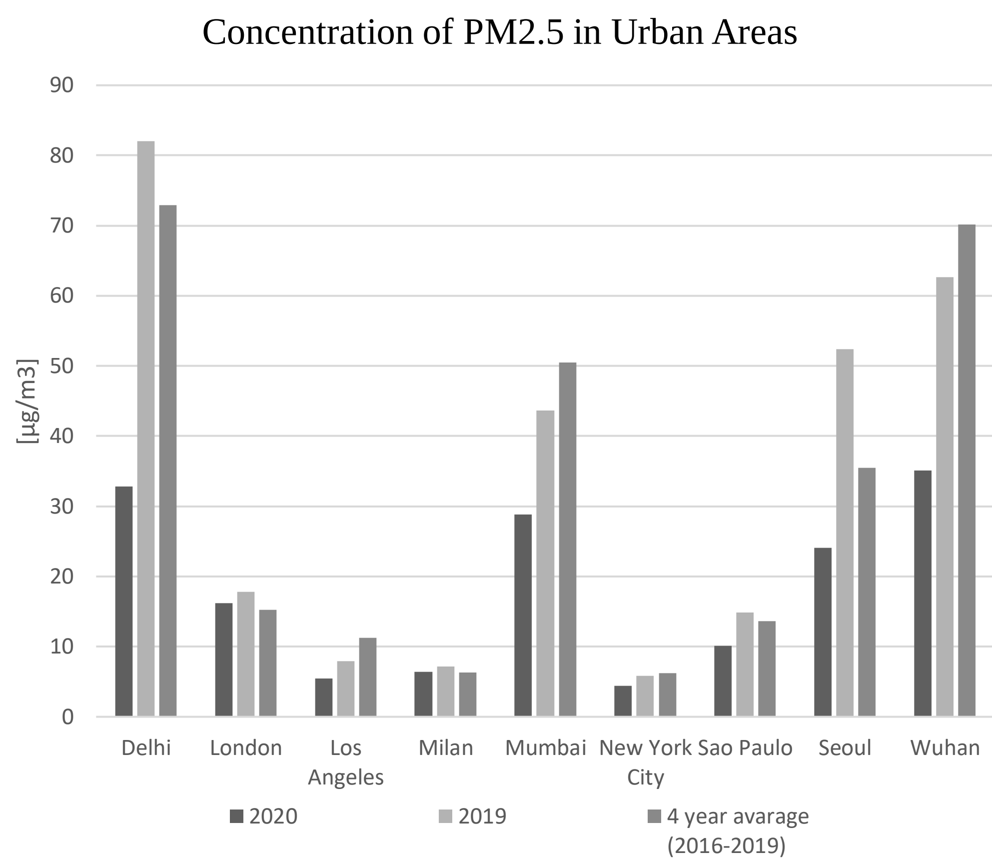

Figure 2.3: Average concentration of Particulate Matter 2.5 during a 3-week lockdown.

Cities that historically have presented extremely high levels of air pollution, mostly due to transportation and power generation, were the most positively impacted in relative terms during the complete or partial lockdowns. Los Angeles saw its best air quality since systematic PM 2.5 data collection started in the 1980s. Similarly, Wuhan saw its lowest measured pollution level[66]–[68]. In Sao Paulo

[69], a decrease of 64.8% in C.O. concentration was followed by a reduction of 77.3% in NO, 54.3% in NO2, and 30% in O3.

COVID-19 confinement measures have resulted in continuing social and economic impacts [70]. The International Monetary Fund (IMF) estimated a Global GDP reduction of 3% in 2020, with a decrease of 4.5% in developed countries and 2.1% in emerging markets, led by India and China. Global GDP is estimated to grow by approximately 6% in 2021 [71]. The economy's recovery is bringing CO2 emissions levels back to 2018-2019, consistent with the increased use of coal and oil [59].

2.3 Building a Greener Future

There was a "V" effect in CO2 emissions growth in past crisis events. This was the pattern of emission trajectory growth seen during the U.S. Savings and Loans crisis in the mid-1980s, the collapse of the Soviet Union in 1988-1991, and the Global financial crisis of 2008/2009. The global oil crisis in the 1970s presented an L-shape in the growth trajectory of CO2 emissions. The main cause was the implementation of structural changes in the energy sector, reducing the reliance on oil while adopting natural gas and nuclear energy [72]–[74].

The oil crisis started a race to develop new technologies to improve the efficiency of energy systems in the transportation and industry sectors, thereby reducing the carbon intensity of the economy (the CO2 emission ratio relative to gross domestic product (GDP), as shown in Figure 2.4.

Even with continuing economic growth in developing countries and the consistent growth of CO2 emissions, the global carbon intensity of the economy maintains a declining trajectory, which means that globally, we are producing fewer CO2 emissions to maintain consistent levels of economic development [75]–[77]. However, reducing the economy's carbon intensity is not enough to limit global warming and the looming climate crisis.

Developed economies presented a reduction in the CO2 emission levels of 1.3% in 2008 and 7.6% in 2009, followed by a growth of 3.4% in 2010 (one year after the 2009 global economy crisis). Developing countries, on average, presented a consistent increase in emissions of 4.4% in 2008, 2.9% in 2009, and 7.6% in 2010 [72]. In 2021, global CO2 emissions rebounded to 2019 levels, primarily due to the use of coal for electricity generation and the return of mobility [78].

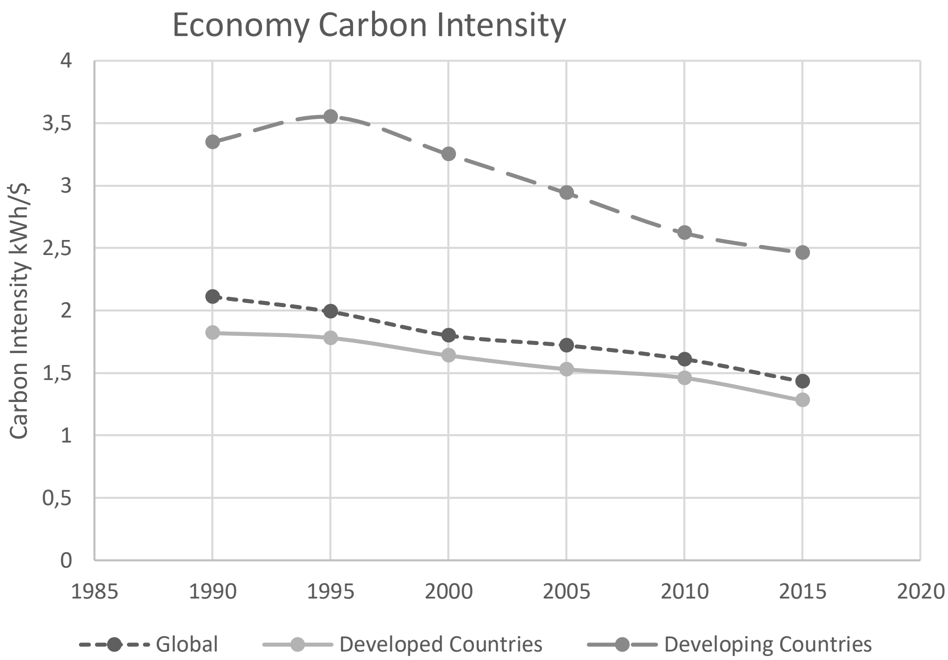

Figure 2.4: Carbon Intensity of the Global Economy since the '90s [76].

Energy source shares are changing due to structural changes in the energy sector, implemented since the oil crisis and, more recently, due to a rise in concerns about climate change. The share of coal as a primary source has remained stable since the '70s, while the share of oil is reduced, and natural gas has increased. The percentage of renewables other than hydroelectric, e.g., solar and wind, started to grow in 2010 when efforts to fight climate change intensified. Figure 2.5 shows that coal and oil remain the leading energy sources for electricity generation and transportation globally.

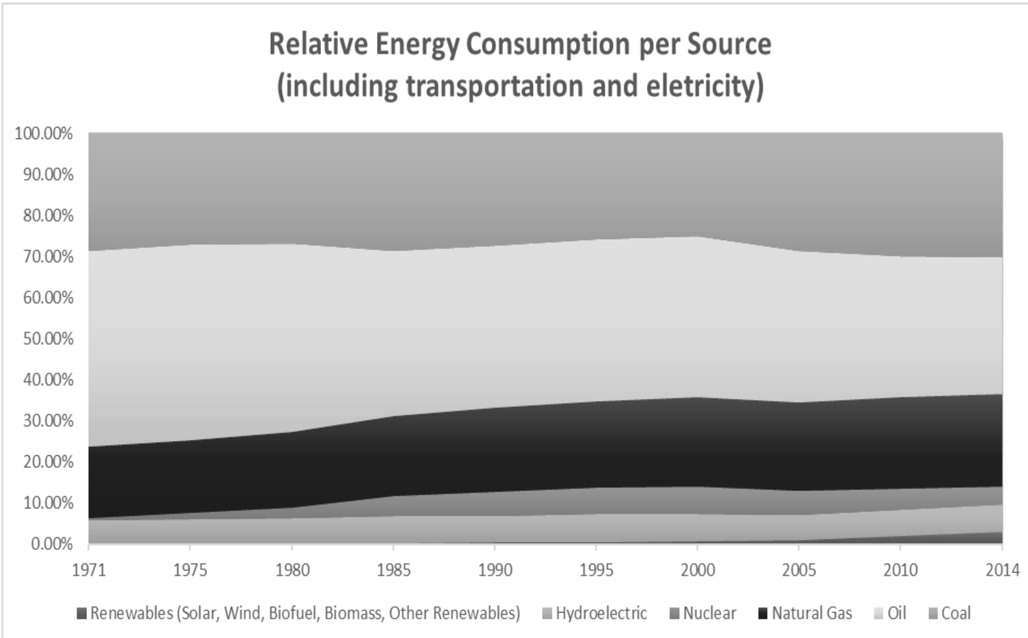

Figure 2.5: Energy Sources mix since 1971 [58].

Structural changes in the energy sector are an effective way to transition to a low-carbon economy. As presented by [79], there is a direct correlation between the implementation of policies and regulations and the reduction in emission levels and air pollution. However, the growth of capacity to generate and offer renewable electricity in the grid and the electrification of the transportation sector is not keeping pace with the growth in the energy demand, which results in an increasing share of renewables in the energy mix but does not reduce the global use of coal and oil, as shown in Figure 2.5.

In [80], a mix of the electrification of the energy sector and carbon capture technology is mentioned as a pathway to meet the goals of the Paris Agreement. Table 1 shows that during the COVID-19 "Great Lockdown", the transportation and power energy sectors combined accounted for a daily reduction of 12.5 $MtCO_2$; of which 7.5 $MtCO_2$ came from the transportation sector alone. That amounts to a decrease of 7% in the global demand for electricity and a significant decline of approximately 50% in the usage of surface transportation – and exceeds the daily reduction in emissions needed to meet the Paris Agreement targets of about 7 $MtCO_2$.

Even with a new normal, the World still strongly depends on vehicular forms of mobility, and a sustainable reduction of 50% in global mobility will not last long. With the easing of confinement measures, vehicle traffic is beginning to return to normal and is expected to do so when travel restrictions are fully lifted.

The concept of Transportation 2.0 is proposed as a paradigm shift for the transportation sector. A significant component of this shift involves moving from a reliance on fossil fuels to a wholly electrified transportation system, where the electricity is generated by a mix of renewable sources [81].

The technology for electrifying the propulsion system for surface vehicles, e.g., passenger vehicles, public transportation, commercial trucks, and off-road vehicles, is a reality today. Technological challenges still need to be addressed to enable electrification on a large scale. Batteries with higher energy density and charging power are required to increase electric range and reduce charging time. The adequate deployment of charging infrastructure and reduced reliance on rare earth materials to produce electric motors are typical of the technical challenges of all types of ground vehicles.

Transportation 2.0 could also be applied to the aviation sector, offering the potential for cost reduction and increased flexibility in operations; however, many innovations are still necessary. The primary challenge is the need to increase the energy and power density of the propulsion system [82].

On the other hand, the transition to an electrified transportation system increases the demand for electricity. Based on the concept of Transportation 2.0, electricity generation also moves to be based on renewable sources. Transportation 2.0 finds the best energy mix trade-off when up to 70% of the grid is supplied with renewable sources [83].

The transition to a wholly electrified future is capital-intensive. The necessary investment in infrastructure, globally, in the energy system is estimated in the range of $3.5-6 trillion by 2030 [84]. Although there are political roadblocks and capital limitations to funding the energy transition[85], there is a need for this paradigm shift in the energy sector and transportation sectors. The COVID-19 "Great Lockdown" has been an excellent opportunity to see the effects of how a greener energy and transportation sector could impact emissions and climate change for good.

The CO2 emission reduction experienced in 2020 is predicted to be in the range of 0.8-3.0 GtCO2. Based on the temporary reduction of CO2 emission, presented in Table 2.1, it is possible to elaborate a scenario by which electrification of a range between 20-40% of the transportation fleet, if powered by renewable sources, can reduce daily CO2 emissions to the range of 2.8-5.6 MtCO2. The annual

CO2 reduction in this scenario will fall into the range of 1-2 GtCo2, the estimated amount of CO2 emissions reduction to limit global warming.

2.4 Summary

COVID-19 is the worst health crisis since the 1918 Pandemic and has resulted in an economic downturn that dramatically impacted energy demand. "The Experiment," during the COVID-19 "Great Lockdown," gives us a perspective of how measures to electrify the transportation system and drastically increase the share of renewable sources in electricity production can reduce CO2 emissions and air pollution. An estimated electrification of 40% of the surface transportation fleet, powered by renewable electricity, is an effective way to meet the Paris Agreement targets.

The transition to Transportation 2.0 could help to save millions of lives. The needed structural changes in the energy and transportation sectors are highly capital-intensive. Governments should also work to strengthen air pollution and CO2 emission regulations and to remove incentives to the fossil fuel industry. The transition should start with the electrification of surface transportation, investments in developing technologies to reduce reliance on rare earth materials, and electrification costs. Also, there is a strong need to expand the charging infrastructure system and generate electricity from renewable sources. Massive investments in innovation and research are still necessary to make the electrification of the aviation sector economically feasible. However, the electrification of this sector can cause a paradigm shift in its entire business model. A transition of the aviation supply chain is also necessary, and incentives are essential to change the mobility industry.

The impact of the COVID-19 "Great Lockdown" and the "return to normal" effect on the CO2 emission and pollution footprint is an excellent example of how a major sector of the economy impacts the global CO2 emission and air pollution profiles. We have also seen where and by how much measures to reduce the pollution of economic sectors could simultaneously help limit global warming.

Chapter 3

Electrified Automotive Propulsion System

Some estimations predict that the number of motorized vehicles used for transportation can surpass more than 1 billion cars [1]. The number of new vehicles on the roads in 2018 reached about 80 million units, with a growth rate of about 10% compared with the number of produced vehicles by 2015 [2]. This growth in the automotive industry is mainly due to the enormous increase in economies of developing countries such as China and India, which are creating an entirely new automotive market, with yearly production volume estimated at 30 million units per year in China, for example [86].

On the other hand, the United States is known as a country on wheels, and the vehicle market has mostly plateaued. More than 280 million vehicles are on the road in the USA, and about 35% are light passenger vehicles – at least four wheels, no more than eight seats, and a maximum GVW of 8500 lbs [3]. However, in 2016, 90% of the miles in the USA were driven by light passenger vehicles [87]. The International Council on Clean Transportation (ICCT) estimates that transportation causes 23% of global emissions. About 40% of the total emission is from light passenger vehicles [4]. The Environmental Protection Agency (EPA) estimates that in the United States, the level of Global Carbon emission caused by fossil fuels rose about 90% when compared with the status of the 1970s, and 28% of the total gas emission comes from the transportation system [5].

The ICCT presents the perspectives of the regulatory landscape for the most important automotive markets in the world regarding the target CO2 emission, parametrized for the same test procedure, the New European Drive Cycle (NEDC).

European Union is leading many efforts to establish the metrics to reduce harmful gas emissions. The average CO2 emission by cars in the European region has decreased from 185 g/km in 1995 to 118 g/km in 2018. The European target for 2020 is to meet, on average, 95 g/km of CO2 and about 80 g/km by 2025 [4]. The mandatory average reduction of CO2 emission is about 40% in the United States and Canada from the 2012 level by 2025, and the regions that comprehend the most important automotive markets in the world will have a target to meet an average CO2 emission of about 100 g/km [4].

To meet the requirements, over the past 20 years, automakers have invested in many incremental technologies to reduce CO2 emissions. The development of those new technologies focused on optimizing the internal combustion engine, including direct fuel injection, engine downsizing combined with the gearbox down speeding, engine cylinder deactivation, and engine start-stop [88], [89]. These technologies, combined with weight reduction through the application of new materials and body design techniques, vehicle aerodynamics, and the development of tires with improved drag resistance, were the most critical enablers of CO_2 emission reduction in the past years [90].

However, in 2018, the EPA estimated that only 25% of the vehicles sold at that time were able to meet the 2020 requirements, and only 5% would be able to reach 2025 needs which about 50% of these cars sold in 2018 used a gasoline engine serving as the main propulsion. Of that 5% able to meet 2025 requirements, all are pure electric vehicles [90].

The adoption of the electrification of the propulsion system is hence mandatory to meet the CO_2 emission targets of 2025. The electrification of the propulsion is defined as the utilization of "more electrical energy to power traction and non-traction loads of the vehicle" [91].

The electrification of the powertrain consists of the addition of electric machines, batteries, and power electronics [92]. The electric machines have a high torque response, relatively low cost, and high power density, which facilitate a wide range of installation possibilities in the propulsion system; however, the cost of permanent magnet machines is expected to rise shortly due to the rise in the cost of rare earth material [93], [94]. On the other hand, batteries are still relatively expensive, and there are many complexities in battery installation in the vehicle. In many cases, the vehicle platforms are developed uniquely to accommodate internal combustion engines and conventional gearboxes, which create additional complexity for integrating electric machines, batteries, and charging features. Automakers and suppliers frequently face the challenges of developing powertrains that improve vehicle propulsion energy efficiency, reduce greenhouse gas emissions, meet regulatory requirements, and achieve business profitability and economy of scale.

This chapter aims to present a comprehensive review of electrified propulsion systems. It presents the propulsion system from its definitions and subsystems, detailing the degrees of electrification and the possible architectures to be designed combining electric motors. The potential operational modes for each architecture are also presented, dividing them into primary and secondary operation modes.

3.1 Vehicle Propulsion Subsystems

The definition of the powertrain consists of a system in which a group of components work together as a system and deliver power and torque to the vehicle. The powertrain system is sometimes split into two different categories: powertrain – responsible for providing the torque and power, and drivetrain or driveline – responsible for transmitting the power and torque to the wheels [91]. In this chapter, the powertrain is called the propulsion system. The propulsion system is one of the systems which integrates a vehicle. This chapter proposes dividing the propulsion system into four subsystems: the power unit, the driveline, the energy subsystem, and the thermal subsystem. Each subsystem is defined by the group of functionalities that the subsystem performs. Figure 3.1 shows an example of a plug-in hybrid vehicle propulsion system.

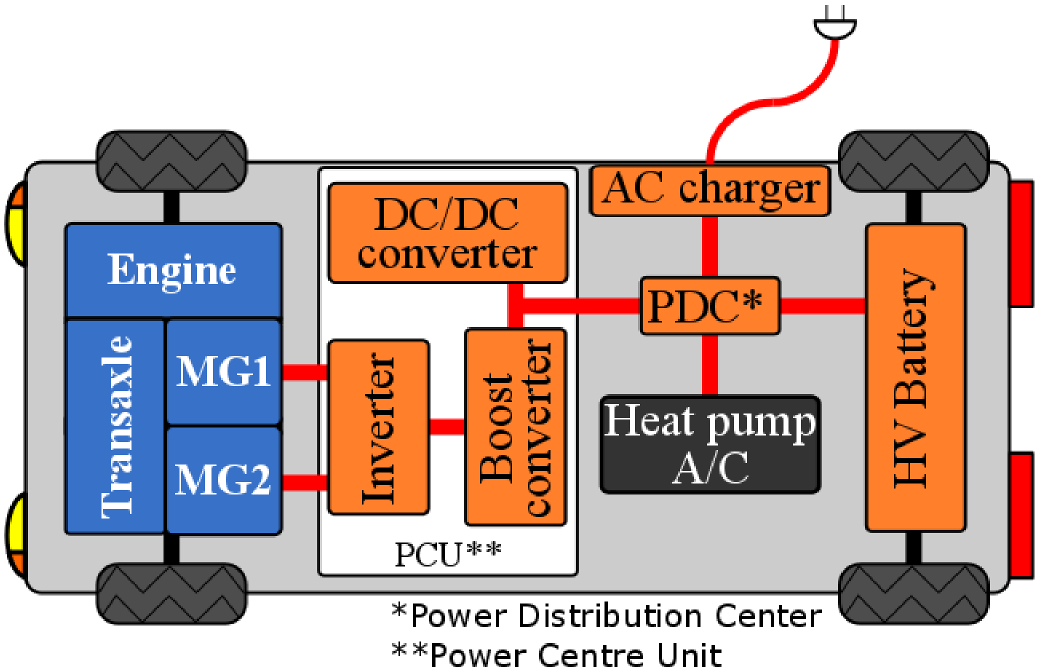

Figure 3.1: An electrified powertrain subsystem configuration example

Figure 3.2 shows the organization of the propulsion system and the hardware organized as subsystems.

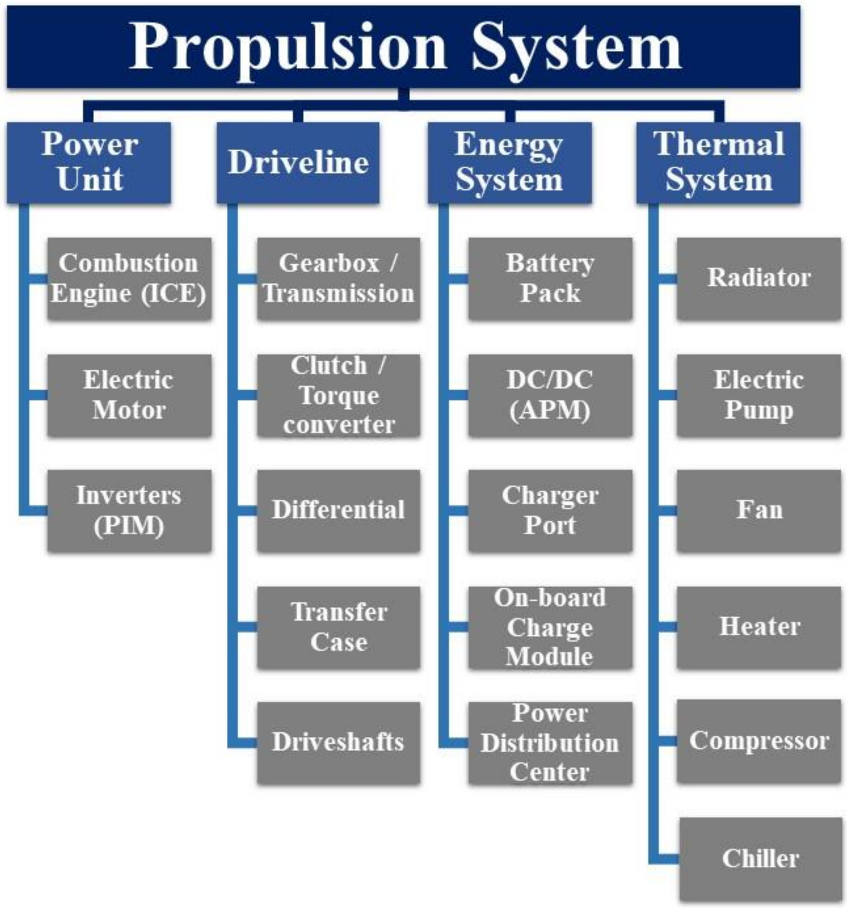

Figure 3.2: Propulsion System Breakdown Structure.

3.1.1 Power Unit Subsystem

The power unit subsystem: the internal combustion engine (ICE), the electric machines (EM), the inverters (AC/DC) – also called the power inverter module (PIM), and the DC/DC booster.

The power unit subsystem provides power to the vehicle for propulsion and auxiliaries. The internal combustion engine (ICE) is the primary power source in conventional cars. Electric machines are the primary power source in electric vehicles, including battery-electric and fuel-cell vehicles. While in hybrid, plug-in hybrid, and range-extended vehicles, the ICE and electric machines provide power [95].

3.1.1.1 Internal Combustion Engine

The internal combustion engine, ICE, produces power through a thermodynamic process, burning fuel. The ICE is a complex mechanism with many moving parts. The combustion of the fuel produces the thrust force in the combustion chamber (the cylinders), translationally moving the pistons and turning the engine crankshaft. The engine crankshaft has two outputs: the front-engine accessory drive (FEAD) and the engine flywheel (or heavy disc). The FEAD connects with the alternator, the hydraulic steering pump, and the air-conditioning compressor via engine belts and pulleys [96]. The flywheel (or heavy disc) has three main functions: to keep the engine balanced due to the inertial of the disc, to deliver power to the vehicle wheels through the transmission, and to crank the ICE with the starter [97][98].

The engine can be of a spark ignition type or a compression ignition type, depending on the fuel that the engine is designed to operate. The most common type of spark ignition operation cycle is the Otto cycle. Gasoline is the most common fuel used on this type of engine, but ethanol, methanol, and natural gas are also used in this type of engine. The spark-ignition engine can also be a flex-fuel type when the ICE can operate with two or more fuels of the listed above [99], [100]

In electrified propulsion systems, the engine is often designed to operate in different combustion cycles, such as the Atkinson and the Miller cycle. The

Atkinson cycle consists of a short compression stroke combined with a longer expansion stroke, making this the ideal cycle for low Speed and low torque engine operation, which is the primary vehicle operation mode in urban traffic. The engine's overall efficiency is improved when working in the Atkinson cycle. However, the peak power performance reduces for all engine operation speeds [101].

3.1.1.2 Electric Machines

In electrified powertrains, traction machines are applied in the propulsion system as the primary source of power and torque to the vehicle or work to assist the ICE during accelerations and regulate the engine speed for higher fuel efficiency. The traction machines are also responsible for processing the electrical power flow in the reverse direction during the regenerative braking or propelled by the internal combustion engine during charging, converting mechanical power to electric power as generators [102].

The alternate current (AC) machine type is the predominant technology applied to electrified propulsion systems, such as permanent magnet (PM) machines, such as those in the Toyota Prius. Nissan Leaf and Chevy Bolt [103]–[105], and the induction machines (IM) – such as applied in Tesla Model S and Model X [106], [107].

Meanwhile, switch reluctance machines (SRM) are intensively researched, showing a good potential for traction application in electrified vehicles， and are gaining ground in electrified powertrain systems such as electric parking lock actuators and integrated starter generators [108]–[112].

The PM machine is the most used electric machine type applied in automotive propulsion systems, mainly because this type of machine provides the best efficiency. The PM machine also offers the best power density, which requires less packaging space. This is especially beneficial for traction applications since the electric machines are installed inside the transmission. However, the PM machine has a higher cost due to the intense usage of rare earth materials. The always-existing flux from the permanent magnets also results in high back electromotive force (EMF) at high speed and, in cases of winding short-circuit, could lead to hazardous situations when control fails [113]

The IM machine, when compared with the PM machine, operates at a lower power factor and lower efficiency. IM machine has the advantage of lower cost and more straightforward configuration, as the squirrel cage rotor does not contemplate permanent magnets, typical of asynchronous machines. The design and control techniques for IM machines have been mature for decades; when compared with PM machines, they can operate at higher speeds since the magnets generate no back EMF. However, to generate torque, there is always a speed gap, i.e., asynchronous, between the rotor and the stator magnetic field, and the rotor resistance must be estimated, reducing the accuracy of the motor control. The IM machine also increases the drag resistance to the vehicle motion when the machine is operating above the synchronous Speed when it is not powered [114].

The SRM machine has the simplest and most robust design and the lowest cost. It utilizes the reluctance torque between the salient stator and rotor teeth for propulsion. However, due to the significant torque ripple generated between phase transition, noise, and vibration propagation caused by the radial forces of the machine, this type of machine is not often directly applied to the traction application. In contrast, they are currently more used as actuators and motors/generators for smaller power electrified propulsion systems in passenger vehicles. They are also more accepted in commercial vehicles due to their robust performance and fault-tolerant characteristics [109].

Figure 3.3 shows a comparison of the three basic electric machine architectures.

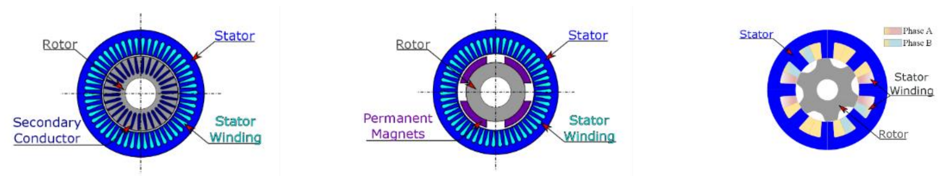

IM **PMSM** **SRM**

Figure 3.3: Common schematic types of different electric motor architectures [115]

3.1.1.3 Power Inverter Module (PIM)

The inverter is a power electronic device whose primary function is to convert DC into AC to drive the electric machine or vice-versa when the electric machine works as a generator. When applied to the vehicle power unit subsystem, the inverter converts AC to DC from the electric machine to the battery while the electric machine is operating as a generator during regenerative braking or engine charging and DC to AC from the battery to the electric machine, when the EM works as the primary source for propulsion, or to provide power to assist the ICE. A total of six main parts make the automotive inverter: the switching devices (IGBT and MOSFETS, for example), the diodes, the gate driver, the capacitor, the inductor, the bus bars, and the controller. Wide-band gap semiconductors based on Silicon Carbide (SiC) or gallium nitrate (Gan) have been researched and developed recently to improve the efficiencies of automotive electric drive units [114].

The switches are controlled by the gate driver to supply three-phase AC current into the machine winding. Typically, two switches are used per one-phase leg, and PWM techniques are applied to control the switching sequence. Diodes are used in parallel to the switches to protect the switches and allow reverse flow of current during regenerative braking or fault conditions. The capacitor and inductor are used to stabilize the DC link voltage and filter the current waveform. Finally, a microcontroller controls the gate driver and provides a diagnostic of the machine status to the upper-level vehicle electronic control unit (ECU) [116], [117].

3.1.1.4 Booster (DC/DC)

As the name indicates, the DC/DC converter steps up or down the DC voltage. When the DC/DC is part of the propulsion system, the primary function is to perform the buck-boost mode, which stabilizes the apparent voltage to the inverter and extends the base operation speed of the machine, resulting in an extended peak torque curve. This can be a cost-saver compared with adding more expensive battery packs, as it offers more flexibility on the voltage selection of the battery pack. High DC link voltage also boosts the EM efficiency as less current is needed for high voltage to achieve the same amount of power [118].

3.1.2 Driveline Subsystem

The driveline is the subsystem that allows the propulsion system to meet the following drive commands: stay stationary when the vehicle stops, but the engine is running idle, achieve and perform the transition from static to mobile state, control the vehicle forward or backward state, perform the torque and rotational speed adjustment at different vehicle speeds smoothly, and compensate for the wheel speed variation on the same axle while the vehicle is cornering. The components of the driveline subsystem include clutches, torque converter, differential, driveshaft, and transfer case [97].

3.1.2.1 Transmission

Transmission is used to adjust the driveline output torque and Speed to fit the engine characteristics, as the engine has low efficiency outside limited regions. There are two types of automotive transmissions: manual and non-manual. In manual transmissions, the driver shifts the gears manually, whether on the non-manual; the engaged gears are changed automatically and controlled by a controller depending on the driving conditions [119].

Manual transmission is the most common transmission used, with the most uncomplicated design, lower cost, and smaller space claimed. Manual transmissions are usually the choice for many vehicles sold in growing automotive markets such as South America and India. Many small vehicles in Europe also implement manual transmissions.

In non-manual transmissions, the most common transmission is the automatic transmission (AT) with a set of planetary gears. Others include automatized manual transmission (AMT), dual-clutch transmission (DCT), and continuous variable transmission (CVT).

The AT is the most common automatic transmission. This type of transmission is coupled to the engine principally by a torque converter, and the gear ratios are built with a set of planetary gears. The AT provides smooth shifting and better drivability when compared to the others. However, AT is the transmission with the higher cost and worst transmission efficiency due to the torque converter [120].

The AMT is a robotized manual transmission. This type of transmission has the same internal layout as the manual transmission; however, the gear shifting is controlled by an electronic control unit (ECU), which controls a hydraulic system that acts over the shifter inside the transmission, shifts the gears, and manages the clutch. This system has a relatively low cost compared to manual transmission but has the main disadvantage of a "torque gap feeling" while shifting [119] [121].

The DCT uses two clutches and two primary shafts: one for the even gears and the other for the odd gears. In this type of transmission, while one shaft is engaged to the engine, the transmission controller selects the Gear of the other primary shaft. When the gear shifts, the next Gear is already set, reducing the shifting time and the torque gap feeling while shifting gears. The DCT can be coupled to the engine using dry or wet clutches [119], [122].

A transmission capable of continuously varying the speed ratio between the input shaft and the output shaft without discrete gear ratios is defined as a CVT transmission. This is also called shiftless transmission or stepless transmission. In the CVT, a belt and variable-diameter pulleys or toroidal roller are implemented to create a continuous speed variation between the higher engine speed and the lower output wheel speed. The continuous shifting mechanism makes it possible to keep the engine operating at the maximum efficiency region for a broader range of torque and Speed, improving the vehicle's fuel efficiency. The coupling element can be a dry or wet clutch or a torque converter [119], [123].

Figure 3.4 shows a typical propulsion system of an AWD vehicle equipped with ICE only.

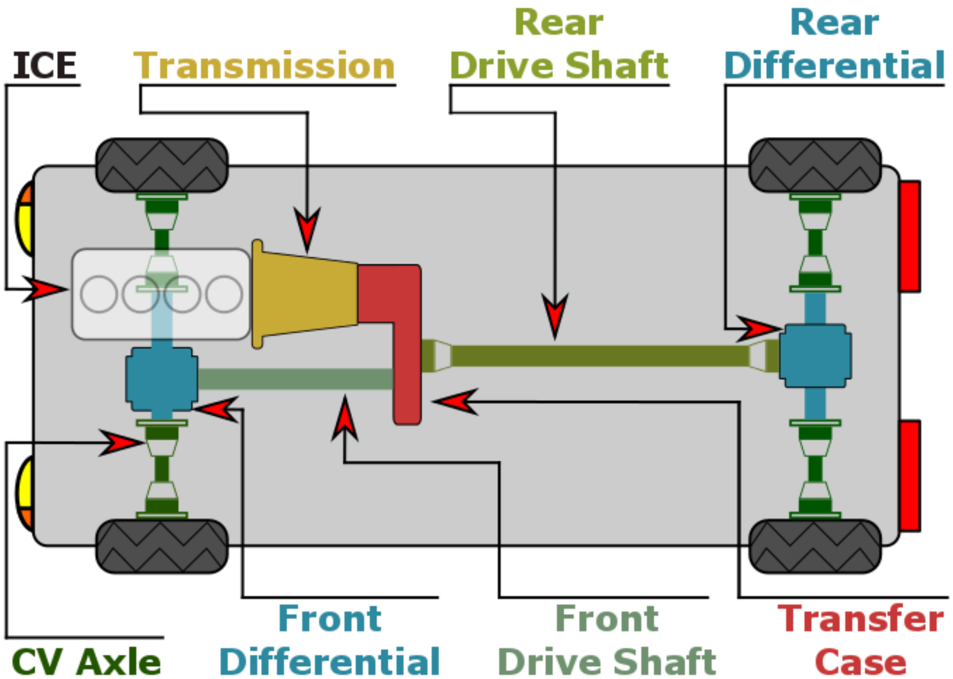

Figure 3.4. An example of typical driveline subsystem components

3.1.2.2 Clutch

The primary function of a clutch is to disconnect the power unit from the transmission and, therefore, from the driveline subsystem to allow the power unit to operate idle while the vehicle is not moving or will enable the Gear shifting when the vehicle is moving. Dry and wet clutches are the primary clutches used in automotive transmissions [97]. The dry clutch is a primary application for MT, AMT, and DCT, while the wet clutch is more utilized in AT, DCT, and CVT. The wet clutch allows a better thermal performance against the dry-clutch, while the dry-clutch provides better efficiency in converting the torque and Speed [124].

3.1.2.3 Torque Converter

The torque converter, also named the hydrodynamic torque converter, is a component filled with oil, which transmits torque using the viscosity oil through a conversion from mechanical energy to hydraulic energy by the impeller and then from hydraulic energy back to mechanical energy by the turbine blades [120]. The torque converter is composed mainly of three elements: the turbine - the driven component; the impeller - the driver component; and the stator, which assists the torque conversion function. A locker is used in the torque converter to improve the efficiency of the torque converter during steady-state operations, such as in highway conditions, eliminating the two-step energy conversion process [125].

3.1.2.4 Differential

The differential is a mechanical element that allows the two wheels of the same axle to rotate at different speeds while the vehicle is cornering, providing appropriate distribution of the forces to the wheels. A type of locker can be added to the differential to limit the differential effect when one of the wheels is slipping. The locker differential can provide additional torque to limit the differential impact or fully lock the differential to allow the drivetrain to propel both wheels with the same torque [125][97].

3.1.3 Energy Subsystem

The energy subsystem: the battery pack and the DC/DC converter. The auxiliary power module (APM), and the power distribution center (PDC). In the case of chargeable electrified vehicles, the charge port and AC/DC charger are also called on-board charger modules (OBCM).

3.1.3.1 Battery

In automotive applications, the battery is a portable source of electrical energy for vehicles. For vehicles equipped only with an ICE as a power unit, the battery's primary function is to power the engine cranking and to balance the power of the electric loads of the vehicle. In electrified vehicles, the battery is part of the propulsion system, works as an energy storage source for the power unit, and stores the recovered energy from regenerative braking. [102].

The battery in the electrified propulsion system is an integration of multiple chemical cells, connected in series and in parallel, to deliver the appropriate power at the desired voltage and store the proper energy. This integration of cells is named battery pack [126]. Battery packs keep the chemical energy at a specific voltage, and the output electric power is delivered in the DC format. The components in a typical battery pack include cells, modules, current and voltage sensors, bus bars, cooling plates and tubes, cover plates, contactors, high voltage (HV) connectors, HV fuses, and the battery management system (BMS) [127], [128].

The key characteristics of the battery pack are the power density that determines the charging and discharge rate and the energy density that determines the electric drive range. However, these two characteristics are typically trade-offs. For hybrid vehicles, the power density is an essential characteristic of the battery, while for electric vehicles, the energy density is most important. For plug-in hybrids, a balance between the two aspects is necessary [129] [102].

There are different types of battery chemistries utilized in the automotive industry, and they differ by the base chemistry and, consequently, the energy and power density and cost. For traction applications, the most utilized batteries are the Nickel Metal Hydride (NiMH), mostly used by Toyota in its hybrid vehicle, and the Lithium-Ion type, the dominant traction application technology. Within the lithium-ion technology domain, different types of materials are utilized on the positive or the negative electrode. Table 3.1 shows the most common types of anodes and cathodes [114].

Table 3.1: Lithium-ion battery cathode and anode typical materials [130].

Cathode		**Anode**		
		Non-Carbon Material	**Carbon Material**	
Nickel (LNO)		Silicon Based Composites	Non-Graphite	Graphite
Cobalt (LCO)		Nitrogen	Soft Carbon	Synthetic Graphite
Manganese (LMO)		$Li_4Ti_5O_{12}$	Hard Carbon	Natural graphite
Iron-phosphate (LFP)		Lithium Metal		
Nickel-manganese-cobalt (NMC)				
Nickel-cobalt + Aluminum (NCA)				

3.1.3.2 Auxiliary Power Module (APM)

There are multiple applications for a DC/DC converter in automotive systems. Except for the DC/DC converter used in the power unit, they are also widely implemented to charge battery and power auxiliaries. This section focuses on the DC/DC converter as part of the energy subsystem.

When the DC/DC is part of the energy subsystem, the primary function is to convert the DC current from the high-voltage battery to charge the auxiliary battery. Another vital role of the auxiliary power module (APM) is to stabilize the auxiliary battery's voltage while the battery receives a high-power demand [131].

3.1.3.3 On-board Charger Module

When used as part of the energy subsystem, the inverter operates as a battery charger, converting the AC current from the grid to charge the battery with a DC current. In some cases, the inverter can be bi-directional, allowing the vehicle battery to provide power to the grid of charge other applications [132].

3.1.4 Thermal Management Subsystem

The thermal subsystem: the radiators, electric pumps, fans, heaters, compressors, chillers, etc. The thermal subsystem is a large standalone topic and is not part of this chapter's scope. Readers may refer to separate works [133], [134].

3.2 Classifications of Electrified Propulsion System

This section aims to provide a general understanding of the different degrees of electrification and their definitions, introducing the concept of primary and secondary operational modes of an electrified propulsion system.

3.2.1 Electrification Degree

The most common way to classify a hybrid vehicle is by the electrification degree [97]. These classifications are based on three different factors: the plug-in capability, the hybridization factor, and the operational modes enabled by the electrification of the propulsion system.

3.2.1.1 Plug-in Capability

The plug-in capability is the possibility of the vehicle being connected to the grid to charge the battery and use the energy to power the electric machines. Based on plug-in capability, electrified vehicles can be categorized into two main groups: non-plugin and plug-in [114].

3.2.1.2 Hybridization Factor

The hybridization factor is proposed by [135] as the ratio between the total electric power available divided by the full power available. Equation (3.1) represents the hybridization factor (HF) mathematically.

$$\boldsymbol{HF = \frac{W_{EM}}{W_{EM} + W_{ICE}}} \tag{3.1}$$

Where:

$\mathrm{HF} =$ Hybridization factor;

$\mathrm{W_{EM}} =$ Electric Motor Power;

$\mathrm{W_{ICE}} =$ Internal Combustion Engine Power.

The hybridization factor is an excellent metric to quickly analyze the effect of electric power on the fuel economy, where the higher the hybridization factor, the higher the fuel economy tends to be.

However, this ratio is valuable only for a non-plugin vehicle. For plug-in vehicles, as part of the energy is from the grid, it is also necessary to analyze the relation between the energy from the grid and the total energy consumed by the fuel and grid electricity. In [136], the authors defined the plug-in hybrid electric factor Pihef in the form of the Equation (3.2):

$$Pihef \ = \frac{E_{grid}}{E_{grid} + E_{fuel}} \tag{3.2}$$

Where

$\mathrm{Pihef} = \mathrm{Plug} - \mathrm{in\ hybrid\ electric\ factor};$

$\mathrm{E_{Grid}} =$ Average energy from the grid over time (Battery capacity divided by charging efficiency);

$\mathrm{E_{Fuel}} =$ Average energy from the fuel over time.

3.2.2 System Operational Modes

The traditional powertrain equipped with an internal combustion engine and transmission has two main operational modes: ICE mode – when the power supplied to move the vehicle comes from the internal combustion engine; and fuel cut-off – when the fuel injection is shut-off while the vehicle is deaccelerating [137].

The electrification of the propulsion systems, depending on the electric machine position and total electric power, will enable other operational modes. Primary and secondary operational modes are the proposed classifications for the new functions of the electrified propulsion system. The primary operational modes are the functions directly associated with the reduction of fuel consumption. The secondary operational modes are the functions related to the optimization of fuel consumption, drivability improvement, increased comfort and safety, and enhancement of dynamic performance and handling.

3.2.2.1 Primary Operational Modes

Stop-start (SS) – the ICE is shut-off while the vehicle is stopped or stopping and starts again when the driver presses the clutch pedal in manual transmissions or releases the brake pedal on automatic transmissions. In some conditions, the engine restarts after reaching a certain vehicle speed while the electric machine propels the vehicle before that [138].

Electric torque-assist (TA) – the EM provides power and torque to assist the ICE, improving the overall system efficiency [139].

Regenerative braking (RB) – The EM provides a braking torque during decelerations, converting kinetic energy into electric energy. Then energy accumulates in the form of chemical energy in the battery pack [140].

Generator mode (GM) – the EM operates as a generator, powered by the ICE, charging the battery pack or creating a power flow to another EM [141].

Pure electric drive (PE) – the EM provides torque and power to the wheels to keep a constant speed or accelerate the vehicle. There are two types of PE mode: limited PE (LPE) – pure electric propulsion with limited range and performance, and full PE – pure electric propulsion that can provide total vehicle performance [142].

3.2.2.2 Secondary Operational Modes

The secondary operational modes are functions enabled due to the different approaches taken in the propulsion system torque management and its distribution to the vehicle wheels. Some of these operating modes impact the fuel economy of the vehicle; others can enhance the drivability of the car by improving the engine cranking time, the torque response in the wheels to the driver's command, or the feeling of rolling resistance. The comfort can be improved mostly by reducing NVH or improving the driver's perception of vibration in traffic jam situations. Performance and safety are added by managing the different sources of torque, controlling the torque distribution to the wheels, enhancing the accelerations, and handling control at cornering maneuvers.

Table 3.2 presents the definition of secondary operation modes and how each of them impacts vehicle performance. The definition of each of the secondary operational modes is presented as follows.

3.2.2.2.1 One-Pedal-Driving

Regenerative braking is when the brake pedal is fully released, and the accelerator pedal has a negative variation, indicating the driver desired to reduce the vehicle speed and the vehicle is performing any level of braking using the electric machines. [143]

3.2.2.2.2 Power Split

In architectures with two or more electric machines, one machine operates as a generator, while the other serves as a motor to optimize the operation of the internal combustion engine to its best specific fuel consumption region. [144]

3.2.2.2.3 E-smoothing

Torque gap filler during gear shift or turbo lag. [145], [146]

3.2.2.2.4 Cold Cranking

Cranking the engine without the utilization of an engine fly-wheel starter at any temperature condition, up to -40ºC. [147]

3.2.2.2.5 E-Coasting or e-Sailing

The engine is decoupled from the drivetrain and maintained idle, or the engine is off, with no fuel burning, at high vehicle speeds when the driver releases the accelerator pedal completely. [148]

3.2.2.2.6 Advanced Start-Stop

The ICE is turned-off at speeds higher than 0 km/h (extended start-stop) when the driver presses the brake pedal and can be re-started at vehicle speeds above 0 km/h when the driver releases the brake pedal completely. [149]

3.2.2.2.7 E-launch

Pure electric propulsion motion at very low speeds, usually bellow 20 km/h. [150]

3.2.2.2.8 ZEV Mode

Pure electric propulsion when the driver selects the EV mode button. ICE will be cranked when the driver presses the accelerator pedal, and the electric machine is not capable of providing the demanded power and torque. [151]

3.2.2.2.9 E-Creeping

Limited pure EV performance to support vehicle stop and go, long low-speed motions during traffic jams, and parking maneuvers. [152], [153]

3.2.2.2.10 E-Boost

Additional transient torque and power, including the electric machine and the internal combustion engine torque and power, will improve the vehicle's maximum output power, acceleration, and maximum speed. [154]

3.2.2.2.11 E-Burning

In architectures with two or more electric machines, one machine operates as a generator, and the other servers as a motor, operating very inefficiently, with the purpose of burning electric power during regen (to avoid battery over-voltage) or to generate heat to warm-up the propulsion system in cold weather.

3.2.2.2.12 Torque Vectoring

When to electric motors are on the same driving axle and powering different wheels, additional torque (positive or negative) is applied to the wheels when the torque domain controller identifies that the vehicle is not following its intended path. [154]

Table 3.2: Secondary Operational Modes of an Electrified Propulsion Systems

	Benefits				
Mode	**Fuel Economy**	**Drivability**	**Comfort**	**Safety**	**Performance**
One Pedal Driving	X	X	X		
Power Split	X		X	X	
e-Smoothing		X	X		X
Cold Cranking			X		
e-Coasting or e-Sailing	X		X		
Advanced Start-Stop	X	X			
e-Launch	X	X	X		
ZEV Mode		X	X		
e-Creeping			X		
e-Boost					X
e-Burning		X		X	
Torque Vectoring				X	X

3.2.3 Types of Electrified Propulsion Systems

The classification of electrified vehicles can be grouped by the different degrees of electrification: micro-hybrid electric vehicle (mHEV), mild-hybrid electric vehicle (MHEV), full hybrid electric vehicle (HEV), plug-in hybrid electric vehicle (PHEV), range extender electric vehicle (REEV) and pure electric vehicle (EV) [91].

Table 3.3 presents a summary comparing the different degrees of electrification according to the operational modes and fuel economy.

Table 3.3: Comparison of different electrification levels and vehicle applications

	mHEV	**MHEV**	**HEV**	**PHEV**	**REV**	**BEV**
(SS)	+	+	-	-	NA	NA
(TA)	+/-	+	++	++	NA	NA
(RB)	+/-	+	++	++	++	++
(PE)	-	-	+/-	+	++	+++
Plug-in	-	-	-	+	+	++
FE	2-5% [8]	Up to 20%[8]	20-50% [8]	35-80% [155], [156]	>70% [157]	100% [8]
Vehicle Application	Peugeot 208 eHDi [158], Fiat Panda [159],	Jeep Wrangler [160], Mercedes-AMG GLE 53 [161]	Toyota Prius [162], Peugeot 3008 [163]	Pacifica Hybrid [164], BMW X5 [165]	GM Volt [166], BMW i3 [167]	Jaguar iPace [168] Audi eTron [169]

3.2.3.1 Micro-Hybrid Electric Vehicles (mHEV)

The micro-hybrid systems, also named start-stop systems, have the lowest degree of electrification, where the vehicle is propelled only by the ICE, and a small electric machine can be used to recover a small amount of energy through regenerative braking [91]. The integrated starter generators (ISG) and belt alternator starters (BAS) are the forms in which the micro-hybrid system can work in the propulsion system. The operational modes associated with the mHEV vehicles are the start-stop (SS), regenerative braking (RB), and generator mode (GM).

The electric power installed is in most of the cases between 3-5kW and improves between 2%-5% of fuel economy when compared with the base vehicle equipped only with an ICE. [91]

3.2.3.2 Mild Hybrid Electric Vehicles (MHEV)

The mild-hybrid vehicles are the next level of electrification. In addition to the SS and RB functions, the torque assist (TA) capability is the additional operational mode with the MHEV [91]. However, the electric machine alone is not capable of propelling the vehicle [124]. The ICE is the primary source of the power unit, and the electric machine provides power assist to the ICE to improve the specific fuel consumption of the engine, improving the overall efficiency of the system [125]. In MHEV, the fuel economy can improve by up to 20% [114], and in general, the DC voltage of the system is under 60V, and the installed electric power is between 7-15kW [91].

3.2.3.3 Full Hybrid Electric Vehicles (HEV)

The full hybrid propulsion system has the highest degree of electrification compared with the micro and mild hybrid vehicles. The total electric power installed is 30kW or more. In the full hybrid systems, both the ICE and the EM can provide enough torque and power to move the vehicle alone. In general, according to data extracted from [170], full hybrid vehicles have a high voltage electric system (>60V) and can improve the fuel economy by 40% or more in urban driving conditions, such as an FTP 75 cycle.

3.2.3.4 Plug-in Hybrid Electric Vehicles (PHEV)

The plug-in hybrid electric vehicle is an HEV in terms of performance and hybrid capability; however, with a larger battery and with the capacity to have the battery charged by an external source, i.e., by plugging the vehicle into the power grid [8] A PHEV can improve the fuel economy by between 40-60% when compared with a conventional vehicle. The total electric power of a PHEV is the same as that of a full HEV, with a major 30kW, depending on the vehicle size. In a PHEV, the engine is also fully capable of powering the vehicle to meet all required performances [170].

3.2.3.5 Range Extender Electric Vehicle (REEV)

The REEV is a type of PHEV; however, the REEV is better defined as an electric vehicle with an extended range capability. A small engine, in combination with an electric machine operating as a generator, is installed to charge the high-voltage battery, increasing the electric range of the vehicle [8].

In the REEV, the traditional operational modes are not present, and the vehicle is propelled only by electric machines. The total electrical power available should be enough to guarantee the full performance of the vehicle. In REEVs, the operational modes available are pure electric (PE), RB, and GM.

3.2.3.6 Pure Electric Vehicle (PEV)

The PEV, also named battery electric vehicle (BEV), uses electrical power as the only source of motion to propel the vehicle. In this case, the hybridization factor has a maximum value equal to 1. In a PEV, only PE and RB operational modes are present. Considering only the tank-to-wheel concept, the PEV operates at zero-emission, and the electrification factor reaches 100% when compared to an ICE vehicle, as it is only propelled by the electric machine [8], [136].

3.3 Electrified Propulsion System Architectures

The electrified propulsion system's performance depends not only on the size of the components that form the subsystems but also on the system layout or powertrain architecture and the type of operation of the architecture. The powertrain architecture and operation will impact the system's energy efficiency and the performance of the primary and secondary operational modes.

The number of EMs in the architecture, the location where the EMs are in the drivetrain, how they are connected via transmission devices from input to output, and whether it operates in series, parallel, or series-parallel mode, are all critical factors that determine the performance and operation of the electrified propulsion system. The better choice of the architecture of a given product or a basket of products should be the one that provides better trade-offs for the specified functional objectives, which are driven by customers' desires, business, and regulatory requirements.

This section aims to review the possible propulsion system architectures and operations, whether it is a single-electric machine architecture or a multi-electric machine solution. It will give a definition and classification of the different electrified propulsion architectures following the electric machine positions.

3.3.1 Hybrid Propulsion System Operation

3.3.1.1 Series Hybrid

The vehicle is propelled by a traction electric machine, while a generator group, composed of an ICE and an EM, generates the electrical power that feeds the primary traction machine.

The series hybrid operates in six different operational modes: (1) The traction electric machine provides torque to the wheels using only power from a battery (PEV), (2) the electric traction machine provides torque to the wheels using power from a battery, and the generator group (SHEV-1), (3) the traction electric machine provides torque to the wheels using power only from the generator group (SHEV-2), (4) the traction electric machine provides torque to the wheels using power exclusively from the generator group and the exciding power charges the battery (SHEV-3), (5) regenerative braking (RB-1), and (6) the generator group only charges the battery while the vehicle is not moving, or while braking or coasting (CH). Vehicle examples of a series hybrid are the BMWi3 extended range and the Karman Fisker [171], [172]

3.3.1.2 Parallel Hybrid

The traction electric machine and the internal combustion engine can provide torque to the wheels together or separately, and it is preferable to have another electric machine primarily working as a generator be positioned on the drivetrain in a way that the engine can charge the battery in any drive condition [124].

The parallel hybrid architecture has mainly four operational modes depending on the electrification level: (1) ICE provides torque to the wheel (ICE), (2) the traction electric machine provides torque to the wheel (PEV), (3) the ICE and the traction electric machine give torque to the wheel (HEV), and (4) regenerative braking (RB-2)[114]. Examples of parallel hybrids are the Land Rover Range Rover P400e, the Lincoln Aviator, and the BMW X5 530e [173]–[175].

3.3.1.3 Series-Parallel Hybrid

A series-parallel hybrid, as the name says, is a combination of the series and the parallel hybrid, and as [97] presented, the series-parallel hybrid architecture can also be seen as a blend of two basic parallel architectures.

This type of hybrid can operate either in a parallel mode when the EM and the ICE work together or individually when providing torque and power to the vehicle, or in series mode when one EM provides torque to the wheel while the ICE and the second EM are working as a generator unit to generate electric power [124]. The series-parallel architectures are also "more flexible" and controllable in the ratio of power distribution, operation modes, and propulsion system architecture [97]. Examples of parallel hybrids are the Hyundai Ionic, the Kia Niro, and the Jeep Compass [176]–[178].

3.3.2 Single Electric Machine Architectures - SMA

A common practice in the automotive industry is to name the architecture type by the position of the electric machine in the system. The possible places for the electric machine are P0 or P1f, P1 or P1r, P2, P3, and P4.

3.3.2.1 Position P1f or P0

The EM is connected to the crankshaft of the ICE as part of the front engine accessory drive (FEAD) belt. At this position, the electric machine can be disconnected from the transmission [179]. The minimum pulley ratio between the electric machine and the crankshaft pulleys is defined according to the electric machine torque and the engine crank peak torque. In contrast, the maximum pulley ratio is set such that the EM top speed matches the top ICE speed. The ideal pulley ratio should be selected at this interval and designed to maximize the fuel economy. A typical layout of the P0 architecture is presented in Figure 3.5.

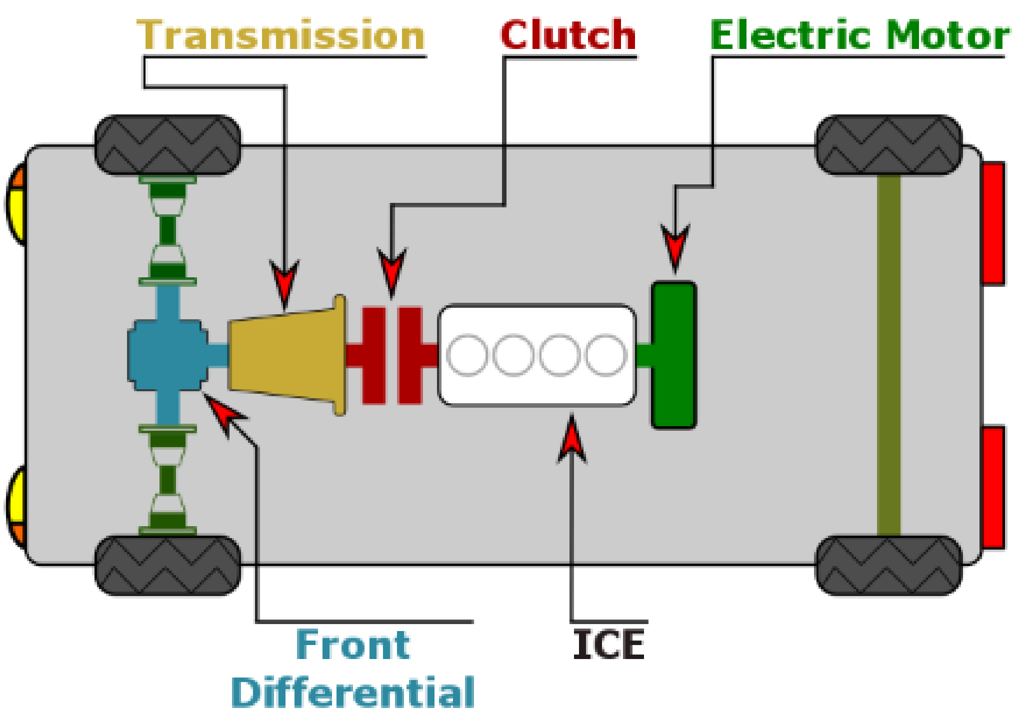

Figure 3.5: Electrified Propulsion System Single Machine Architectures - P1f or P0.

3.3.2.2 Position P1 or P1r

The EM is connected to the engine flywheel and has two mounting possibilities - coaxial with the crankshaft, which means that the Speed of the electric machine will always be the same as the ICE or geared to the engine flywheel with a specific gear ratio. At this position, the electric machine can be disconnected from the transmission. The minimum and maximum gear ratios are defined based on the same principles as in the P0 architecture. The ideal gear ratio is limited to this interval to maximize the fuel economy [180]. A typical layout of the P1 architecture is presented in Figure 3.6.

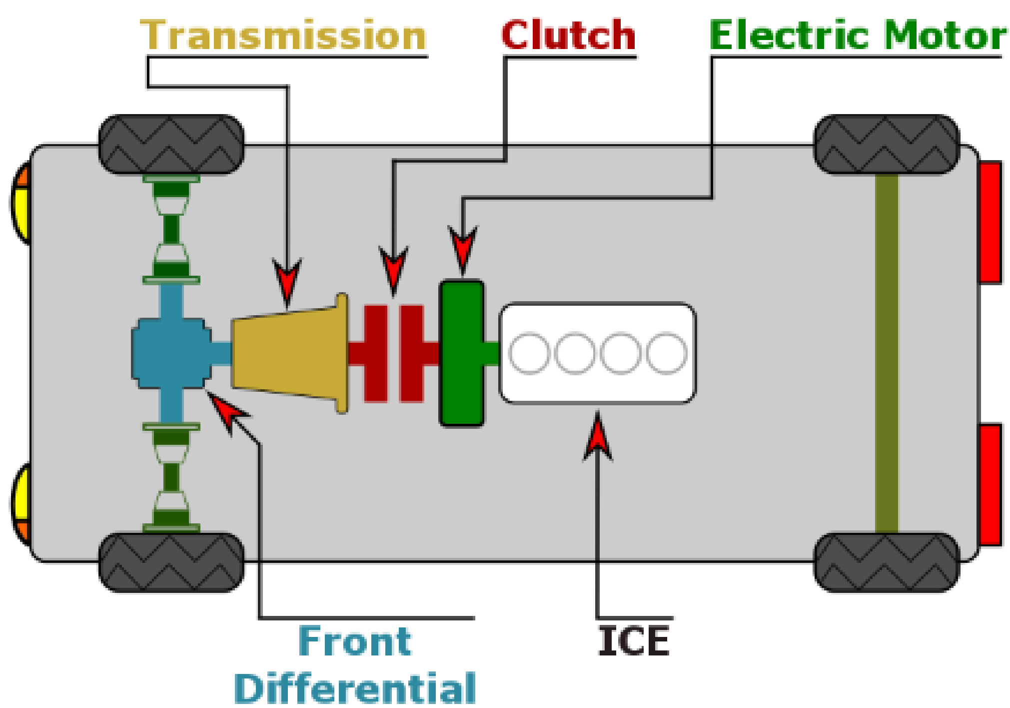

Figure 3.6: Electrified Propulsion System Single Machine Architectures - P1r or P1.

3.3.2.3 Position P2

The EM is coupled to the transmission and can be completely decoupled from the engine; as illustrated in the torque path of the drivetrain, the EM is positioned "after" the clutch or torque converter. In this configuration, the electric machine can be placed in different forms: coaxial to the primary transmission shaft or geared to the primary transmission shaft. In the case of a DCT transmission, the electric machine can be coaxial or geared but is connected to only one of the primary shafts, i.e., either the odd or the even shaft. In the case of a geared machine, the top Gear will be calculated for the maximum required Speed of the electric machine such that it is not higher than the maximum engine speed when the transmission is engaged in the lowest possible Gear [181]. A typical layout of the P2 architecture is presented in Figure 3.7.

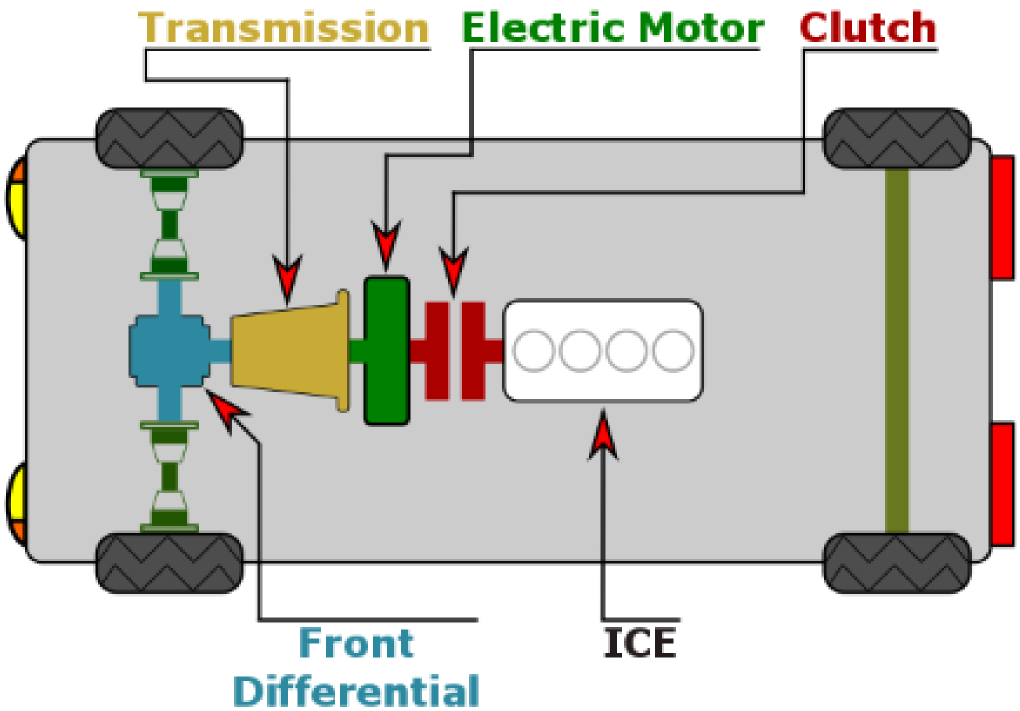

Figure 3.7: Electrified Propulsion System Single Machine Architectures - P2.

3.3.2.4 Position P3

The EM is positioned on the secondary axle of the transmission or the transfer case – in AWD applications. In this case, the electric machine can be disconnected from the ground only if a clutch is included in the torque path. In a P3, the EM is subjected exclusively to the speed reduction of the differential. There is the option to connect the electric machine using a coaxial or geared approach. For the P3 architecture, the optimum solution will be designed to maximize the fuel economy. However, if a clutch is not present at the torque path, the EM maximum speed should be above the maximum vehicle speed [181]. A typical layout of the P3 architecture is presented in Figure 3.8.

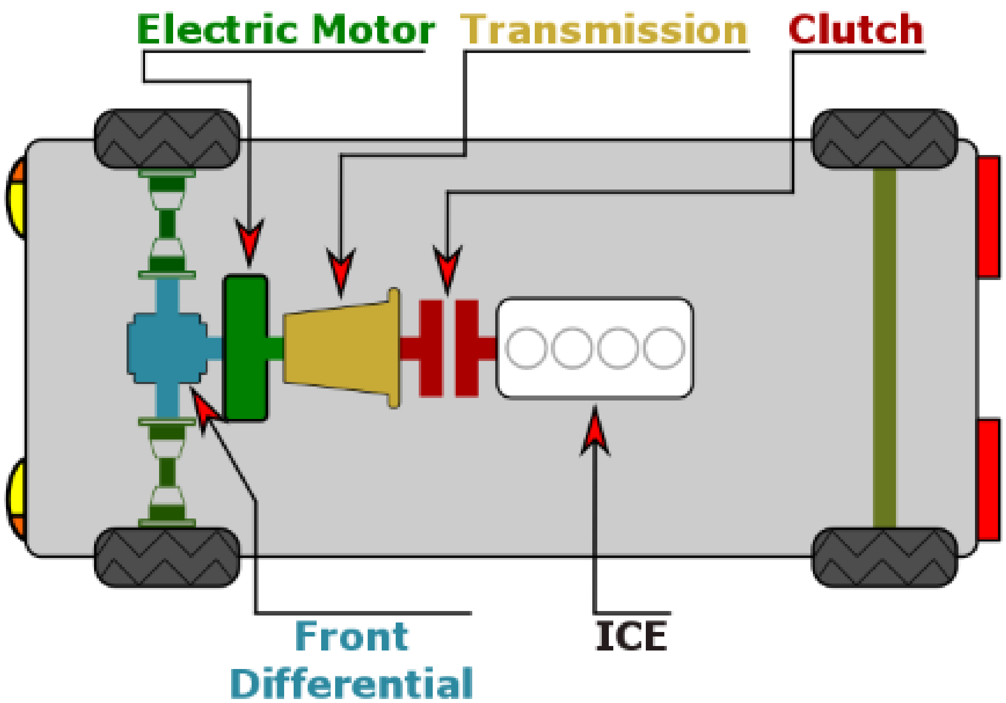

Figure 3.8: Electrified Propulsion System Single Machine Architectures - P3.

3.3.2.5 Position P4:

The EM is connected to the wheels directly by a dedicated gearbox with a gear ratio and differential. The gearbox can be an off-set type – set of helical gears with a primary and secondary shaft or a coaxial type - set of planetary gears. In this position, differently from the other possible locations - where the electric machine is installed in the engine or the drivetrain subsystem - the P4 electric machine is on a primary drive axle by itself. The P4 power unit can be single Gear or multi-gear, and it is also possible to use a disconnected element such as a dry clutch [182]. A typical layout of the P4 architecture is presented in Figure 3.9.

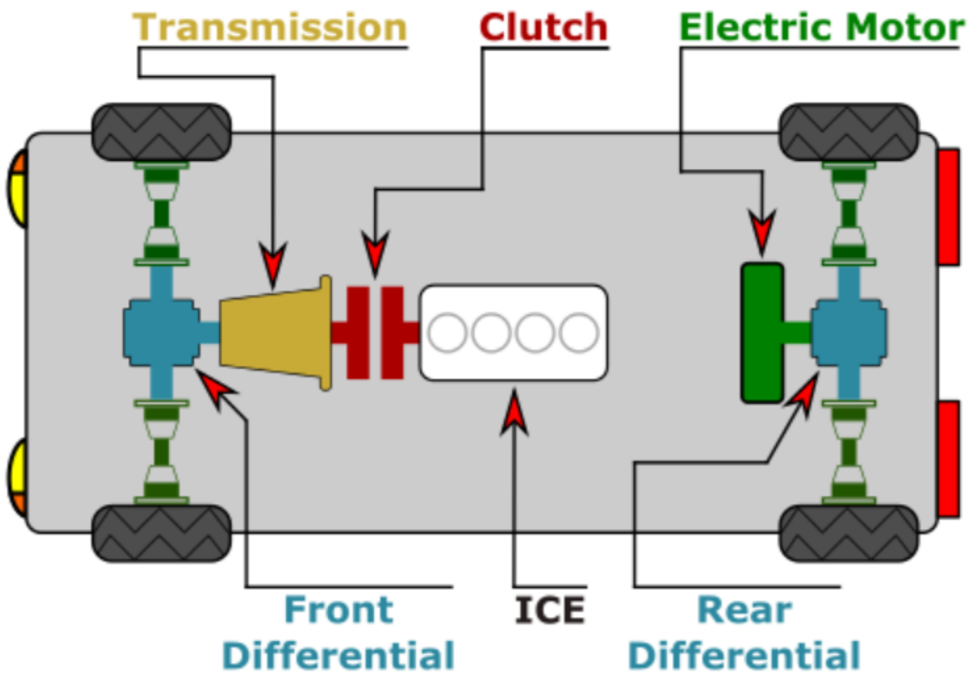

Figure 3.9: Electrified Propulsion System Single Machine Architectures - P4.

3.3.2.6 Operational Modes and Electrification Degree for SMA

Sections 3.2.2.1 and 3.2.2.2 define the operational mode of the electrified propulsion system as primary and secondary operational modes, respectively, and provide an overview of how each operational mode affects the different performances of the vehicle. This section provides all possible locations for the EM in single-motor propulsion architectures and gives its definitions. However, not all operational modes are available for all possible EM positions. Table 3.4 and Table 3.5 show, respectively, the primary and secondary operational mode's applicability for each EM position in a single motor electrified propulsion system architecture.

Table 3.4: Availability of Primary Operational Modes in SMA

	P0	P1	P2	P3	P4
Torque Assist (TA)	X	X	X	X	X
Regenerative Braking (RB)	X	X	X	X	X
Generator Mode (GM)	X	X			
Start-Stop (ESS)	X	X	X		
Pure Electric (PEV)			X	X	X

Table 3.5: Availability of Secondary Operational Modes in SMA

	P0	P1	P2	P3	P4
One Pedal Driving	X	X	X	X	X
e-Smoothing			X	X	X
Cold Cranking	X	X			
Advanced Start-Stop	X	X			
e-Motoring			X	X	X
e-Launch		X	X	X	X
e-Parking		X	X	X	X
e-Creeping		X	X	X	X
e-Boost	X	X	X	X	X
Torque Vectoring				X	X

Table 3.6 shows the electrification degrees for each possible EM positions is SMA architecture.

Table 3.6: Electrification Degree as a function of EM position on SMA architectures

	P0	P1	P2	P3	P4
mHEV	X	X			
MHEV	X	X	X	X	
HEV		X	X	X	X
PHEV					
REV					
BEV					X

3.3.3 Multi Electric Machine Architectures - MMA

Combining at least two electric machines is essential to build an electrified propulsion system capable of operating in a series, parallel, or series/parallel hybrid. It also enables a pure AWD electric vehicle, which is especially important to reduce the complexity of underfloor packaging and create more space for battery packaging and vehicle architecture sharing between pure electric and hybrid vehicles.

Another advantage of utilizing the dual-motor architecture is the ability to perform a fast warmup of the catalysts, reducing emissions during the cold phases of the homologation cycles.

3.3.3.1 MMA Architectures EM Positions

Usually, multi-electric machine propulsion systems are developed with two or three electric motors, deriving from the SMA architectures with the following EM positions: P0, P1, P2, P3, and P4.

Variations of the MMA architectures are presented in the following sections.

3.3.3.1.1 MMA Architectures derived from P0

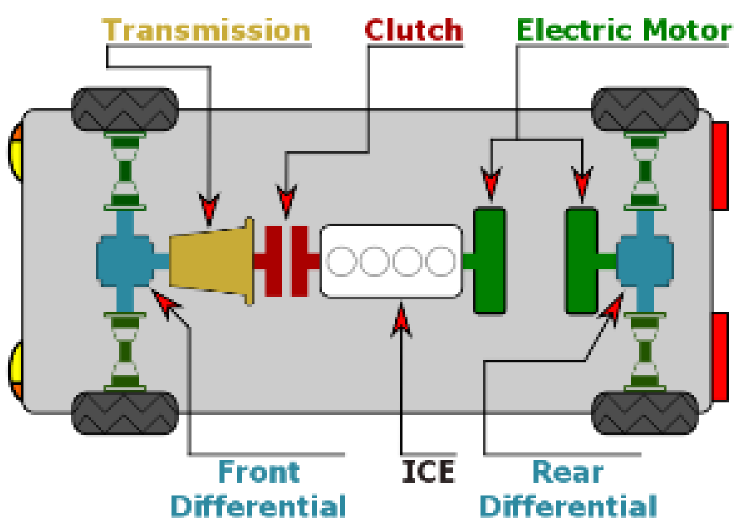

Figure 3.10: P0P4 MMA Architecture

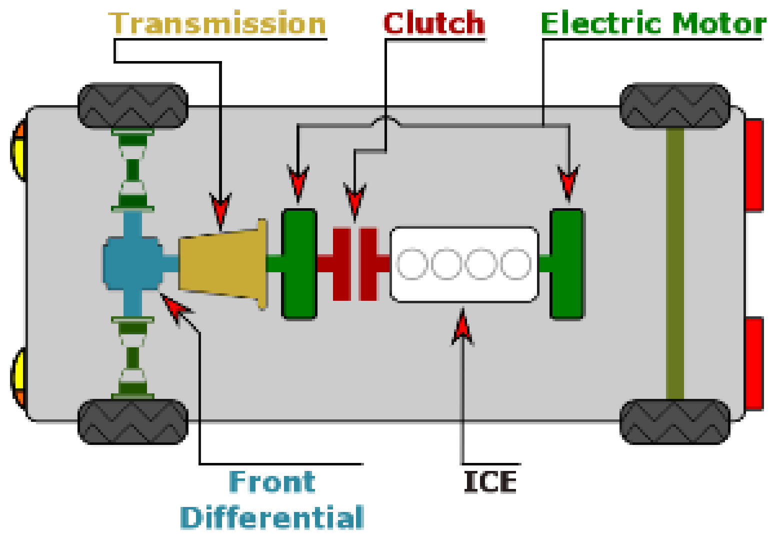

Figure 3.11: P0P2 MMA Architecture.

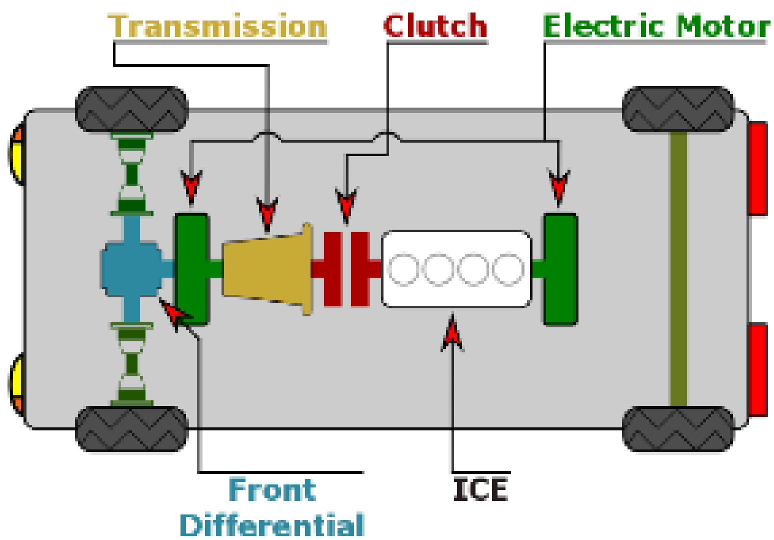

Figure 3.12: P0P3 MMA Architecture.

3.3.3.1.2 MMA Architectures derived from P1

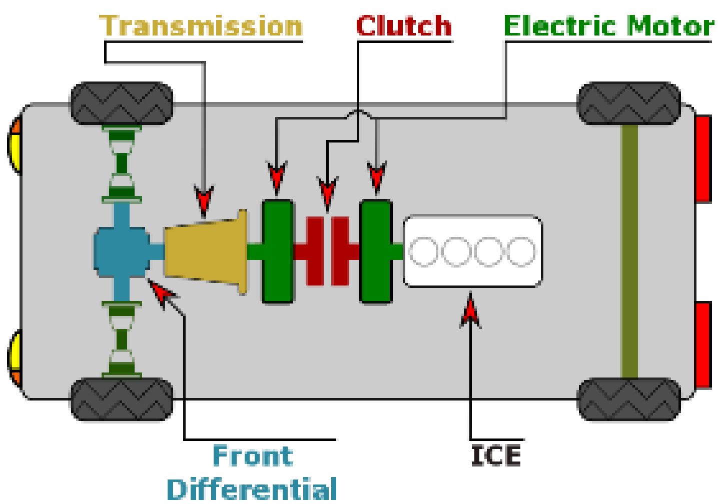

Figure 3.13: P1P2 MMA Architecture.

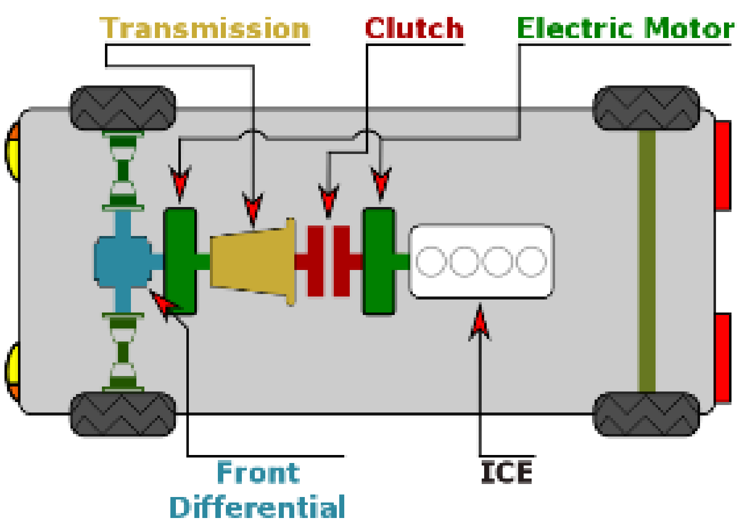

Figure 3.14: P1P3 MMA Architecture.

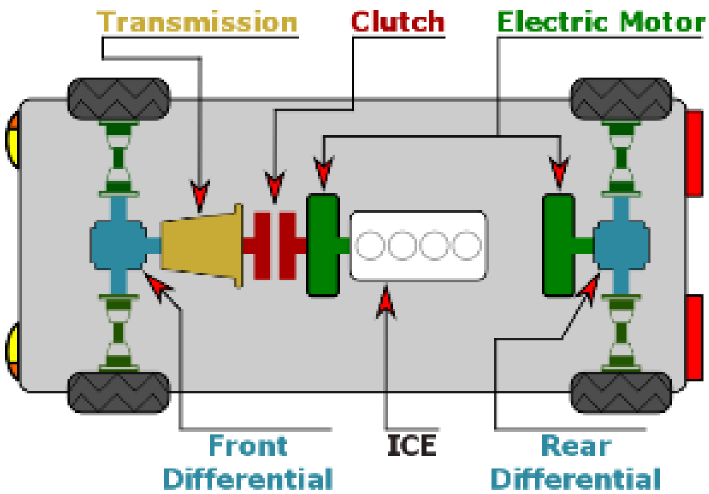

Figure 3.15: P1P4 MMA Architecture.

3.3.3.1.3 MMA Architectures derived from P2

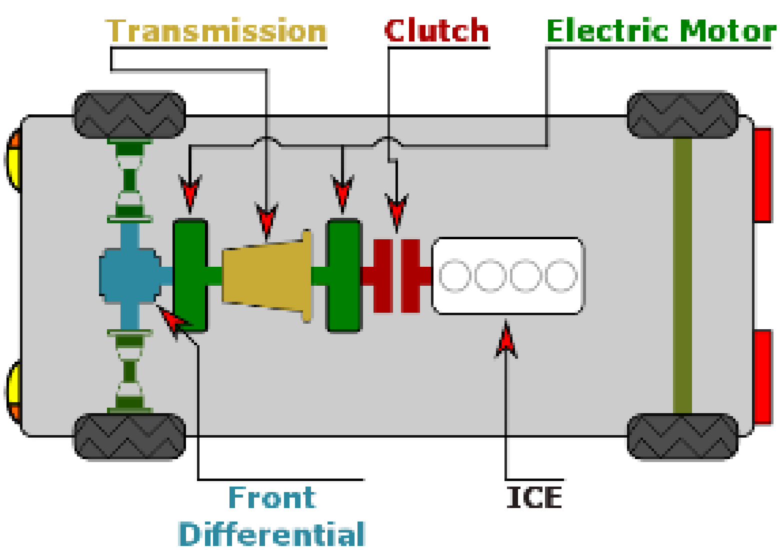

Figure 3.16: P1P4 MMA Architecture.

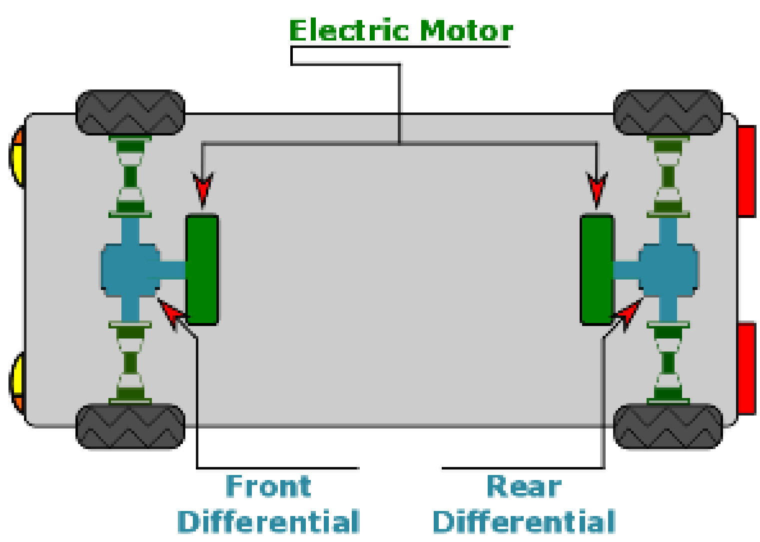

Figure 3.17: P4P4 MMA Architecture.

3.3.3.2 MMA Architectures EM Positions

This section shows the possible locations for the EM in a multi-machine architecture. However, not all operational modes and electrification degrees are viable for all possible configurations.

Table 3.7 and Table 3.8 show, respectively, the applicability of the primary and secondary operational modes for each EM position in MMA architectures. Table 3.9 shows the electrification degrees for each possible EM position in SMA architectures.

Table 3.7: Availability of Primary Operational Modes in MMA Architectures

Operation Modes	P0P4	P1P4	P0P2	P1P2	P0P3	P1P3	P2P3
Start-Stop (ESS)	X	X	X	X	X	X	X
Torque Assist (TA)	X	X	X	X	X	X	X
Regenerative Braking (RB)	X	X	X	X	X	X	X
Generator Mode (GM)	X	X	X	X	X	X	X
Pure Electric Mode (PEV)	X	X	X	X	X	X	X

Table 3.8: Availability of Secondary Operational Modes in MMA Architectures

	P0P4	P1P4	P0P2	P1P2	P0P3	P1P3	P2P3
One Pedal Driving	X	X	X	X	X	X	X
e-Smoothing	X	X	X	X	X	X	X
Cold Cranking	X	X	X	X	X	X	
Advanced Start-Stop	X	X	X	X	X	X	X
e-Motoring	X	X	X	X	X	X	X
e-Launch	X	X	X	X	X	X	X
e-Parking	X	X	X	X	X	X	X
e-Creeping	X	X	X	X	X	X	X
e-Boost	X	X	X	X	X	X	X
Torque Vectoring	X	X					

Table 3.9: Electrification Degree as a function of EM position on MMA architectures

	P0P4	P1P4	P0P2	P1P2	P0P3	P1P3	P2P3	P4P4
mHEV								
MHEV								
HEV	X	X	X	X	X	X	X	
PHEV	X	X	X	X	X	X	X	X
REV		X				X	X	
BEV								X

3.3.4 Advanced System Architectures

Various advanced electrified propulsion systems can be configured by utilizing dual machines combined with multiple planetary gear sets or clutches. For instance, Toyota Prius implements two electric machines and two planetary gear sets to enable the power split configuration [114], [183].

General Motors developed the two-mode hybrid system with two electric machines, three planetary gear sets, and four clutches [184]. FCA used a planetary gear set combined with a one-way clutch to form the single-input electronic variable transaxle (SI-EVT) [185].

These advanced powertrains adjust the planetary gear set ratios to split the power between the engine and electric machines, and clutches and brakes are used to change the operational modes. They are all variants of a P2P3 configuration. Enhanced fuel economy and performance can be achieved throughout a wide range of vehicle speeds. Detailed analysis of these advanced electrified propulsion systems can be found in [183] [184], and Figure 3.18 illustrates their architectures.

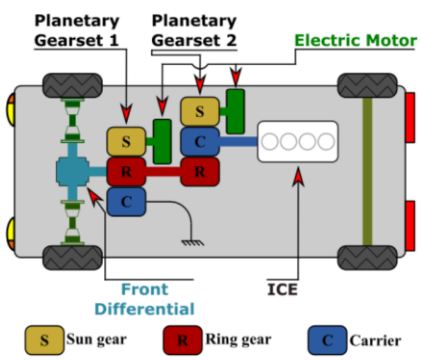

(a) Toyota Prius power-split architecture

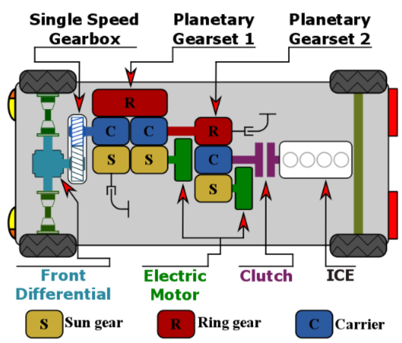

(b) Toyota Highlander Hybrid architecture using Ravigneaux gear

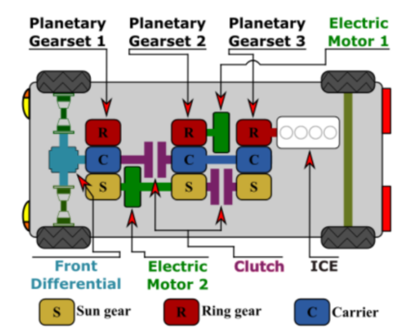

(c) GM two-mode architecture

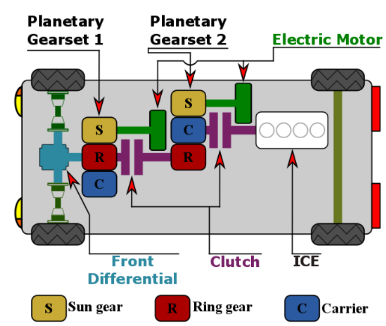

(d) FCA SI-EVT architecture

Figure 3.18. Advanced electrified propulsion architectures

3.4 Propulsion System Architecture Selection

The selection of the most appropriate propulsion system architecture is an interactive process made of multiple trade-off analyses using requirements and constraints as inputs with detailed study to feed a decision matrix that is used to compare the different architectures against the functional objectives [186].

These requirements and constraints can be internal or external to the environment of the project and are established to reflect the business and market goals, which are translated into functional objectives. The functional objectives define what the electrified propulsion system should do and how well the system should perform.

Examples of functional objectives are the vehicle acceleration time, the vehicle top speed, the vehicle fuel economy, and the ability of the vehicle to launch on grade or full electric range and capacity to be charged from an external power source [187].

On the other hand, the design constraints define the barriers that the system design and operation cannot cross for different reasons. The constraints of a propulsion system design are an essential input to reduce the options of architecture in the design space, eliminating those that cross the boundaries of the constraints.

Examples of design constraints are the nature of the vehicle traction axle – (FWD, AWD, or RWD), the selection of required operational modes, and constraints that the vehicle architecture might implement to the design of the propulsion system, such as available space claim for packaging.

Figure 3.19 shows a summary of a propulsion system architecture selection process.

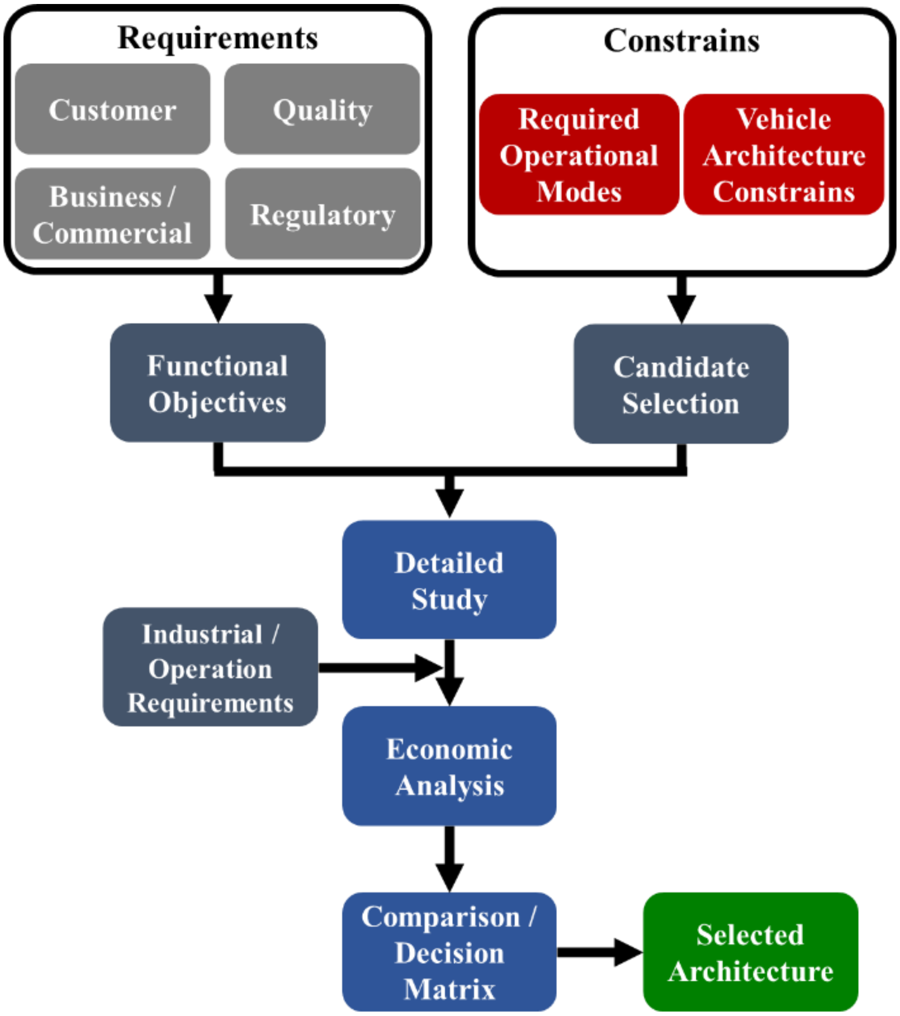

Figure 3.19: Electrified Propulsion Architecture selection process.

With the functional objectives and the design space wholly defined, the candidates are then studied in detail. In this phase, virtual models of each of the candidates are developed. The performance and fuel economy of each candidate are calculated in an interactive looping of system simulation and component sizing to optimize the ideal size of each of the components that are part of the propulsion system, and that closely meets the functional objectives. In parallel, a bill of material, BOM, for each studied architecture is defined, and macro packaging feasibility is performed for all the intended vehicles to receive the electrified propulsion system under development.

The industrial and operational constraints represent barriers to the manufacturing and assembly process and also include logistics challenges and limitations of the supply chain. In this stage, DFM (Design for Manufacturing) and DFA (Design for Assembly) are assessed to guarantee the architecture candidates can be designed to be efficiently and economically manufactured [188]. These constraints are used to feed the economic analysis and, in some cases, to identify hard constraints for some of the candidates, reducing the size of the design space even more.

The Economic Analysis includes the valuation of the system BOM and the efforts and investments to develop and manufacture the system. The metrics evaluated in this phase are the DMC – direct material cost, the EDD – engineering and development cost, and the CAPEX – capital expenditure, which is necessary to manufacture the components and assemble the subsystem and the system Economic Analysis.

The results of the detailed studies and the economic analysis are listed in a table called the decision matrix. This table is a multi-dimensional matrix used to compare all the candidates against the initial requirements to make a recommendation for the best architecture candidate to meet all the program targets.

Table 3.10, Table 3.11, and Table 3.12 show, respectively, the examples of FE and Emissions, economics, and performance comparison matrixes. Those tables can be used as a starting point to evaluate the selection and application of an electrified propulsion system for a certain vehicle or a group of vehicles, and they will vary depending on the market region or type of vehicle.

Table 3.10: fuel consumption, electric range, and emissions comparison.

Functional Objective				Target	Arch 1	Arch 2
FE and Emissions	EPA (USA - North America)	EPA Combined Label	[Mpg]			
		EPA Combined Label	[Mpge]			
		All Electric Combined Range	[mi]			
		EPA Combine CAFÉ	[Mpg/Mpge]			
		EPA Unadjusted Combined CO2	[g/mi]			

Table 3.11: Cost and investment comparison.

Functional Objective				Target	Arch 1	Arch 2
Economics	DMC	Direct Material Cost	[$]			
	EDD	Engineering and Development	[$]			
	CAPEX	Investment in Capital for manufacturing	[$]			

Table 3.12: Performance comparison.

Functional Objective				Target	Arch 1	Arch 2
Performance	Acceleration maneuver	0-50 km/h	[s]			
		0-100 km/h	[s]			
		0-max Speed	[s]			
	Passing maneuver	60-100 km/h	[s]			
		80-120 km/h	[s]			
	Maximum Speed	30 minutes continuous	[km/h]			
	Max Launch on Grade (forward)		[%]			
	Max Launch on Grade (rewards)		[%]			
	Davis Dam Max Speed	6% grade constant Speed	[km/h]			
	Towing Capability	max towing	[kg]			

3.5 Summary

The electrification of the propulsion system is mandatory to meet all the stringent compliance requirements. It not only allows the improvement in fuel economy and CO2 emission but can also help to improve vehicle drivability, comfort, and safety. Each propulsion system architecture provides a different balance between the various performances.

This chapter reviews the core components of electrified powertrains and the state-of-the-art technologies for each subsystem. To help the architecture selection process, the electrified propulsion systems are classified based on the electrification degree, types of electrified powertrains, and the operational modes, where primary and secondary operational modes are proposed. According to the number and position of electric machines, various architectures of electrified propulsion systems and their functions are presented in terms of their impact on vehicle performance and fuel economy. The selection of the most appropriate electrified propulsion system is a multidisciplinary interaction process where technical and business requirements should be taken into consideration.

Chapter 4

Electric Vehicle Modelling

The need for propulsion system electrification is increasing globally due to urban restrictions on conventional vehicles and potential bans by 2030-2040. CO2 emission regulations are prevalent in major automotive markets. UK studies indicate lower ownership costs for Electric vehicles than fossil fuel-powered vehicles. With mature lithium-ion battery technology and cost in Europe, 60% of new road vehicles could be electrified by 2030, potentially reaching 100% in the small vehicle segments (A and B segments). [7], [189]–[192] The current scenario of market and regulation in all the important automotive markets is building the bridge to an electrified future, as indicated in Chapter 2.

The wide range of road vehicles, including buses, trucks, light commercial vehicles, and passenger vehicles, each with distinct segments and performance needs [7], demands a system design optimization, which focuses on adequately sizing the propulsion system design [97].

Chapter 3 indicates various architecture configurations for electrified propulsion systems, with different degrees of electrification and electric machine quantities. Vehicle performance and energy efficiency rely on the collaboration of multiple subsystems. The vehicle's capabilities hinge on the number of driving axles, electric motors, battery energy and power, and the coordination of power electronics for synchronizing multiple power units simultaneously. Consequently, electrified vehicles are highly intricate systems [8], [9].

Figure 4.1 shows the interaction of different subsystems to perform the propulsion system functions.

Chapter 3 also indicates the need for virtual models capable of simulating multiple scenarios of what-if analysis and optimizations to determine the ideal propulsion system architecture candidates and to size the subsystem of the propulsion system.

Figure 4.1: Propulsion System and the Subsystems interconnections.

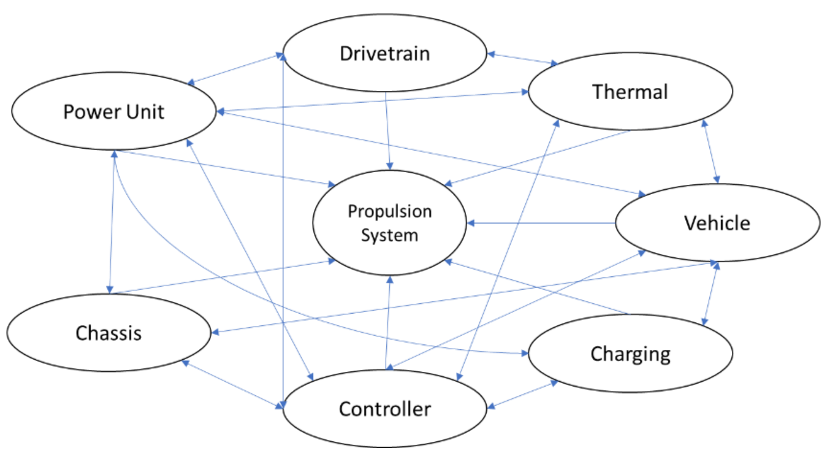

Bureaucratic and hierarchical organizations pose challenges to developing optimal electrified propulsion system architectures and their subsystems and components [193], [194]. These organizations heavily rely on human interactions for information flow and knowledge sharing, which limits the exploration of what-if scenarios and tradeoff studies. With hundreds of design possibilities, depending solely on the experience of a few engineers, it is insufficient to find optimized solutions.

The transition to large-scale production of electrified vehicles represents a paradigm shift in the transportation industry, requiring knowledge development and collaboration among OEMs and the supply chain [195], [196]. These factors affect design quality, cost optimization, and decision-making processes, which lack system simulations to assess performance impacts and accommodate late design changes throughout the product development cycle. [197]

Studies show that 85% of product costs are determined during the initial design concept phases, including architecture selection, component sizing, and supplier choices. [198]

The adoption of a model-centric approach, since the early stages of the development, allows the application of a continuous loop of design-build-test-optimize in a virtual environment, performing many different design tradeoffs within the propulsion system boundaries and across the propulsion system boundaries, creating a multidisciplinary virtual domain. This process can occur from the beginning to the end of the development cycle.

A model-centric approach enables continuous design optimization within the boundaries of the propulsion system, extending to a multidisciplinary virtual domain. This approach spans from translating requirements into targets to freezing component designs for manufacturing and production, covering the entire development cycle. In 2007, authors highlighted the need for tools to model electric and hybrid vehicles, including embedded software and vehicle details. [199]

While market tools now support performance and fuel economy analysis, integration of these tools and methods for a model-centric development approach remains lacking.

This Chapter reviews a model-based engineering approach and an electric vehicle model. The Chapter also verifies the correlation of the model results with physical results, available at [200]. The chapter demonstrates the dynamic responsiveness of the model, ensuring reliable results for design choices and energy efficiency assessment, as well as software and control calibration of various subsystems.

4.1 Model-Based Design Engineering

4.1.1 Model-Based Design Engineering

Models are a very unexpansive tool for investigating the many details of a system with all the subsystems and components, capturing complexities at many different levels of design complexity, and hiding or exposing details and complexities as needed. Executable models, at any level of sophistication, allow to perform tradeoffs and what-if analysis at any stage of product development and permit the execution of verifications and validations of the design in the initial stages of the development, fully or partially virtual, reducing the risk and the cost of changes. There are multiple levels of modeling complexity and techniques. The choice of the modeling method and the level of complexity will depend on the end goal of the model simulation [201].

Different types of models are used based on the desired outcomes. Models can be classified according to the number of dimensions employed. Some models focus solely on the time domain without spatial consideration (0D), while others incorporate spatial dimensions alongside time (1D). Additionally, 2D and 3D models encompass two or three spatial dimensions (X, Y, Z), and 4D models account for all three spatial dimensions in the time domain. 1D simulations are particularly effective in representing complex systems and capturing interactions between various subsystems and components [202].

Model-based design engineering (MDB) is a method that focuses on developing controls, signal processing, dynamics systems, and communication in a model-centric manner. It proves most effective when applied to complex systems like aircraft or electrified propulsion systems. MDB facilitates information sharing and serves as a workspace for the engineering team. Design decisions and changes are captured through modifications in the model, which then propagate to other models. By utilizing knowledge-based engineering processes, these modifications ensure that all models reflect the latest information while safeguarding intellectual property and preserving generated knowledge [203].

Models, at any level, are linked with requirements in a way that makes it possible to keep track of design decisions while making sure that the design meets the product criteria. In the MBD approach, the model increases its complexity along the development process, and the complexity can be hidden or exposed, depending on the study's focus [203].

Figure 4.2 shows how the model increases complexity during the V-Cycle development process.

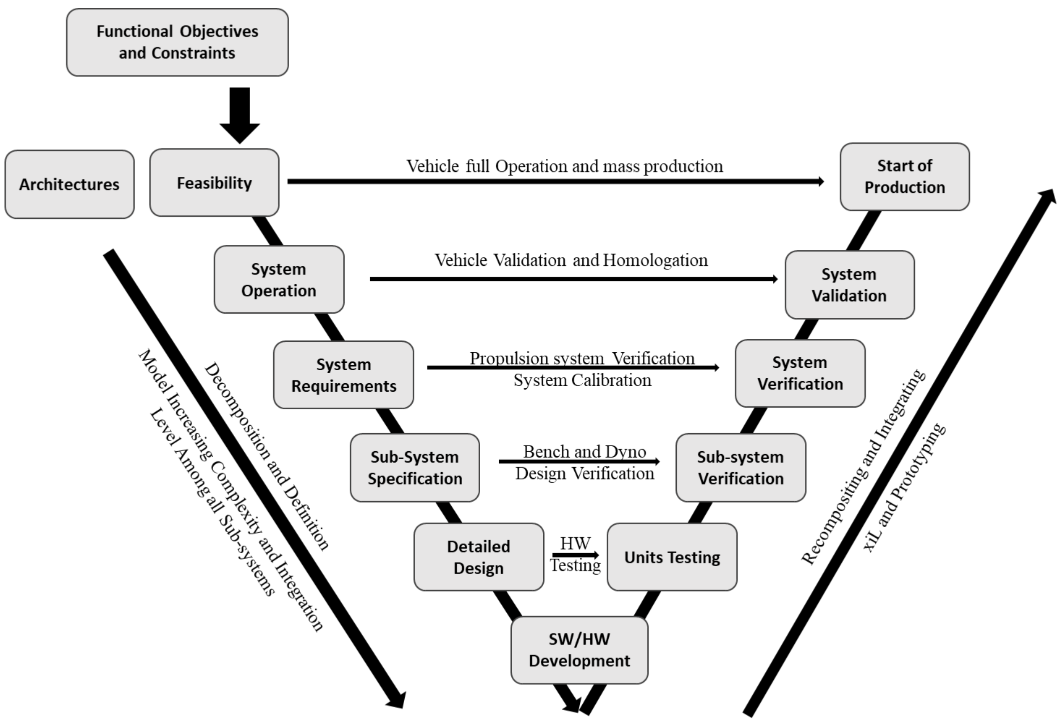

Figure 4.2: Simplified system development approach applied to propulsion system development.

In the MDB approach, the model captures all the design information, such as requirements, test scenarios, and any database with any relevant information, such as efficiency maps and control strategies. The model of the system allows the simulations to check the design and subsystems' performances and define their interactions. During the architecture selection phase, the model provides a very low-cost way of testing ideas and learning about the system; at the same time, tradeoff studies compare the different possible solutions of the design space.

Model elaboration is an interactive process of creating a model from high-level architecture to detailed design. As the model increases its complexity, a virtual prototype, or digital twin of the product, performs a continuous loop of test and verification of the system.

Using scripts and optimization tools, these tests could be automated to perform repetitive tasks, accelerating the development time and improving the issue resolution process. Models are also a way of passing information and knowledge and serve as design documentation.

In MBD, different methodologies utilize models to test and validate systems. Model-in-the-loop (MiL) involves the model representing the system's hardware features, while the controller means the system's logic. In Software-in-the-loop (SIL), the controller logic model is replaced by the actual control code intended for embedding in the physical controller processor. Processor-in-the-loop (PiL) tests the embedded code in the processor itself. Hardware-in-the-loop (HiL) simulation connects a real-time computer to the electronic control unit(s) (ECU) to simulate the plant and validate the controllers using appropriate analog, digital, and CAN signals. Driver-in-the-loop integrates a real driver into a driving simulator to simulate real-world driving conditions [204], [205].

This research uses MiL and DiL.

4.1.2 System Simulation Models

There are two types of system modes techniques for application in MBD, classified according to the speed and torque propagation: Forward-feeding and backward-feeding [206]. The application of each model has a different fit depending on the purpose of the modeling.

The Backward Model, the average operating point or kinematic model, employs driving cycles to input speed and grade, while torque (or force) and speed propagate from the wheel to the propulsion system [207]. This model is commonly used for initial component sizing [208]. However, the backward model is static and cannot capture dynamic effects like rotational inertia, inductance, and thermal propagation. Additionally, it cannot simulate complex electrified propulsion systems. Figure 4.3 illustrates a high-level backward model, while Figure 4.4 demonstrates the propagation of force and speed in a simple electric vehicle.

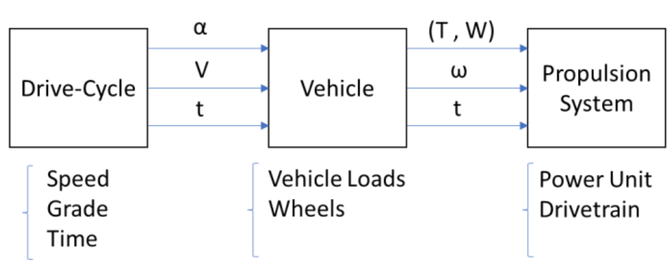

Figure 4.3: Backwards model simulation flow concept.

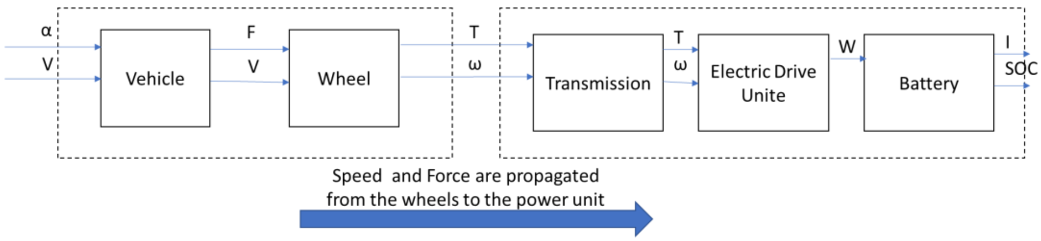

Figure 4.4: Backwards model physical propagation.

The Forward Model utilizes a driver model to compare the desired speed with the actual vehicle speed obtained from the plant model. This model captures dynamic phenomena and incorporates variables that can be measured in the real world. It also requires a supervisory controller model to develop and test control functions of the propulsion system, enabling designers to optimize operations and logic for minimizing energy consumption [209]. Figure 4.5 depicts a high-level system model using the forward approach, while Figure 4.6 illustrates the propagation model within the propulsion system of a basic electric vehicle.

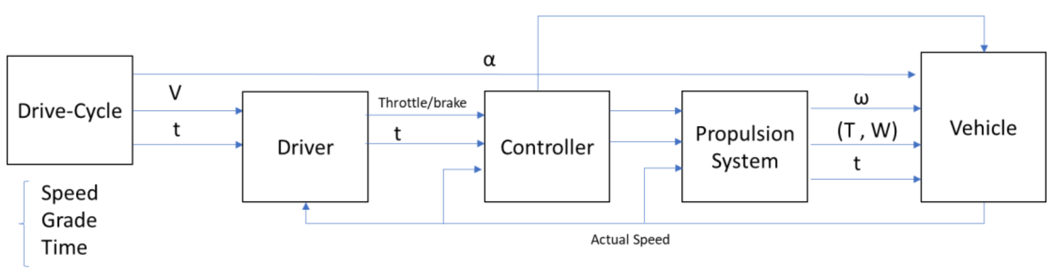

Figure 4.5: Forward model simulation flow concept.

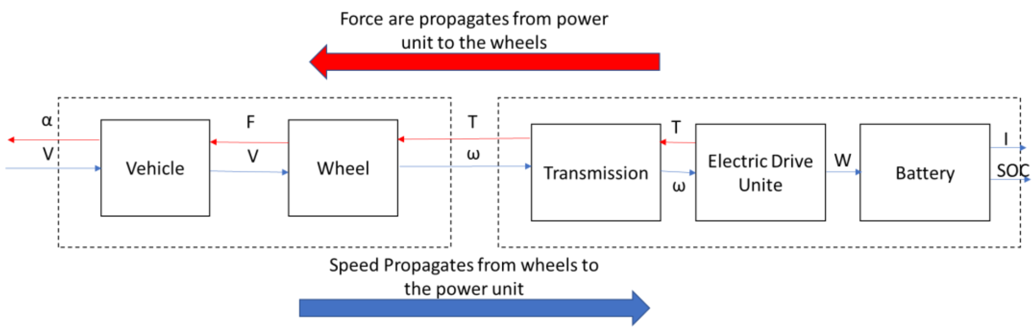

Figure 4.6: Forward model physical propagation.

4.1.3 Plant Models

Accurate component modeling is crucial for successful powertrain models since a powertrain comprises various components. The modeling methods can differ depending on the component, typically categorized as static, quasi-static, and physics-based models.

Quasi-static Models assume static behavior at each moment and linearize non-linear problems. In propulsion system modeling, these models simplify the process, reduce computational time, and maintain a representation of physical phenomena inherent to the system's behavior. For instance, energy consumption is calculated through efficiency maps interpolation, component limits are modeled using 1D tables, and algebraic equations represent dynamic effects. These models employ look-up tables derived from experimental testing. Quasi-static models are preferred when modeling complex powertrain systems that are not the primary focus of interest in the simulation since their transient (dynamic) response is limited [210].

Physics-based Models are employed when analyzing the dynamics of a component of interest. These models are constructed based on the governing physical laws of the component. Dynamic models utilize differentials, algebraic equations, or lumped coefficients to approximate the component's behavior. Most variables influencing the component and system behavior are included in dynamic models. They are commonly used for modeling DC machines, converters, and batteries (using electrochemical models) [211].

Static Models: Static models assume a constant state without dynamic effects [212].

4.2 Modelling

This section presents the modeling equations and the model used in this research. A one-dimensional simulation model developed in Simulink, shown in Figure 4.7, was developed for this research.

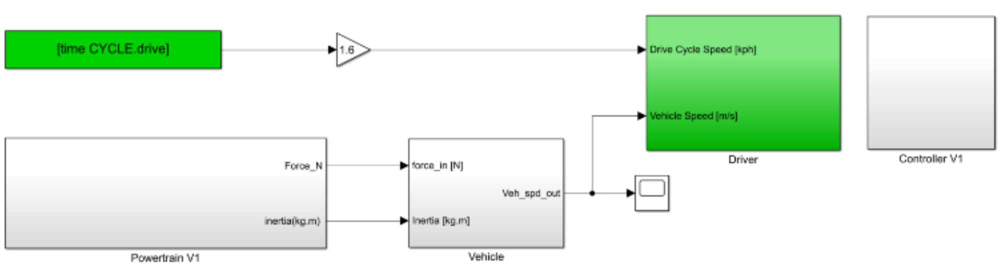

Figure 4.7: One-Dimensional propulsion system modelling.

The driver model uses a proportional integral derivative (PID) in a closed loop forward simulation model to maintain the vehicle simulated output speed close to the target speed from the driving cycle. The output of the PID controller produces a simulated accelerator or brake pedal signal to the propulsion system controller, which then commands the torque to actuators (electric machines and brake calipers), which are modeled in the plant model.

Figure 4.8 presents the layout of the closed-loop one-dimensional model.

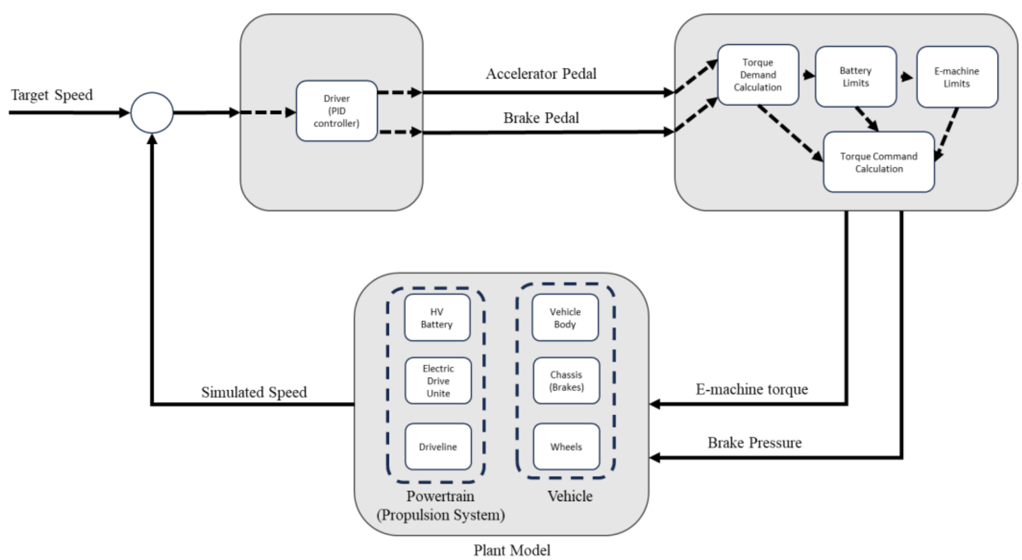

Figure 4.8: Layout of the one-dimensional simulation model.

4.2.1 Plant Model

Road loads encompass the inherent losses associated with the vehicle's forward movement, including aerodynamic resistance, tire rolling resistance, and grade resistance [213].

The electric vehicles' longitudinal dynamics can be expressed by Equation (4.1), assuming no slip occurs on the wheels, and using a quarter vehicle model as a reference.

$$m\dot{v} = \frac{\tau_{wh}}{r_{wh}} - mg \sin \emptyset - A \cos \emptyset - Bv - Cv^2 \tag{4.1}$$

Where m is the vehicle equivalent mass, v is the vehicle speed, τ_{wh} is the torque at the driving wheels, r_{wh} are the dynamic wheel radius $\emptyset$ road grade, and g is the gravity acceleration.

Factor A corresponds to the vehicle rolling resistance and weight and is expressed by Equation (4.2). Where f is the rolling tire resistance.

$$A = mfg \tag{4.2}$$

Factor B corresponds to the linear relationship of the rolling resistance with vehicle speed, usually originating from disc brake contact with the calipers and half shaft assemblies, and the dynamic effects of the tire rolling resistance. Factor B in empirical value, measured during coast-down tests.

Factor C corresponds to the aerodynamic resistance and is expressed by Equation (4.3). Where ρ is the air density, A_f is vehicle projected frontal area, and C_d is the aerodynamic drag resistance coefficient.

$$C = \frac{1}{2}\rho A_f C_d \tag{4.3}$$

4.2.2 Propulsion System

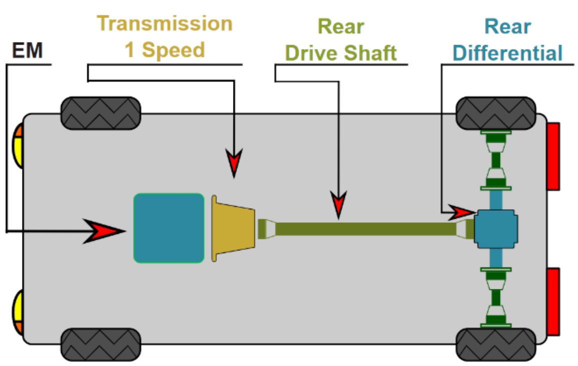

Figure 4.9: Single motor with a single-speed gearbox electric vehicle architecture.

The propulsion system torque and power propagation in electrified propulsion systems determine whether the electric machine is propelling or braking the vehicle. Equation (4.4) shows the torque at the wheels for propelling, and Equation (4.5) shows the torque at the wheels for regenerative braking.

$$\tau_{wh} = \varphi_p i_p \tau_{em} \tag{4.4}$$

Where φ_p Is the overall propulsion system efficiency, i_p is the overall propulsion system gear ratio – including the differential and τ_{em} is the electric machine's torque. The variables φ_p, and i_p are a function of the driveline architecture and are described in the driveline topics of this section.

$$\tau_{wh} = \frac{i_p \tau_{em}}{\varphi_p} - \tau_{br} \tag{4.5}$$

Where τ_{br} is the torque from the hydraulic brakes during deceleration.

4.2.2.1 Driveline

The driveline model depends on the transmission architecture used in the propulsion system. Equations (4.6) and (4.7) express the torque efficiency and gear ratio for a single-speed electric drive unit with one electric motor and a one-stage speed reduction connected to a differential. Figure 4.9 shows the driveline architecture.

$$\varphi_{p,1=} \varphi_{gb}\varphi_{ps}\varphi_{diff} \tag{4.6}$$

$$i_{p,1=} i_{gb} i_{diff} \tag{4.7}$$

Where φ_{gb} is the gearbox efficiency, φ_{ps} is the efficiency of the propulsion shaft with its joints and φ_{diff} is the efficiency of the differential.

4.2.2.2 Electric Machine

The electric machine efficiency is expressed by the combination of the inverter and the electric machine efficiencies and is calculated from three-dimensional efficiency maps as a function of the motor speed, high-voltage battery DC Voltage, and torque command.

4.2.2.3 High Voltage and Low Voltage Battery

The battery current calculation is expressed by Equation (4.8) as a function of battery open circuit voltage (Voc), Battery internal resistance (Ri), and demanded power Pem.

$$I_b = \frac{V_{oc} - \sqrt{V_{oc}^2 - 4R_iP_{em}}}{2R_i} \tag{4.8}$$

The battery state of charge is calculated by using coulomb counting, expressed by Equation (4.9), where SOC is the battery SOC, and Cb is the total battery capacity.

$$SOC_t = SOC_{t_0} - \int_{t_0}^{t} \frac{I_b}{C_b}\, dt \tag{4.9}$$

4.2.2.4 Auxiliary Power Module

The APM model efficiency is calculated by the Equation (4.10).

$$W_{HV,dc} = \frac{W_{LV,dc}}{\varphi_{apm}} \tag{4.10}$$

Where $W_{HV,dc}$ and $W_{LV,dc}$ are the charge or discharge electric power of the high voltage and low voltage batteries, respectively, and φ_{apm} is the efficiency of the APM, represented by a constant value.

4.3 Model Correlation

The Chevrolet Spark Electric 2015 was used as a reference vehicle for this model correlation study. The Argonne tested this vehicle, and detailed test data is available at [200]. For this correlation examination, the data used are from the test dynamometer - driving cycle speed, time step, and rolling dyno force; from sensors installed on the vehicle – battery terminal voltage and DC current; and from the vehicle CAN - battery SOC.

The combined performance and efficiency of the electric machine and the power inverter were estimated from publicly available work [214]. The battery OCV-SOC was calculated using the OCV-SOC curve for the NCM Lithium battery, which was found at [215]. The terminal voltage model used was an OCV-R model.

Table 4.1 summarizes the vehicle's basic technical specifications, and Table 4.2 shows the OEM's declared performances, and the results are estimated using the vehicle model built for this research.

The model's performance was evaluated using a normalized RMSE approach and then a box plot to compare the significant trend of the values (median), its dispersion, and distribution.

Table 4.1: Base vehicle technical specifications.

Specifications	
Battery	
Cells	96S2P
Energy	19 kWh
Total Capacity	54 Ah
Battery Power	120 kW
Electric Motor/Drive Unite	
Power	105kW
Torque	444Nm (540Nm peak)
Final Ratio	3.87:1

Table 4.2: Base vehicle declared versus calculated performances.

	Declared	**Simulated**
Top speed*	90 mph	~145kph/90mph
0-30 mph*	3s	~3s
0-60mph*	7.2s	~7.2s
MPGe Combined	119	119mpge
MPGe City	128	135mpge
MPGe Highway	109	100mpge
Kwh/100mi	28	27kWh/100mi
Adjusted combined Range	82 mi	72.5mi

The RMSE was chosen for this comparison as it gives the same weight to the positive and negative values for the differences. It is mandatory to evaluate the current and rolling dyno force, which has negative values. The drawback of the RMSE is an increased error due to spikes in the data set, as it overscales the errors at the peaks. The normalization of the RMSE was then calculated to bring all the errors to the same scale and compare the different physical metrics the problem is dealing with.

The overall performance of the model is measured by comparing the ability of the model to follow the input (target) speed from the tested vehicle for the given driving cycles and the estimation accuracy of the battery state of charge, the DC current from the battery to the power electronics, the high voltage battery terminal voltage, and the tangential force applied by the tires to the rolls of the dynamometer used to drive the car on the driving cycles.

Table 4.3 shows the parametrized RMSE for each of the driving cycles evaluated.

Table 4.3: Normalized RMSE to evaluate the model's ability to represent an electric vehicle.

Normalized RMSE

Driving Cycle Description	SOC Initial	Voltage	SOC	HV DC	Force	Speed
Acceleration maneuver: 0-80-0 mph, 0% Slope	83.50%	0.0192	0.0032	0.209	0.0202	0.0053
Acceleration maneuver: 0-80-0 mph, 6% Slope	65.86%	0.0376	0.0073	0.1651	0.0256	0.011
Passing Maneuver: 0% Slope	31.75%	0.0241	0.0147	0.1809	0.0237	0.0108
Passing Maneuver: 3% Slope	25.87%	0.0301	0.0124	0.2248	0.0263	0.0128
Passing Maneuver: 6% Slope	30.58%	0.0362	0.0194	0.2677	0.0253	0.0156
Driving Cycle: UDDS Ph 1+2, HWY Ph3, UDDS Ph 4+5, US06 Ph 6+7	99.96%	0.013	0.0197	0.159	0.0128	0.0078
Driving Cycle: 65mph deplete +US06 ph 3+4	62.33%	0.0363	0.0099	0.0933	0.0158	0.0098
Driving Cycle: UDDS Ph 1+2, HWY Ph3, UDDS Ph 4+5	38.02%	0.0203	0.0164	0.1159	0.0216	0.0092
Driving Cycle: UDDS Ph 1+2	38.02%	0.0234	0.0126	0.1722	0.0261	0.0116
Driving Cycle: UDDS Ph 4+5	21.17%	0.0155	0.0259	0.119	0.0265	0.0115
Driving Cycle: HWY Ph3	32.14%	0.0188	0.007	0.126	0.013	0.0063

Figure 4.10 shows that the error for the HV DC current has much higher dispersion, where 50% of data are within a range of 10% error, and the 25% of data in the upper quartile are also within a range of 10% error. The HV DC current data also presents a greater error when compared to the other analyzed variables, reaching an average normalized RMSE of 16.5%. This more significant variance is primarily due to the more dynamic behavior of the HV DC current, varying in seconds from a very high negative value to a very high positive value. The high dispersion of the DC estimation limits the evaluation of the other physical metrics in the same graphic.

Figure 4.11 excludes the HV DC from the analysis and shows a very low RMSE dispersion for the battery terminal voltage, the battery SOC, the wheel Force, and the vehicle speed. With a mean error varying from 2.5%-1.5% and the median varying from 2.2%-1.0%. The box plot in Figure 4.10 also indicates an equivalence of the model's accuracy in estimating the battery terminal voltage, battery SOC, wheel force, and the mathematical driver model's ability to follow the given speed profile.

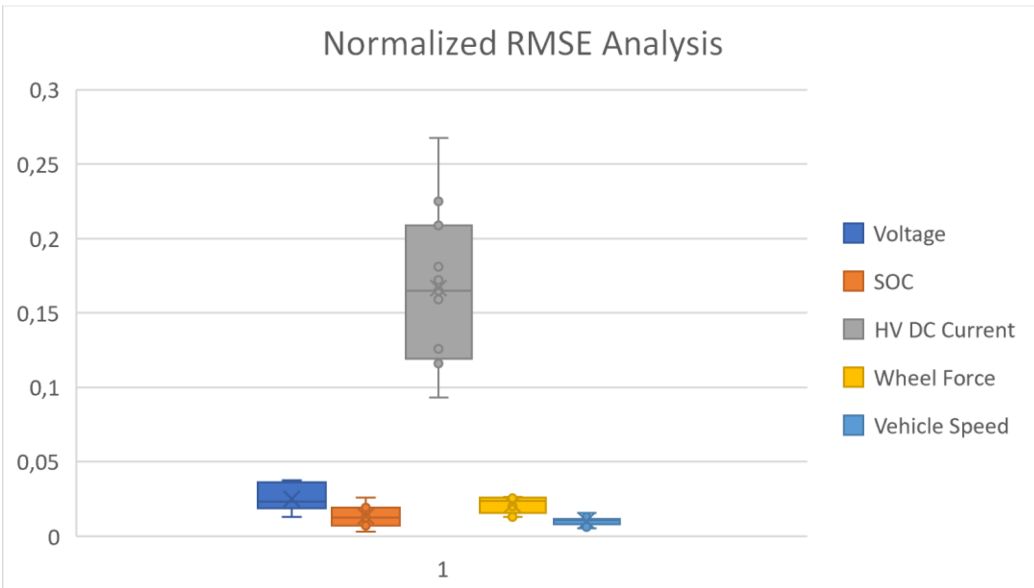

Figure 4.10: Boxplot analysis for battery terminal voltage, battery SOC, DC current, wheel tangential force, and vehicle speed.

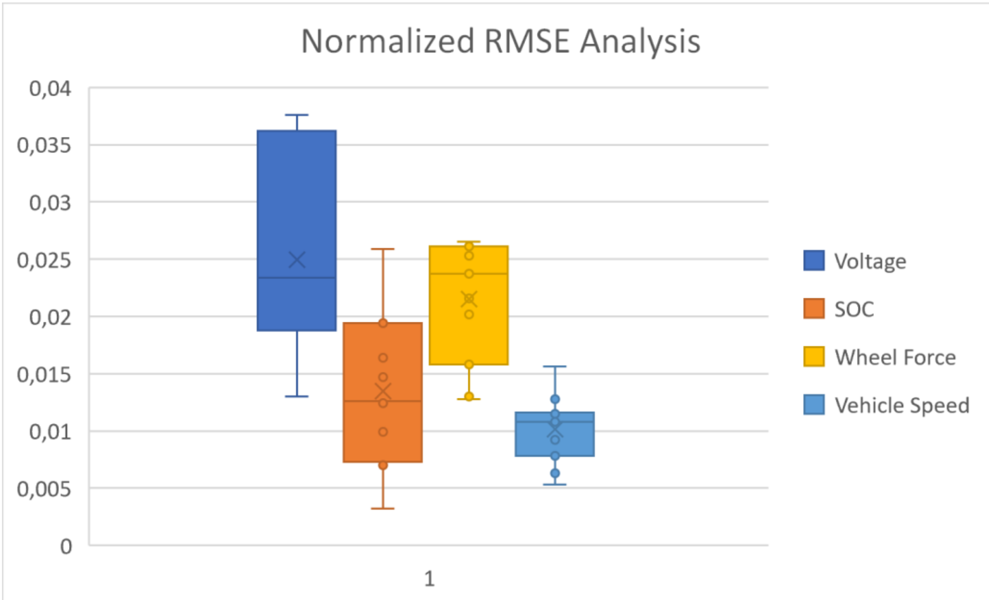

Figure 4.11: Boxplot analysis excluding the DC current from the date set. Battery terminal voltage, battery SOC, wheel tangential force, and vehicle speed.

Nevertheless, it is crucial to acknowledge that both the battery's state of charge (SOC) and its terminal voltage are inherently and directly contingent on the high-voltage direct current (HV DC) flowing through the system. Given the model's ability to closely approximate the battery terminal voltage and SOC (which is calculated through Coulomb counting) and their strong alignment with experimental data, it becomes evident that the normalized Root Mean Square Error (RMSE) metric may not comprehensively capture the overall deviation when assessing the adherence of DC current estimation to empirical data.

We undertake a deeper analysis of the data to provide a more comprehensive assessment of the model's performance. Specifically, we delve into the simulation outputs of battery DC current, battery terminal voltage, and battery SOC. This examination is conducted across three distinct driving cycles, namely: an acceleration maneuver involving a speed profile of "0-80-0 mi/h" with a 6% slope, a passing maneuver characterized by the same slope, and a simulation encompassing the 65 mph deplete phase followed by the US06 phase 3 and 4. The selection of these driving cycles enables a comprehensive evaluation containing the best, worst, and average model performance scenarios.

Figure 4.12, Figure 4.13, Figure 4.14 show the simulation output for the acceleration maneuver; Figure 4.15, Figure 4.16, Figure 4.17 show the simulation for the passing maneuver; and Figure 4.18, Figure 4.19, Figure 4.20 are the results for the driving cycle with a 65mi/h depleting plus US06 cycle.

All driving cycle results are in Appendix A.

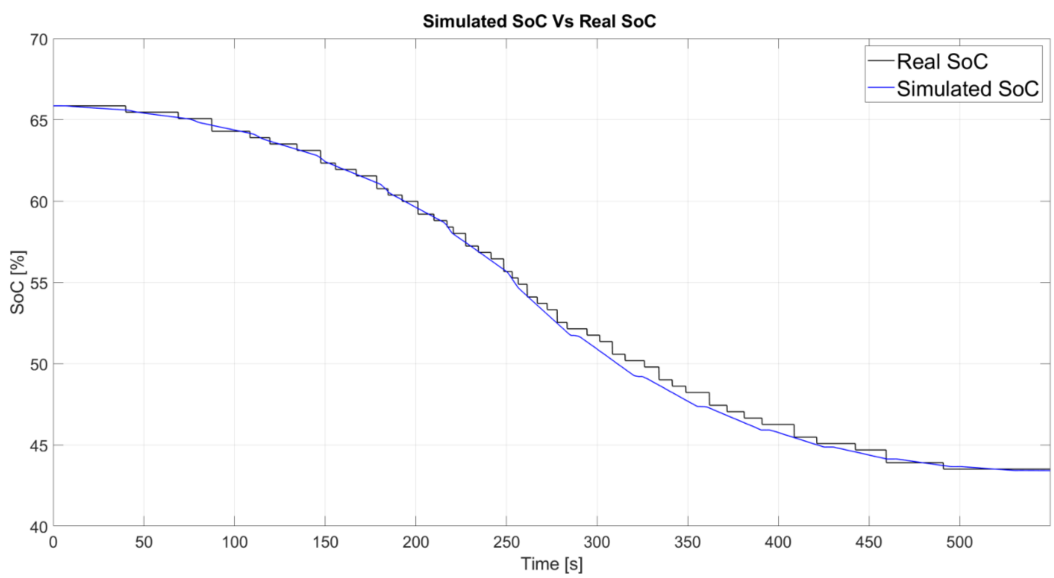

Figure 4.12: Model Correlation - Acceleration maneuver: 0-80-0 mph, 6% slope - battery state of charge.

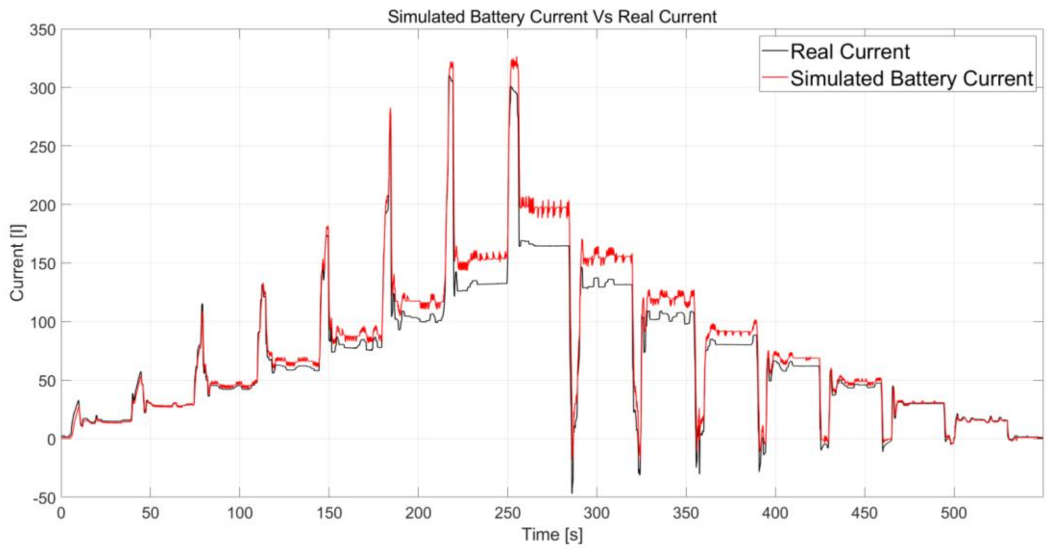

Figure 4.13: Model Correlation - Acceleration maneuver: 0-80-0 mph, 6% Slope - HV Battery DC Current.

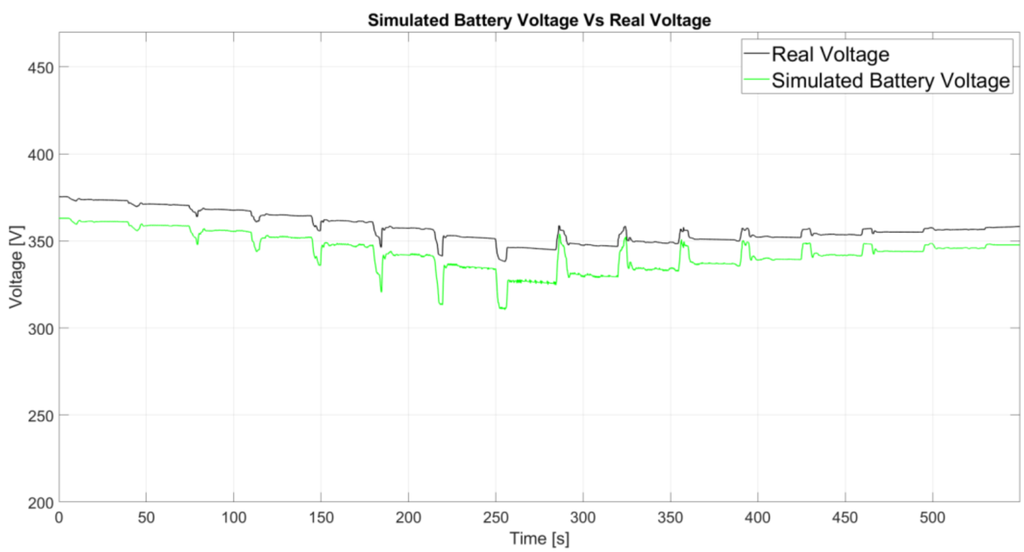

Figure 4.14: Model Correlation - Acceleration maneuver: 0-80-0 mph, 6% Slope - battery terminal voltage.

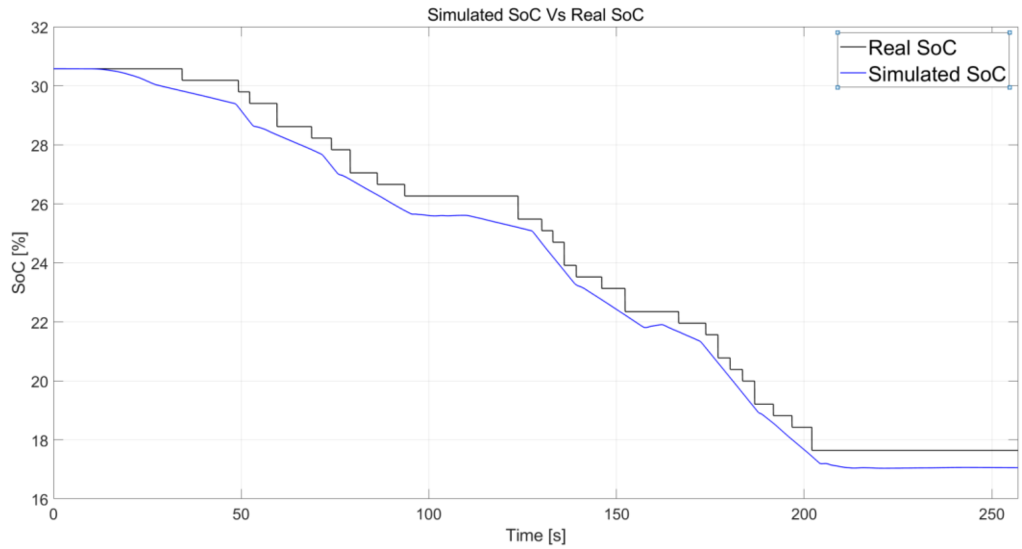

Figure 4.15: Model Correlation - Passing Maneuver: 6% slope - battery state of charge.

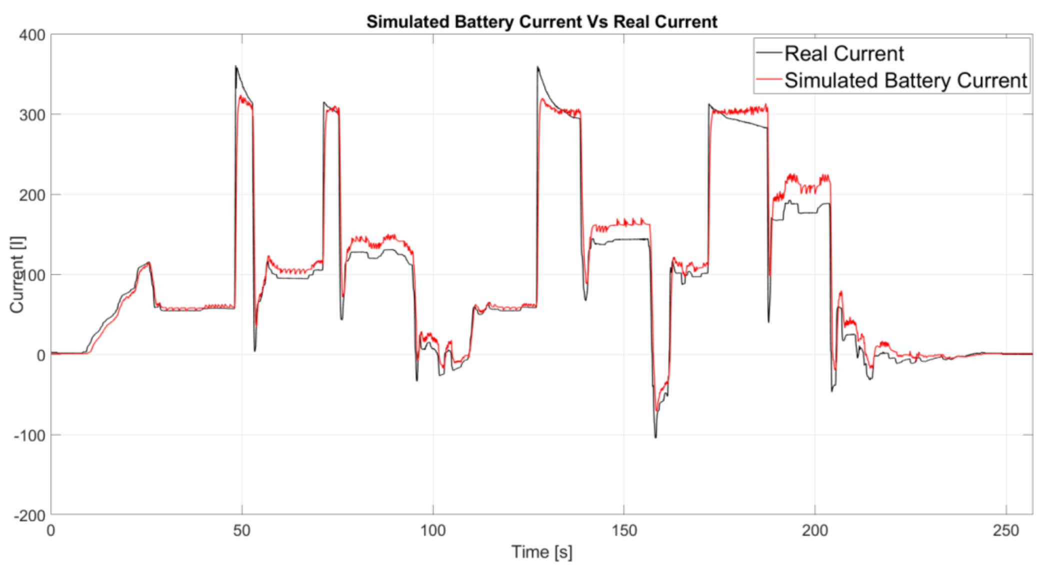

Figure 4.16: Model Correlation - Passing Maneuver: 6% slope - battery DC Current

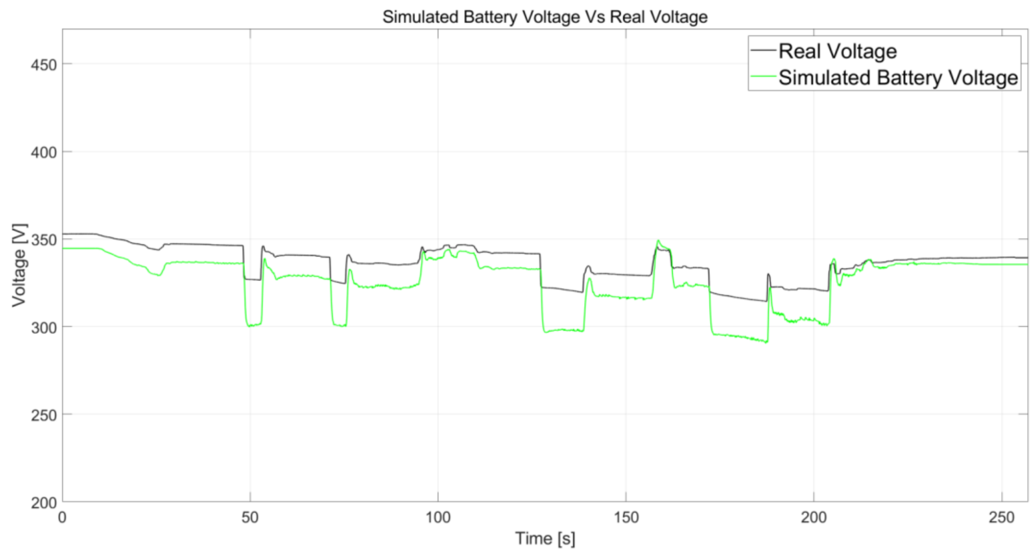

Figure 4.17: Model Correlation - Passing Maneuver: 6% Slope - Battery Terminal Voltege.

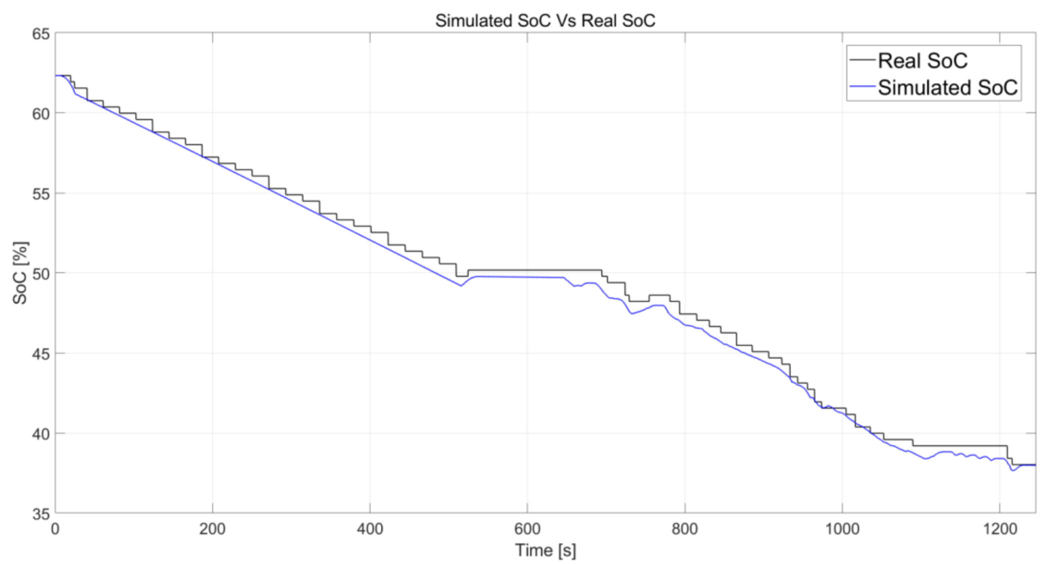

Figure 4.18: Model Correlation - 65mph deplete +US06 ph 3+4 - battery state of charge.

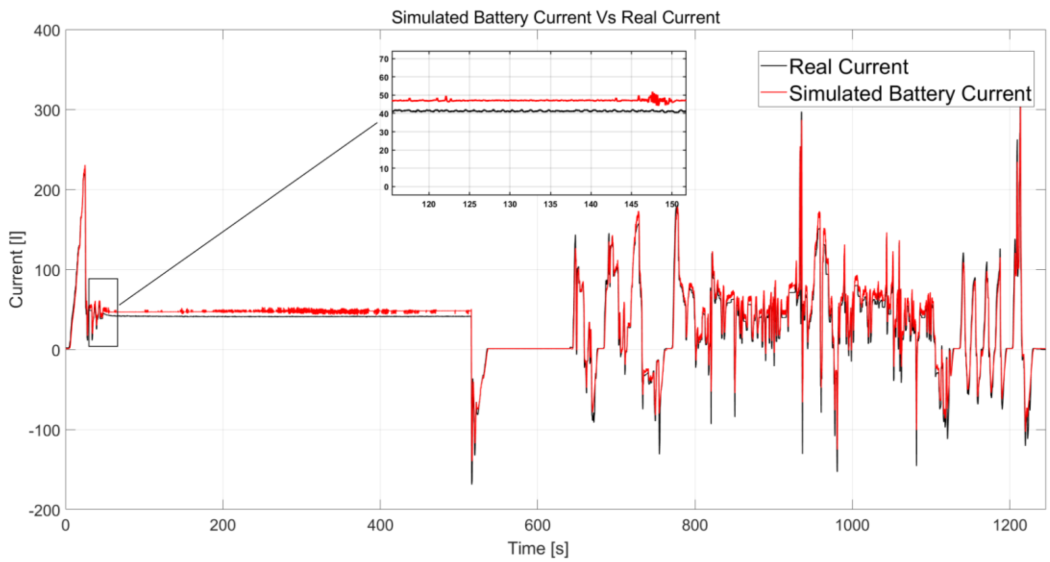

Figure 4.19: Model Correlation - 65mph deplete +US06 ph 3+4 - battery DC Current.

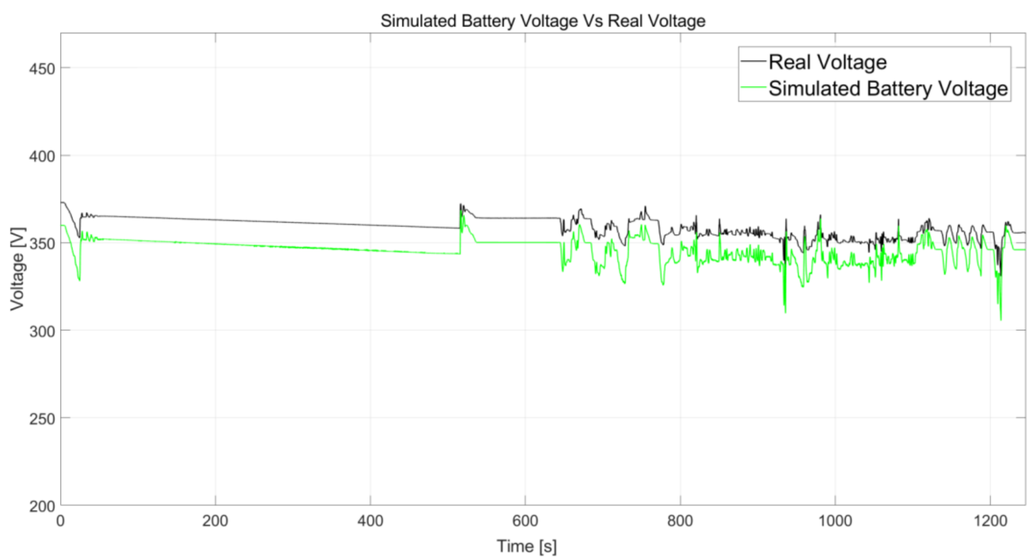

Figure 4.20: Model Correlation - 65mph deplete +US06 ph 3+4 - Battery Terminal Voltage.

4.4 Summary

In conclusion, this Chapter has explored the imperative need for propulsion system electrification in the face of global urban restrictions and mounting CO2 emission regulations. The evolving landscape of automotive markets, as discussed in Chapter 2, emphasizes the growing shift towards electrified vehicles. These transformations necessitate the development of optimal electrified propulsion system architectures and subsystems. This task becomes increasingly complex due to the myriad of design possibilities and the limitations of traditional bureaucratic organizations.

Adopting a model-centric approach, as introduced in this Chapter, is invaluable in addressing these challenges. This approach enables continuous design optimization and tradeoff analysis within the boundaries of the propulsion system. Bridging the gap between requirements and component designs offers a holistic perspective throughout the product development cycle. However, integrating tools for modeling electrified vehicles and their associated software remains a crucial need in the industry.

The review of model-based engineering highlighted the versatility of models in capturing system complexities and facilitating tradeoffs at various levels of design complexity. It showcased how model-based design engineering (MDB) serves as an effective method for developing complex systems like electrified propulsion systems. Moreover, the Chapter emphasized the importance of models in maintaining traceability of design decisions and supporting the continuous loop of test and verification.

The results presented in this Chapter, particularly the model's correlation with physical data, reinforce the efficacy of the simulation tool developed. Despite some challenges in modeling high-voltage DC current dynamics, the model demonstrates its reliability in estimating key variables such as battery terminal voltage, battery SOC, wheel force, and driver model adherence to speed profiles. The comprehensive assessment across various driving scenarios underscores the model's ability to perform optimally under different conditions.

The model-centric approach proposed in this research offers a promising avenue for addressing the complex challenges of electrified propulsion systems. The successful correlation of the model with physical data instills confidence in its capability to guide design choices, enhance energy efficiency assessment, and facilitate software and control calibration. As the automotive industry continues to embrace electrification, this research provides a valuable tool for achieving efficient and optimized electrified propulsion system architectures and components.

Chapter 5

Electric Vehicle Architecture Design

Governments of all major automotive markets are imposing regulations to limit the transportation sector's usage of fossil fuels and establishing strict limits on the emission of air pollutants. In [1], a comparison of emissions requirements for light-duty vehicles in the four primary automotive markets - the United States, China, the European Union, and Brazil is detailed. It states that from 2010 to 2030, emissions from new cars are expected to drop from more than 500 mg/km of NMHC/NMOG+NOx 2010 to below 100 mg/km in 2030.

In Brazil, the Brazil National Council for the Environment (CONAMA) approved the introduction of a new emissions standard for light and heavy-duty vehicles called PL-8, starting the new requirements phase-in in 2025 for light-duty vehicles, with complete adoption in 2031. The new regulation establishes emissions requirements for standard and real-world driving cycles and the minimum durability requirement of 160,000 km or ten years [2]. CONAMA is defined as light-duty passenger vehicles (PV) and light-commercial vehicles (LCV). A summary of both is in Table 5.1.

Table 5.1: Vehicle Type Definition according to CONAMA.

	(PV)	(LCV)
Curb weight (CW)	<2,720kg	
Gross Vehicle Weight (GVW)	<3,856 kg	
Payload	<1000kg	≥1000kg*
Number of Passengers	≤8	>8 *
*Payload ≥1000kg or more than eight seats added to the driver seat		

LCVs represent 15-20% of the light-duty vehicles in the Brazilian market, with an average annual sale of approximately 400 thousand units. About 40% of LCVs are body-on-frame vehicles with diesel engines [3]. Therefore, slowing down diesel engine technology development could heavily impact a market size of roughly 6 billion dollars in revenue if alternative technologies are not in place.

The PVs and LCVs have different phase-in requirements strategies, starting in 2025, but emissions limits align in 2031. In [1], the report also compares the PL-8 requirements for light-duty vehicles with EU, China, and US emissions standards and shows the Brazilian standards aligned with major automotive markets by 2031. By 2030, an extensive electrification program will achieve 47% of the total emissions reduction in the EU [4]. The EU approved to end the sales of all CO2-emitting vehicles by 2035 [5]. This decision establishes a deadline that causes a natural reduction in the development of technologies to improve fuel quality and combustion engine emissions, with consequences to the long-term adoption of gasoline and diesel engines in other automotive markets, primarily in developing countries [6], [7].

Brazil, South and Central America have one of the cleanest electric grids in the world. In South and Central America, the electric power generation from renewables counts for 66%, while in Brazil, renewables count for approximately 84%, equivalent to 520TWh [8], with average equivalent CO2 emissions of 0.09 gCO2/kWh. For comparison, in the USA, in 2020, the equivalent CO2 emission was 0.371gCO2/kWh [9].

The electrification of the transportation infrastructure stands as a pivotal catalyst for the overarching reduction in the economy's carbon footprint, particularly in regions like Brazil, characterized by its distinctive energy generation matrix primarily dominated by hydroelectric, solar, and wind resources. However, it is imperative to acknowledge that the electrification of the transportation sector also plays a pivotal role in reshaping the Total Cost of Ownership (TCO) dynamics, particularly within the context of commercial fleets. According to specific estimations, there exists the potential for an astounding 80% reduction in TCO when comparing electrified fleets to their internal combustion engine (ICE) counterparts.

The complete phase-out of incumbent vehicle fleets, predominantly ICE-powered vehicles, entails a protracted timeline spanning several decades. Within this intricate landscape, the retrofitting of pre-existing ICE vehicles, wherein these vehicles are endowed with electrified propulsion systems, emerges as an expedient avenue to expedite the transformative transition from a fossil fuel-centric economy towards an electrified paradigm.

This Chapter thoroughly explores the retrofitting of commercial vehicles, delving into a meticulous analysis of four distinct electric vehicle propulsion configurations.

Our investigation extends beyond a mere assessment of energy efficiency, encompassing a thorough examination of the acquisition costs and the overarching Total Cost of Ownership (TCO) considerations, thereby scrutinizing the viability of electrified vehicles as a financially sound and profitable investment opportunity, analyzing its internal rate of return (IRR), payback period (PB), and return on investment (ROI). The architecture assessment is adapted from the process proposed by [10].

5.1 Study Case Architectures

Selecting the ideal driveline architecture is crucial when designing an electric vehicle since it dramatically affects its performance, energy efficiency, cost, and how it fits together. Electric vehicles can have various driveline setups, including single, dual, or multiple electric machines. The choice depends on what characteristics you want for the vehicle and its intended application.

In this Chapter, only two-wheel-drive setups are investigated, keeping the drive axle and differential the same as a typical internal combustion engine vehicle. This research aims to find the best option for making commercial vehicles electric by studying four different setups.

The baseline ICE vehicle is shown at Figure 5.1.

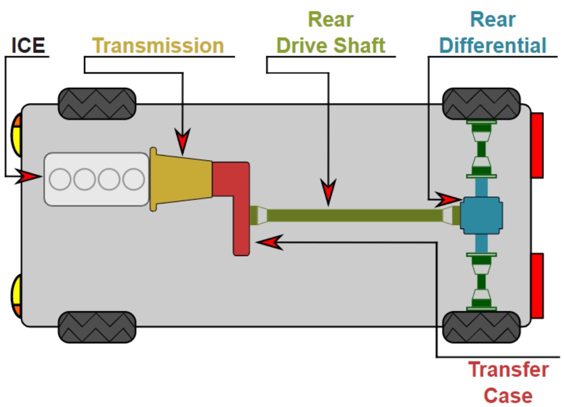

Figure 5.1: Base Internal Combustion Engine (ICE) Vehicle Propulsion System Architecture.

A differential torque limit curve is defined from the peak input torque observed at the base ICE vehicle and works as a constraint to the design of the electric propulsion system, intending to limit the influence of the electric motor torque on the mechanical durability of the driveline system. The maximum driveline input torque curve is in Figure 5.2.

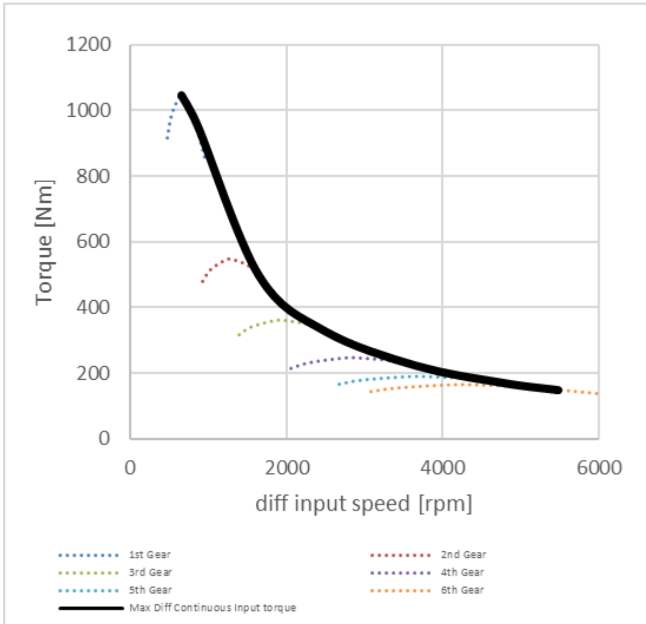

Figure 5.2: Differential maximum input torque calculated from the base ICE vehicle.

5.1.1 Architectures

This Chapter delves into a comprehensive examination of four distinct two-wheel drive (2WD) architectures, each characterized by variations in parameters such as motor peak torque, power and speed, gearbox utilization, number of gear speeds, or the incorporation of a dual electric machine system. Figure 5.3, Figure 5.4, Figure 5.5, and Figure 5.6 illustrates architecture 1, 2, 3, and 4 respectively.

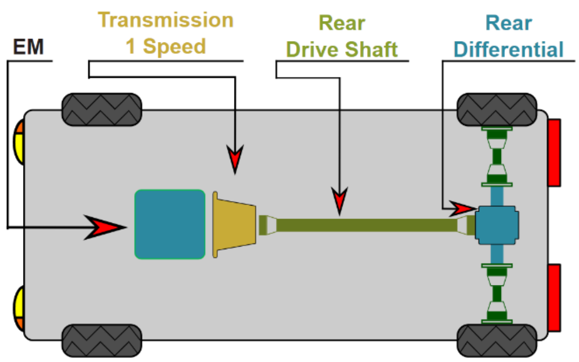

Figure 5.3: Single motor with a single speed gearbox electric vehicle architecture.

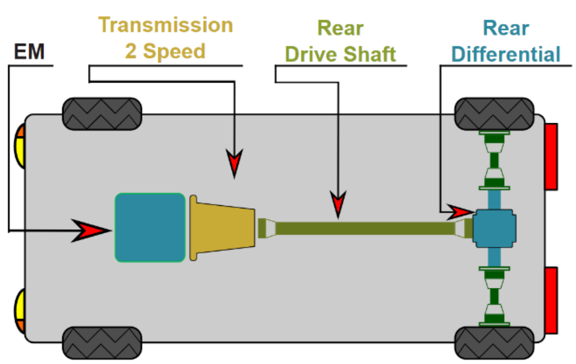

Figure 5.4: Single motor with a two-speed gearbox electric vehicle architecture.

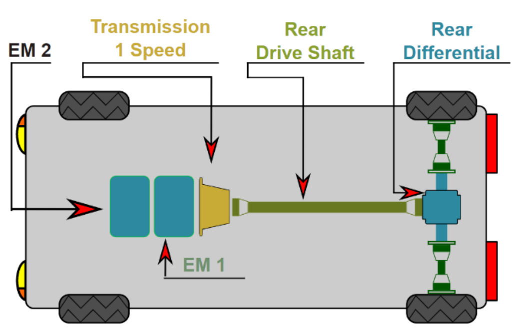

Figure 5.5: Dual motor with a single-speed gearbox electric vehicle architecture.

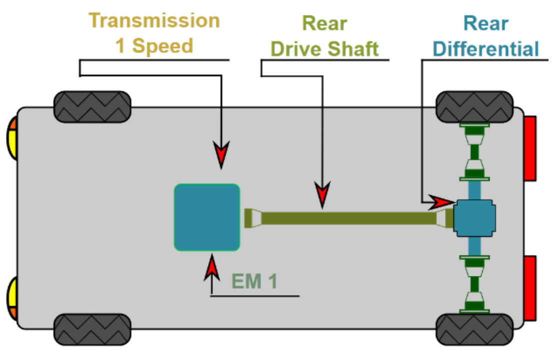

Figure 5.6: Single motor directly connected to the propulsion shaft.

5.2 Modelling

In Chapter 4, we introduced propulsion system modeling. For the architecture assessment that this chapter presents, models for each driveline architecture we're investigating have been developed. These models take into account the unique features and specifications of each system. The reason for doing this is twofold: first, it allows us to assess how efficient and performant each design is thoroughly, and second, it helps us pinpoint areas that might need improvement, reaching the optimum sizing for each architecture.

Overall, this modeling approach helps us understand the strengths and weaknesses of different architectures.

5.2.1 Propulsion System

The propulsion system torque and power propagation in electrified propulsion systems are determined by whether the electric machine is propelling or braking the vehicle. The equations were presented in Chapter 4.

Equation (5.1) shows the torque at the wheels for propelling, and Equation (5.2) shows the torque at the wheels for regenerative braking.

$$\tau_{wh} = \varphi_p i_p \tau_{em} \tag{5.1}$$

Where φ_p Is the overall propulsion system efficiency, i_p is the overall propulsion system gear ratio – including the differential and τ_{em} is the electric machine's torque. The variables φ_p, and i_p are a function of the driveline architecture and are described in the driveline topics of this section.

$$\tau_{wh} = \frac{i_p \tau_{em}}{\varphi_p} - \tau_{br} \tag{5.2}$$

Where τ_{br} is the torque from the hydraulic brakes during deceleration.

5.2.2 Driveline

The driveline model depends on each architecture.

Equations (5.3) and (5.4) express the torque efficiency and gear ratio for Architecture 1, Equations (5.5) and (5.6) for Architecture 2, Equations (5.7) and (5.8) for Architecture 3, and Equations (5.9) and (5.10) for architecture 4.

$$\varphi_{p,1=}\ \varphi_{gb}\varphi_{ps}\varphi_{diff} \tag{5.3}$$

$$i_{p,1=}i_{gb}i_{diff} \tag{5.4}$$

Where φ_{gb} is the gearbox efficiency, φ_{ps} is the efficiency of the propulsion shaft with its joints and φ_{diff} is the efficiency of the differential.

$$\varphi_{p,2=}\ \varphi_{gb,z}\varphi_{ps}\varphi_{diff} \tag{5.5}$$

$$i_{p,2=}i_{gb,z}i_{diff} \tag{5.6}$$

Where z is the gear selected.

$$\varphi_{p,3=}\ \varphi_{gb}\varphi_{ps}\varphi_{diff} \tag{5.7}$$

$$i_{p,3=}i_{gb}i_{diff} \tag{5.8}$$

$$\varphi_{p,4=}\ \varphi_{ps}\varphi_{diff} \tag{5.9}$$

$$i_{p,4=}i_{diff} \tag{5.10}$$

5.2.3 Electric Machine

The electric machine efficiency is expressed by the combination of the inverter and the electric machine efficiencies, calculated from the efficiency map of Figure 5.7.

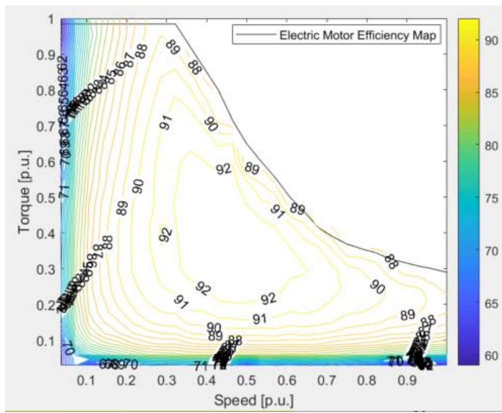

Figure 5.7: Electric machine efficiency map in per unit (p.u.) system.

5.2.4 High Voltage and Low Voltage Battery

The battery current calculation is expressed by Equation (14) as a function of battery open circuit voltage (Voc), Battery internal resistance (Ri), and demanded power Pem.

$$I_b = \frac{V_{oc} - \sqrt{V_{oc}^2 - 4R_iP_{em}}}{2R_i} \tag{5.11}$$

The battery state of charge is calculated by using coulomb counting, expressed by Equation (15), where SOC is the battery SOC, and Cb is the total battery capacity.

$$SOC_t = SOC_{t_0} - \int_{t_0}^{t} \frac{I_b}{C_b}\, dt \tag{5.12}$$

5.3 Architecture Assessment

In this investigation, the performance prerequisites for the electrified vehicle were meticulously delineated to ensure parity or surpass the performance metrics exhibited by its internal combustion engine-equipped counterpart. Furthermore, we have judiciously formulated the battery electric vehicle (BEV) range specifications to align with an average performance benchmark concerning other electric vehicles inhabiting the same vehicular segment.

We present a concise representation of the targets in Table 5.2. This table offers a detailed exposition of the multifaceted parameters that the electrified vehicle must adhere to attain the status of a viable alternative to its internal combustion (IC) counterpart.

This effort focuses on evaluating the possibility of electrifying commercial vehicles while ensuring that the resulting vehicle meets the needs of its intended users. This is achieved by setting clear and specific performance and range criteria.

Table 5.2: Design Requirements.

Performances	Units	Targets
Adjusted Combined Range (FTP75/highway)	[km]	260
0-100 km/h	[s]	12s
Maximum Speed	[km/h]	146
Launch on grade @GVW	[%]	25%
Launch on grade @PBT	[%]	33%
6% grade constant speed	[km/h]	141

Several constraints restrict the design space to ensure a rigorous architecture analysis and guide the system sizing process. In particular, four main restrictions apply to this problem: the differential input speed and torque should remain the same as in the donor vehicle, as illustrated in Figure 5.1 and Figure 5.2; the system voltage should be 350V nominal, with a peak DC current not exceeding 600A, thereby limiting the total power of the electric machine to 200kW; and the payload should not be lower than 1000kg.

Table 5.3 shows the sizing results for the electric machines, gearbox, and high-voltage battery.

Table 5.3: Architecture Subsystem Sizing.

Architecture	e-machine	gearbox	Battery
1	200 kW	2.97:1	80 kWh
2	150 kW	1^{st} gear = 4.5:1 2^{nd} gear = 2.97:1	72 kWh
3	100 kW	2.97:1	65 kWh
4	200 kW	1:1	80 kWh

By imposing these constraints, this study aimed to assess the feasibility of electrifying the donor vehicle while considering its intended use's practical limitations and requirements. These constraints enabled a more comprehensive analysis of the candidate architectures, allowing for a more accurate evaluation of their performance and suitability for the specific application.

The assessment comprehends the simulation of the investigated architectures using the base modeling presented in Chapter 4, which is adapted for each of the four architectures. For the evaluation, regulatory EPA driving cycles, such as FTP75 and Highway cycles, are used for energy efficiency and electric range calculations. Vehicle capabilities comparison uses the ability of the propulsion system to sustain a constant speed at a 6% road slope and to launch on grade at its gross vehicle weight.

Table 5.4 presents the performance results for all architectures compared to the target.

Table 5.4: Architecture assessment results.

	Units	Target.	Architectures			
			1	2	3	4
FT75 Range	[km]	-	360	393	440	346
Highway	[km]	-	219	241	264	219
Adjusted Combined	[km]	260	260	260	260	260
FTP 75	[kwh/km]	-	0.154	0.141	0.126	0.16
Highway	[kwh/km]	-	0.253	0.23	0.21	0.253
Adjusted FT75 Range	[kwh/km]	-	0.221	0.201	0.183	0.228
Adjusted Highway	[kwh/km]	-	0.361	0.328	0.309	0.361
Maximum Speed	[km/h]	146	146	146	146	146
Launch on Grade @GVW	[%]	25	25	29	25	29.6
Launch on Grade @PBT	[%]	33	33	38.3	33	39.1
6% grade constant speed	[km/h]	141	100	91.6	100	108

Figure 5.8, Figure 5.9, Figure 5.10, and Figure 5.11 show the electric machine operation for FTP75 and Highway EPA cycles for Architecture 1, 2, 3, and 4, respectively.

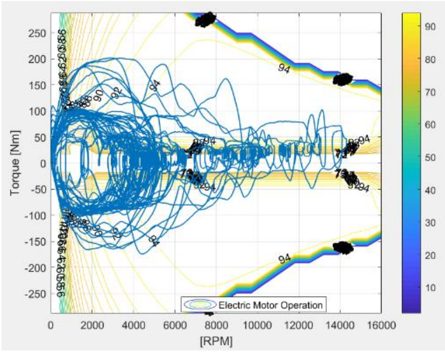

Figure 5.8: Architecture 1 - Electric machine operation on FTP75 and highway cycle.

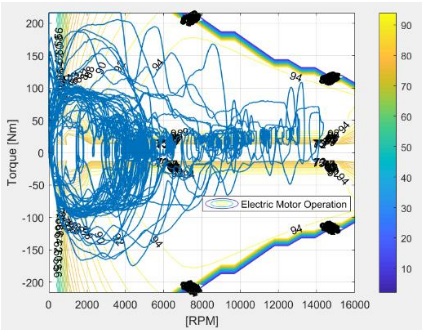

Figure 5.9: Architecture 2 - Electric machine operation on FTP75 and highway cycle.

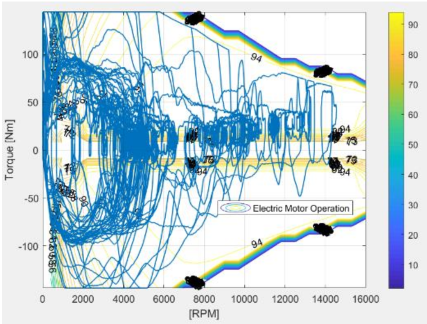

Figure 5.10: Architecture 3 - Electric machine operation on FTP75 and highway cycle.

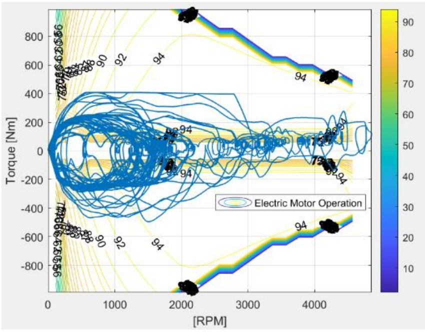

Figure 5.11: Architecture 4 - Electric machine operation on FTP75 and highway cycle.

Figure 5.12 shows the difference in SOC variation among the four investigated architectures for the FTP75 and highway driving cycles.

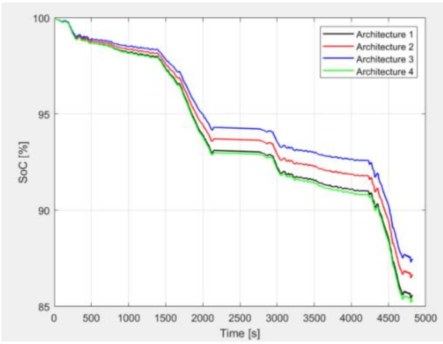

Figure 5.12: SOC variation comparison for different architectures on FTP75 and Highway driving cycles.

5.4 Financial Assessment

The financial assessment of the diverse driveline architectures entailed formulating a cost model, serving as a mechanism for estimating the aggregate material costs requisite for the product's realization. Furthermore, a comparative examination of the total cost of ownership for each architectural configuration was undertaken, complemented by developing a cash flow analysis for each prospective option.

To gauge the financial viability of these architectures as potential investments, critical financial metrics, including Return on Investment (ROI), Internal Rate of Return (IRR), and Payback Period (PB), were subject to rigorous scrutiny.

Through the execution of this all-encompassing financial appraisal of the various driveline architectures, the principal aim of this section was to furnish valuable insights into the economic feasibility surrounding the electrification of commercial vehicles and retrofit of existing ICE vehicles, thereby serving as a guiding compass for decision-making processes within this domain.

5.4.1 Cost of Acquisition Model

The studies [11] [12] were used for overall system cost estimation based on an actual vehicle tear-down. [13], [14] were used for the gearbox and driveline cost estimation. [15], [16] were used for the power electronics and e-machine cost estimation, and [17] for battery cost estimation. The MSRP, Manufacturer Suggested Retail Price, was then estimated based on an electric vehicle industry average of 30% gross margin over the total base material cost. The MSRP calculated for the vehicle, with each of the propulsion system architectures, is shown in Figure 5.13

Figure 5.13: Vehicle MRSP for different architectures to meet the same functional objectives.

5.4.2 Total Cost of Ownership

The study [18] defines a product's total cost of ownership (TCO) as an approximation of all the capital and operational expenses associated with purchasing, deploying, using, and retiring the product. This study compares the TCO of an LCV originally equipped with an IC with the exact vehicle but with a fully electric propulsion system operating in Sao Paulo, Brazil.

The capital costs considered in the study are the acquisition of the vehicle and, in the case of the electric car, an external level 2 wall charger. The operational costs considered in the study are energy consumption (liquid fuel or electricity), tire replacement, insurance, maintenance, and state license tax. The yearly drive distance is - according to [19] - and the estimation is 50.000 km per year.

A 10-year lifetime is used for the cash flow projection. Costs are considered at present value and on an annual basis. The battery traction replacement is not part of the operational cost estimations since the battery lasts between 4,000 to 8,000 complete cycles after years of usage.

This paper also compares the investment by examining four electricity cost and generation scenarios. Commercial and residential prices are taken according to [20], and industrial prices are taken from the free electricity market [21]. The investment to produce electricity to charge the vehicles using solar panels is estimated from [22].

The variable costs of ownership, such as energy and solar panels, are in Table 5.5. The fixed costs are presented in Table 5.6.

Table 5.5: Electricity and diesel cost.

Energy Commodity	**Unit**	**Cost**
Diesel	[BRL/L]	6.58
Residential (Class B)	[BRL/kWh]	1.02
Residential (ClassA)	[BRL/kWh]	0.62
Industrial (Free market)	[BRL/kWh]	0.35
Solar Painels	[BRL/kWp]	4.00

Table 5.6: Fixed annual cost of ownership.

	Diesel	Electric
Tires Replacement	BRL 2,000.00	BRL 2,400.00
Insurance	BRL 2,000.00	BRL 4,210.53
Maintenance	BRL 2,000.00	BRL 1,000.00
Yearly Tax	BRL 3,800.00	BRL -

The yearly fuel and energy cost for each architecture is presented in Figure 5.14

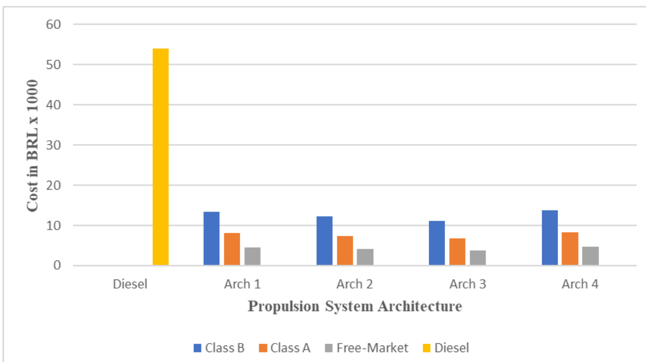

Figure 5.14: Total variable annual cost of ownership as a function of propulsion system architecture and energy cost.

5.4.3 Financial Analysis

Several methods are available to evaluate capital expenditures (CAPEX) investments, including the net present value (PB), (IRR), (ROI). This approach allows for a comprehensive comparison of the different architectures' performances and provides valuable insights into the economic feasibility of electrifying commercial vehicles.

5.4.3.1 Internal Rate of Return

The internal rate of return considers the investment's time value and operation costs during the investment period. It's commonly used to compare different investments and support the decision-making process of capital expenditure allocation by constantly looking at the investment performance.

The minimum IRR to reach an investment equilibrium is expressed by Equation (5.13).

$$0 = \sum_{t=1}^{T} \frac{C_t}{(1 + IRR)^t} - C_0 \tag{5.13}$$

Where T is the number of time periods, C_t is the net cash flow during the period T, and C_0 is the capital expenditure.

5.4.3.2 Return on Investment

The return on investment compares the value of an investment to its cost and is expressed by Equation (5.14). It's commonly used to compare the efficiency of one investment against another. In the case of this study, the ROI provides the overall efficiency of the electric vehicles as an investment compared to a baseline diesel vehicle.

$$ROI = \frac{Current\ Value - Cost\ of\ Invesment}{Cost\ of\ Invesment} \tag{5.14}$$

Figure 5.15 shows the cash flow projections for the exact vehicle charged in two ways: commercial electricity from the grid and auto-generation using solar panels. The electric vehicle as an investment is compared with the baseline IC vehicle in regards to its internal rate of return (IRR), return of investment (ROI), and the investment time to pay back (PB).

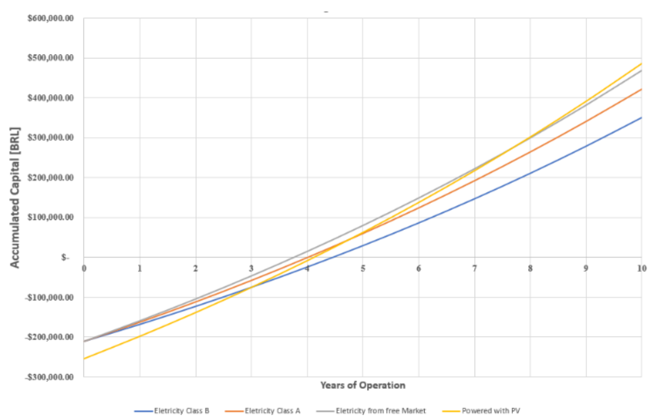

Figure 5.15: Electric vehicle with architecture 4 - Operation Cash flow.

5.4.3.3 Pay Back

Investment payback is defined as the time it takes to recover capital expenditure and reach its breakeven point. In this study, the payback analysis gives the time to recover the delta acquisition cost of the electric vehicle over an LCV equipped with a diesel engine. The payback period is expressed by Equation (5.15).

$$PB = \frac{C_0}{Average\ Annual\ Cash\ Flow} \tag{5.15}$$

5.4.4 Financial Assessment

A comprehensive cash flow analysis was meticulously conducted for each of the examined driveline architectures. This analysis considered the initial capital expenditure, computed as the disparity between the acquisition cost of the electric vehicle and the infrastructural investment cost relative to the baseline diesel vehicle. Additionally, the discrepancies in total cost of ownership between the electric vehicle and its internal combustion engine counterpart were subjected to discounting. The computation of the initial capital expenditure was achieved through the application of Equation (5.16). At the same time, the determination of the operating income, characterized by the delta Total Cost of Ownership (TCO), was ascertained through Equation (5.17).

$$C_0 = C_{MRSP} + C_{inf} \tag{5.16}$$

Where C_0 is the total capital expenditure, C_{MRSP} is the electric vehicle cost of acquisition, and C_{inf} is the total investment in infrastructure to operate the electric vehicle fleet.

$$Operate\ Income = TOC_{IC} - TCO_{EV} \tag{5.17}$$

Table 5.7 summarizes the financial analysis for all architectures evaluated at different electricity costs, where the best product presented is architecture 3, especially when the battery is charged by buying electricity from the free market.

Table 5.7: Financial assessment summary

Electricity Cost		Architecture			
		1	2	3	4
Class B	IRR	21%	25%	26%	21%
	Profit	354k	393k	408k	350k
	ROI	169%	207%	215%	167%
Class A	IRR	24%	28%	29%	24%
	Profit	424k	456k	468k	421k
	ROI	202%	240%	249%	201%
Free Market	IRR	26%	30%	31%	26%
	Profit	470K	498k	506k	469k
	ROI	224%	262%	269%	223%
Solar Panels	IRR	23%	26%	27%	23%
	Profit	487k	514k	520k	486k
	ROI	193%	224%	233%	191%

5.5 Summary

In summary, the findings elucidated within this technical exposition underscore that each of the four propulsion architectures subjected to investigation yields a commendable payback period of approximately four years, accompanied by an impressive return on investment, averaging around 200%. This robust return on investment remains consistent irrespective of the electricity procurement methodology employed to compute the total cost of ownership for electric vehicles.

However, upon a meticulous examination of the architectures from an investment perspective, it becomes evident that Architecture 2, characterized by utilizing a multispeed gearbox, and Architecture 3, distinguished by incorporating two electric machines in series, emerge as the most economically favorable options. Both Architecture 2 and Architecture 3 manifest an Internal Rate of Return (IRR) that surpasses their counterparts by a notable margin of 20%, coupled with a residual value of approximately 5% at the culmination of their investment lifecycle. This advantageous performance is attributed to the adept operation of the electric machine within these architectures, consistently operating within the most efficient regions of the electric machine efficiency map.

Collectively, this technical treatise furnishes invaluable insights into the economic feasibility of electric vehicles while underscoring the pivotal significance of judiciously selecting the most efficient propulsion architecture to optimize financial outcomes.

Chapter 6

Regenerative Braking Efficiency and Driveability

Vehicle electrification is growing in all major markets and segments. The light-duty electrified vehicles market grew three times from 2018 to 2021 and 8 times when comparing 2021 sales volume with 2016. The light commercial vehicle sales volume grew 70% from 2020 to 2021. The number of light-duty electrified models offered in 2022 is 450, five times more than in 2015. In the heavy-duty segment, the sales volume of electric buses went up, reaching 40% higher sales volume in the last year alone. [216]

The average EV range of light-duty electric vehicles improved by three times from 2010 to 2020. This significant improvement was mainly due to technological advances in battery chemistry (energy and power density), electric motor and power electronics efficiency, and thermal management advancements. [216]

The technological shift from internal combustion engines to total electrification of the propulsion system is a continuous process, and in three years, a product can become obsolete regarding its performance. This scenario of a fast technology shift and technology improvement creates the need to introduce many products quickly, forcing the manufacturers to find design methods and processes to reduce product development time and its associated investments.

An essential feature of improving electric vehicle energy efficiency is the ability of these vehicles to recover the kinetic energy during decelerations and store it as chemical energy in the battery back instead of dissipating this energy in the form of heat when friction brakes are used. This recovered energy could be used to propel the vehicle or to power the auxiliary loads, increasing the overall vehicle energy efficiency.

During the regenerative braking event, the electric machine applies a negative torque to the driveline, which decelerates the car. Three high-level strategies can be used to execute regenerative braking, two of them using the brake pedal as the main actuation from the driver, and one where the accelerator pedal is the main actuation from the driver (this is called one pedal drive strategy - OPD) [217]. The strategies for using the brake pedal are the focus of this chapter. OPD will be discussed in Chapter 7.

Figure 6.1 shows a schematic of each regenerative braking strategy for low-level accelerations. In the following sessions, the three regenerative braking strategies are presented together with the strategy developed for this work.

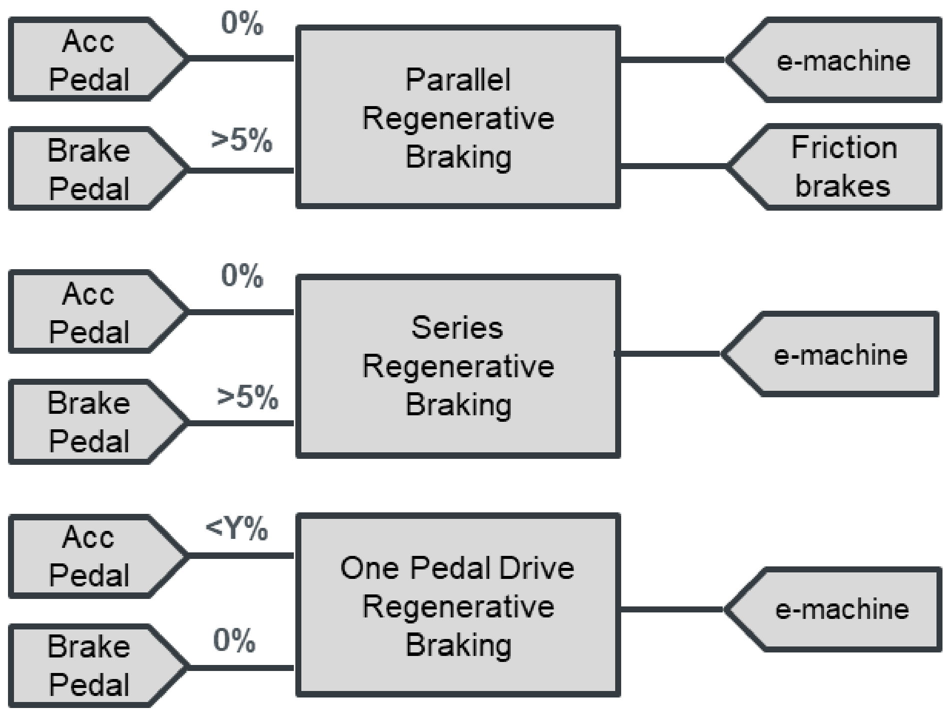

Figure 6.1:Regenerative braking strategies overview.

Another form of regeneration strategy, which the driver does not control, is the e-coasting, where without any command from the driver (both accelerator and brake pedal are released), the vehicle "freely coasts" with a minimum braking torque applied by the electric motors (or because the back electromagnetic force) or for some calibrated torque curve in the function of the vehicle speed [218], [219].

Regenerative braking is essential for the total energy efficiency of the vehicle and to reduce the maintenance cost of the braking system components while reducing the total cost of ownership. The regenerative braking system also heavily impacts the vehicle's drivability and the driver and passengers feeling during the deceleration maneuvers. The design of the braking system architecture and its interactions with the propulsion system is an emerging field of study introduced in the electrification era. Its interactions' resultant performance impacts the system's energy efficiency and braking performance, which are vital customer performance indicators.

Electric vehicle clients of different segments are looking for diverse product attributes. For example, in light passenger vehicles, the clients are looking for the total electric range and the charging time; whether in light commercial or heavy-duty segments, the clients are looking more at the total cost of ownership and the reliability of the vehicle as a system.

However, for all types of vehicles and all segments, energy efficiency is of central importance as it is the main factor behind the total electric range and operation cost of an electric vehicle [219].

This Chapter investigates different regenerative braking strategies applied to light commercial electric vehicles and compares them regarding their energy efficiency and drivability. The energy efficiency assessment simulates the vehicle's different regenerative braking strategies in five driving cycles. The drivability in decelerating maneuvers is performed using a driver-in-the-loop simulation using a static driving simulator.

The Chapter proposes an integrated model-in-the-loop (MiL) and driver-in-the-loop (DiL) approach, where the interactions of the propulsion system with the braking system could be evaluated in both aspects, energy efficiency and drivability (objectively and subjectively).

The development of the different systems and their control strategies uses a model-in-the-loop tool capable of representing the system and its interactions by using one-dimensional (1D) static, quasi-static, and physical models. 1D models are a very inexpensive tool that provides the capability to test many different architecture solutions at the system and subsystem levels, allowing the application of hundreds of trade-off studies without building numbers of prototypes. However, the traditional 1D models use a PID controller to represent the driver. They use known driving cycles as input to the simulation, making the model-in-the-loop limited for simulations focused on the driver's interactions with the system.

Driving simulation, due to the possibility of creating virtual scenarios, such as different weather and traffic conditions, brings the ability to develop the system in a virtual environment, including the driver in the loop, without building any prototype, allowing the engineering organizations to shorten the development time and to reduce the associated investments in product development.

Driver-in-the-loop simulation is being extensively used in the development of chassis subsystems and their components (e.g., suspension, tires, brakes, ABS calibration, etc.), but it's also being used to study the driver behavior and the driver interaction with the vehicle, to develop autonomous and advanced driver assistance systems (ADAS). Nevertheless, its application as a tool to develop electrified propulsion systems is not yet broadly used.

This chapter presents the comparison of two different regenerative braking strategies' energy in regard to their energy efficiency and drivability performance using the pedal travel and longitudinal acceleration and acceleration ratio as the evaluation metrics.

6.1 Regenerative Braking Strategies

The performance of the braking system and the braking feeling performance is recognized as one of the most critical factors in the automotive industry's voice of customers.

The most used metric of braking performance evaluation is the stopping distance and timing with the brake pedal fully pressed. In the real world, braking a car is related to continuing braking maneuvers for speed reduction or light decelerations with the brake pedal gradually pushed. The essential braking performances are a quick response time, with less brake pedal force, smooth deceleration, and low or no body motion. Braking performance with jerky behavior, which means rapid brake response to the pedal command, is considered exhausting and discomfort for the driver and vehicle passengers. At the same time, a response that is too slow causes a longer braking distance and provides the worst feeling of bad braking performance. Another essential characteristic of a well-designed braking system is its linearity. A slow initial response followed by a fast response later or vice versa makes it hard for the driver to control the deceleration during braking maneuvers and causes additional uncomforting deceleration conditions for the driver and the passengers [220].

It's possible to classify the deceleration maneuver according to its intensity: low level, with decelerations up to 0.3 g's; medium level, with decelerations in the range of 0.3 g's up to 0.8 g's; and emergency braking, with decelerations above 0.8 g's, when the ABS usually starts to influence the braking. [220] shows that daily driving decelerations are not greater than 0.3g and are always considered low-level decelerations.

The authors in [220] propose that quick braking response time, brake pedal force, and brake pedal travel are the main design metrics for an excellent braking system. In this study, we develop all the analyses based on brake pedal travel.

The electrification of the propulsion system and the addition of the regenerative braking function create an interaction between the braking system and the propulsion system torque management control. The deceleration performances and the braking feel are impacted by the operation of the electric motor. At the same time, the overall propulsion system energy efficiency is affected by how much kinetic is dissipated as heat using friction brakes and how much is recovered using an electric machine brake.

The braking feeling and performance shall be maintained constant, regardless of how much braking torque is coming from each actuator (friction brake or electric machine). Thereby, regenerative braking strategies presented in this study are developed to meet a trade-off between energy efficiency and braking comfort.

6.1.1 Target Brake Pedal Curves

In the analysis presented in [220], the author proposes three different brake pedal curves with deceleration as a function of pedal travel. These curves are for various vehicle segments and are shown in Figure 6.2. This study focuses on developing a regenerative braking strategy for a light commercial vehicle (LCV) and uses the truck brake pedal curve as a design target.

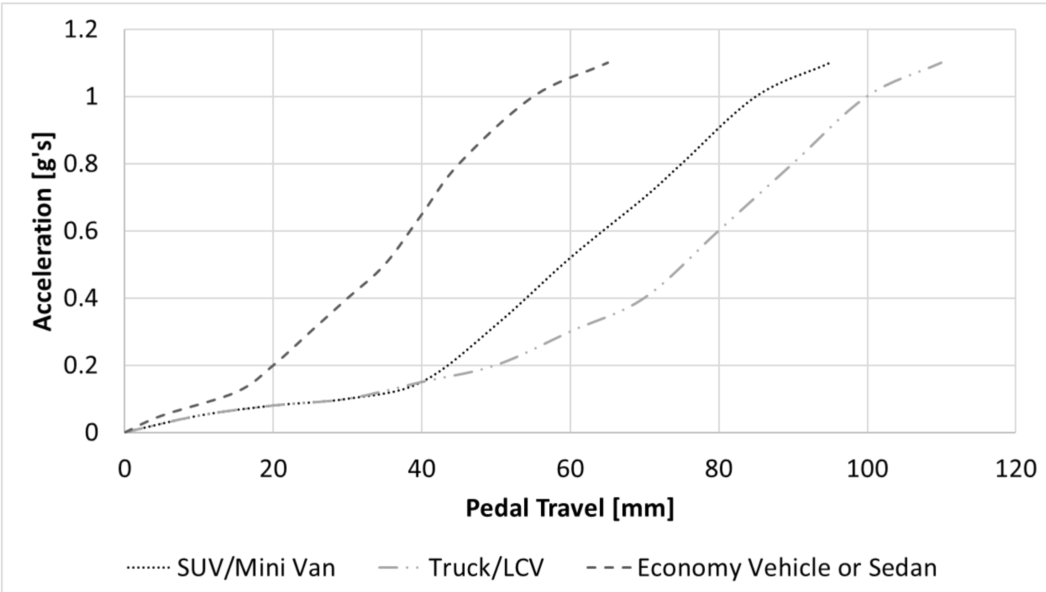

Figure 6.2: Theoretical brake pedal deceleration curves as a function of pedal travel for different vehicle applications.

Figure 6.3 shows the proposed pedal brake travel target curve concerning the desired deceleration and the longitudinal braking force at the wheels.

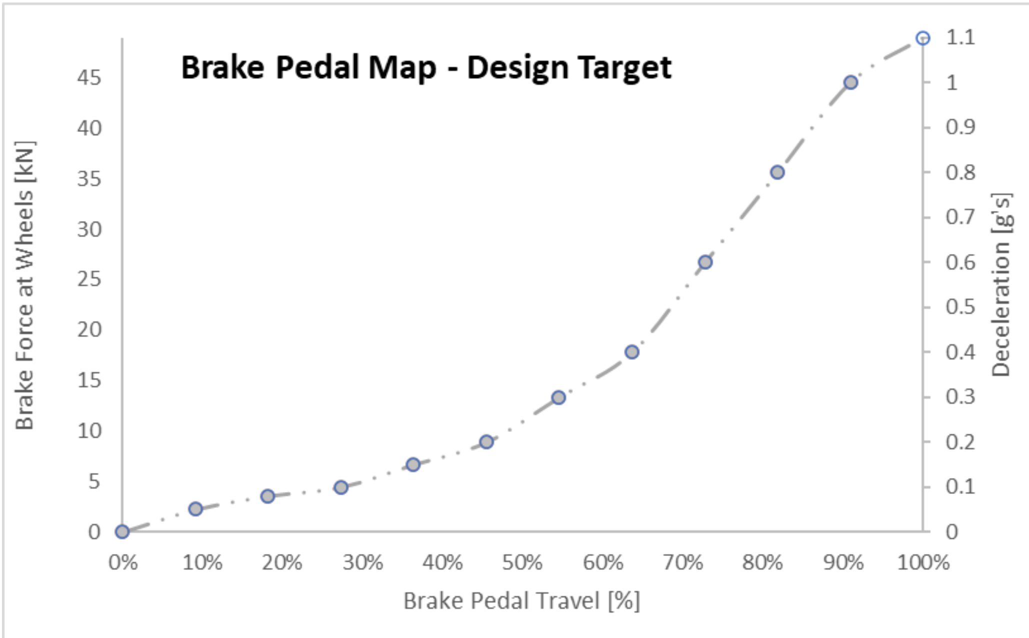

Figure 6.3: Target brake pedal curve developed for a light-commercial vehicle with 4540kg GVW.

6.1.2 Series Regenerative Braking Strategy

The series regenerative braking requires a braking-by-wire system that, based on the pedal travel requested by the driver, estimates the total force needed at wheels for the desired vehicle deceleration and adjusts the amount of friction brake from the calipers and mechanical brake from the electric machines. This integrated control strategy is calibrated for energy recuperation maximization while maintaining good braking performance and feel. In the technical literature, some authors present that a series regeneration may improve the energy efficiency by 30% in official driving cycles; however, due to its more complex hardware architecture and software, better system efficiency comes with a higher material cost and higher development cost [221].

The brake pedal curve developed for this paper, which represents the series regenerative braking strategy, is presented in Figure 6.4. The amount of mechanical brake from the electric machine was defined as the maximum amount to maximize the kinetic energy recovery in low-level decelerations or decelerations of up to 0.3g when the vehicle is loaded with its Gross Vehicle Weight (GVW).

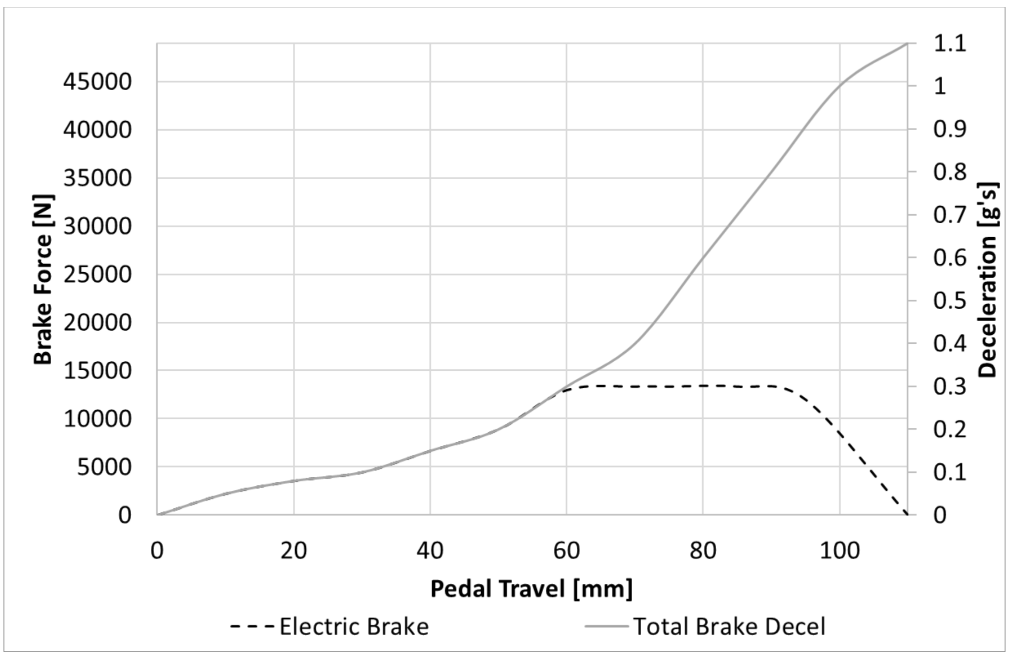

Figure 6.4: Serie regenerative braking strategy to maximize energy recovery for accelerations up to 0.3 g.

6.1.3 Parallel Regenerative Braking Strategy

The parallel regenerative braking strategy developed for this paper is applied in parallel to the friction brakes without any integrated chassis-propulsion system controllers. The regenerative braking force from the electric motors works in parallel with the friction brakes and increases as a function of the pedal travel. In the technical literature, some authors present an improved efficiency of up to 18% in energy efficiency; however, it compromises the braking feeling since it increases the pedal response time [221].

To improve the energy regeneration efficiency, the proposed brake pedal curve for the parallel regenerative braking strategy, shown in Figure 6.5, deviates from its original target. Consequently, the total brake force and the resultant deceleration performance are like the proposed curve for SUVs and Mini Vans, as shown in Figure 6.6.

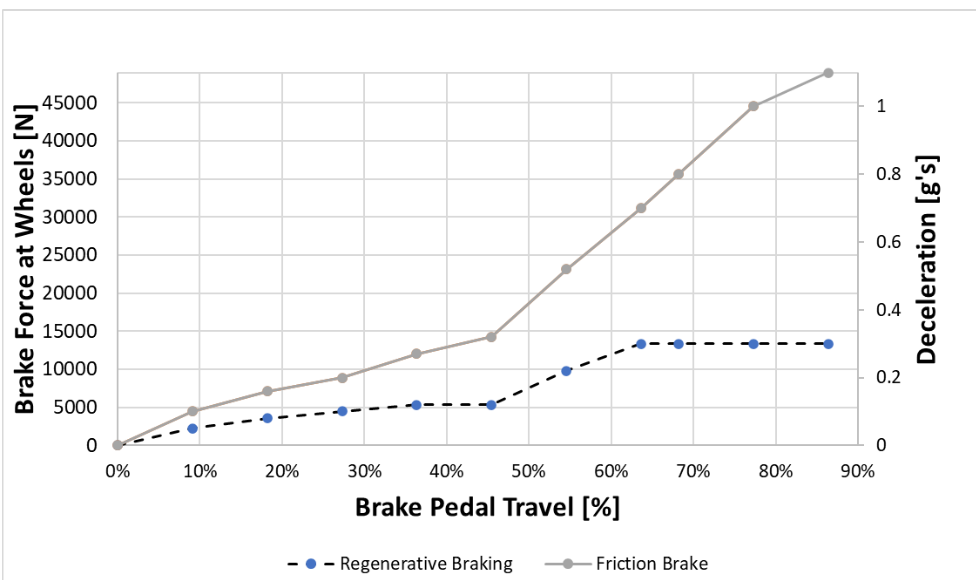

Figure 6.5: Parallel regenerative braking strategy to maximize energy recovery for accelerations up to 0.3 g with a compromise to the brake feel the performance.

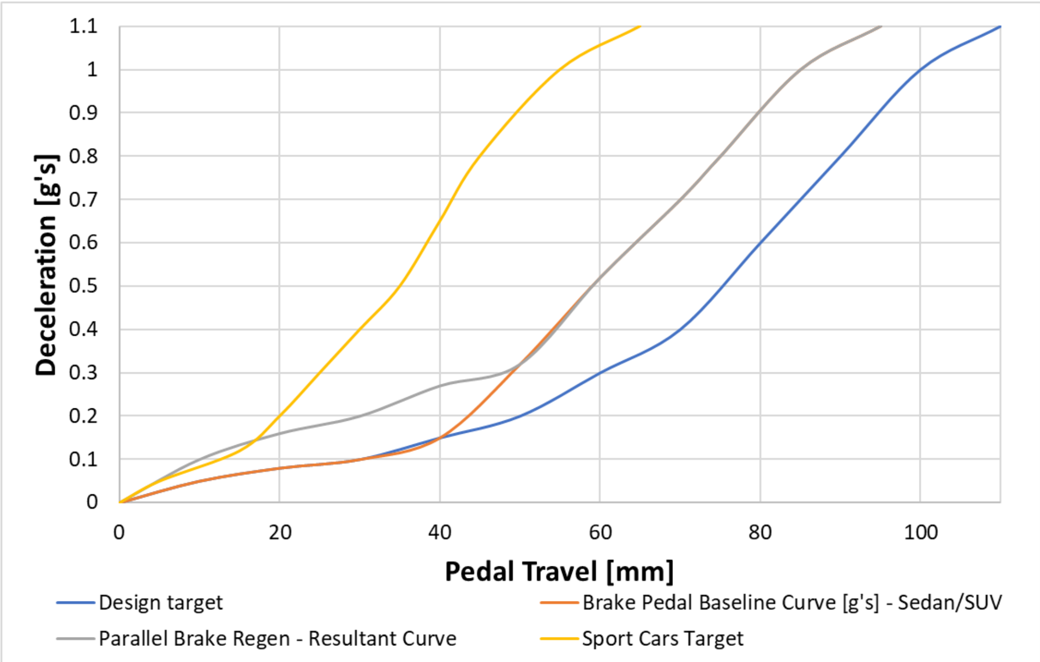

Figure 6.6: Parallel regenerative braking strategy brake pedal curve compared with the target and theoretical brake pedal curves.

6.2 Study Case

6.2.1 Vehicle

The study focuses on its application in a light commercial vehicle. The vehicle characteristics are shown in Table 6.1.

Table 6.1: Battery electric front wheel drive light-commercial vehicle.

		Curb	**GVW**
Road Load Coefficients	A [N]	210	270
	B [N/kph]	0.4067	0.4067
	C [N/kph2]	0.09185	0.09181
	Weight [kg]	2530	4540
	Tire type	215/75R16	
	Tire length [m]	2.2898c	

6.2.2 Modelling

This study adopted a forward vehicle model for the one-dimensional model. The forward model uses a driver model, modeled as a PID controller, which compares the desired speed with the vehicle's output speed, calculated on the plant model [207]. The forward model propagates the dynamic phenomena, deals with measurable variables in the real world, and requires a supervisory controller model, where the torque management and regenerative braking strategies are modeled. Figure 6.7 shows a high-level system, while Figure 6.8 shows the propagation model at the level of the propulsion system of an electric vehicle.

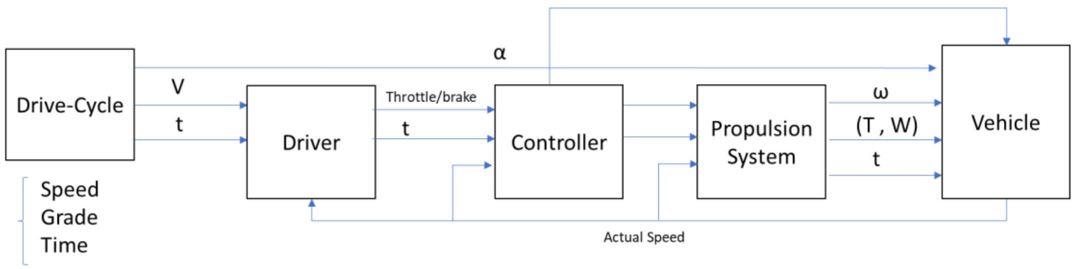

Figure 6.7: 1D model architecture used to simulate a Front Wheel Drive (FWD) electric vehicle with different regenerative braking strategies.

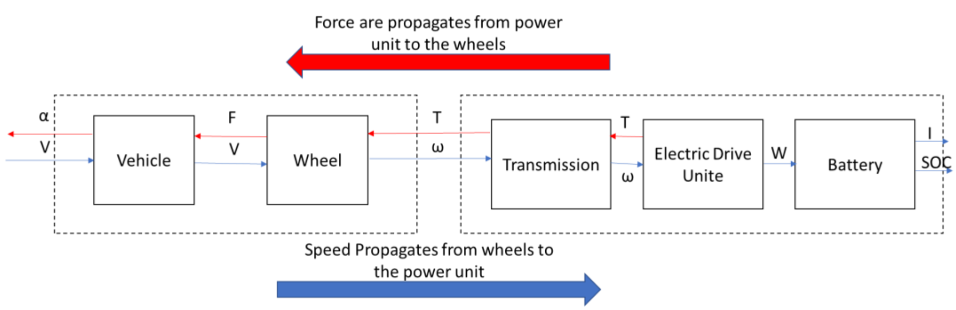

Figure 6.8: 1D model system interaction propagation.

In Figure 6.7 and Figure 6.8, V is the driving cycle input speed, t is the driving cycle input time, and α is the driving cycle input slope. The throttle and brake signals are relative to pedal travel, and the actual speed is the calculated vehicle speed measured at the contact point of the tires and the driving surface. The HV Battery DC is represented by I, and the State of Charge is represented by SOC. ω is the angular wheel speed.

6.2.3 Driver-in-the-Loop (DiL)

The driving simulator used in this work is a static simulator located at the McMaster Automotive Resource Centre (MARC), in Hamilton, Canada. The MARCdrive simulator has been presented and detailed in [205]. It houses a highly immersive environment, using a real vehicle body in Front of a 210-degree curved screen. The active steering, seat, and seatbelts give motion cues. As exemplified in [222], such a setup can be used for drivability evaluation. The present work aims to leverage such a tool for performing realistic brake pedal inputs. Figure 6.9 shows the driving simulator used for this experiment.

Figure 6.9: The MARCdrive simulator, located at McMaster Automotive Resource Centre (MARC), in Hamilton, Canada.

The model presented in Figure 6.7 was implemented, replacing the PID pedal control with a real driver. Given the open-loop nature of driving simulation, where an actual human driver performs the maneuver, the driving cycle inputs are suppressed from the model, and a real driver commands the accelerator and brake pedals. The static vehicle model gives room to a 14 DOF vehicle model that accounts for translational and rotational motion of the vehicle's body in all three dimensions, plus the rotational and bounce of each wheel. The tests are conducted in a virtual environment – an infinite three-lane test track. The virtual road emulates a flat, dry asphalt condition that is consistent and smooth throughout the entire route.

6.3 Results and Analysis

6.3.1 Energy Efficiency

The energy efficiency of different regenerative braking strategies is compared using official driving cycles representing various urban and highway traffic conditions. The driving cycle and its main characteristics are shown in Table 6.2.

Table 6.2: Driving cycle summary and characteristics.

	Driving Cycles		
	Distance	Max Speed	AVG Speed
	[km]	[km/h]	[km/h]
LA92	17.7	107.5	36.7
NY_city	1.9	44.3	11.4
US06	12.8	128.5	77.3
FTP75	17.7	90.7	33.9
WLTP High	7.2	97.4	24.6

The energy efficiency of each regenerative braking strategy was calculated from its energy consumption (kWh/km) in each driving cycle. Table 6.3 shows the energy consumption for each driving cycle with the vehicle at its curb weight plus 100kg, representing an 80kg driver plus carry-on items. Table 6.4 shows the energy consumption for each driving cycle with the vehicle at GVW.

Table 6.3: Electric energy consumption in the driving cycles with the vehicle at curb weight plus 100kg.

	Energy Consumption [kWh/km]		
	Curb+100		
	Series Regen	Parallel Regen	dif
LA92	0.076	0.097	22%
NY_city	0.125	0.205	39%
US06	0.346	0.380	9%
FTP75	0.164	0.205	20%
WLTP High	0.816	0.914	11%

Table 6.4: Electric energy consumption in the driving cycles with the vehicle at GVW.

Energy Consumption [kWh/km]

	GVW		
	Series Regen	Parallel Regen	dif
LA92	0.086	0.126	32%
NY_city	0.165	0.294	44%
US06	0.366	0.432	15%
FTP75	0.179	0.256	30%
WLTP High	0.845	1.042	19%

The series regenerative braking strategy improves energy consumption for all studied conditions. The benefit reaches a maximum of approximately 44% in the new york city cycle when the vehicle is fully loaded and a minimum of 9% in the US06 cycle when the vehicle is at curb weight plus 100kg. Two examples of the difference in the SOC for each regeneration strategy are shown in Figure 6.10 and Figure 6.11; the LA92 and US06 cycle plots provide a better visualization of regeneration events.

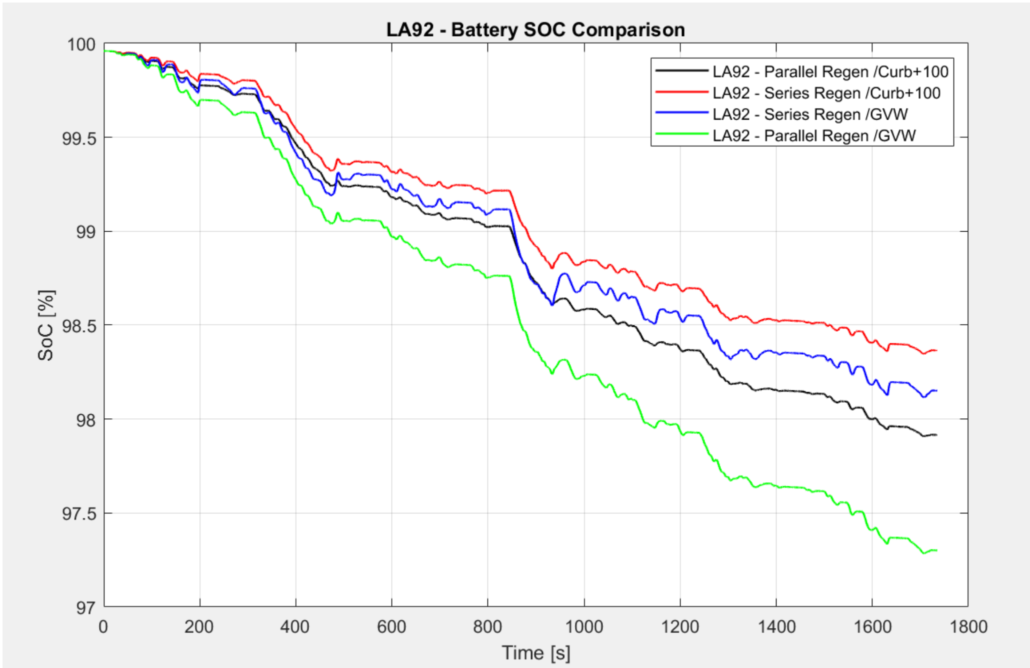

Figure 6.10: High voltage battery state-of-charge for all simulated cases on the LA92 driving cycle.

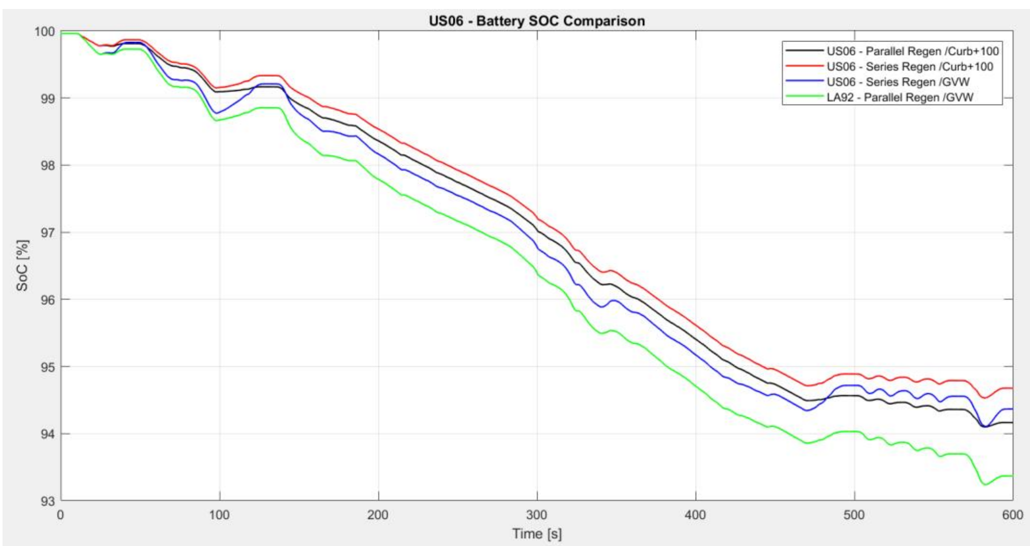

Figure 6.11: High voltage battery state-of-charge for all simulated cases on the US06 driving cycle.

To calculate the efficiency of the regenerative braking strategy, the total kinetic energy available on wheels was compared with the total electrical energy stored in the battery pack. The results are presented in Table 6.5. On average, the parallel regenerative braking strategy showed an efficiency of 28% and 33% for the vehicle at curb+100kg and GVW, respectively. The series regenerative braking strategy presented an efficiency of 69% and 75%, respectively, for curb+100kg and GVW.

Table 6.5: Energy recovery global efficiency.

	Regenerative Braking Efficiency			
	Curb+100		**GVW**	
	Series Regen	Parallel Regen	Series Regen	Parallel Regen
LA92	67%	28%	73%	32%
NY_city	69%	29%	73%	33%
US06	72%	30%	77%	35%
FTP75	70%	28%	76%	33%
WLTP High	68%	27%	75%	32%

An energy balance is presented in Figure 6.12 and Figure 6.13 for the driving cycle with higher and lower improvement.

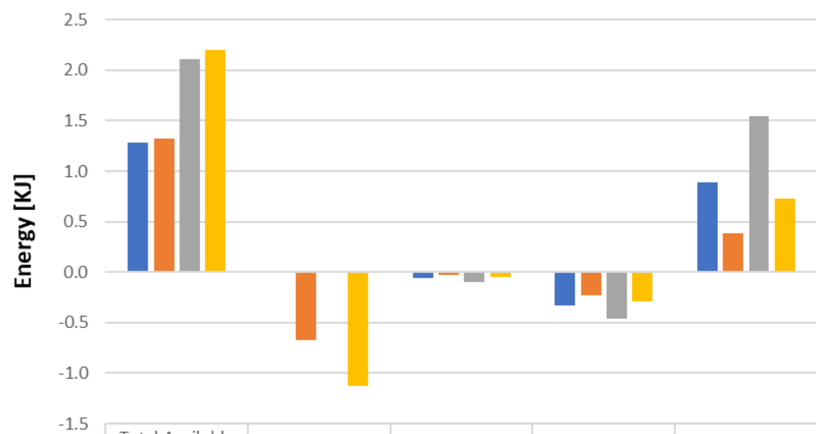

	Total Available Energy to Recover	Friction Braking Loss	Gearboss Regen Loss	e-Machine Regen Loss	Total Recovered
Curb+100 Series Regen	1.3	0.0	-0.1	-0.3	0.9
Curb+100 Parallel Regen	1.3	-0.7	0.0	-0.2	0.4
GVW Series Regen	2.1	0.0	-0.1	-0.5	1.5
GVW Parallel Regen	2.2	-1.1	-0.1	-0.3	0.7

Figure 6.12: NY city cycle regenerative braking energy balance.

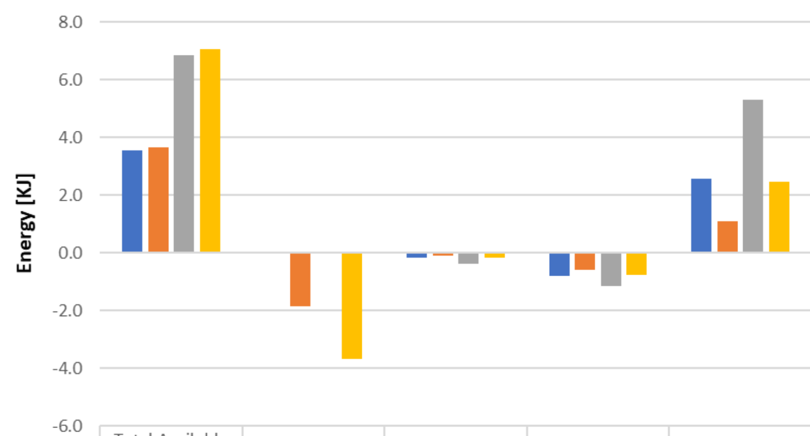

	Total Available Energy to Recover	Friction Braking Loss	Gearboss Regen Loss	e-Machine Regen Loss	Total Recovered
Curb+100 Series Regen	3.5	0.0	-0.2	-0.8	2.6
Curb+100 Parallel Regen	3.6	-1.9	-0.1	-0.6	1.1
GVW Series Regen	6.8	0.0	-0.4	-1.2	5.3
GVW Parallel Regen	7.1	-3.7	-0.2	-0.8	2.4

Figure 6.13: US06 cycle regenerative braking energy.

6.3.2 Drivability

An experienced driver tested the virtual model in the driving simulator on a flat road for the driveability evaluation. One vehicle configuration was tested using the full virtual driving simulator to develop the brake travel curves for each percentage of brake pedal used in this study.

Driver instructions included accelerating the vehicle until a velocity higher than 90 kph, releasing the throttle, letting the vehicle coast to 80 kph, and then applying the brake pedal to the desired level. The ramp should reach the desired level in less than a second, with a tolerance of ± 5%, and then a constant pedal should be achieved within the next second, with a tolerance of ± 2%. The steady pedal remains until the vehicle stops.

Using a real driver to acquire the brake pedal profile adds realism to the simulated experiments. The maneuvers are conducted for the parallel topology in the Curb+100 configuration. The difficulty in maintaining low pedal values (10-20%) is noted in the results, as well as the aggressive response of the vehicle to higher levels (60-70%). Such human perceptions were used in defining the range in which the systems were tested (10-70%). For medium-level pedals (30-50%), the difficulty lies in reaching the desired level in a consistent ramp and remaining with the constant pedal. That difficulty is more remarkable for the 30-35% pedal position.

In summary, seven levels of brake pedal were tested from 10% to 70%, evenly spaced by 10% each. Four vehicle configurations were simulated: vehicle at curb weight plus 100kg with series and parallel regenerative braking strategy curves, and vehicle at GVW with the series and parallel regenerative braking strategy.

In addition, the simulator enables the recording of the human-performed brake profile and its identical reproduction between the different test cases. That repeatability is difficult, if not impossible, to achieve in physical experiments. That promotes a fair performance comparison since it evaluates every system with the same input.

Seven different metrics evaluate the vehicle's performance in deceleration maneuvers [223]. The metrics are listed below:

1. Longitudinal acceleration in m/s^2
2. Jerk while releasing accelerator pedal in m/s^3
3. Jerk while pressing the brake pedal m/s^3
4. Jerk while releasing the brake pedal m/s^3
5. Jerk while pressing the accelerator pedal from a braking maneuver m/s^3
6. Quickness in s^{-1}
7. Minimum trailing distance and time

Nonetheless, with the driving simulator, all seven metrics could be evaluated without any change to the model; for this study, the longitudinal acceleration, measured at the vehicle center of gravity, and the jerk, measured at the driver seat, while pressing the brake pedal are evaluated.

Figure 6.14, Figure 6.15, and Figure 6.16 show the deceleration curves of each evaluated scenario for 10%, 20%, and 30% brake pedal travel, respectively. For short pedal travel, the parallel regeneration strategy develops a 25% higher deceleration level than the series regeneration strategy, which is a metric that shows a faster braking response for the parallel strategy. An average of 25% quickness for the parallel regeneration is seen along all the brake pedal curves.

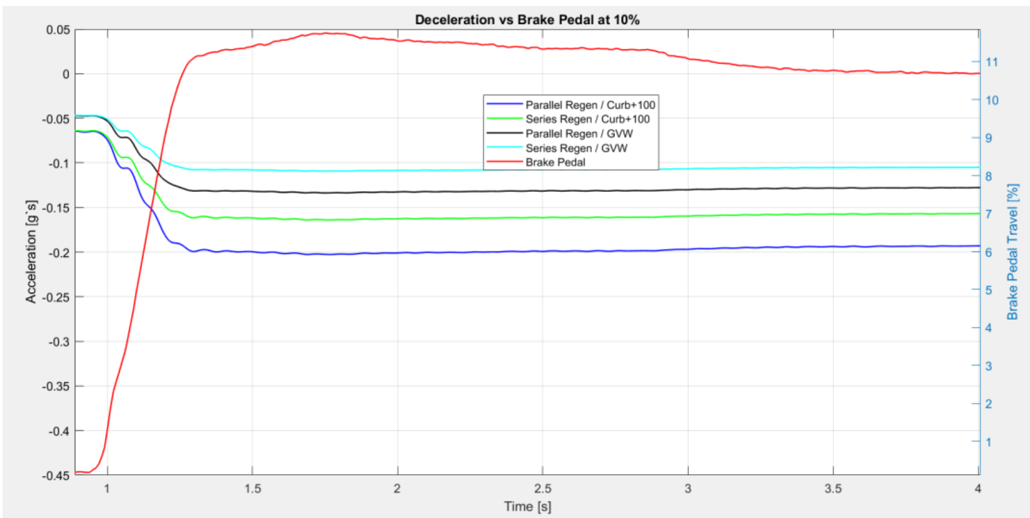

Figure 6.14: Braking Maneuver at a 10% brake pedal.

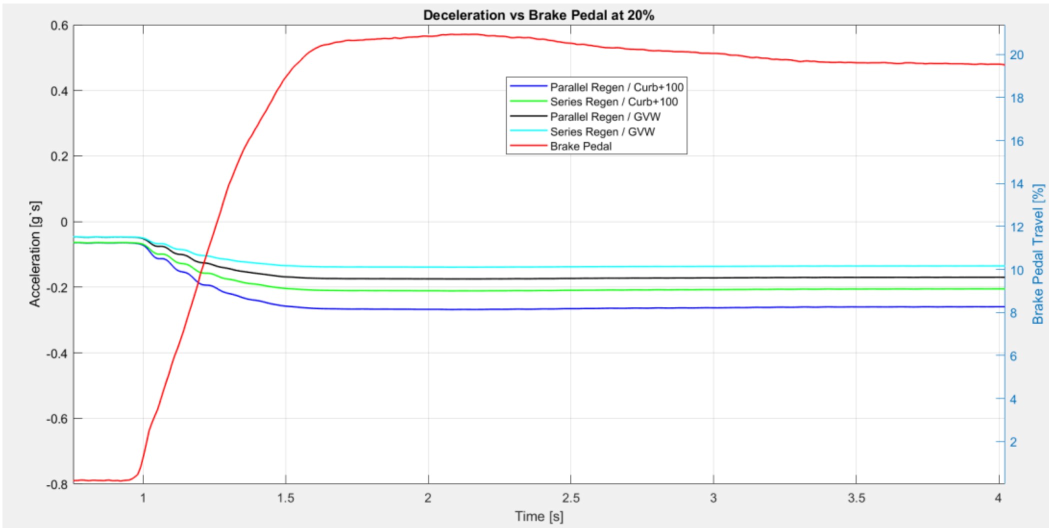

Figure 6.15: Braking Maneuver at a 20% brake pedal.

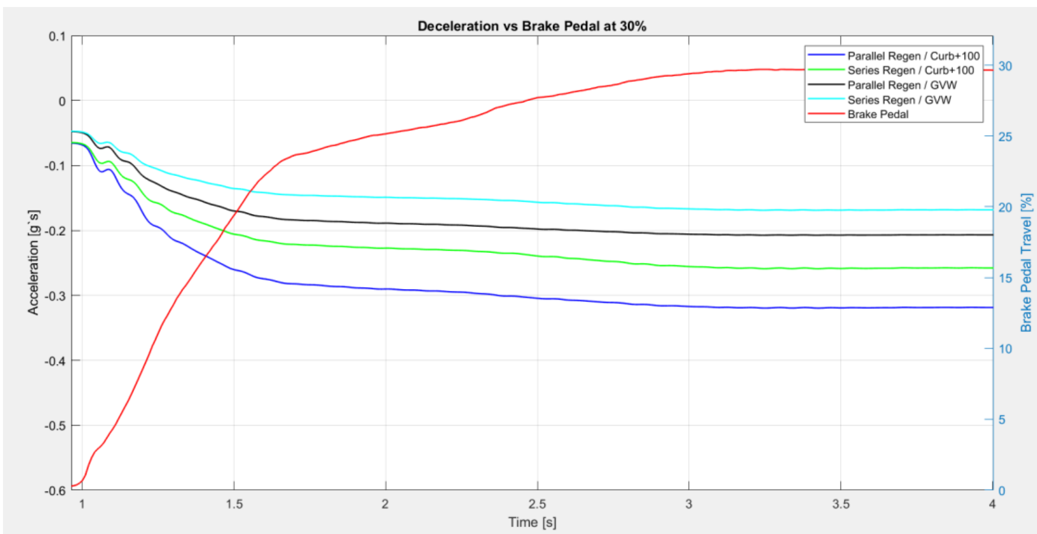

Figure 6.16: Braking Maneuver at a 30% brake pedal.

The perception of an uncomfortable maneuver increases almost linearly with the longitudinal acceleration level. Longitudinal accelerations greater than 2 m/s^2, or approximately 0.2 g's are considered uncomfortable [224]. The parallel regeneration strategy delivers its deceleration at 10% brake pedal position when the vehicle is at curb weight plus 100kg. Meanwhile, the series regeneration strategy presented this acceleration at a 30% brake pedal position.

In non-emergency longitudinal accelerations, jerks of 1-1.5 m/s^3 are considered normal and comfortable, and jerks of to 5 m/s^3 are considered acceptable, and above that are considered uncomfortable, with jerks above 8 m/s^3 being acceptable only for emergency accelerations [224].

The comfort comparison of each brake regeneration strategy relies on the jerk analysis while pressing the brake pedal for all four studied cases and all seven levels of pedal position. The jerk was calculated from the acceleration measured at the driver's seat, as proposed by [225]. The results estimated from the maneuvers executed using the driving simulator are presented in Figure 6.17.

The uncomfortable limit of 5 m/s^3 jerk is achieved at 10% of brake pedal travel when the vehicle is at curb weight plus 100kg and 55% of brake pedal travel at GVW. The jerks caused by braking maneuvers using the parallel strategy were always above the range considered comfortable (1.5 m/s^3), regardless of the pedal position and vehicle deceleration.

On the other hand, the series regen strategy delivers very comfortable acceptable jerk behavior for all low-level accelerations (below 0.3 g's) when in its curb weight plus 100kg and comfortable braking conditions when in GVW. The series regeneration shows a better braking performance for comfort.

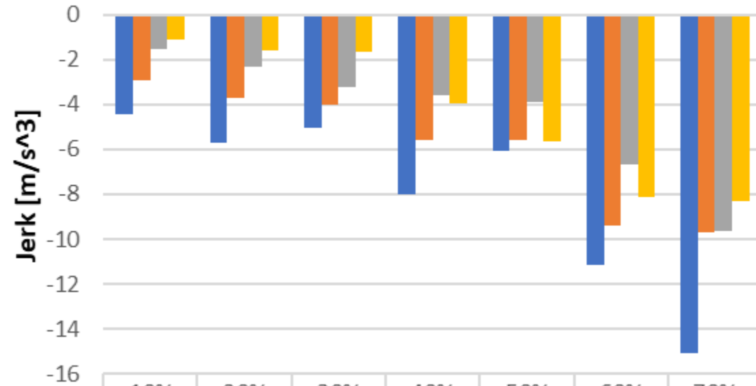

	10%	20%	30%	40%	50%	60%	70%
Parallel Regen Curb+100	-4.45	-5.71	-5.06	-8.03	-6.04	-11.15	-15.1
Series Series Curb+100	-2.91	-3.74	-4	-5.6	-5.6	-9.4	-9.67
Parallel Regen GVW	-1.52	-2.32	-3.22	-3.6	-3.92	-6.7	-9.65
Series Regen GVW	-1.1	-1.6	-1.65	-3.95	-5.65	-8.15	-8.3

Figure 6.17: Jerk while pressing the brake pedal for four vehicle configurations and seven different pedal positions.

6.4 Summary

This chapter intends to demonstrate the ability to integrate a propulsion system model developed in a one-dimensional model-in-the-loop approach applied in a driver-in-the-loop simulation to evaluate different regenerative braking strategies. The logged data from the driver-in-the-loop simulation confirmed the subjective perceptions of the driver.

Nevertheless, the study case demonstrates a better energy efficiency and driveability performance of the series regenerative braking system compared to the parallel regenerative braking system. The efficiency difference is bigger when compared with the vehicle at full load and can be as high as 44% for urban application, as seen in the New York City Cyle. The drivability difference is bigger when the vehicle is empty.

Efficiency is even more important for commercial vehicles since it directly impacts the total cost of ownership, which is the most important functional objective for these vehicles. In future studies, the author foresees the need for research that solves the efficiency of parallel braking systems without the need to add complex and expensive brake-by-wire systems.

Chapter 7

Adaptative One-Pedal-Drive Regenerative Braking

The transportation system is one the most significant contributors to air pollution and CO2 emissions, being one of the leading causes of the global average temperature increase. During the COVID-19 great lockdown, with the shutdown of the economy, we have seen the transportation system contributing to a daily -7.5 MtCO2, as mentioned in Chapter 2, a 36% reduction compared to the previous year.

More than a billion vehicles are on the streets worldwide, and every year, more than 80 million new vehicles get to our cities' streets and highways. The electrification of 40% of the transportation system, powered by renewable electricity, is a way of helping meet the targets defined in the Paris Agreement to limit the average temperature increase to 1.5C by 2030, as concluded in Chapter 2.

Electric vehicles are economically attractive since their total cost of ownership is about 80% lower than the equivalent vehicle equipped with an internal combustion engine. These differences will vary depending on the daily mileage and factors such as total system efficiency. The benefit limits of electric vehicles do not include their positive environmental impacts. Still, their lower total cost of ownership makes electric vehicles very attractive economically, therefore being a natural choice for fleet operators.

In 2022, electric buses and trucks represented 4.5% and 1.2% of the total sales, respectively, and 90% of the electric trucks were boxe trucks with a max GVW of 10,000 lbs [226]. [227], indicates that by 2035, 50% of all new buses and trucks will be electric and that by 2040, 40% of all commercial vehicles worldwide will be full electric vehicles.

The utilization of electric motors creates a wide range of new operational modes, as stated in Chapter 3, and one operating mode is crucial to improving the electrified vehicles' efficiency: regenerative braking. According to Chapter 6, there are three ways of performing regenerative braking: series and parallel, which both uses the brake pedal as the sensor to command the braking, and one-pedal-drive (OPD), which uses the accelerator pedal to command positive and negative Torque.

The performance of the braking system and the braking "feeling" are essential safety and driveability attributes. As stated in Chapter 6, decelerations of up to 0.3 g's are considered low-level accelerations and, in electric vehicles, can be fully executed by the electric motors.

Regenerative braking increases the total propulsion system efficiency of electric vehicles; however, the benefits of regenerative braking are a function of the brake subsystem architecture and the control calibration. The energy consumption difference between series regenerative braking and parallel regenerative braking in a 10,000 lbs commercial vehicle can reach up to around 50%, depending on the driving cycle [228].

Although the series regenerative braking provides clear benefits to the system's energy efficiency, its application depends on a complex braking control module, which integrates electronic and anti-lock braking systems (EBS and ABS) with a brake-by-wire pedal, allowing the braking system to control the electric motors without acting to the hydraulic or pneumatic braking circuit. The development of such a system requires a number of vehicles to be tested in a "zero" drag surface, which makes its development very expensive.

Even if ABS and EBS are very common in light-passenger vehicles, and brake-by-wire is becoming the standard for electric vehicles, the same is not valid for commercial vehicles, which usually are produced in low volume and don't receive technologies that require high volume production to pay back the investment of developing its application. In this context, the OPD becomes a vital option to optimize the ability of commercial vehicles to recover energy during decelerations.

The OPD allows the driver to launch, accelerate, brake, park, and stop the vehicle only using the accelerator pedal. The accelerator pedal generates the signal, and the electric machines work as a single actuator to brake the vehicle. The OPD allows the driver to operate the vehicle naturally by only using one pedal while freely selecting the intensity of the accelerations or allowing the vehicle to coast or creep, depending on the pedal's position [217].

However, the braking acceleration is a function of the vehicle mass and the applied braking force. For a vehicle with a gross vehicle weight 100% heavier than its weight when empty, the same braking force that produces a braking acceleration of 0.3 g's at GVW will deliver an acceleration of 0.6 g's at its curb weight. This level of acceleration is seen during an emergency braking.

An efficient OPD calibration for the loaded vehicle wouldn't be safe and comfortable in the empty vehicle, and an optimum OPD calibration for the empty vehicle wouldn't be efficient and generate enough braking torque for the loaded vehicle.

This Chapter proposes an adaptative one-pedal drive (A-OPD) strategy for electric commercial vehicles, which addresses the problem of an optimum OPD for commercial vehicles with significant differences between curb and gross vehicle weight (GVW).

The proposal consists of an algorithm that estimates the actual vehicle running mass and road grade using an RLS (recursive least square filter). The estimated running mass is a classification variable that chooses between pre-calibrated A-OPD regenerative torque maps. For this Chapter, three levels of A-OPD torque maps are used.

The strategy allows the driver to feel the OPD operating similarly, independent if at the curb or GVW or at an intermediate weight between the lower and upper weight limit. The A-OPD is intended to increase the overall energy efficiency of real-world driving while simultaneously maintaining driveability, performance, and safety.

In this Chapter, we presented the drive-by-wire pedal for torque management control and how it is used to control the conventional one-pedal-drive (OPD) braking. Then, we present an A-OPD method application and the central role of the RLS filter for mass estimation in addressing this challenge. Subsequently, we outline the results of the A-OPD method compared to a conventional OPD and series and parallel regenerative braking, which are commanded by using the braking pedal.

7.1 Electric Vehicle Controls

During an automotive product development phase in the 1970s, the auto industry spent about 5% of the vehicle's validation resources on electro-electronic components and software. In the 2010s, this number reached 35% of all validation tests and resources. With the introduction of electric vehicles, complex ADAS systems, and newer OTA (over-the-air) features, today, 50% of all test resources are dedicated to electro-electronics and SW validation. Entry-level vehicles have approximately 100 electric control units (ECUs), while high-end electric vehicles have around 150 ECUs, reaching about 150 million lines of code [229].

Vehicles are becoming software-defined machines, whereas mechanicals are becoming commodities, and at the same time, their software application features significantly impact the product value. Software is what differentiates automobiles [230].

Typical automotive controls and electro-electronic architecture have several domain controllers that consolidate and control the functionalities of vehicle subsystems, such as propulsion systems, chassis, body, infotainment, and ADAS, among others. The communication between all controllers usually works with high-speed CAN. Still, low-speed communication can also work with LIN protocols, and more advanced architectures have high-speed ethernet and wireless communications between the controllers [231].

Figure 7.1 shows a layout to exemplify the context of a vehicle controls architecture with its domain controllers. This Chapter presents an adaptative one-pedal drive functionality, a function of the propulsion system domain.

All domain controllers have software layers. The interface layer reads and writes digital and analog signals and CAN, LIN, Ethernet, and Wireless IDs. The conditioner layers transform the signal and IDs into physical values or the physical values into signals and message IDs. The application layer is where the software processes its control algorithms [232].

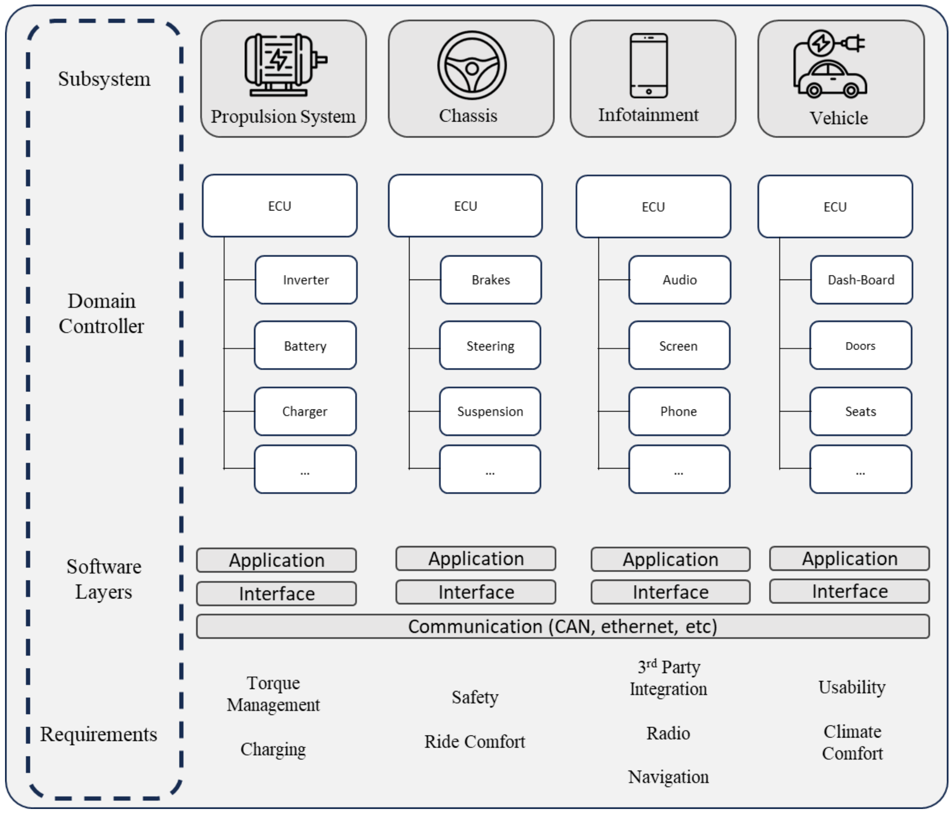

Figure 7.1: Vehicle controls architecture layout.

The application layer of the propulsion system has four main macro-functions: charging, initialization, fault and diagnosis, and drive. It has six other macro-functions inside the drive function, including torque management, which contains the torque request calculation chain. Figure 7.2 shows the simplified macro-layout of the propulsion system domain controller, and Figure 7.3 shows the simplified macro-layout of the propulsion system torque management functions [232].

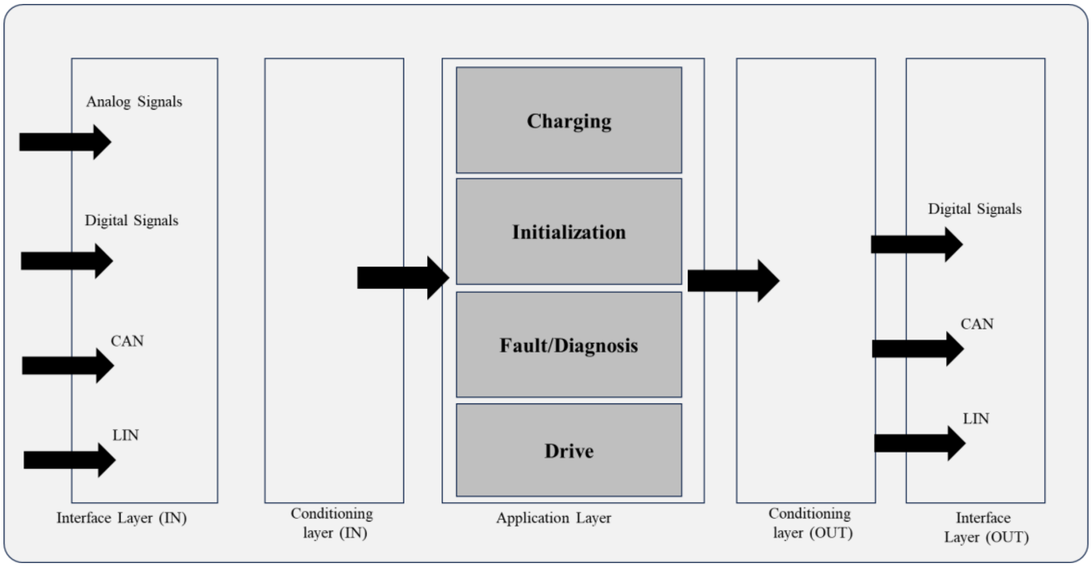

Figure 7.2: Propulsion system controller macro-layout.

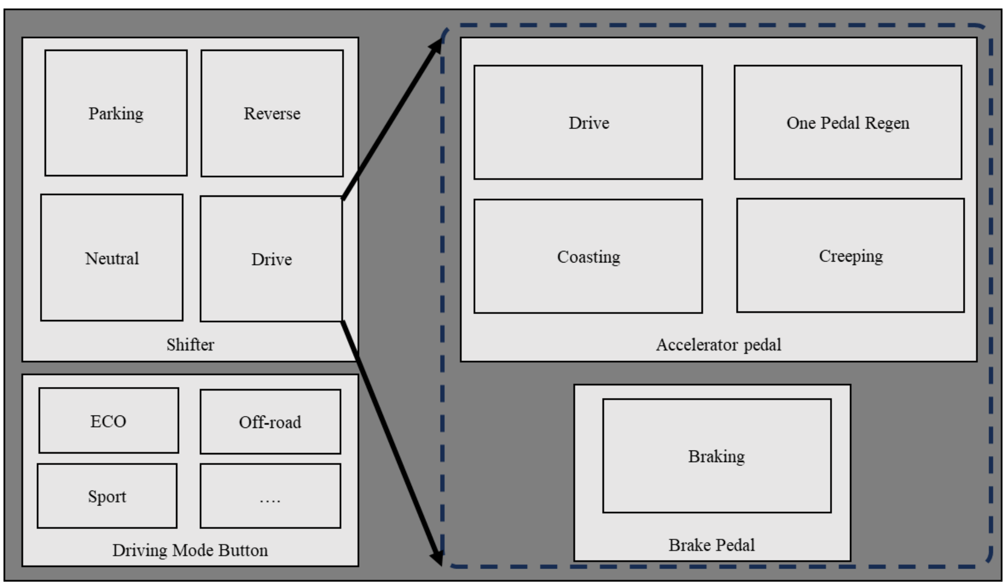

Figure 7.3: Torque Management Function macro-layout.

Figure 3.2, shown in Chapter 3, presents all the subsystems of the propulsion system, and Figure 7.1 eludes the interoperability of the propulsion domain controller with its subsystem controllers. Figure 7.3 illustrates the macro-layout of the torque management, consisting of the vehicle's operational status while turned on.

Figure 7.4 shows the interoperability of the propulsion domain controller with its subsystems, executing the function of producing Torque to move the vehicle. The torque production starts with the driver's command through the accelerator and brake pedals. The propulsion domain controller calculates the torque request and commands the Torque to the electric motors, considering aspects of the e-machine and battery limitations and other inputs to limit Torque and speed (usually from the chassis subsystem while executing the wheel's anti-lock and anti-slipping functions).

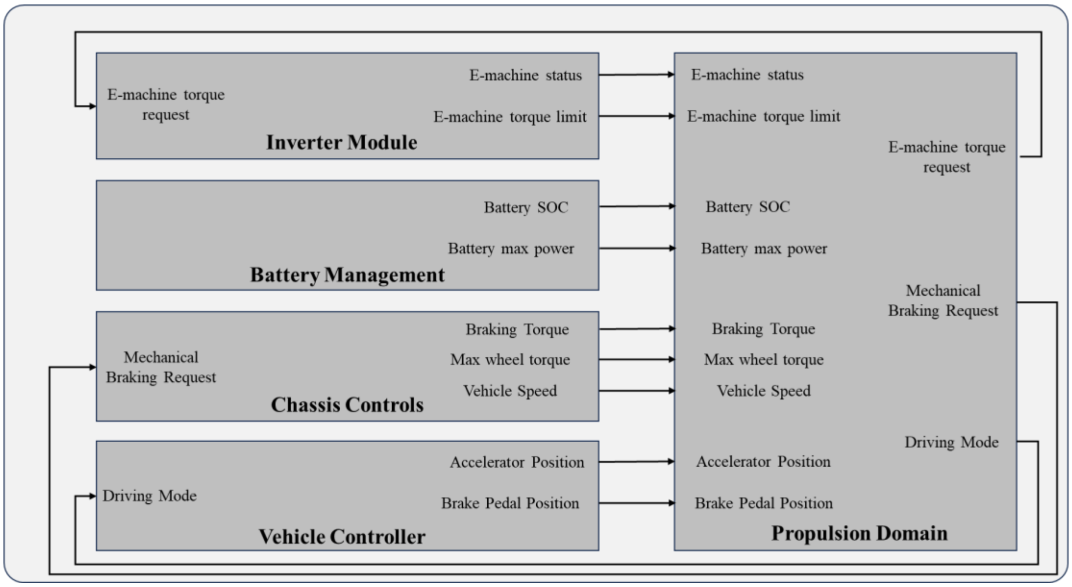

Figure 7.4: Propulsion System Domain Controller Interoperability with Propulsion Subsystems Controllers.

7.1.1 Drive-by-wire accelerator pedal

In modern vehicles, the accelerator pedals are of the drive-by-wire type. It consists of a hall-effect sensor connected to the pedal, which produces a linear voltage signal as the pedal moves [233]. From this physical signal, the propulsion domain controller calculates the Torque required from the drives and determines the Torque delivered to the wheels, considering the constraints imposed by the e-machine, battery, and chassis.

This section explains how a drive-by-wire accelerator pedal works and how it acts as the primary input to the torque request calculation. Figure 7.5 shows how the torque command chain works, from the pedal command to delivering the Torque to the wheels and the speed feedback that closes the control loop.

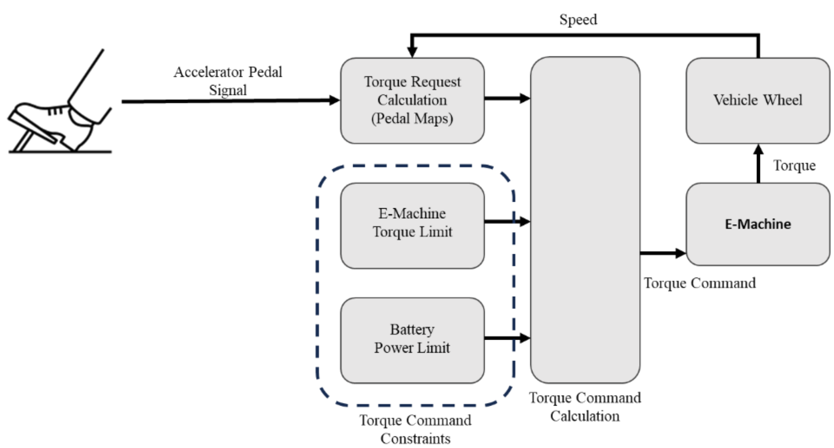

Figure 7.5: Torque command chain.

Figure 7.6 provides a more in-depth view of the torque request calculation. It consists of three main steps: the pedal position calculation, the driver's desired acceleration with a normalized torque curve as a function of the pedal position, and the required torque calculation. These are all calculated from calibratable lockup tables.

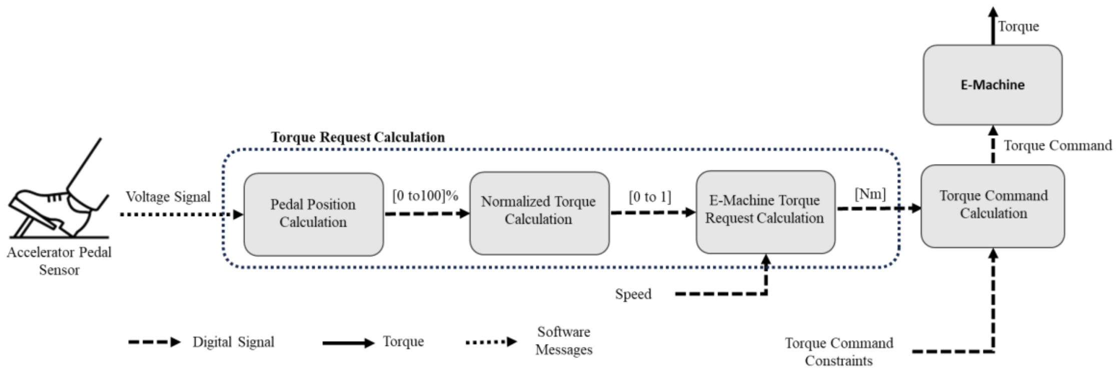

Figure 7.6: Torque command calculation chain using drive-by-wire accelerator pedal.

7.1.1.1 Pedal Position Calculation

Figure 7.7 shows an example of a linear relationship between the pedal position and the voltage signal produced by the drive-by-wire accelerator pedal. Equation (7.1) shows the pedal position calculation, which is the torque request calculation's first step, shown in Figure 7.6.

$$P = \frac{\emptyset_i}{\emptyset_{max}} \tag{7.1}$$

Where P is the pedal position, defined in a percentage, $\emptyset_{max}$ is the voltage measured when the pedal is fully pressed (representing 100% pedal position), and $\emptyset_i$ is the voltage produced at its instant driving position.

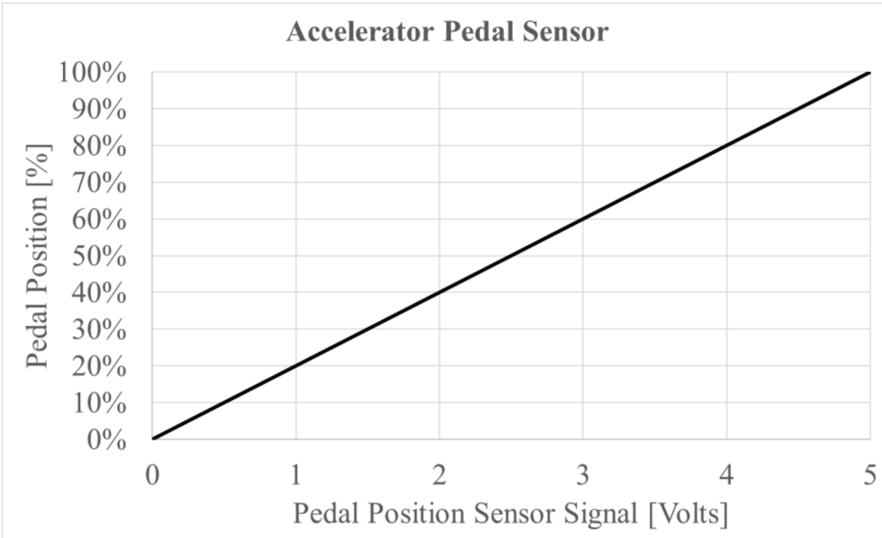

Figure 7.7: Accelerator pedal sensor signal.

7.1.1.2 Normalized Pedal Map Calculation

The pedal position translates the driver's desire for Torque and acceleration. According to [234], the driver-required Torque is calculated from an accelerator pedal curve, which produces a torque fraction output as a function of the pedal position. That curve is calibrated to deliver a specific torque response, such as sportiveness or energy-efficient driving. It is a sensible variable that considerably affects the vehicle's driveability and the quality perception of its performance. Figure 7.8 shows an example of an accelerator pedal map with normalized torque output as a function of the pedal position. This is the second step of the torque request calculation.

Figure 7.8 also shows the curves of linear, sport (aggressive), and eco-driving modes. They differ in regards to how quickly the Torque is delivered from the motor to the wheels and the progressiveness of the torque ramp-up, all variables that influence the vehicle driveability quality and the driver's performance perception.

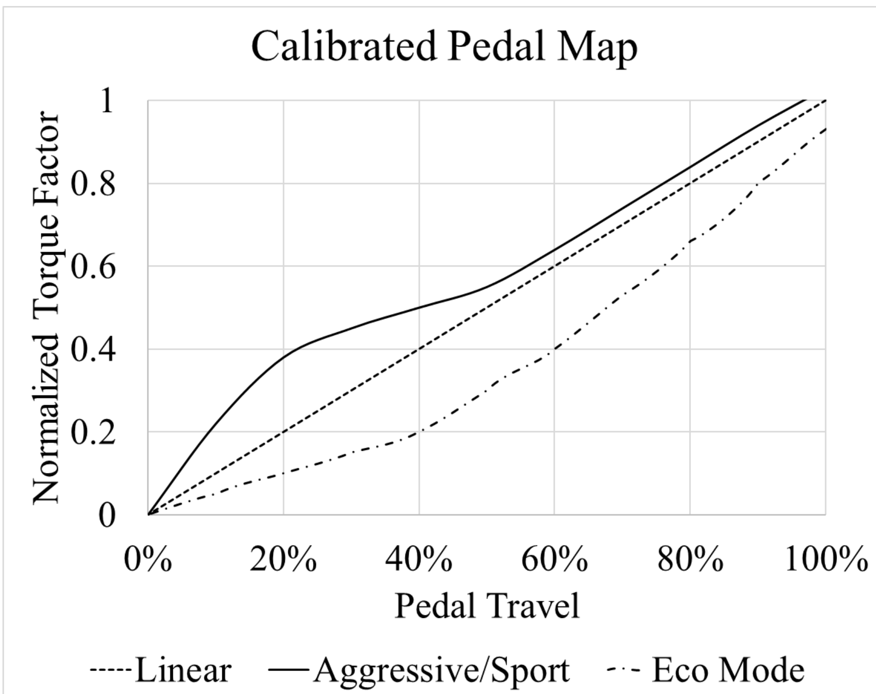

Figure 7.8: Normalized Accelerator Pedal Map for Different Driving Modes.

7.1.1.3 E-Machine Torque Request Calculation

The output of the normalized torque calculation is the input for the e-machine required torque calculation. Equation (7.2) represents the e-machine calculation needed for Torque.

$$T_{e,req} = L.f(T_{max}, rpm) \tag{7.2}$$

Where $T_{e,req}$ is the e-machine required Torque, L is the normalized Torque calculated from the pedal map of Figure 7.8, and $f(T_{max}, \varphi)$ is the peak torque map of the e-machine, where T_{max} is the peak torque for a given motor speed (φ). The replationship of motor speed and wheel speed is linear for single-speed electric drive units.

Equation (7.2) produces the pedal torque map, where the input is the pedal position and motor speed, and the output is the required Torque. Figure 7.9, Figure 7.10, and Figure 7.11 are examples of pedal torque maps calculated using the accelerator pedal maps of Figure 7.8 and the peak torque maps of a typical PM e-machine.

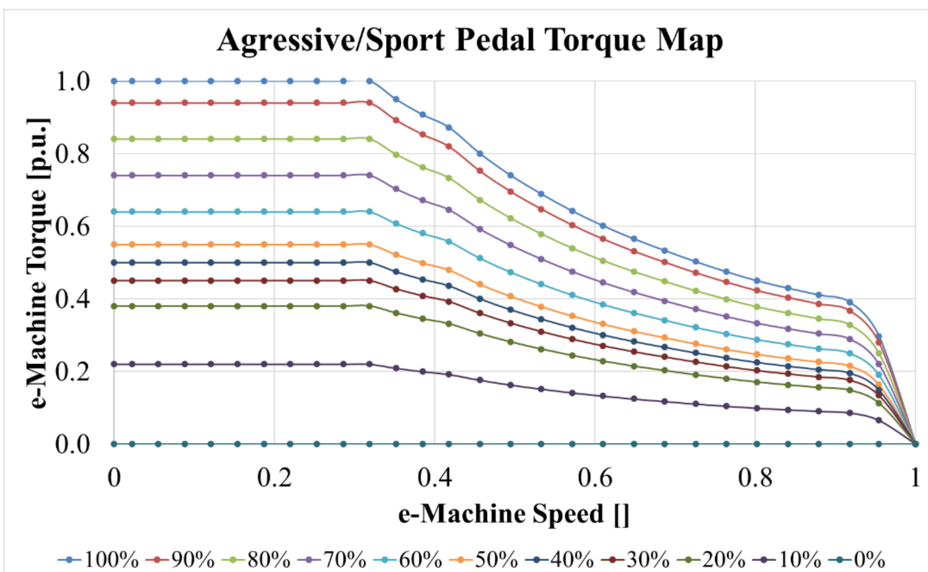

Figure 7.9: Aggressive/Sport pedal torque map.

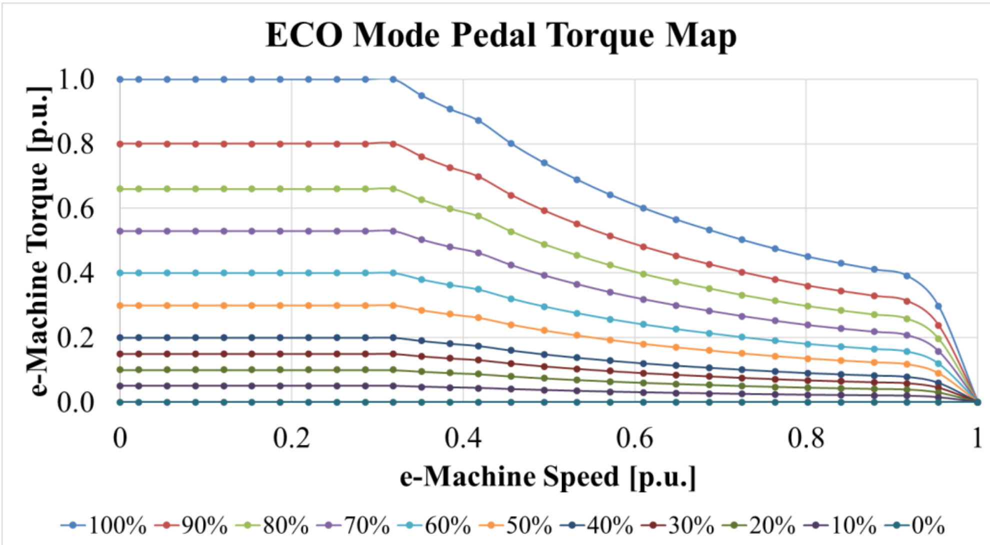

Figure 7.10: Eco mode pedal torq map.

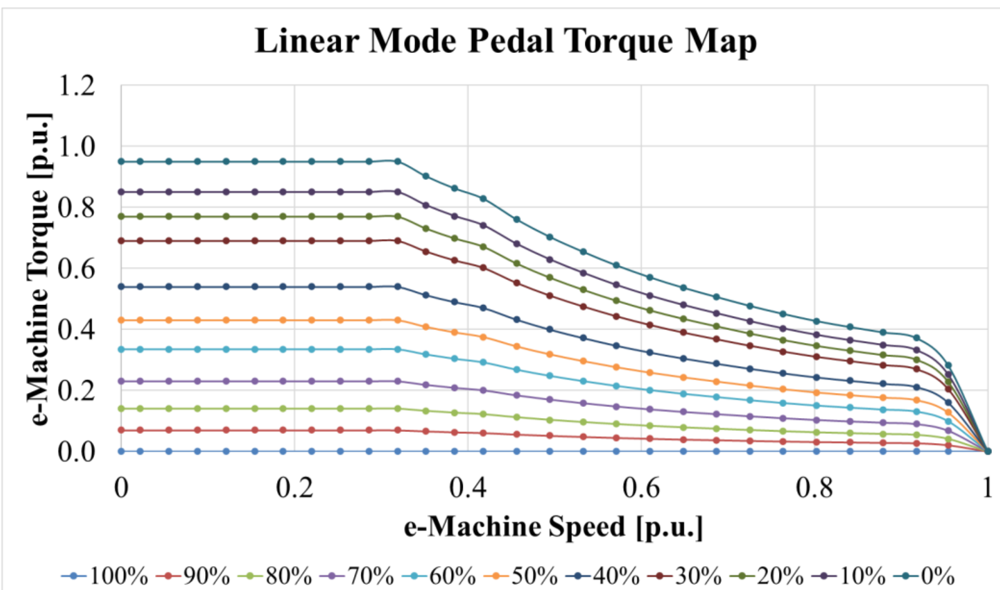

Figure 7.11: Linear pedal torque map.

The above represents the functioning and torque management calculations for a vehicle not equipped with the OPD mode. It means how a pedal map produces positive Torque and acceleration. In this case, coasting is enabled when the pedal is at 0% position. The OPD is presented in more detail in the next session as an evolution of the standard drive-by-wire torque management calculation.

7.2 One-Pedal-Drive

Compared to an ICE vehicle, an electric car can perform decelerations only by using the electric machines as the source of braking torque; simultaneously, it recovers electric energy to the battery pack, the so-called regenerative braking [235].

The OPD strategy uses only the accelerator pedal to perform positive and negative acceleration, braking, and parking. When the driver presses the accelerator pedal, the motor will react with a positive torque to produce a positive acceleration. When the driver releases the pedal, it will produce a negative torque that breaks the car and recovers energy.

Because of the OPD feature, the brake pedal, and as a consequence, the friction brakes are much less used, decreasing the fatigue of stop and go during traffic jams and simultaneously increasing the life and reducing the maintenance cost of the friction brakes. At the same time, it helps to improve overall propulsion efficiency.

In [236], the researchers tested and compared the OPD and conventional two-pedal-driving regarding the driver's emotions, enjoyment of driving, and cognitive working loads (an indication of driving fatigue). The results show increased driving pleasure and reduced mental workload when using OPD. The researchers used an electroencephalography exam to associate questionaries among multiple drivers and objective measurements.

OPD is becoming a mainstream functionality for electric passenger vehicles. For example, Tesla's Model 3, Model Y, Model X, and Model S are all equipped with these features. Teslas also offers, through its HMI (Human Machine Interface) screen, the possibility to calibrate the intensity of the OPD. Other Automakers, such as Volkswagen, Stellantis, and Nissan, also offer OPD in their electric vehicles. However, OPD is not often found in commercial vehicles like trucks and buses [237].

In OPD, the negative Torque produced is a function of the pedal position when the drivers release the accelerator pedal. For example, at very low speeds, the OPD function is disabled to allow efficient creeping, and for high speeds, the amount of deceleration originating from OPD is low, allowing for efficient highway coasting [238].

Figure 7.12 and Figure 7.13 show a deceleration maneuver's electrical and mechanical Power flows with parallel regenerative braking and OPD, respectively.

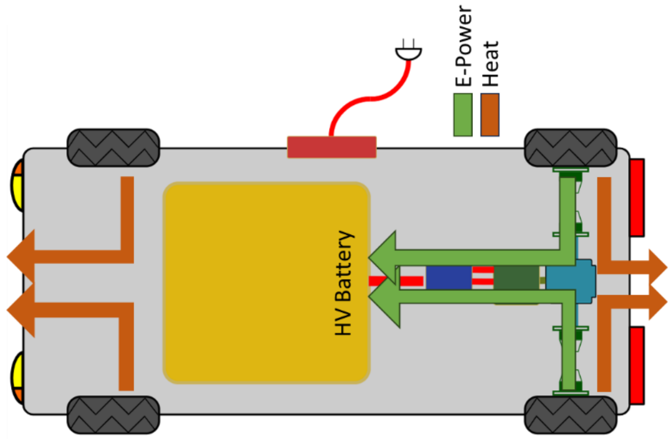

Figure 7.12: Parallel regenerative braking power flow.

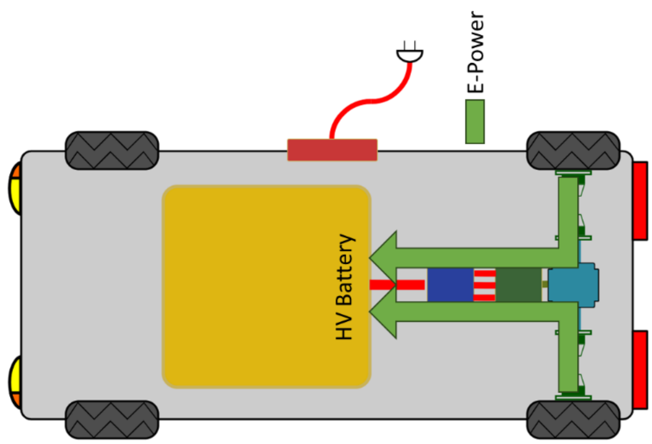

Figure 7.13: One-pedal-drive regenerative braking power flow.

Figure 7.14 shows a four-quadrant view of the pedal maps for a conventional regenerative system with parallel braking architecture. Figure 7.15 shows the four-quadrant pedal map for a simplified OPD strategy.

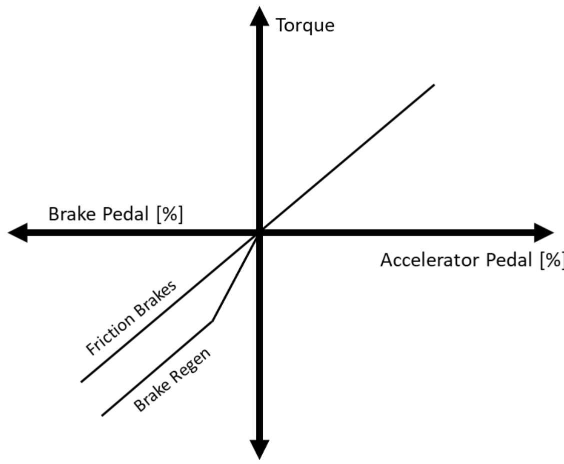

Figure 7.14: Conventional parallel regenerative braking four-quadrant pedal map.

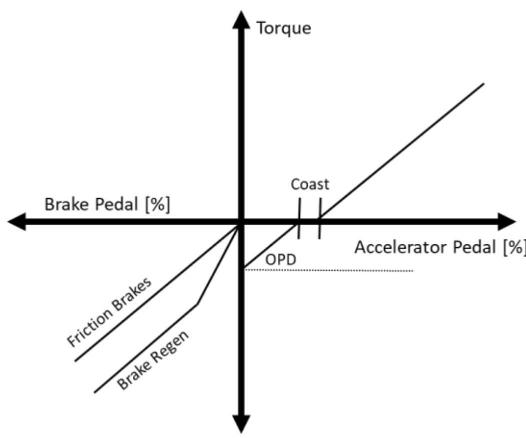

Figure 7.15: Four-quadrant pedal map with OPD and conventional parallel regenerative braking architecture.

An analysis of Figure 7.15 identifies five OPD maneuver moments: launch, accelerating, coasting, braking, and stopping.

Launch is when the driver touches the accelerator pedal, and Torque is delivered to the wheels to start the vehicle's motion and initial acceleration. Launch and acceleration are crucial moments for vehicle driveability, where the feeling of pedal quickness in providing movement and the acceleration buildup impacts the driver's perception of the propulsion's powerfulness. At the same time, the acceleration buildup needs to be smooth without causing jerks and unpredictable accelerations [238].

Coasting is the moment when the vehicle coasts freely, and the only forces acting to slow down the vehicle are the road load forces (Aerodynamics, tire rolling resistance, and mechanical drag resistance from the brakes, transmission, driveline, and the motor back EMF, electro-magnetic force, if of PM type). The transitions from accelerations and brakings to coasting should be smooth, without any unpredictable accelerations, and the driver should naturally find the OPD position to start coasting [238].

Braking and stopping are other maneuvers as critical as the launch and acceleration. During these maneuvers, the driver adjusts the acceleration pedal position to brake the vehicle, and decelerations up to 0.2 g's usually could be achieved. The slowdown can occur until the vehicle stops. However, at speeds close to 0 km/h, the intensity of the regeneration should be very low to allow a comfortable and smooth stopping maneuver and for precise pedal control during parking. Some studies of OPD show that for smooth and safe deceleration control, steps of 5% in the pedal control should be an equivalent of approximately 0.03 g's of deceleration [238].

There are other factors to take into account when designing an OPD. The accelerator pedal tip-in and tip-out at any vehicle speed should not cause any jerk or unexpected behavior. At the same time, the e-machine torque reaction needs to follow the driver's desire for acceleration or braking.

Rule-based OPD, such as Figure 7.15, usually lacks driveability performance. Since the launch and acceleration happen only after the braking and coasting regions, there is a feeling of a free-play area without any positive torque response.

Advanced control methods work in real-time to predict the driver's intention to accelerate, brake, or coast to overcome the driveability issue. In [239], the authors propose a fuzzy fuzzy logic; in [235], the authors propose the utilization of a PID controller.

This Chapter will use the rule-based approach to present the adaptative one-pedal-drive as a function of the vehicle mass.

Figure 7.16 presents the modified torque command chain with an additional step for the driving mode classification: braking, coasting, or accelerating.

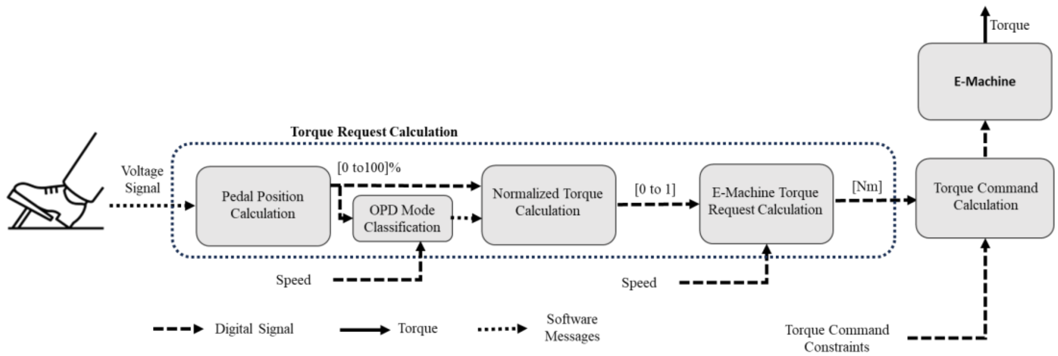

Figure 7.16: Torque command calculation chain using drive-by-wire accelerator pedal with OPD driving mode classification.

The driving mode classification follows the rules as shown bellow:

$$\begin{cases} Accelearting & P > p_{acc} \ and \ \dfrac{\Delta P}{\Delta t} > 0 \\ Braking & P < p_{br} \ ; \\ Coasting & p_{br} \leq P \leq \ p_{acc} \ ; \ \dfrac{\Delta P}{\Delta t} < 0 \end{cases}$$

Where P is the accelerator pedal position, p_{acc} Is the calibrated pedal position where positive torque command begins and $\frac{\Delta P}{\Delta t}$ Indicates the desire to increase the vehicle velocity if greater than zero and the desire to reduce the speed if lower than zero.

7.2.1 Acceleration and Coasting

Figure 7.17 shows a variation of Figure 7.8 linear pedal maps in the acceleration zone, adapted for the rule-based OPD approach, and the resultant torque pedal maps are shown in Figure 7.18.

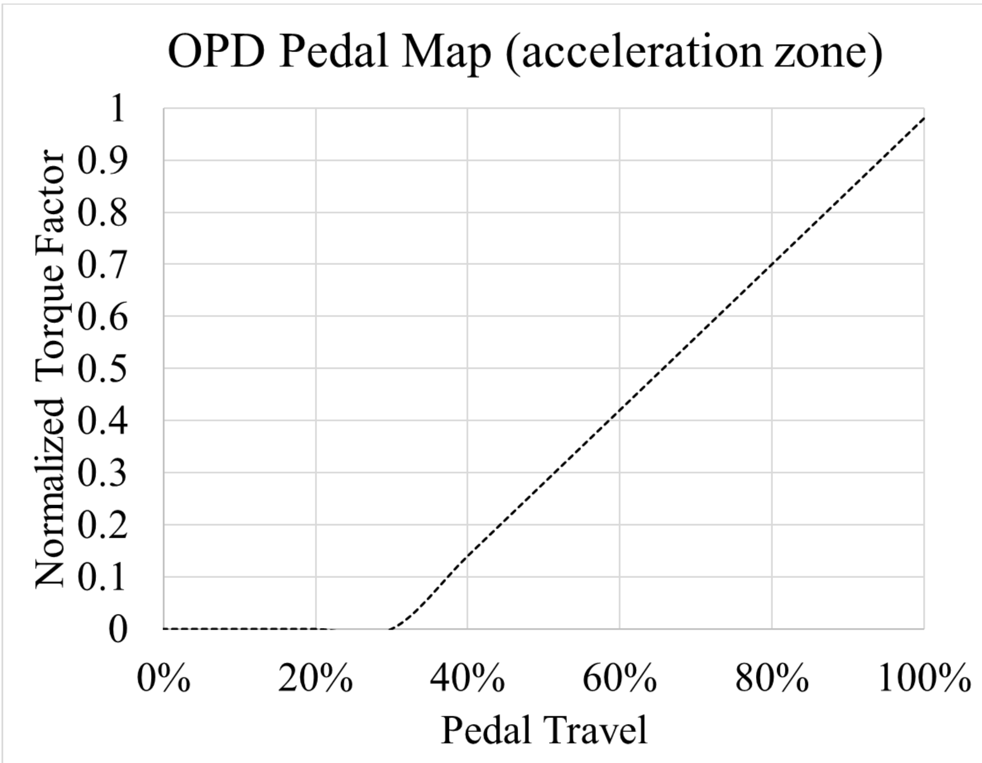

Figure 7.17: OPD Normalized Pedal Map - Acceleration Zone.

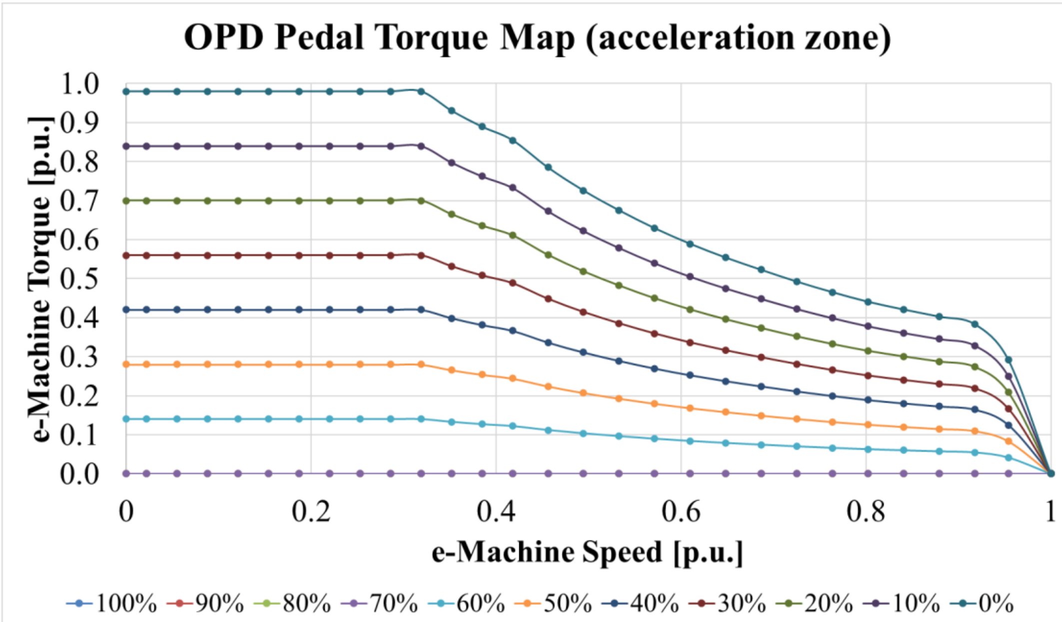

Figure 7.18: OPD Normalized Pedal Torque Map - Acceleration Zone.

When at the coasting region, the torque demand is equal to zero.

7.2.2 Braking

While in the OPD region (braking), the max acceleration for the OPD should not surpass the trash hold of 0.2 g's to provide a safe and comfortable deceleration. However, this level of acceleration makes the OPD uncomfortable and inefficient for highways and low-speed driving and parking maneuvers. For these conditions, lower levels of accelerations are more appropriate. Figure 7.19 presents an example of a desirable max OPD brake regeneration curve where L_{max} represents the maximum OPD torque, and $L_{max,highway}$ is the maximum torque factor at the maximum vehicle speed. The variables v_{low} and v_{high} are speed transition trash holds to set the low, medium, and high speeds. More speed trash holds can be created if needed to improve driveability.

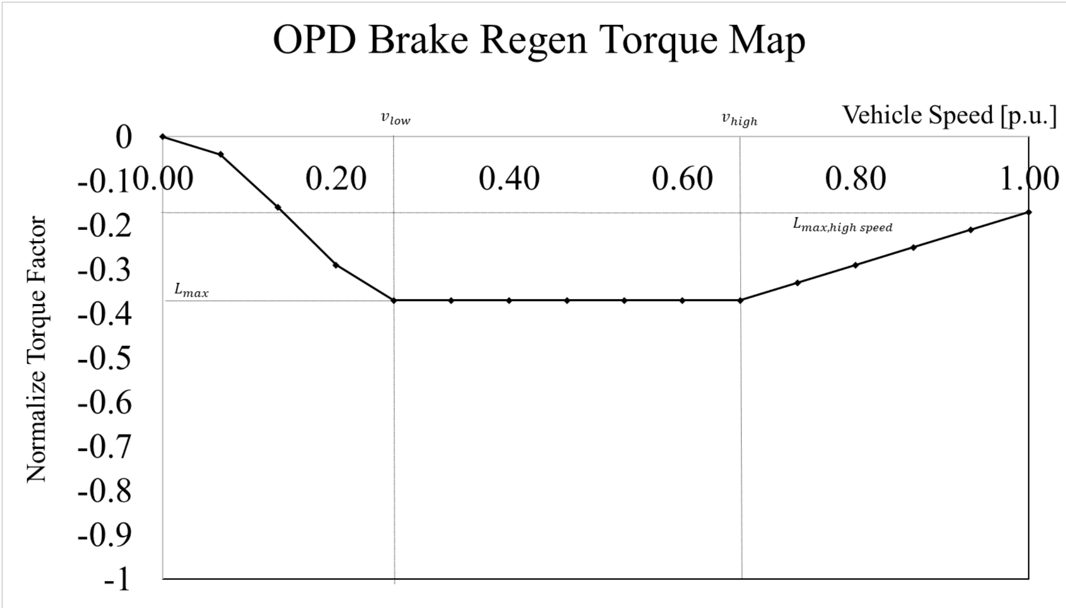

Figure 7.19: OPD Brake Regen - Torque Limit Map.

Figure 7.20 shows an example of the accelerator pedal maps region from the four-quadrant pedal maps shown in Figure 7.15. The OPD zone of the example represents the normalized torque factor of the OPD zone, equivalent to 0.03 g's for each 5% pedal travel step, as proposed in [238].

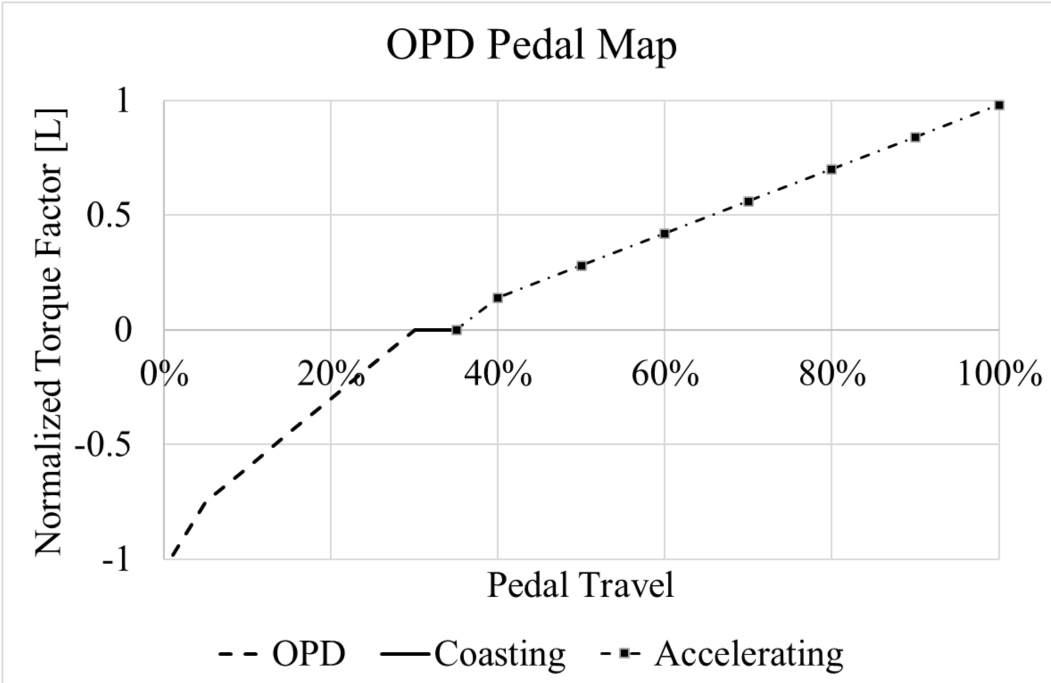

Figure 7.20: OPD Pedal Map.

Combining the OPD map from Figure 7.20 and the OPD brake regen torque limit from Figure 7.19 using Equation (7.2), the OPD braking torque regen map is created and shown in Figure 7.21.

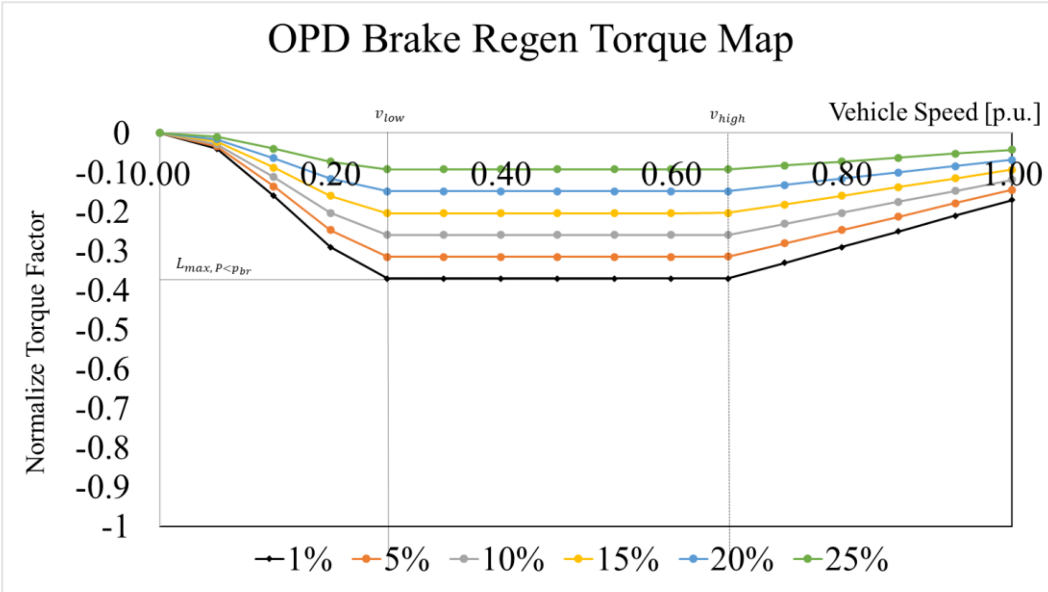

Figure 7.21: OPD Brake Regen Torque Map.

7.3 Adaptative One-Pedal-Drove (A-OPD)

In vehicle dynamics, the deceleration achieved during braking is a function of the vehicle's mass and the applied force from the actuator (e-machine or friction brakes). When a vehicle's at GVW is 100% heavier than its weight when empty with a driver, the resulting deceleration differs significantly when the same braking force is exerted at both GVW and curb weight.

Using the brake torque regen map from Figure 7.21 as a reference, Figure 7.22 shows the braking acceleration in an unloaded vehicle, with this driver in, using an OPD calibrated for a maximum 0.2 g's deceleration on the unloaded vehicle.

At the same time, Figure 7.23 shows a deceleration profile for the same OPD, now calibrated for a max 0.2 g's deceleration when the car is completely loaded.

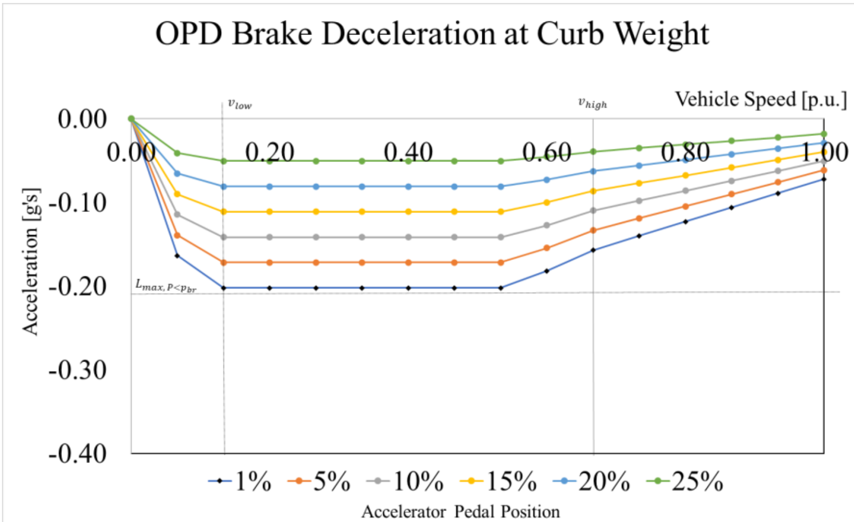

Figure 7.22: Braking acceleration map with OPD at curb weight calibration

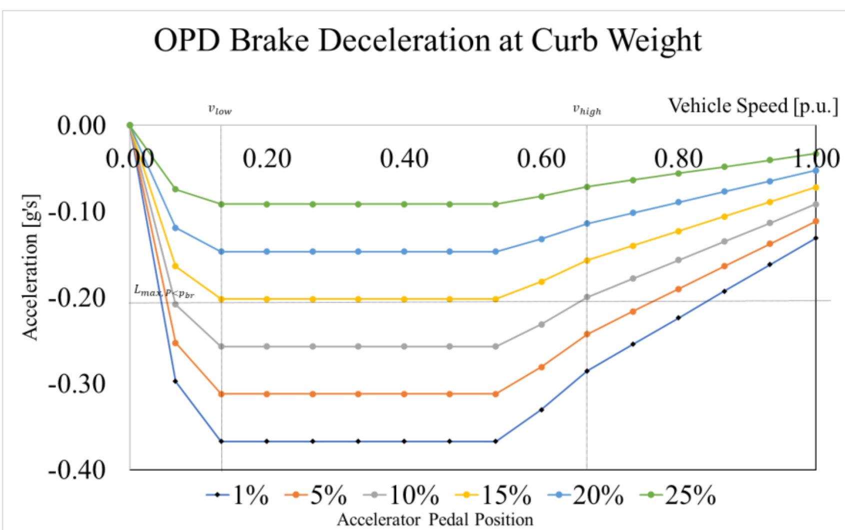

Figure 7.23: Braking acceleration map with OPD at GVW calibration.

Figure 7.23 shows that this braking force decelerates up to 0.37 g's the unloaded vehicle with the GVW calibration. In contrast, at curb weight calibration, Figure 7.22, it translates to a comfortable slowdown of 0.19 g's, a level commonly experienced during typical driving situations.

As mentioned in Chapter 6, the perception of an uncomfortable maneuver increases almost linearly with the longitudinal acceleration level. Longitudinal accelerations greater than 2 m/s^2, approximately 0.2 g's are considered uncomfortable [10], [224].

The problem arises when seeking to calibrate an optimal (OPD) for such a vehicle. An efficient OPD calibration for the fully-loaded vehicle may not deliver a safe and comfortable experience when the car is empty. Conversely, an optimum OPD calibration for the open vehicle might lack the energy efficiency and braking torque necessary for the loaded vehicle's requirements.

The efficiency problem is shown in Figure 7.24, Figure 7.25, and Figure 7.26, respectively. The braking torque profiles for an unloaded and loaded vehicle, generated from the vehicle studied in Chapter 5 and Chapter 6, are compared against the maximum OPD regeneration curve calibrated for the optimum performance of an unloaded vehicle. The following driving cycles are used in the comparison: LA92, NY_City, and WLTP.

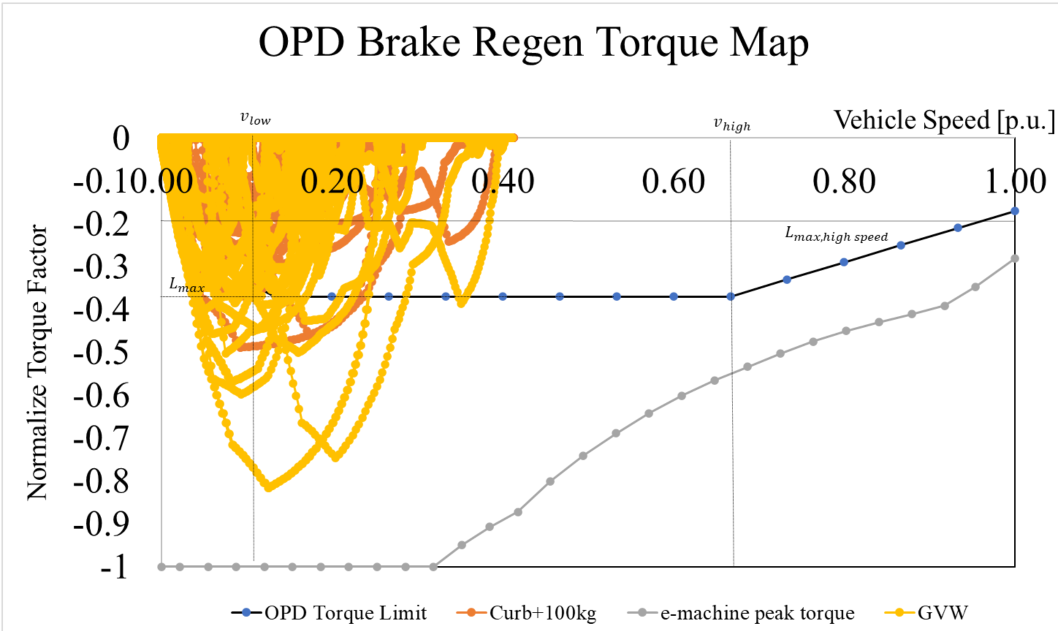

Figure 7.24: Brake Regen Profile Compared to the OPD torque limit in LA92 Driving Cycle.

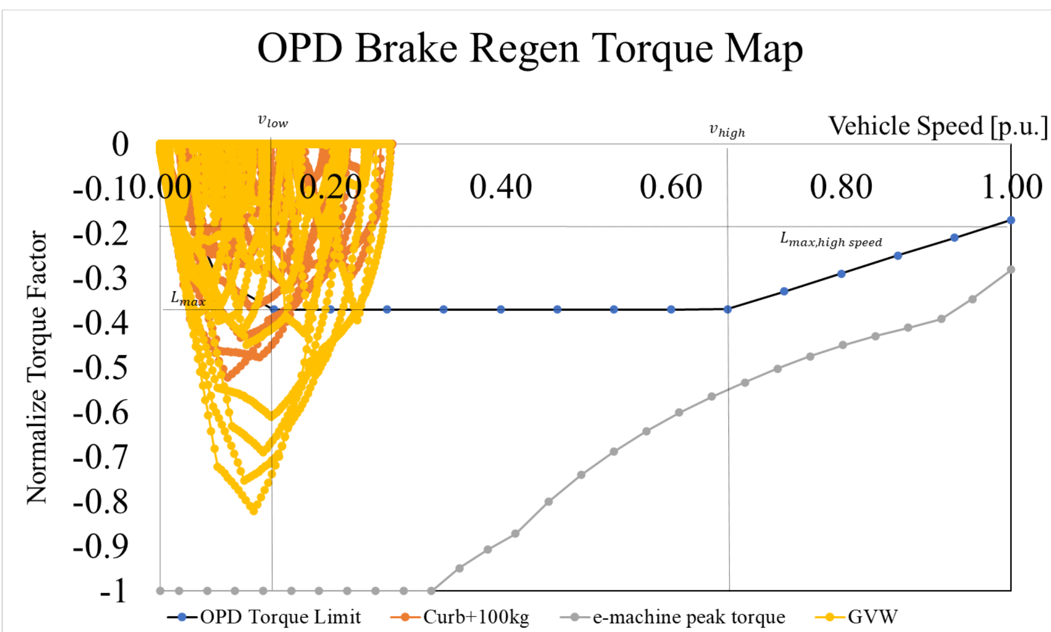

Figure 7.25: Brake Regen Profile Compared to the OPD torque limit in NY_City Driving Cycle.

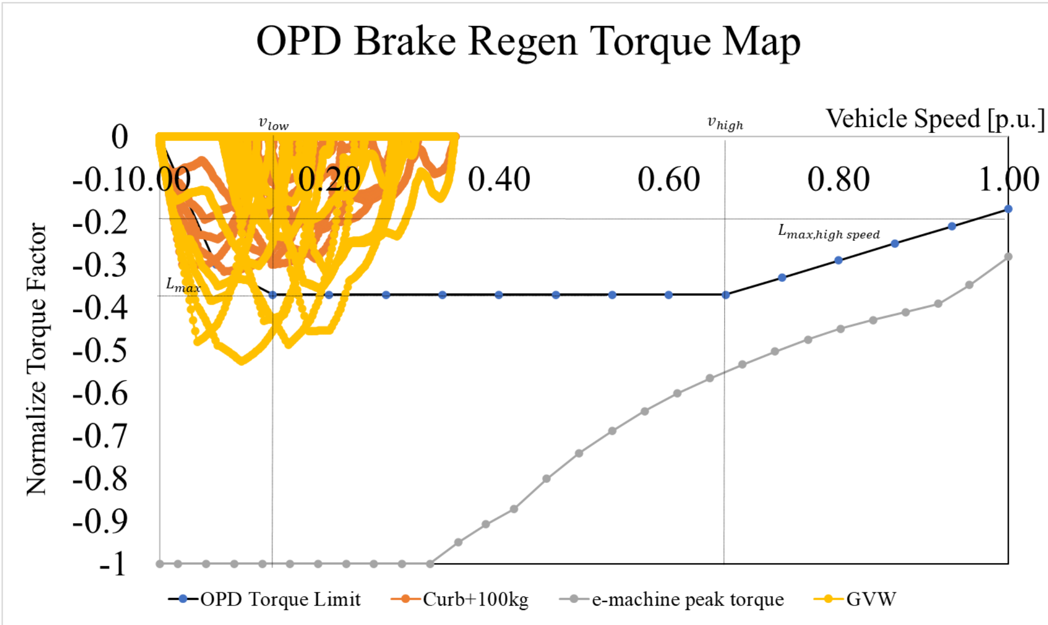

Figure 7.26: Brake Regen Profile Compared to the OPD torque limit in WLTP_High Driving Cycle.

The comparison shows that there may be an efficiency deficit in energy recovery using an OPD when the vehicle is at GVW. When the OPD cannot decelerate the vehicle, necessitating the driver to engage the brake pedal, some energy dissipates in the form of heat. This effect is more evident for the LA92 and NY_City cycles.

Striking a balance between safety, driveability, and efficiency at any vehicle load is critical for the optimum performance of electric commercial vehicles, and the proposal to strike this balance in an Adaptive One-Pedal-Drive (A-OPD).

The A-OPD consists of an algorithm that estimates the vehicle running mass using an RLS (recursive least square) filter. The estimated running vehicle mass is the input for a weight classification calculation, which determines the previous calibrated brake regen torque maps to be used.

Figure 7.27 shows an evolution of the process presented in Figure 7.16, showing the conclusion of the mass recognition, classification, and torque map selection.

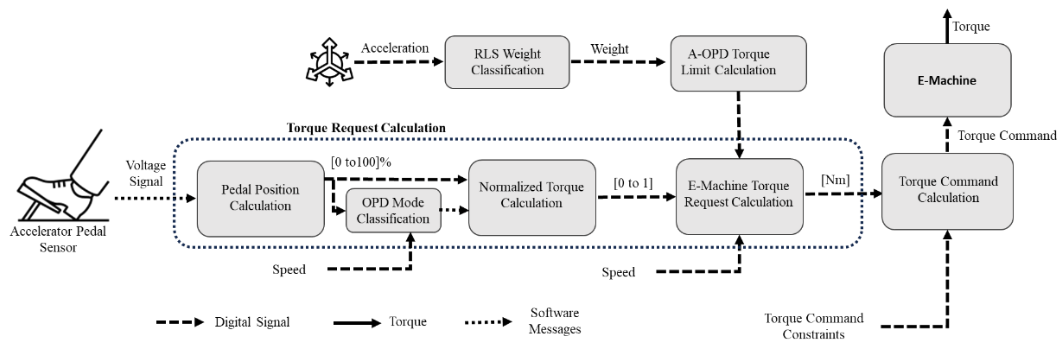

Figure 7.27: Torque command calculation chain using drive-by-wire accelerator pedal with A-OPD

This section explores vehicle mass estimation, delving into its significance in improving regenerative braking using one-pedal-drive (OPD). The method presented in this Chapter is an adaptive one-pedal-drive (A-OPD), which changes its calibration as a function of the vehicle running mass. The A-OPD method involves three steps: weight identification, classification, and selection of torque map.

7.3.1 Weight Identification

Vehicle mass estimation is essential in vehicle dynamics and automotive control development. This parameter finds its applications in various areas of vehicle technology, ranging from heavy-duty vehicles, where it works to improve cruise control and automatic transmission gear shifting strategies, to light passenger vehicles, extensively utilized in enhancing stability control and Advanced Driver Assistance Systems (ADAS) [240].

Different methods for vehicle mass estimation are available, such as extended Kalman filter, machine learning, dynamic grade observer, and parallel mass grade estimator [240]–[242]. However, Recursive Least Squares (RLS) is a particularly prevalent approach [243]–[245].

The Recursive Least Squares (RLS) is an adaptive filter algorithm distinguished by its recursive nature. This algorithm iteratively determines the coefficients that minimize the input signals' weighted linear least squares cost function [246].

The mass estimation problem is linear, as the mass is constant from the moment the vehicle is ON until the moment the vehicle is OFF; the forgetting factor can be assumed to be equal to 1. Equation (7.3) represents the mass estimation system.

$$y(t) = H(t).\delta(t) + \varepsilon(t) \tag{7.3}$$

Where t is the sample time step of the signals, $y(t)$ corresponds to the output of the equation, in this case, the vehicle acceleration. $H(t)$ is the regressor signal, the longitudinal force applied to the tires causes the acceleration. The variable $\delta(t)$

is the estimation variable, in this case, a function of the vehicle mass. The variable $\varepsilon(t)$ is the estimated residual.

Equation 4.1. represents the longitudinal vehicle dynamics. Equation (7.3) shows the same equation organized in the form of Equation (7.2)

$$\dot{v} = (\frac{\tau_{wh}}{r_{wh}} - A\cos\emptyset - Bv - Cv^2)\, {}^{1}\!/_{m} \tag{7.4}$$

Equations below show each of the Equation (7.3) terms, written in the form of the longitudinal vehicle dynamics, where $\dot{v}$ is the longitudinal acceleration, τ_{wh} is the Torque at the wheels, r_{wh} is the wheel radius, v is the vehicle velocity, $\emptyset$ is the road slope, and A, B, and C are road load factors corresponding to aerodynamics and rolling resistance.

$$\dot{v} = y(t)$$

$$\left(\frac{\tau_{wh}}{r_{wh}} - A\cos\emptyset - Bv - Cv^2\right) = H(t)$$

$${}^{1}\!/_{m} = \delta(t)$$

In the case of the mass estimation problem, the RLS uses the vehicle acceleration signal from the vehicle accelerometer, and the longitudinal force applied by the tires to the ground is calculated from the e-machine Torque.

7.3.2 A-OPD Approach

From Figure 7.19 and Figure 7.21, the OPD torque limit and the OPD torque request calculation are determined using calibratable lookup tables. In the conventional OPD method, as illustrated in Figure 7.19, the torque limit is set and fine-tuned to achieve a maximum deceleration of 0.2 g's when it's not carrying any load.

However, the A-OPD approach's torque limit varies based on the vehicle's weight. This means the maximum deceleration of 0.2 g's is reached when the vehicle operates at its actual weight. Figure 7.28 provides an overview of how the A-OPD calculation is carried out in this context.

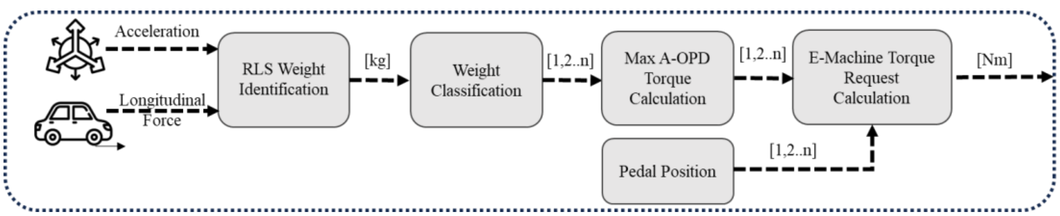

Figure 7.28: A-OPD Calculation Flow.

The weight classification assigns a numerical value based on a predefined weight category determined by comparing the mass obtained through RLS estimation to a specified mass range.

$$\begin{cases} \#1 & m < \vartheta_{curb+100kg} \\ \#2 & \vartheta_{curb+100kg} \leq m < \vartheta_{curb+x} \\ & \vdots \\ \#n & \vartheta_{curb+x} \leq m < \vartheta_{GVW} \end{cases}$$

Where the symbol # represents the weight classification corresponding to the actual vehicle running mass "m" and, ϑ_n corresponding to calibratable weight limits to define the weight limits for each class.

The definition of the A-OPD torque limits for the actual vehicle running mass comes by selecting the corresponding calibration tables to its weight category. Figure 7.29 shows the torque limit curves for different weight categories and compares them to the maximum peak torque of the electric machine.

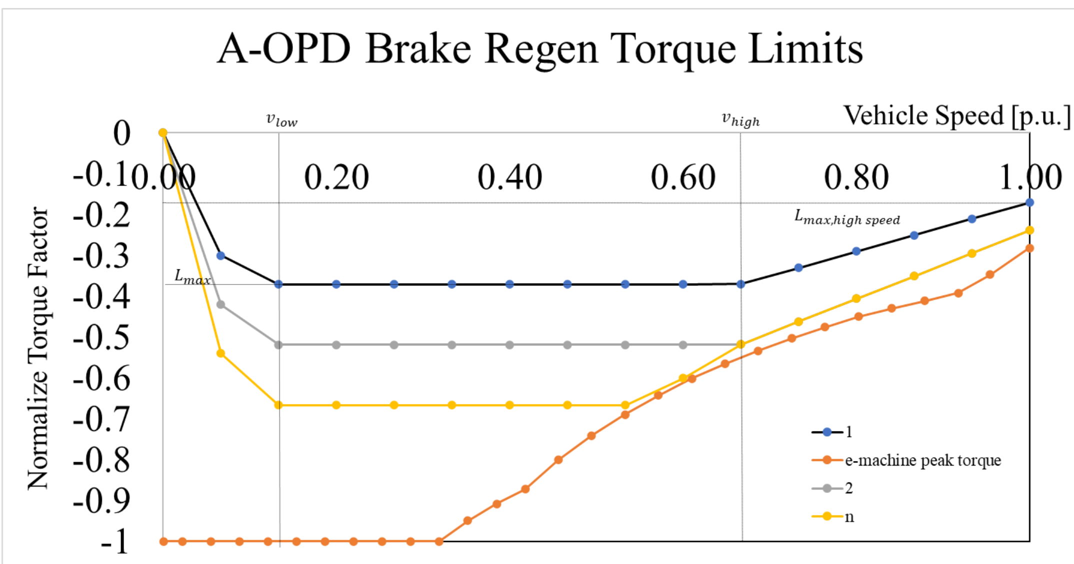

Figure 7.29: A-OPD Braking Torque Limits for different weight classes.

The e-machine torque request calculation is then calculated from Equation (7.2), where L is defined as a function of the pedal position in the OPD, as shown in Figure 7.20, and $f(T_{max,n}, rpm)$ is shown in Figure 7.29, where "n" is the weight category of the torque limit used for the torque request calculation, defined from the RLS vehicle weight estimation.

Figure 7.30 and Figure 7.31 show the implementation of the A-OPD with the RLS mass estimation in the model presented in Chapter 4.

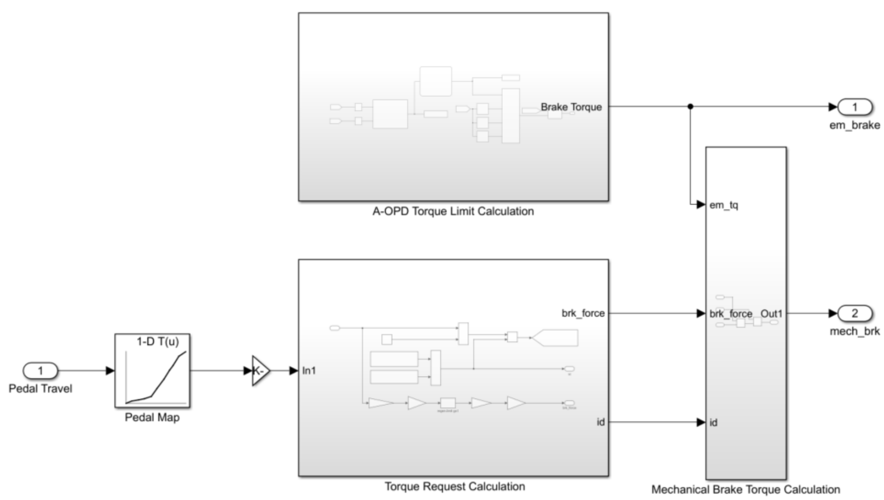

Figure 7.30: Torque request calculation model.

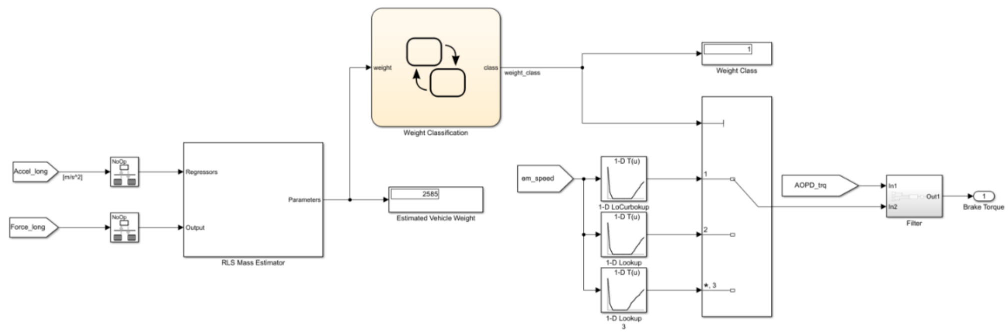

Figure 7.31: A-OPD torque management control model.

7.4 A-OPD Application

For the performance evaluation of the proposed method's efficacy in improving energy efficiency, this research uses the same vehicle as Chapter 5 and Chapter 6.

Table 7.1 shows the main characteristics of the vehicle, and Figure 7.32 shows the propulsion system architecture characteristics.

Table 7.1: Study Case Vehicle Technical Specifications.

Technical Specifications	Units	Targets
0-100 km/h	[s]	12s
Maximum Speed	[km/h]	146
Launch on grade @GVW	[%]	25%
Launch on grade @PBT	[%]	33%
6% grade constant speed	[km/h]	141

e-machine Power	[kW]	200
e-machine Torque	[Nm]	290
Battery	[kWh]	80
Curb Weight	[kg]	2550
Half-Payload Weight	[kg]	3550
GVW	[kg]	4550

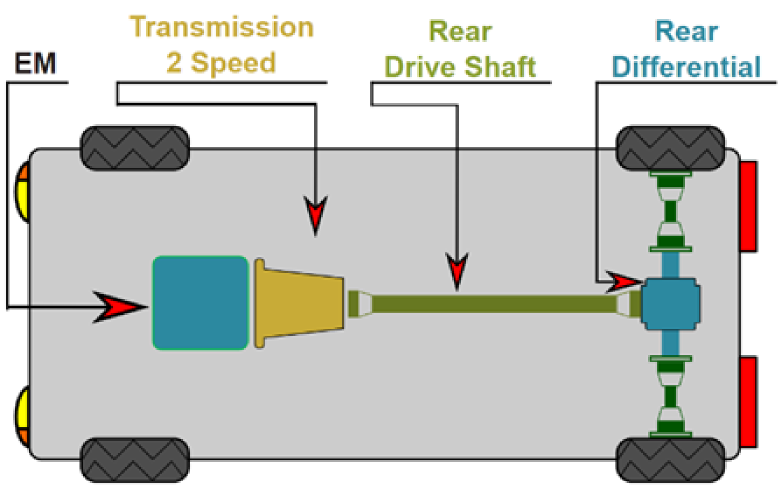

Figure 7.32: Study Case Vehicle Propulsion System Architecture.

Five different driving cycles are used for the energy consumption calculations: LA92, NY-City, US06, FTP75, and WLTP_High. For consistency, they are the same driving cycles used in Chapter 6.

The performance comparisons are from the results of fifty-five simulations using the model presented in Chapter 4. The simulations for the five driving cycles are performed to compare the performance of the presented A-OPD approach when the vehicle is unloaded (Curb+100kg), with half of its maximum payload (half payload), and fully loaded (GVW). Similarly, the simulations were performed using the parallel and regenerative braking architectures, presented in Chapter 6, and the conventional OPD, presented in this Chapter. Table 7.2 shows all simulation cases.

Table 7.2: Study Case Simulation Board.

Driving Cycles	**Vehicle Weight**	**Regen Method**
	Curb+100kg	Parallel
LA92	Half Payload	Parallel
	GVW	Parallel
NY_City	Curb+100kg	**Series**
	Half Payload	**Series**
US06	GVW	Series
	Curb+100kg	OPD
FTP75	Half Payload	OPD
	Half Payload	**A-OPD**
WLTP_High	GVW	OPD
	GVW	**A-OPD**

The results are compared in terms of the percentage of improvement in total energy consumption for the entire driving cycle using three different vehicle weights: Curb+100kg, Half Payload, and GVW.

Table 7.3 shows the A-OPD compared to the conventional OPD. Table 7.4 compares the A-OPD and the series regenerative braking architecture, and Table 7.5 shows the A-OPD efficacy compared to the parallel regenerative braking architecture.

Table 7.3: A-OPD Performance comparison to OPD.

A-OPD Compared to OPD

Driving Cycle	Improvement		
	Curb+100kg	Half Pay Load	GVW
LA92	0%	3.9%	9.3%
NY_City	0%	10.1%	20.7%
US06	0%	3.1%	6.7%
FTP 75	0%	3.5%	10.8%
WLTP_High	0.0%	0.6%	2.9%

Table 7.4: A-OPD Performance comparison to Serie Brake Regen.

A-OPD Compared to Series Brake Regen

Driving Cycle	Improvement		
	Curb+100kg	Half Pay Load	GVW
LA92	-1.4%	-1.8%	-1.4%
NY_City	-3.5%	-4.8%	-3.5%
US06	-2.0%	-2.0%	-2.0%
FTP 75	-0.6%	-0.7%	-0.6%
WLTP_High	-0.1%	-0.1%	-0.1%

Table 7.5: A-OPD Performance comparison to Parallel Brake Regen.

A-OPD Compared to Parallel Brake Regen

Driving Cycle	Improvement		
	Curb+100kg	Half Pay Load	GVW
LA92	33%	34%	39%
NY_City	41%	50%	53%
US06	11%	13%	17%
FTP 75	28%	31%	36%
WLTP_High	21%	18%	23%

The A-OPD approach to control the regenerative braking performance presents a similar performance to the conventional OPD when the vehicle is unloaded. However, it shows an improvement of around 20% in energy consumption for bustling urban traffic, such as the NY-City driving cycle when the vehicle is fully loaded. With half of its payload in the same driving cycle, the gain is approximately 10%. Even for a driving cycle with higher speeds and fewer decelerations and energy recovery opportunities, the A-OPD showed a benefit when compared to the conventional OPD: 2.9% at the WLTP_High, 6.7% at the US06 and 9.3% at the LA92.

Compared to the series regenerative braking, the A-OPD is less effective in recovering energy. On average, A-OPD is -1.6% less efficient than the series regenerative braking. The more considerable difference is on the US06 and NY_City Cycles, and the more negligible difference is on the WLTP_High. This is because the A-OPD only works for decelerations lower than 0.2g's, and for decelerations above this, the brake pedal should be engaged, resulting in energy loss in the form of heat. The series regen architecture can perform any slowdown with the e-machine as far as it does not surpass the torque limits of the e-machine.

The great effectiveness of the A-OPD is perceived when its performance is compared to that of a vehicle equipped with a parallel regenerative braking system. When the vehicle is fully loaded, the improvements reach approximately 50% for the urban cycle (NY_City). Overall, the minimum gain for the loaded vehicle was 17% in the US06 cycle.

This result is very significant since, as mentioned in the sections above, commercial vehicles, especially those designed and built from existing ICE platforms, do not count with advanced ABS, EBS, and ESP systems. For this reason, this vehicles are usually equipped with simplistic parallel regenerative braking systems.

To better present the differences in the performance among the different methods. Section 7.6 shows the SOC profiles for each simulated driving cycle, and Section 7.7 presents the regeneration torque profile for the loaded vehicle on the NY_City and WLTP_High driving cycles.

Figure 7.33, Figure 7.35, Figure 7.37, Figure 7.39, and Figure 7.41 show the SOC profiles for all five driving cycles, using the different regen control methods, for the loaded vehicle.

Figure 7.34, Figure 7.36, Figure 7.38, Figure 7.40, and Figure 7.42 show the SOC profiles for all five driving cycles, using the different regen control methods, for the unloaded vehicle.

Figure 7.43, Figure 7.45, and Figure 7.47 show the brake regen torque profiles for the NY_City driving cycle, comparing the A-OPD to OPD, Series Regen, and Parallel Regen, respectively. Figure 7.44, Figure 7.46, and Figure 7.48 show the torque differences, which explains the efficacy of the A-OPD when compared to the conventional OPD and the parallel brake regeneration.

The same analysis is performed for the WLTP_high driving cycle, and the torque profiles are shown in Figure 7.49, Figure 7.51, and Figure 7.53, while the torque differences are shown in Figure 7.50, Figure 7.52, and Figure 7.54.

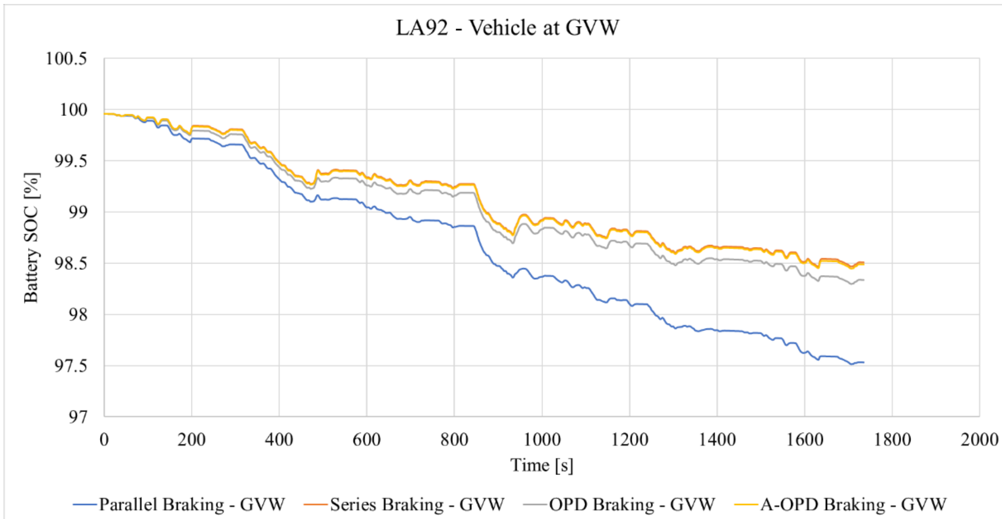

Figure 7.33: LA92 Driving Cycle - GVW - Battery SOC comparison for A-OPD, OPD, Series Brake Regen, and Parallel Brake Regen.

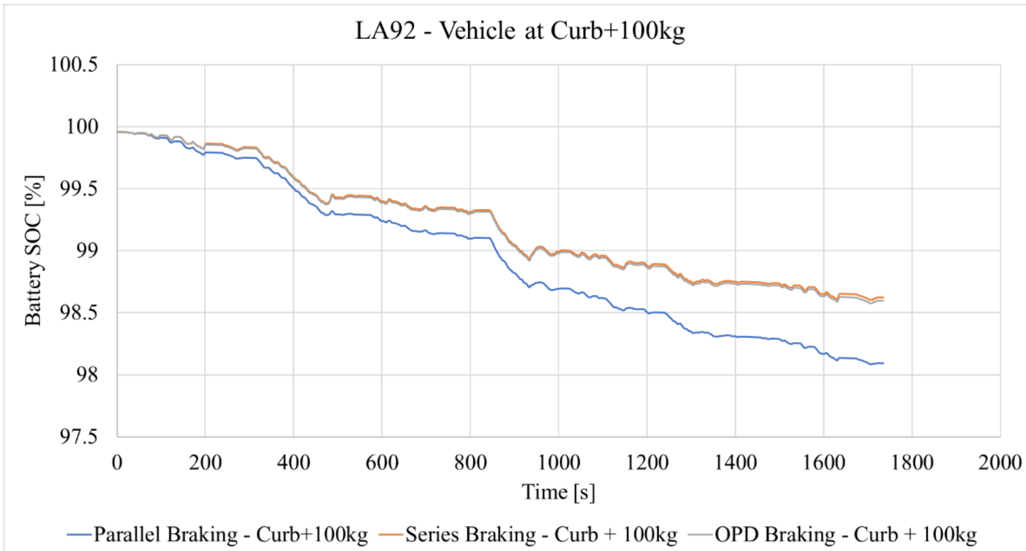

Figure 7.34: LA92 Driving Cycle – Curb+100kg - Battery SOC comparison for A-OPD, OPD, Series Brake Regen, and Parallel Brake Regen.

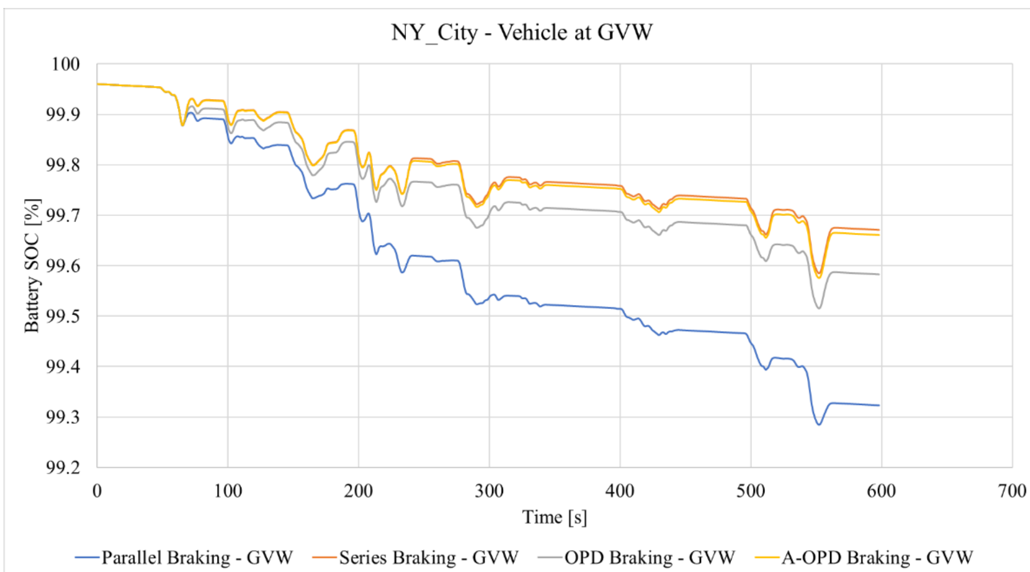

Figure 7.35: NY-City Driving Cycle - GVW - Battery SOC comparison for A-OPD, OPD, Series Brake Regen, and Parallel Brake Regen.

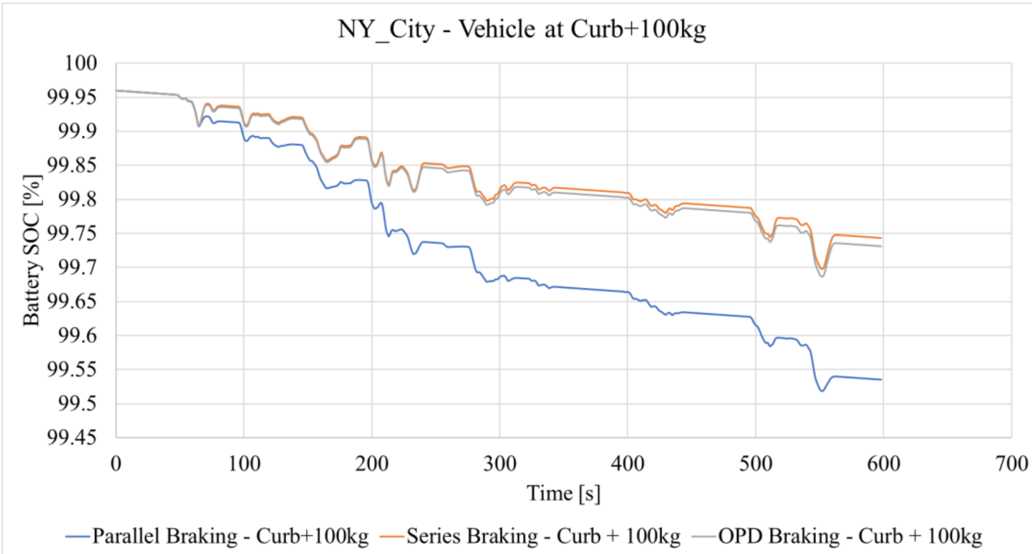

Figure 7.36: NY_City Driving Cycle – Curb+100kg - Battery SOC comparison for A-OPD, OPD, Series Brake Regen, and Parallel Brake Regen

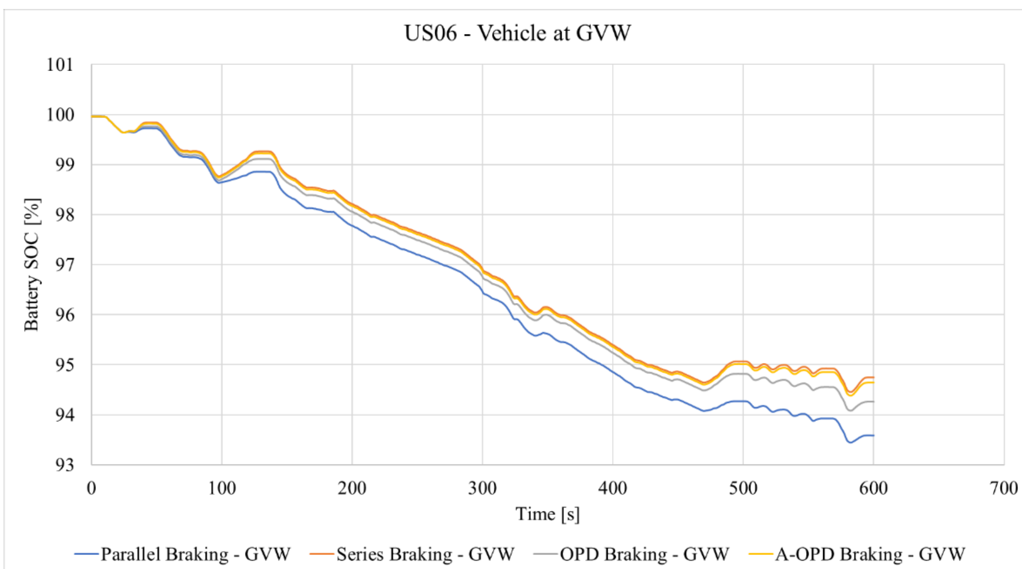

Figure 7.37: US06 Driving Cycle - GVW - Battery SOC comparison for A-OPD, OPD, Series Brake Regen, and Parallel Brake Regen.

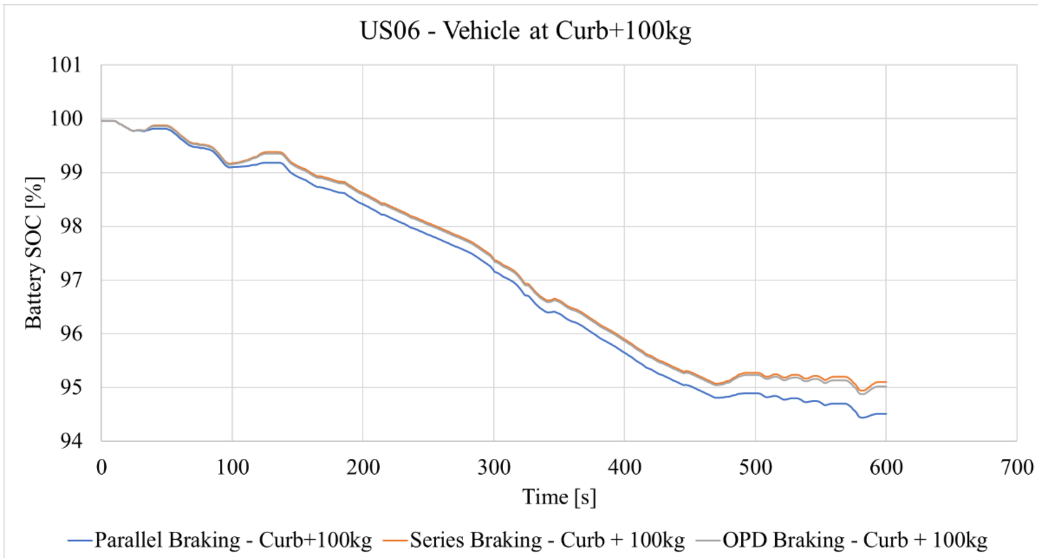

Figure 7.38: US06 Driving Cycle – Curb+100kg - Battery SOC comparison for A-OPD, OPD, Series Brake Regen, and Parallel Brake Regen.

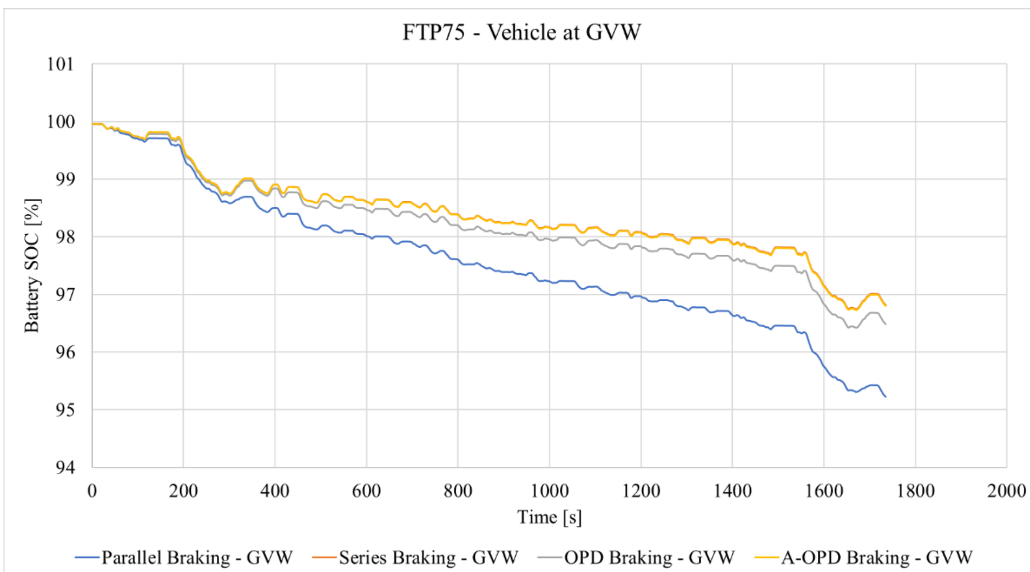

Figure 7.39: FTP 75 Driving Cycle - GVW - Battery SOC comparison for A-OPD, OPD, Series Brake Regen, and Parallel Brake Regen.

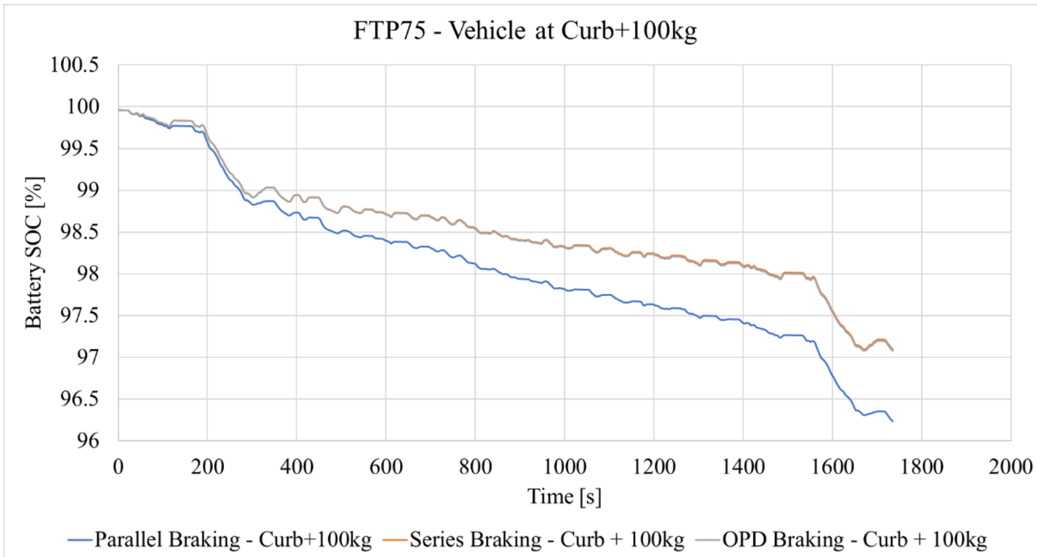

Figure 7.40: FTP 75 Driving Cycle – Curb+100kg - Battery SOC comparison for A-OPD, OPD, Series Brake Regen, and Parallel Brake Regen.

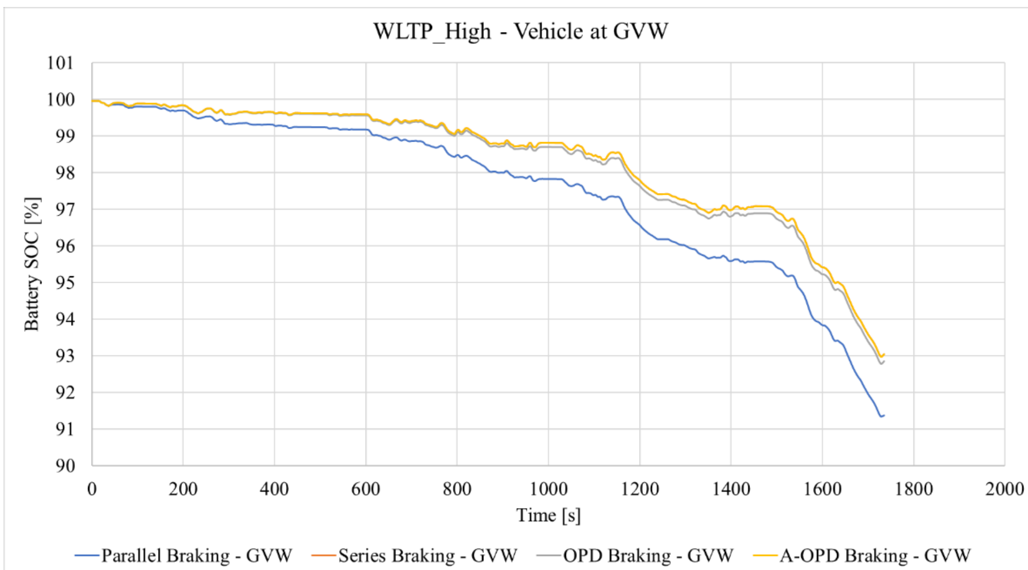

Figure 7.41: WLTP_High Driving Cycle - GVW - Battery SOC comparison for A-OPD, OPD, Series Brake Regen, and Parallel Brake Regen.

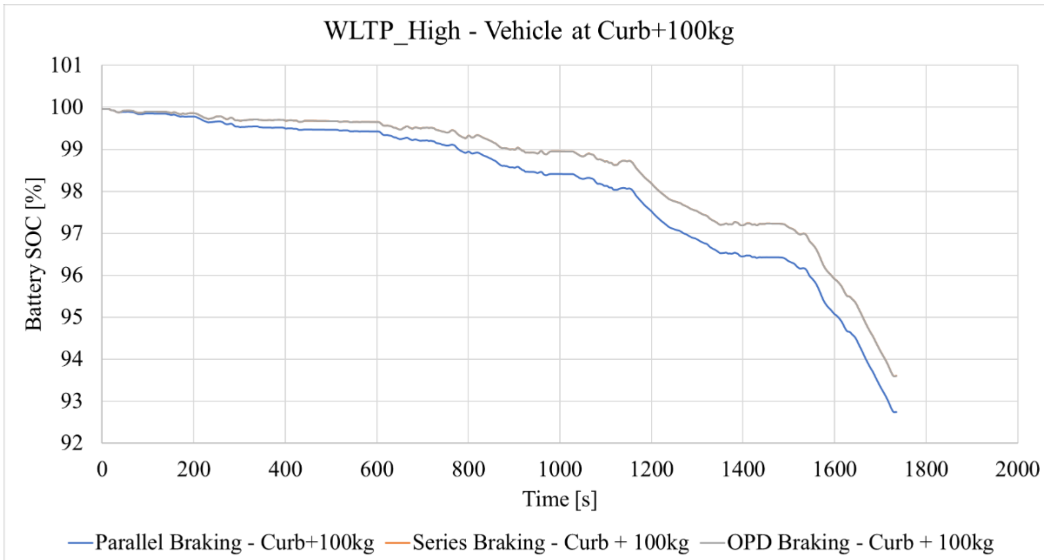

Figure 7.42: WLTP_High Driving Cycle – Curb+100kg - Battery SOC comparison for A-OPD, OPD, Series Brake Regen, and Parallel Brake Regen.

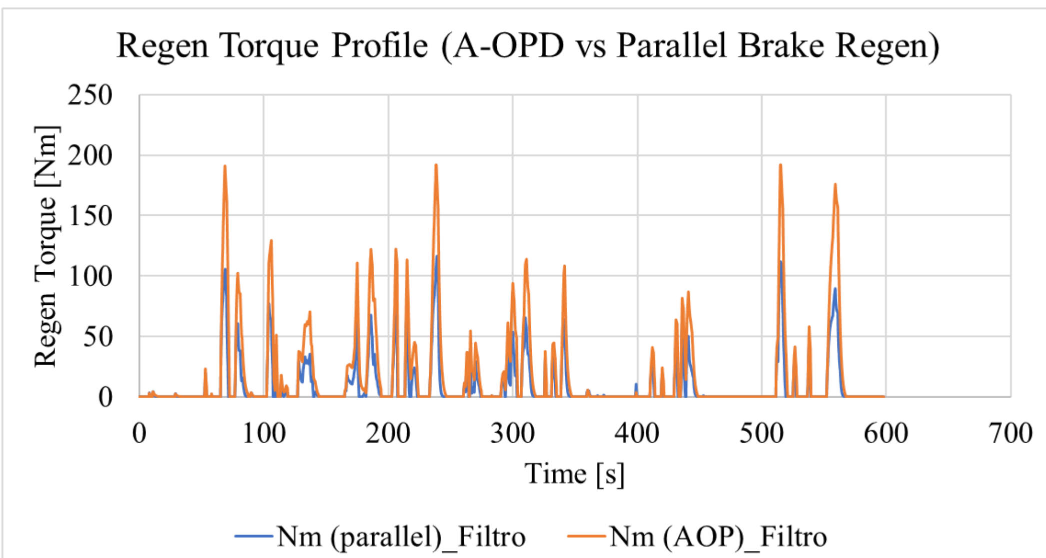

Figure 7.43: NY-City Driving Cycle - GVW – Regen Torque Profile for A-OPD and Parallel Brake Regen.

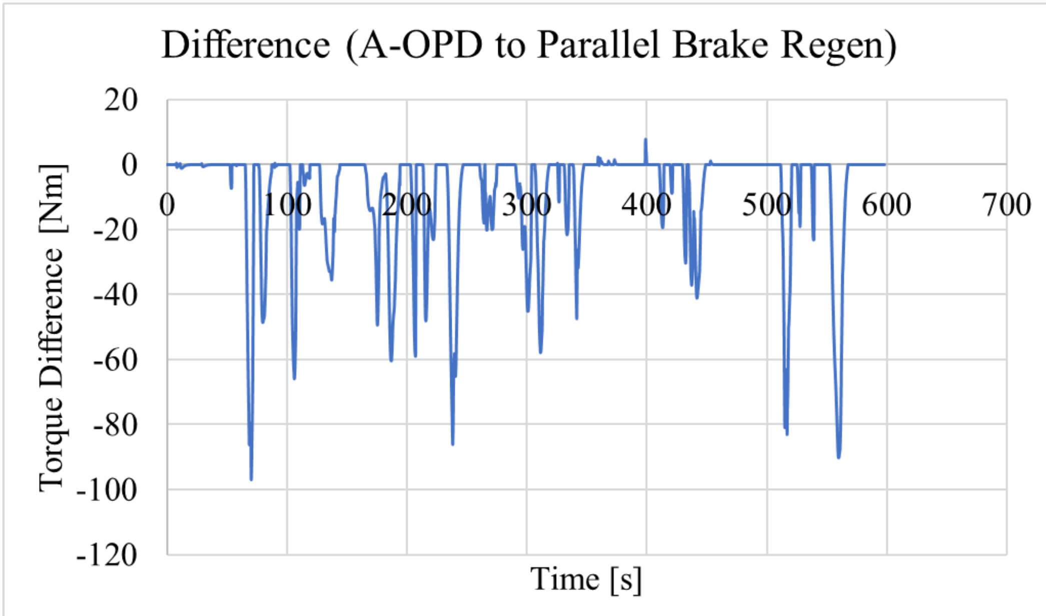

Figure 7.44: NY-City Driving Cycle - GVW – Regen Torque Profile Difference from A-OPD and Parallel Brake Regen.

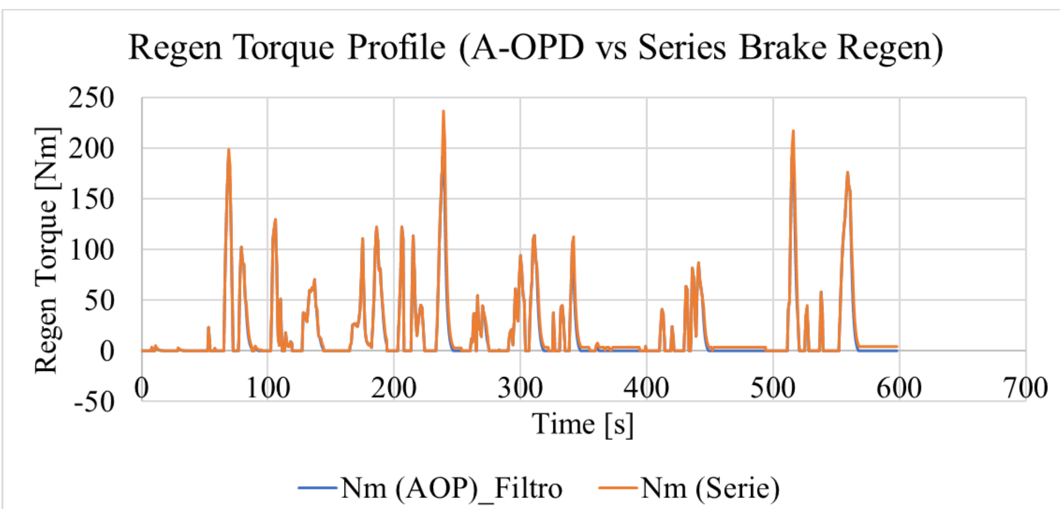

Figure 7.45: NY-City Driving Cycle - GVW – Regen Torque Profile for A-OPD and Series Brake Regen.

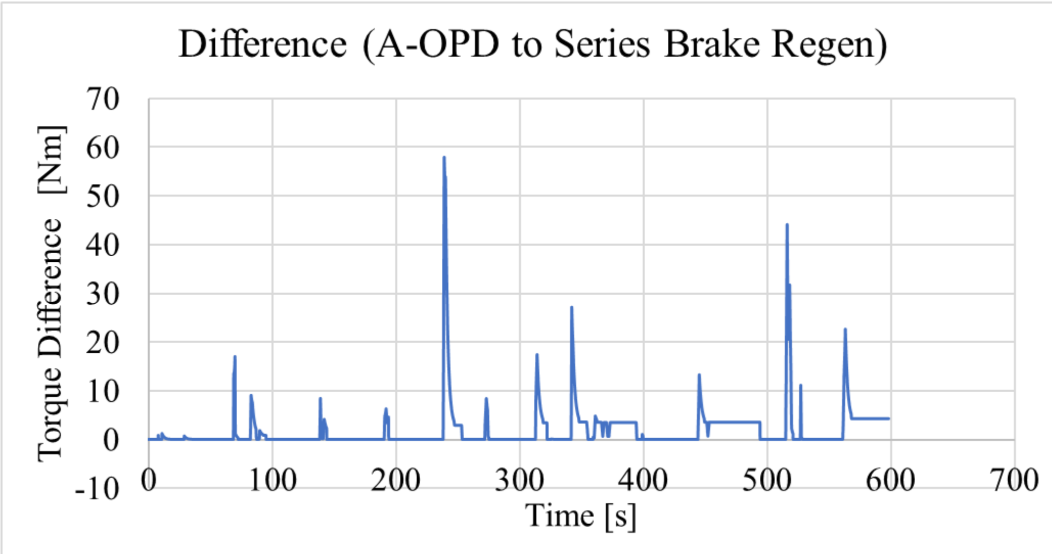

Figure 7.46: NY-City Driving Cycle – GVW – Regen Torque Profile Difference from A-OPD and Series Brake Regen.

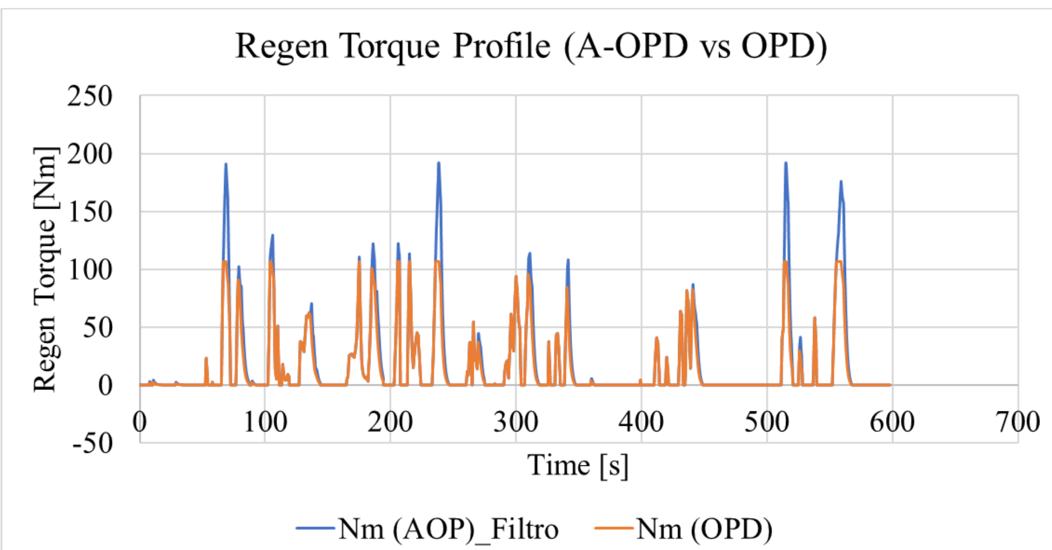

Figure 7.47: NY-City Driving Cycle – GVW – Regen Torque Profile for A-OPD and OPD

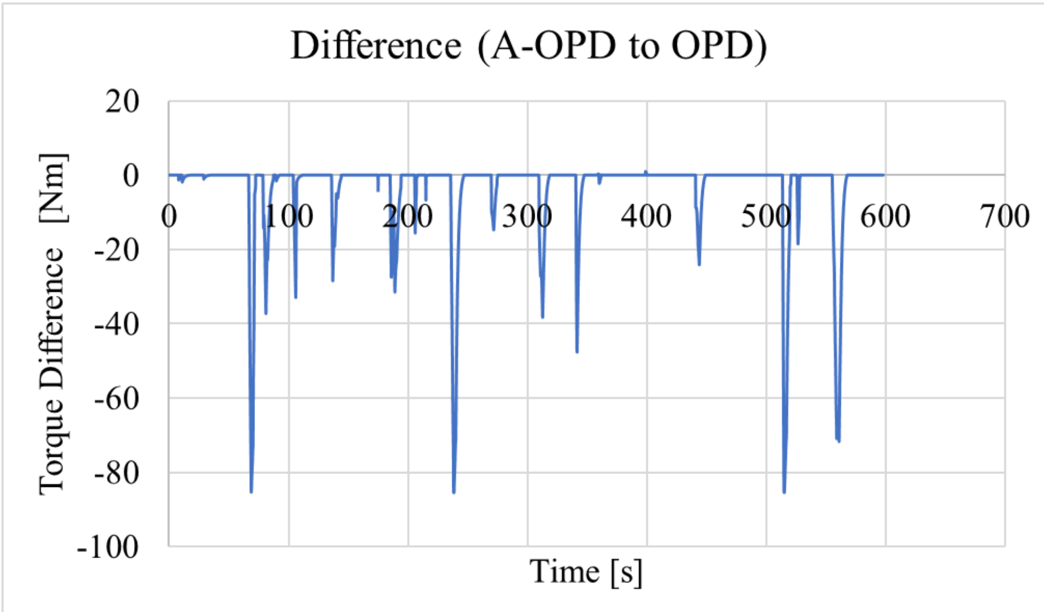

Figure 7.48: NY-City Driving Cycle – GVW – Regen Torque Profile Difference from A-OPD and OPD.

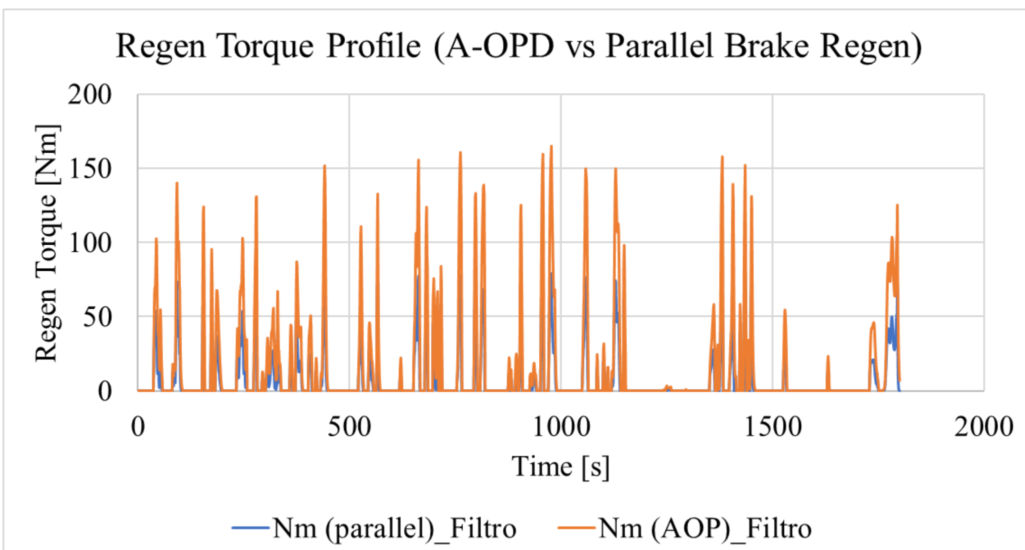

Figure 7.49: WLTP_High Driving Cycle - GVW – Regen Torque Profile for A-OPD and Parallel Brake Regen.

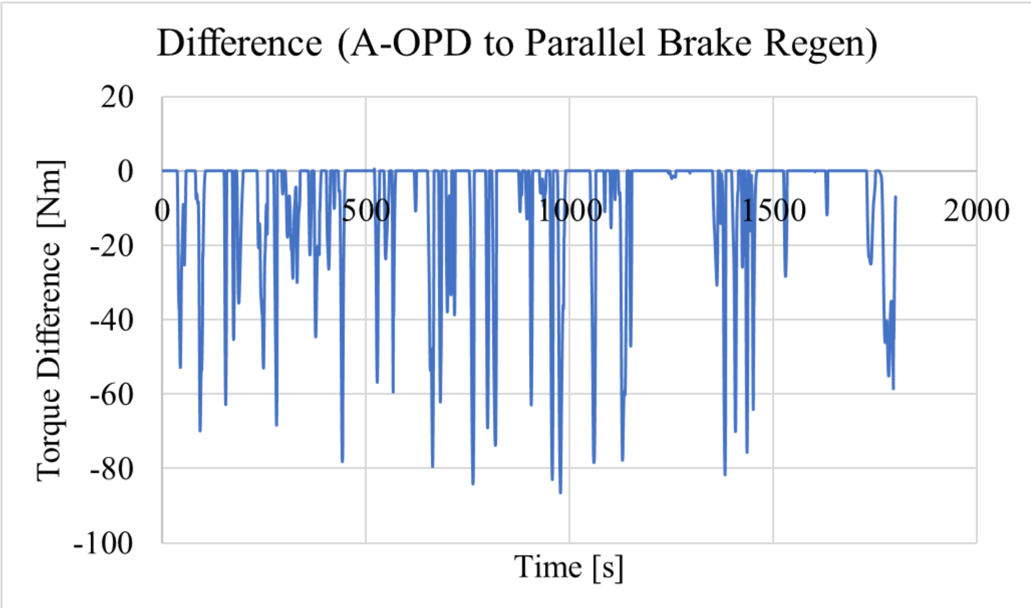

Figure 7.50: WLTP_High Driving Cycle - GVW – Regen Torque Profile Difference from A-OPD and Parallel Brake Regen.

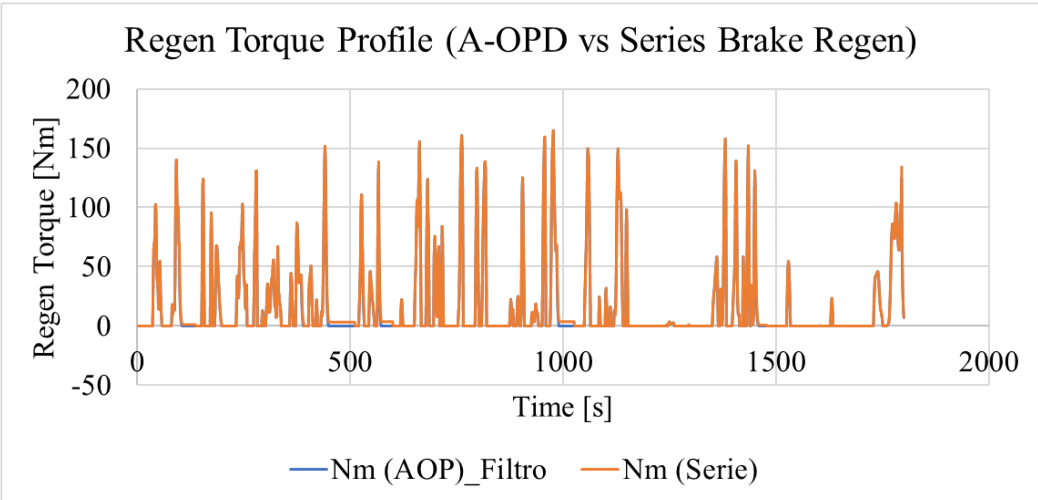

Figure 7.51: WLTP_High Driving Cycle - GVW – Regen Torque Profile for A-OPD and Series Brake Regen.

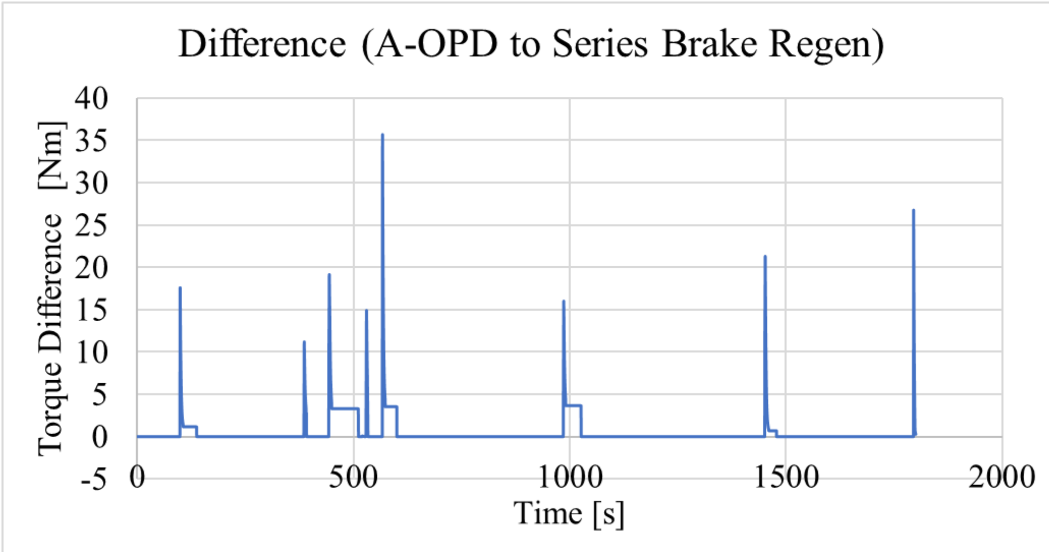

Figure 7.52: WLTP_High Driving Cycle - GVW – Regen Torque Profile Difference from A-OPD and Series Brake Regen.

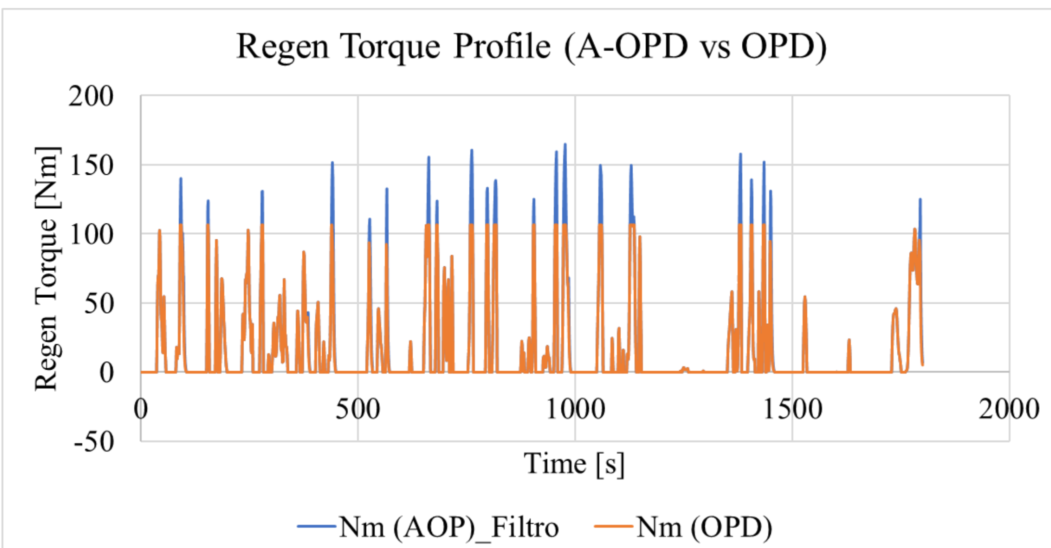

Figure 7.53: WLTP_High Driving Cycle - GVW – Regen Torque Profile for A-OPD and OPD.

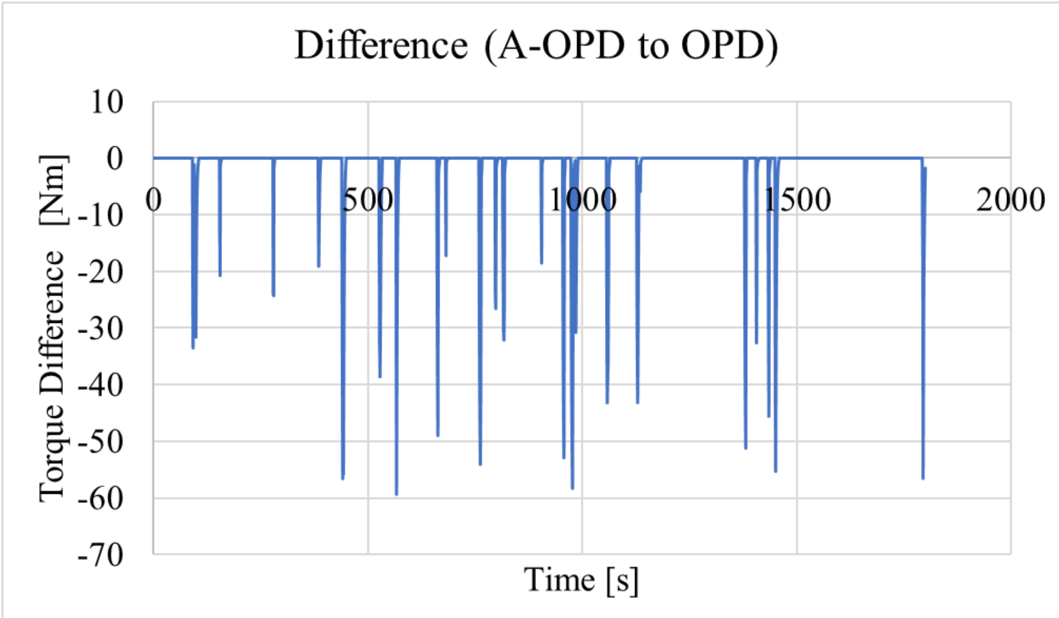

Figure 7.54: WLTP_High Driving Cycle - GVW – Regen Torque Profile Difference from A-OPD and OPD.

7.5 Summary

The substantially lower total cost of ownership, up to 80% less than their internal combustion engine counterparts, positions EVs as an economically attractive choice, particularly for fleet operators. It's important to note that while their environmental benefits are evident, their economic appeal remains a pivotal factor in their widespread adoption.

Integrating regenerative braking systems in EVs has notably improved overall energy efficiency. However, implementing such strategies, especially in commercial vehicles, presents considerable challenges, including the complexity of braking control modules and the need for extensive testing on specialized surfaces.

One-pedal driving (OPD) is an innovative approach that simplifies vehicle operation using only the accelerator pedal. The challenge lies in calibrating OPD effectively for vehicles with varying weights, as what works well for a loaded vehicle may not provide the same safety and comfort for an empty one, and vice versa. The adaptive one-pedal drive (A-OPD) strategy was introduced in response to this challenge, specifically tailored for electric commercial vehicles with significant differences between curb and gross vehicle weight (GVW).

This research has shown that A-OPD significantly improves energy efficiency, especially in dense urban traffic scenarios, compared to conventional OPD. The gains are evident even when the vehicle is partially loaded, demonstrating its practical utility in real-world conditions. While A-OPD may be less effective than series regenerative braking in terms of energy recovery, it outperforms vehicles equipped with parallel regenerative braking systems by a substantial margin.

Considering the limitations of commercial vehicles, often lacking advanced electronic braking systems, the A-OPD approach represents a significant leap forward in enhancing energy efficiency without the need for complex ABS, EBS, and ESP systems. This promising technology holds the potential to transform the efficiency and performance of electric commercial vehicles, contributing to a more sustainable and cost-effective future in the automotive industry.

Chapter 8

Conclusion and Future Work

8.1 Summary and Conclusions

The COVID-19 pandemic, characterized as the most significant health crisis since the 1918 Pandemic, disrupted the global economy, resulting in a substantial decline in energy demand. Chapter 2, titled "The Experiment," draws parallels between the mobility disruptions caused by EVs replacing ICE vehicles and the pandemic's effects. It provides a unique perspective on how electrifying transportation systems and increasing the use of renewable energy sources can effectively reduce CO2 emissions and air pollution. It highlights that electrifying 40% of surface transportation with renewable energy aligns with Paris Agreement targets but underscores the need for substantial capital investments and strengthened regulations against air pollution and CO2 emissions. This chapter emphasizes the importance of transitioning surface transportation to electricity, showcasing the profound impact of the COVID-19 "Great Lockdown" on global emissions and air pollution and emphasizing the interconnectedness of economic industries and climate change.

Chapter 3 delves into the need for electrifying propulsion systems to meet stringent compliance requirements and address growing concerns about CO2 emissions. This chapter navigates the complex landscape of electrified powertrains, highlighting the diversity of architectures and their impact on vehicle performance, fuel economy, drivability, comfort, and safety. It becomes evident that selecting the most suitable electrified propulsion system is a multidisciplinary process where technical and business considerations intersect. As the automotive industry evolves, marked by the shift towards electrified vehicles, this chapter underscores the complexity of designing optimal propulsion system architectures and subsystems in the face of technical and organizational challenges.

The model-centric approach introduced in Chapter 4 emerges as a valuable asset for addressing the intricate challenges of electrified propulsion systems. This methodology enables continuous design optimization and tradeoff analysis, creating a multidisciplinary domain within the propulsion system's boundaries and across the other vehicle systems, bridging the gap between requirements and component designs. The review of model-based engineering showcases the versatility of models in capturing system complexities and supporting decision-making across various design complexities. Furthermore, the chapter reinforces the efficacy of the developed simulation tool, emphasizing its reliability in estimating key variables, but mainly its energy efficiency, while calculating the DC currents, battery terminal voltage, and the forces and torques involved in the vehicle dynamics. This model-centric approach offers a promising solution for the evolving automotive industry as it embraces electrification, guiding design choices, enhancing energy efficiency assessment, and facilitating software and control calibration.

Chapter 5 presents a comprehensive analysis of the economic feasibility of different propulsion architectures for electric vehicles. The findings underscore a commendable payback period and return on investment across all architectures, regardless of the electricity procurement methodology used. However, Architecture 2 (multi-speed gearbox with one electric motor) and 3 (two electric motors connected in series) emerge as economically favorable options, boasting a higher Internal Rate of Return (IRR) and residual value due to their more efficient electric machine operation. This chapter provides invaluable insights into the financial aspects of electric vehicle adoption and highlights the importance of selecting the exemplary propulsion architecture to optimize economic outcomes.

Chapter 6 explores integrating a propulsion system model into a one-dimensional model-in-the-loop approach applied in driver-in-the-loop simulation to evaluate regenerative braking strategies. The results show a significant energy efficiency and driveability advantage for the series regenerative braking system, especially in urban applications, over the parallel regenerative braking strategy. This finding is particularly crucial for commercial vehicles, where efficiency directly impacts the total cost of ownership. While the research highlights the benefits of regenerative braking, it also acknowledges the complexity of implementing such strategies in commercial vehicles, emphasizing the need for additional research to address efficiency challenges, covered in Chapter 7. Still, in Chapter 6, the integration of the driver-in-the-loop was an excellent and reliable opportunity to evaluate the impacts of architecture decisions on vehicle driveability in the very early stages of vehicle development.

Chapter 7 introduces the concept of adaptive one-pedal driving (A-OPD), tailored for electric commercial vehicles with varying weights. A-OPD significantly improves energy efficiency, even under partial load conditions, in dense urban traffic scenarios compared to conventional one-pedal driving, and more particularly, it provides a very significant improvement compared to the parallel regenerative braking strategy. Compared to the series regenerative braking strategy, the A-OPD shows up to 5% inefficiency. However, this is a significant result since this technology offers a practical solution to enhance energy efficiency in commercial vehicles without relying on complex electronic braking systems, which is the case of the series regenerative braking architecture. It holds the potential to transform the efficiency and performance of electric commercial vehicles, contributing to a more sustainable and cost-effective future in the automotive industry.

In conclusion, this journey through chapters 5, 6, and 7 has illuminated several critical points of the light commercial electric vehicle design. First, the economic feasibility of electric vehicles is robust, with the choice of propulsion architecture playing a pivotal role. Second, regenerative braking and adaptive one-pedal driving offer substantial gains in energy efficiency, particularly in urban and commercial settings.

Lastly, as the automotive industry moves toward electrification, innovative approaches and technologies will be essential to ensure a sustainable and efficient future. Virtual engineering has supported this work, facilitated research, and guided decision-making processes. The interplay between technological innovation, economic considerations, and environmental impact underscores the complexity of transitioning to a more sustainable transportation landscape.

8.2 Recommendation for Future Work

This thesis presented a multifaceted exploration of electric commercial vehicle design, assessing the environmental landscape, which works as an electrification motivation tool, and then presenting an electric vehicle modeling and propulsion architectures and regenerative braking strategy assessment for an electric light commercial vehicle. This thesis introduced the A-OPD strategy to enhance commercial electric vehicles' energy efficiency by adapting the regenerative brake torque as a function of the vehicle weight classification.

This research aims to contribute valuable insights into the evolving landscape of electric commercial vehicles and efficiency improvements through the architecture assessment and regenerative braking strategy.

Modeling, architecture assessment, and regenerative braking strategies are wide-open fields of study. Further advances to the presented work will provide a glide path to introducing efficient electrification solutions for commercial vehicles.

On the A-OPD topic, the recommendation for future work is to integrate driving patterns and driver intention recognition into the A-OPD control, together with the weight identification and classification, to improve efficiency and driveability further. Another recommendation is to perform an objective and subjective driveability assessment using a driving simulator to fine-tune the A-OPD controls and calibration.

On modeling and architecture assessment, the proposal for future work is to integrate more architecture models into the simulation tool library and integrate the financial models for vehicle cost and total cost of ownership assessment. Lastly, the automation of the multiple-architecture simulation allows for quicker architecture assessment and optimization algorithms to fine-tune the design of the electric vehicle architectures.

Appendix A

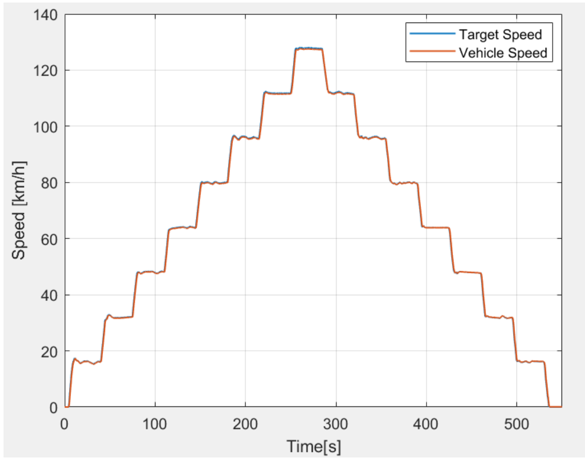

Figure A.1: Acceleration maneuver: 0-80-0 mph, 0% Slope - Vehicle Speed.

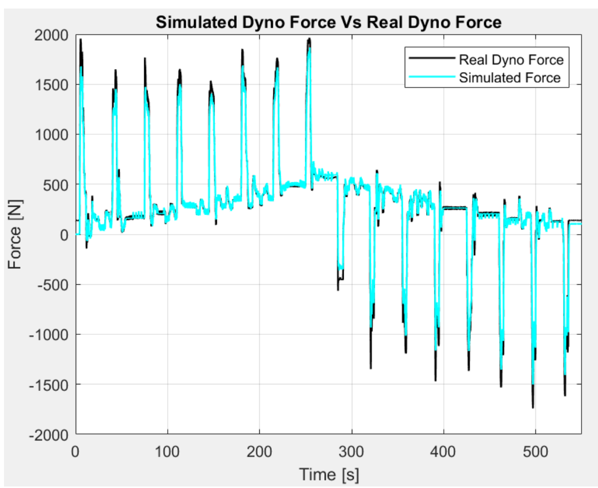

Figure A.2: Acceleration maneuver: 0-80-0 mph, 0% Slope – Tire Force

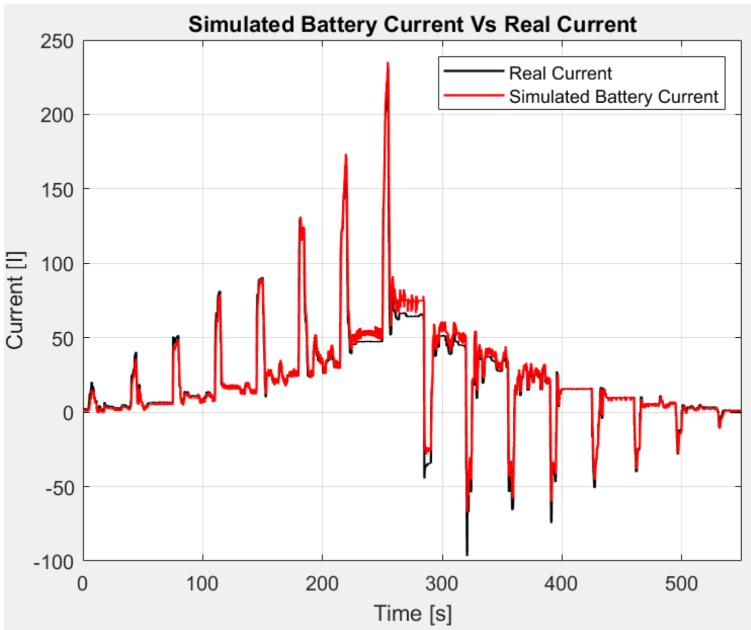

Figure A.3: Acceleration maneuver: 0-80-0 mph, 0% Slope - Battery DC Current.

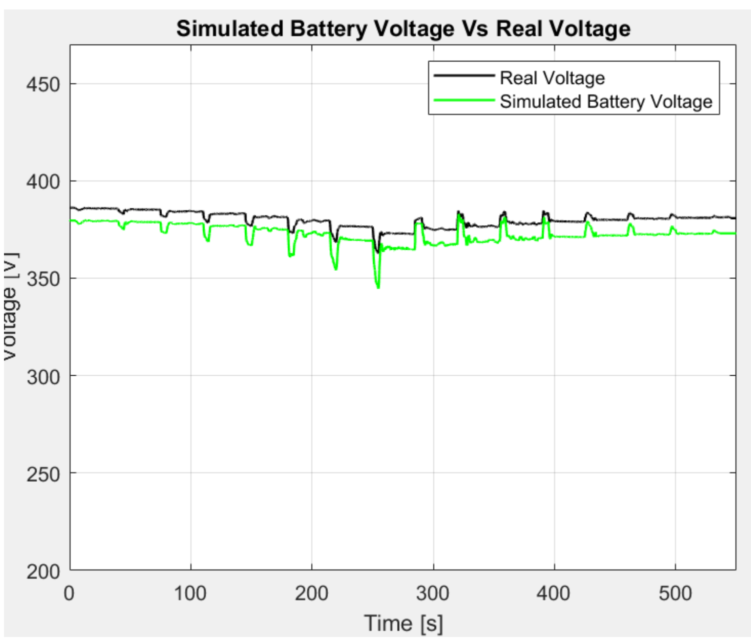

Figure A.4: Acceleration maneuver: 0-80-0 mph, 0% Slope – Battery Terminal Voltage

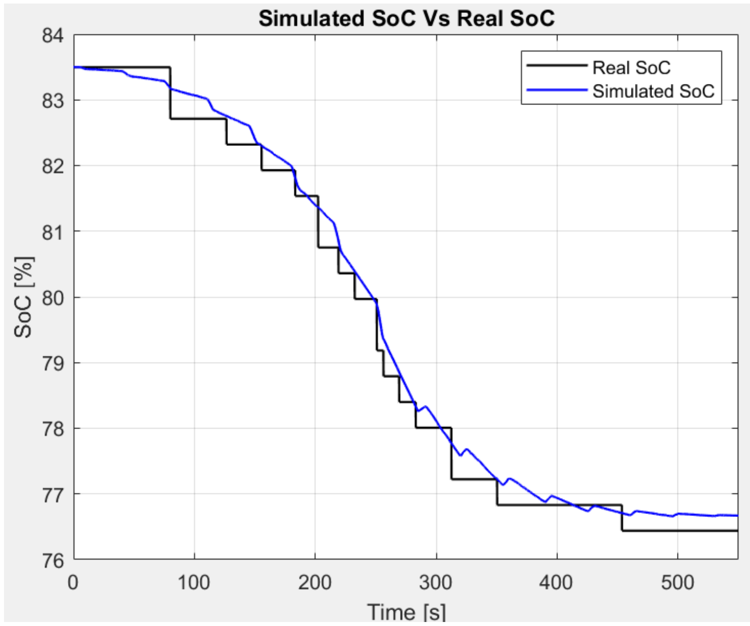

Figure A.5: Acceleration maneuver: 0-80-0 mph, 0% Slope – Battery SOC.

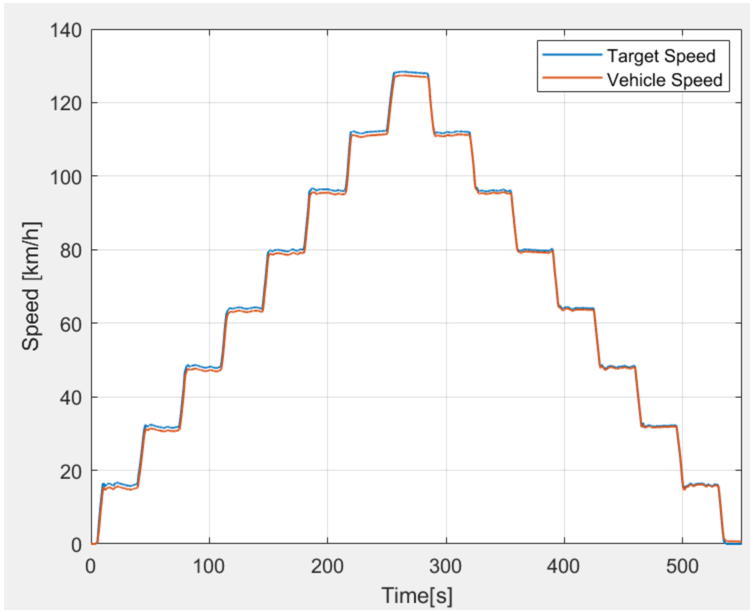

Figure A.6: Acceleration maneuver: 0-80-0 mph, 6% Slope – Vehicle Speed.

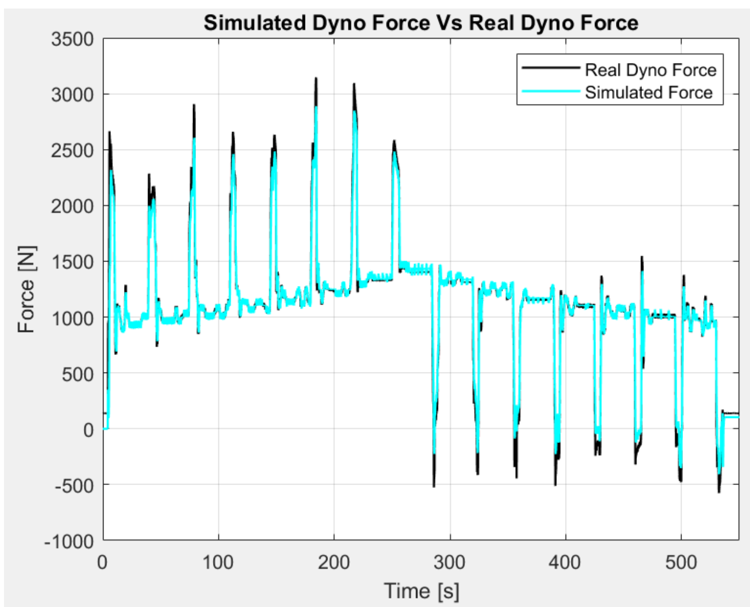

Figure A.7: Acceleration maneuver: 0-80-0 mph, 6% Slope – Tire Force

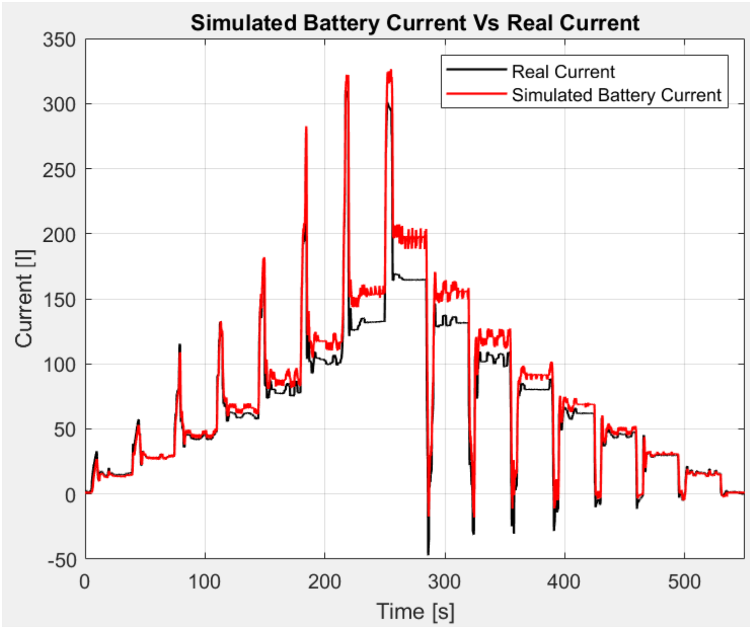

Figure A.8: Acceleration maneuver: 0-80-0 mph, 6% Slope – Battery DC Current.

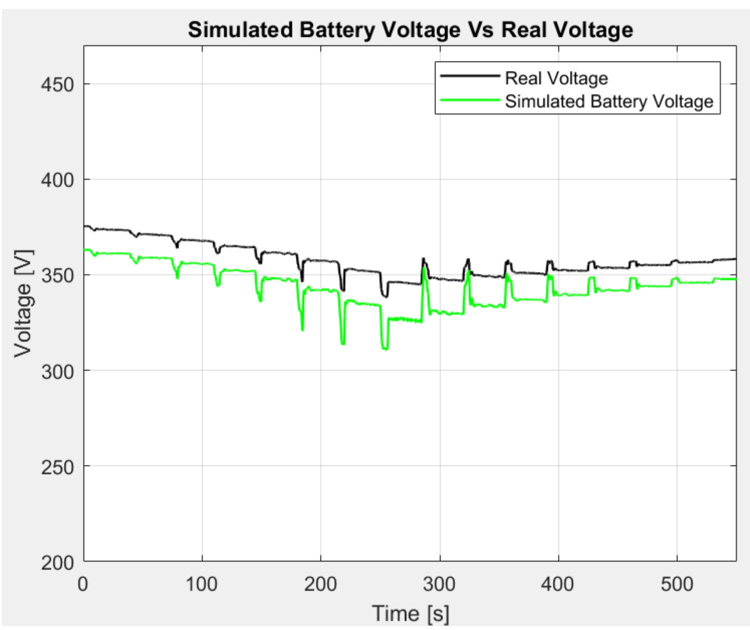

Figure A.9: Acceleration maneuver: 0-80-0 mph, 6% Slope – Battery Terminal Voltage.

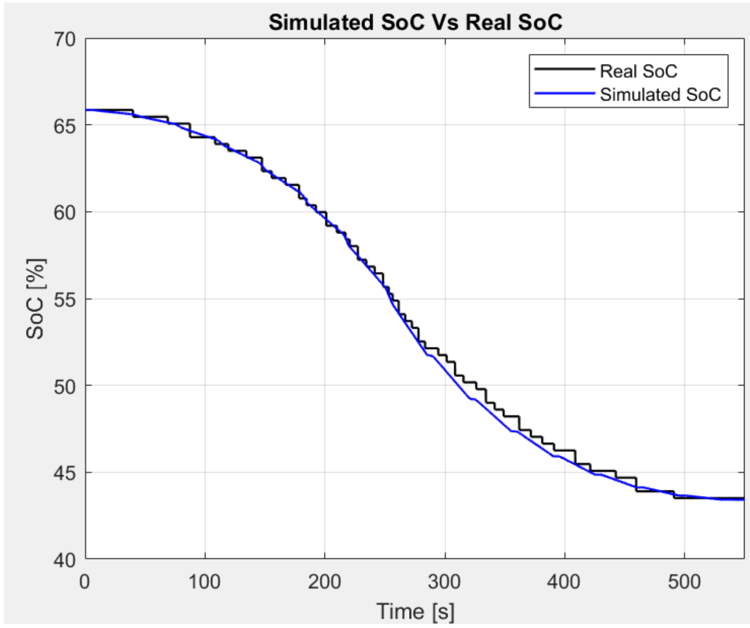

Figure A.10: Acceleration maneuver: 0-80-0 mph, 6% Slope – Battery SOC.

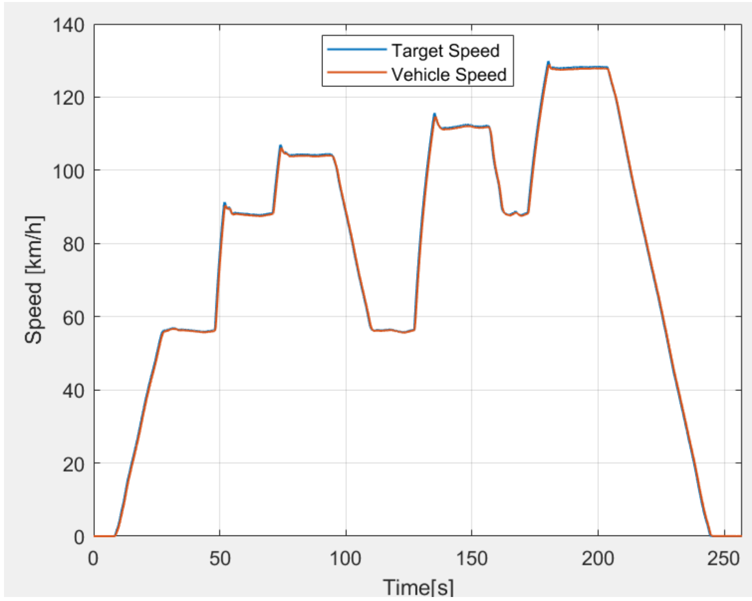

Figure A.11: Passing Maneuver: 0% Slope - Vehicle Speed.

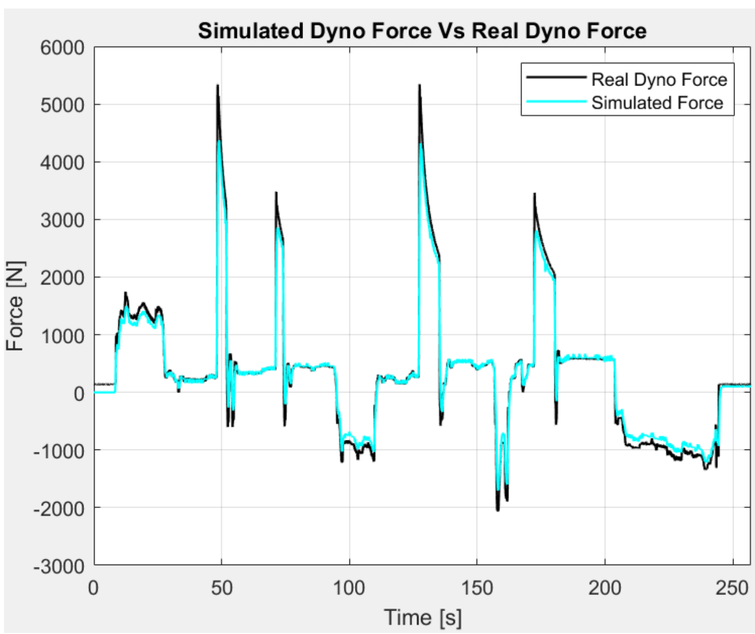

Figure A.12: Passing Maneuver: 0% Slope - Tire Force.

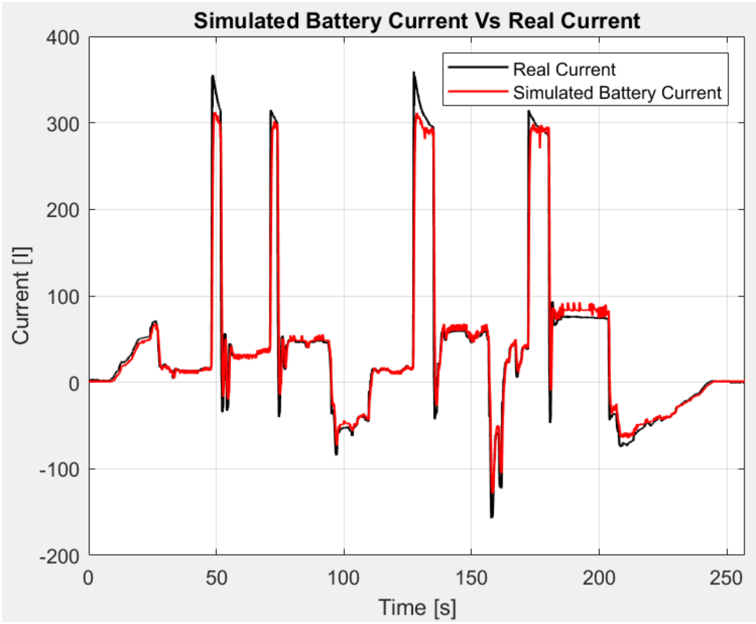

Figure A.13: Passing Maneuver: 0% Slope - Battery DC Current.

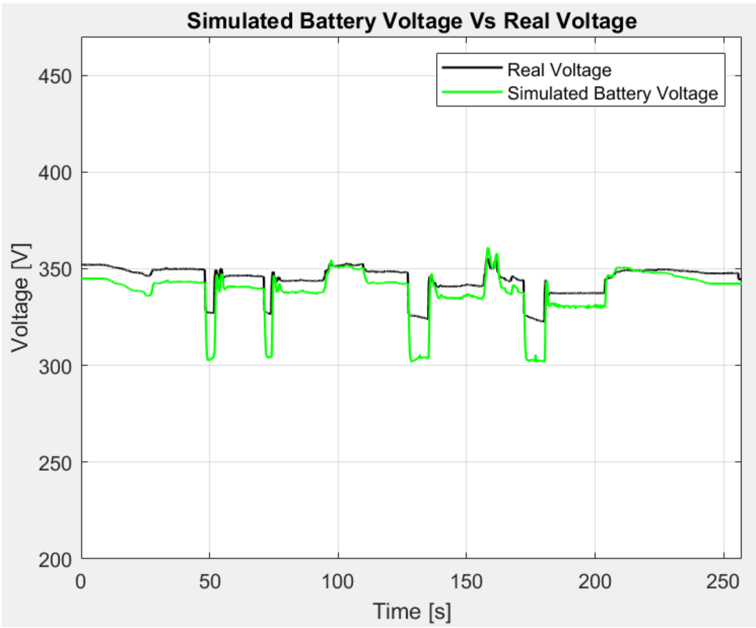

Figure A.14: Passing Maneuver: 0% Slope - Battery Terminal Voltage.

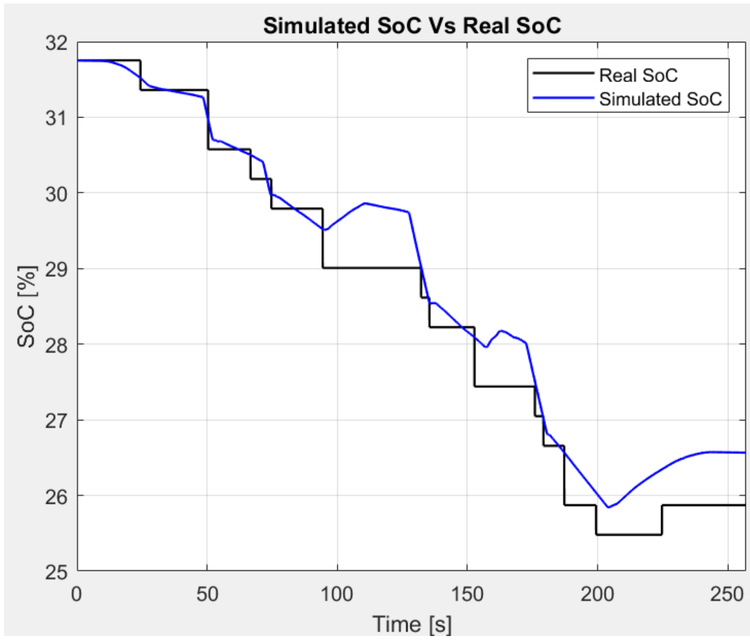

Figure A.15: Passing Maneuver: 0% Slope - Battery SOC.

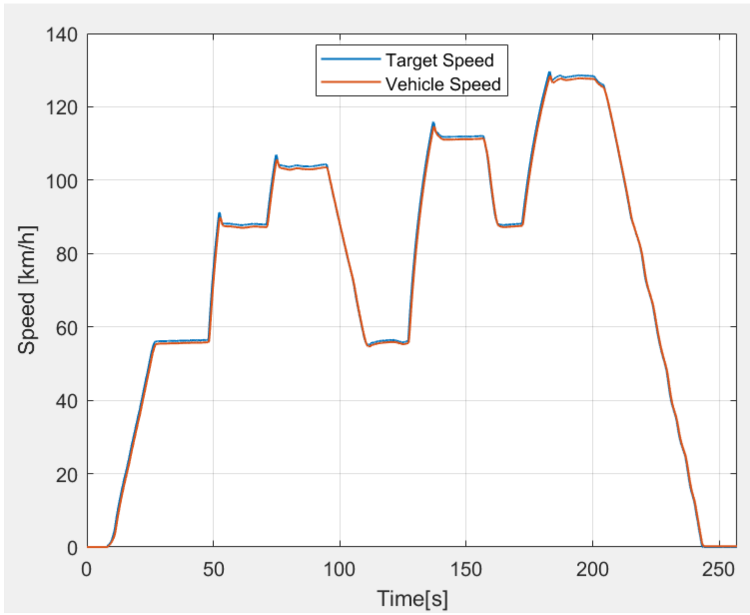

Figure A.16: Passing Maneuver: 3% Slope - Vehicle Speed.

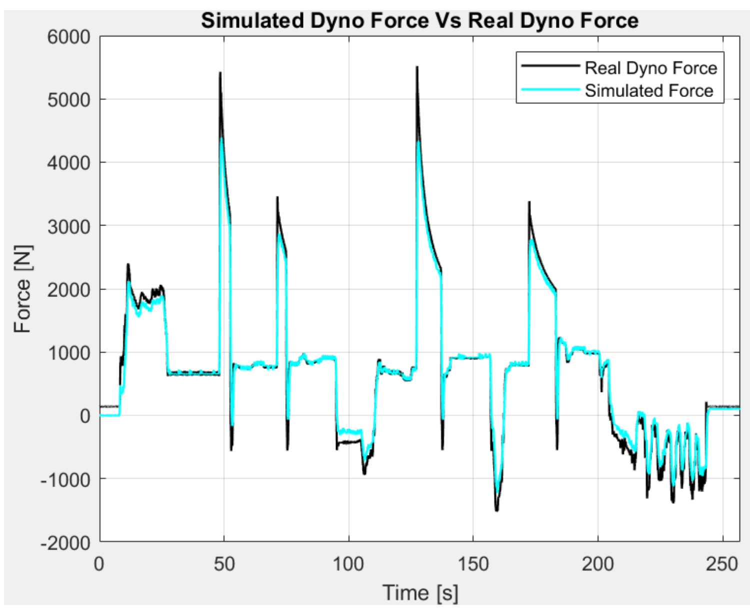

Figure A.17: Passing Maneuver: 3% Slope - Tire Force.

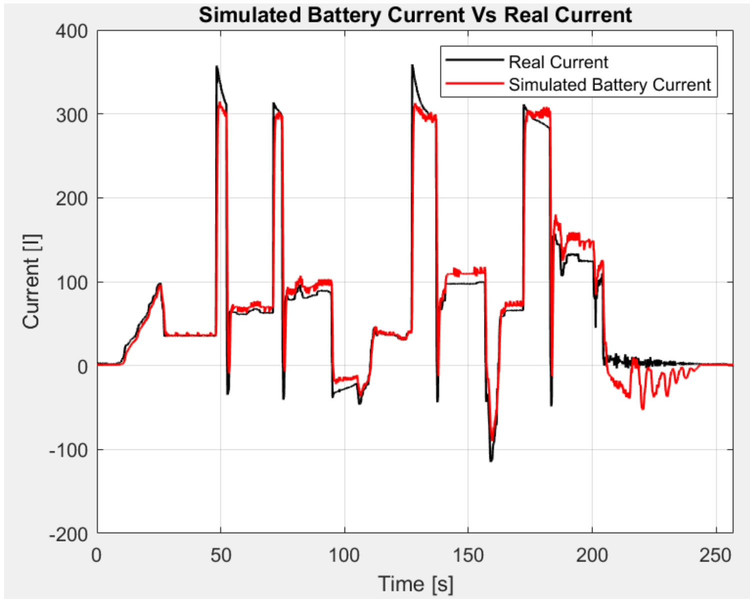

Figure A.18: Passing Maneuver: 3% Slope - Battery DC Current.

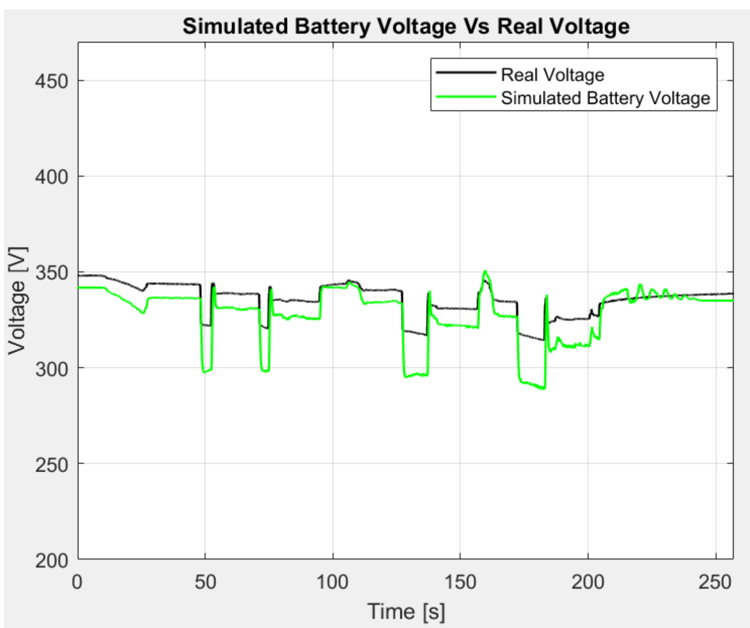

Figure A.19: Passing Maneuver: 3% Slope - Battery Terminal Voltage.

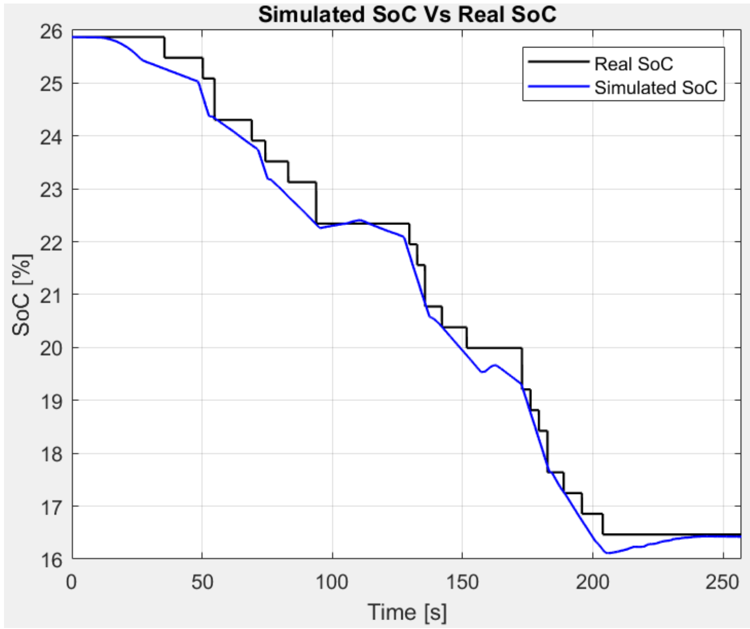

Figure A.20: Passing Maneuver: 3% Slope - Battery SOC.

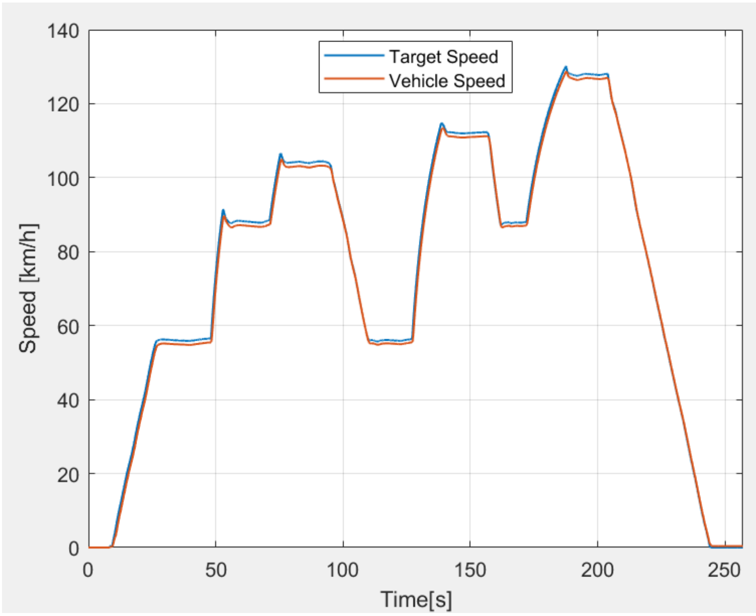

Figure A.21: Passing Maneuver: 6% Slope - Vehicle Speed.

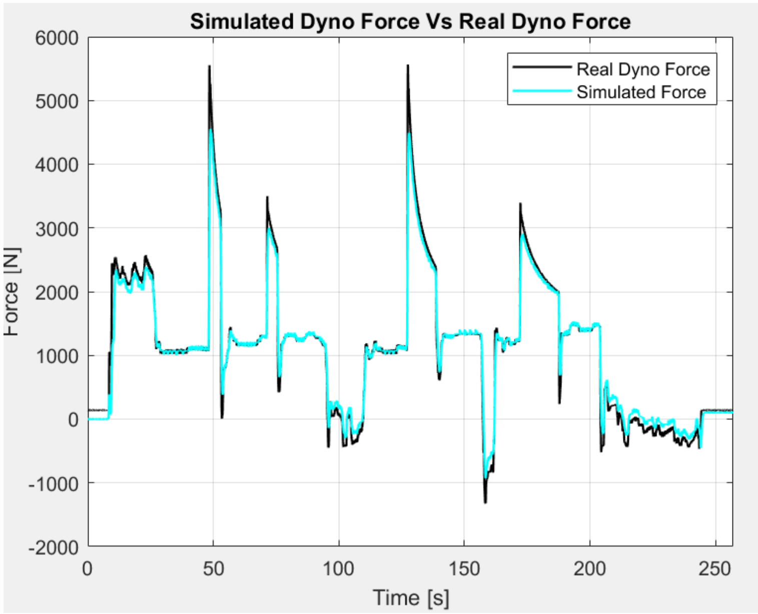

Figure A.22: Passing Maneuver: 6% Slope - Tire Force.

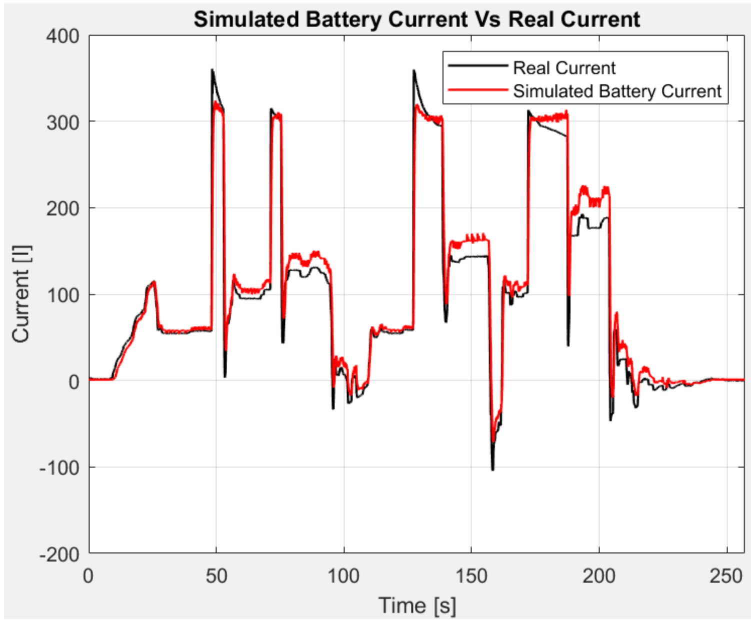

Figure A.23: Passing Maneuver: 6% Slope - Battery DC Current.

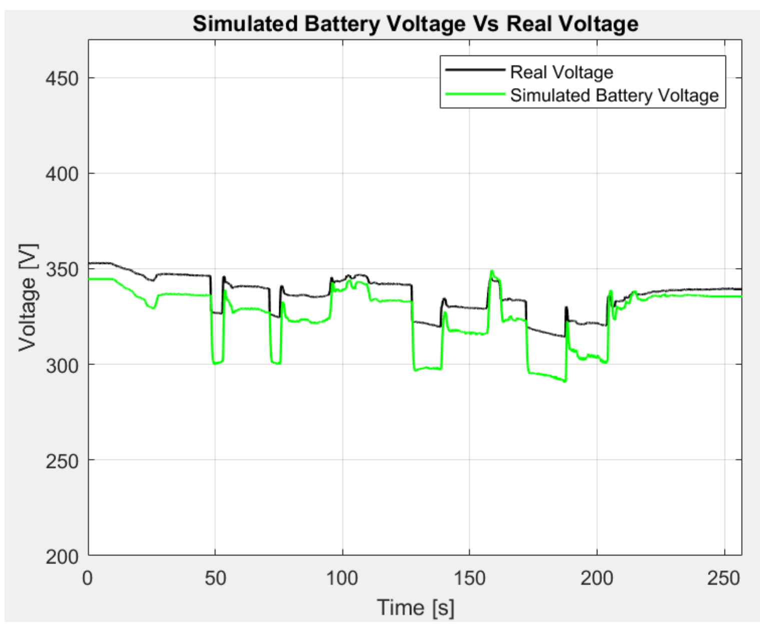

Figure A.24: Passing Maneuver: 6% Slope - Battery Terminal Voltage.

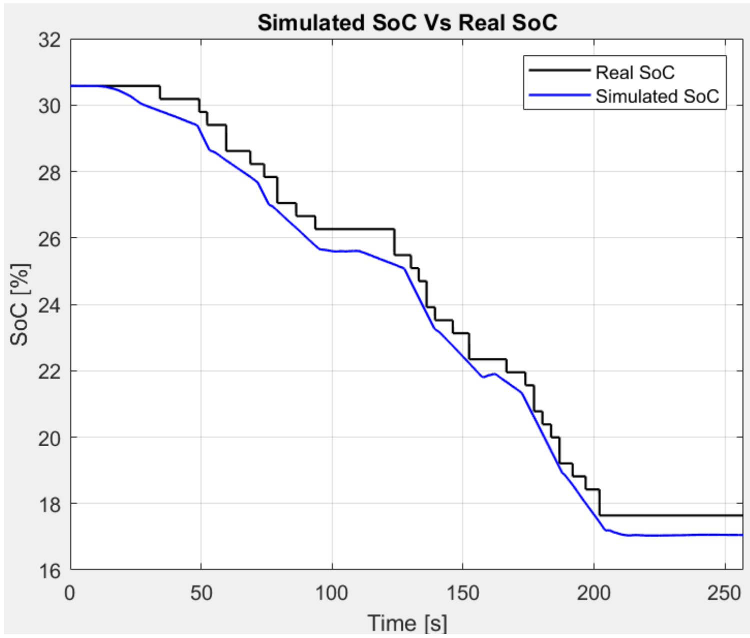

Figure A.25: Passing Maneuver: 6% Slope - Battery SOC.

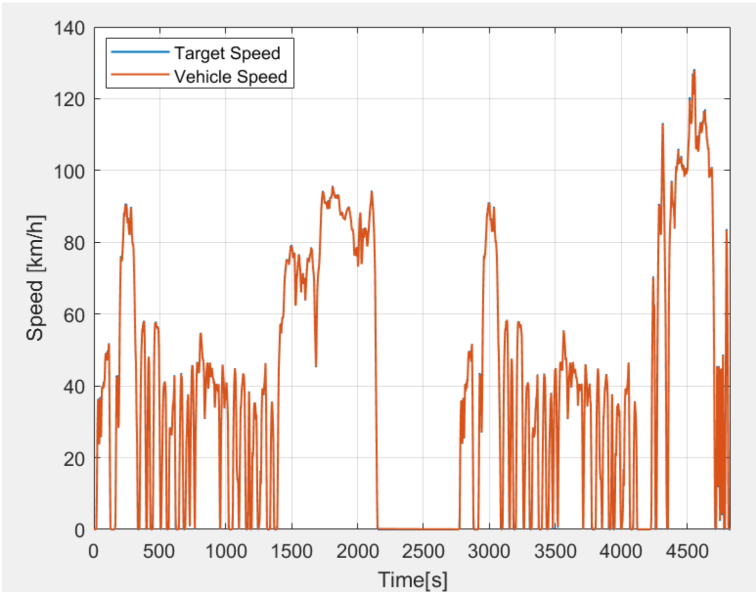

Figure A.26: Driving Cycle: UDDS Ph 1+2, HWY Ph3, UDDS Ph 4+5, US06 Ph 6+7 - Vehicle Speed.

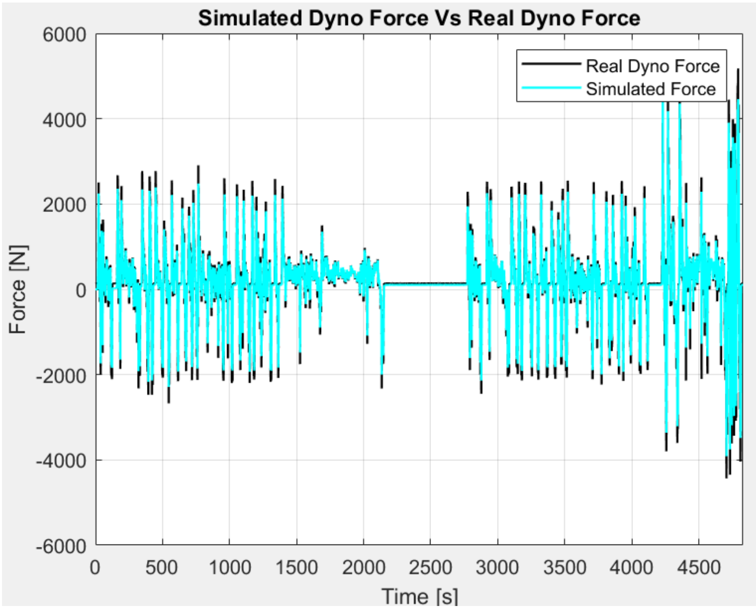

Figure A.27: Driving Cycle: UDDS Ph 1+2, HWY Ph3, UDDS Ph 4+5, US06 Ph 6+7 - Tire Force.

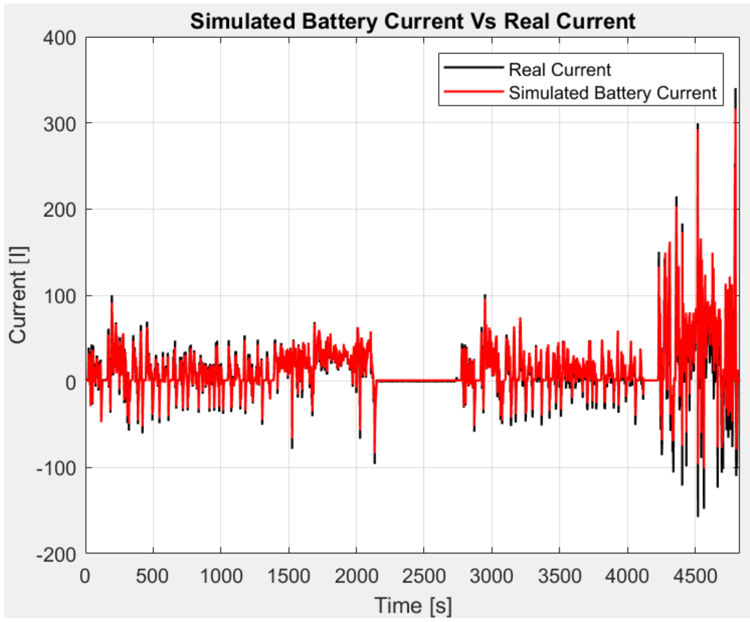

Figure A.28: Driving Cycle: UDDS Ph 1+2, HWY Ph3, UDDS Ph 4+5, US06 Ph 6+7 - Battery DC Current.

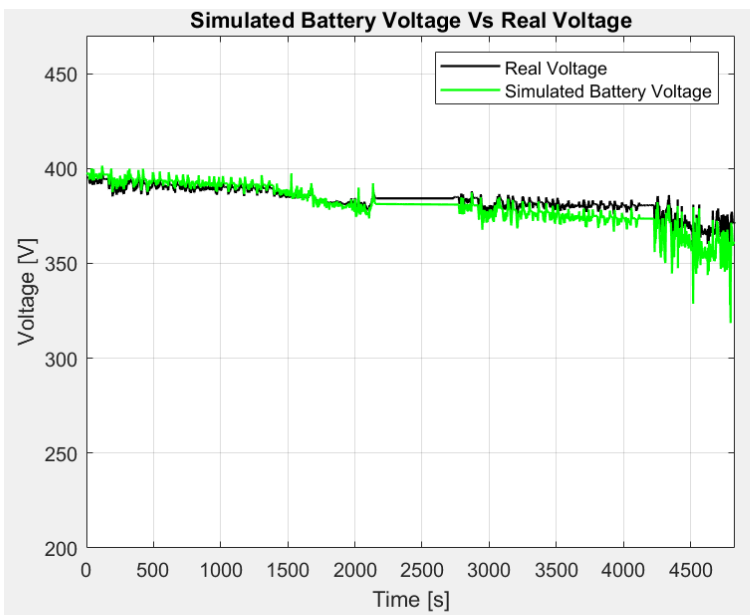

Figure A.29: Driving Cycle: UDDS Ph 1+2, HWY Ph3, UDDS Ph 4+5, US06 Ph 6+7 - Battery Terminal Voltage.

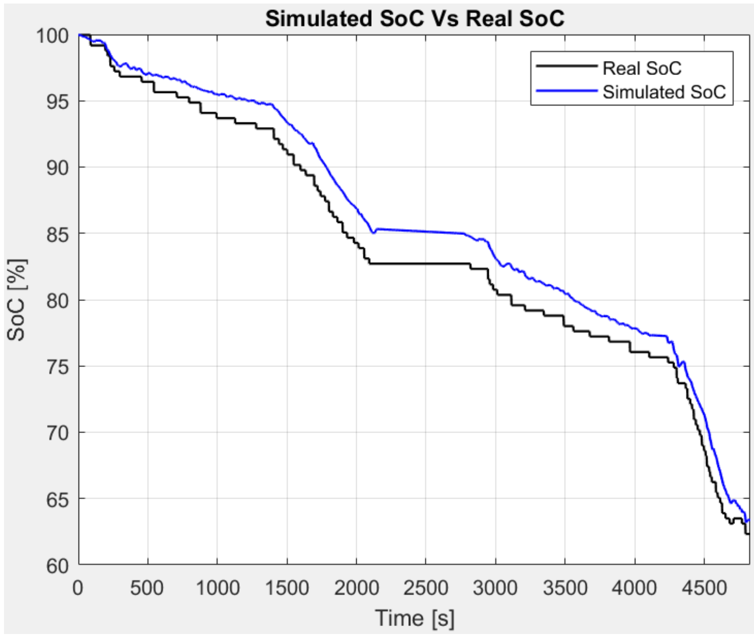

Figure A.30: Driving Cycle: UDDS Ph 1+2, HWY Ph3, UDDS Ph 4+5, US06 Ph 6+7 - Battery SOC.

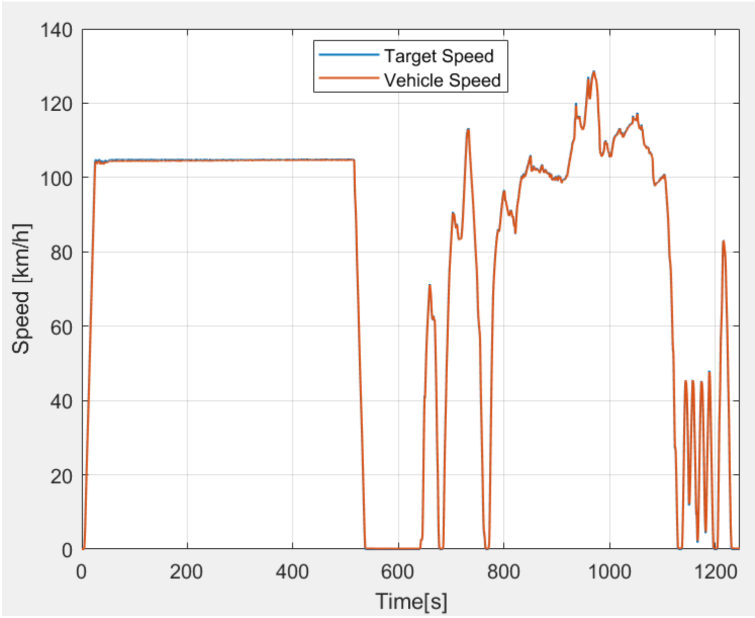

Figure A.31: Driving Cycle: 65mph deplete +US06 ph 3+4 - Vehicle Speed.

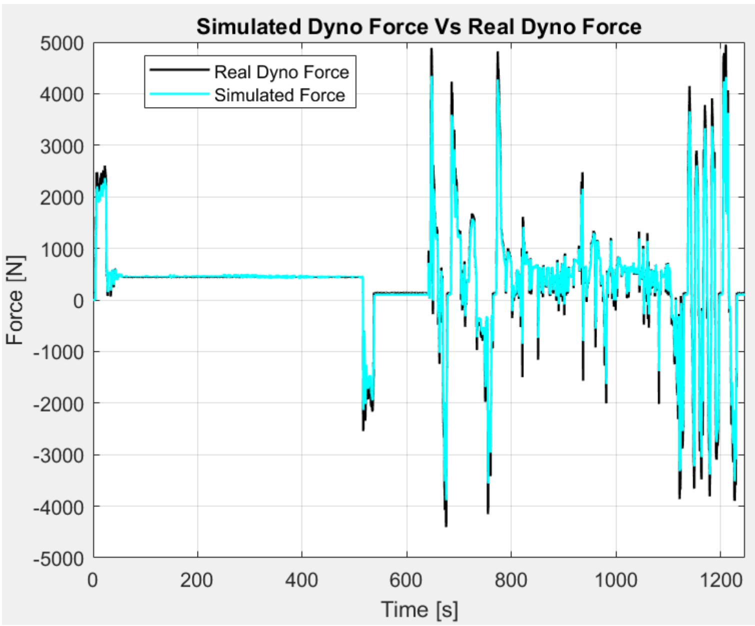

Figure A.32: Driving Cycle: 65mph deplete +US06 ph 3+4 - Tire Force.

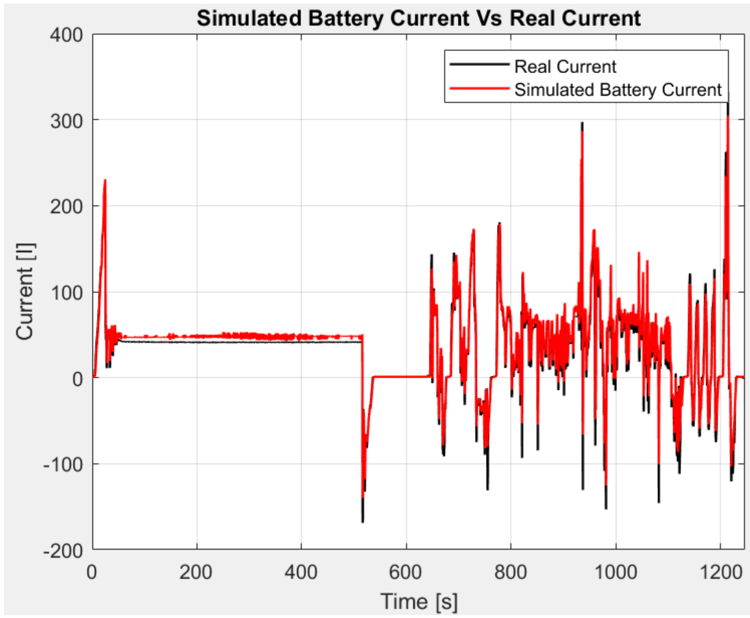

Figure A.33: Driving Cycle: 65mph deplete +US06 ph 3+4 – Battery DC Current.

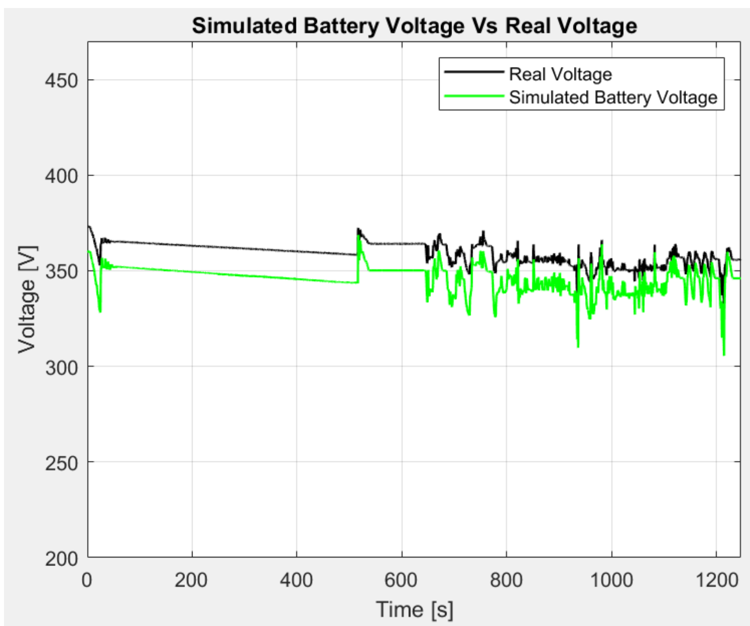

Figure A.34: Driving Cycle: 65mph deplete +US06 ph 3+4 – Battery Terminal Voltage.

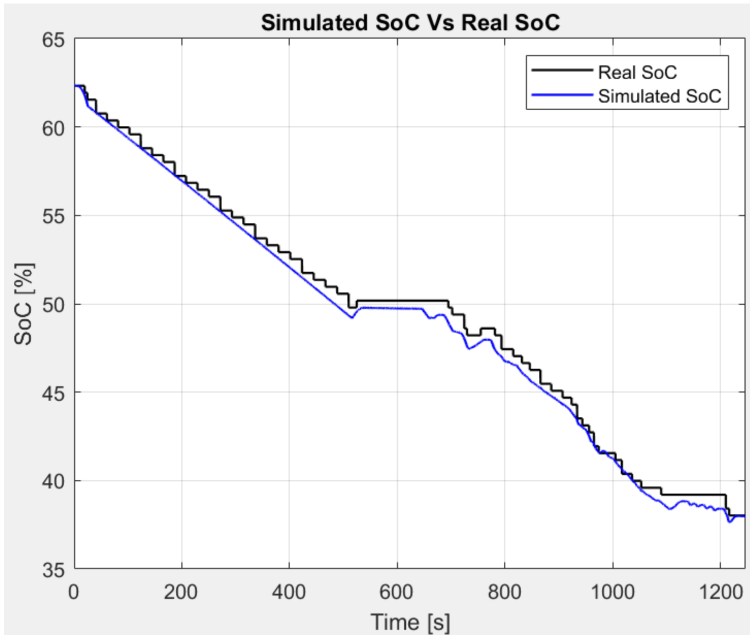

Figure A.35: Driving Cycle: 65mph deplete +US06 ph 3+4 – Battery SOC.

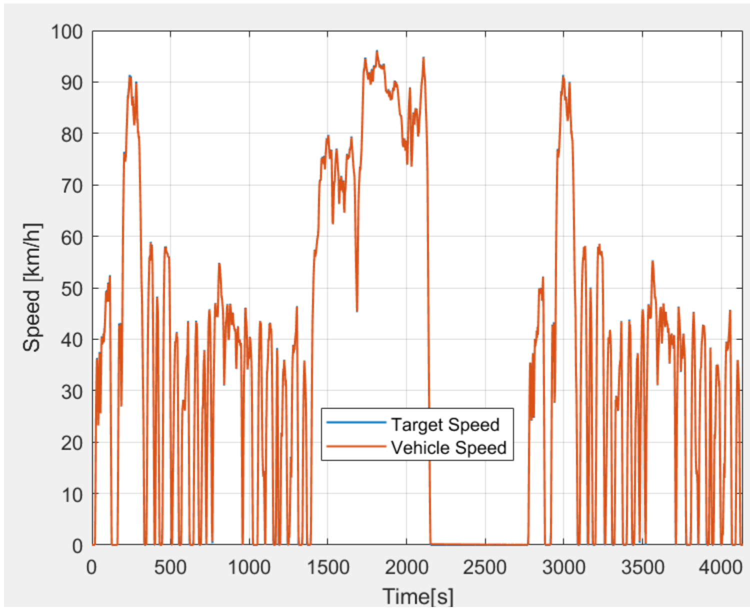

Figure A.36: Driving Cycle: UDDS Ph 1+2, HWY Ph3, UDDS Ph 4+5 – Vehicle Speed.

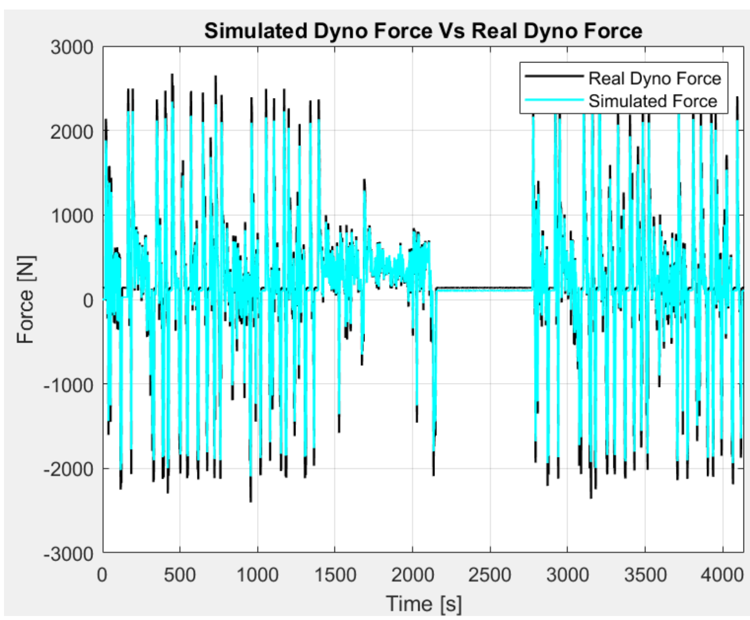

Figure A.37: Driving Cycle: UDDS Ph 1+2, HWY Ph3, UDDS Ph 4+5 – Tire Force.

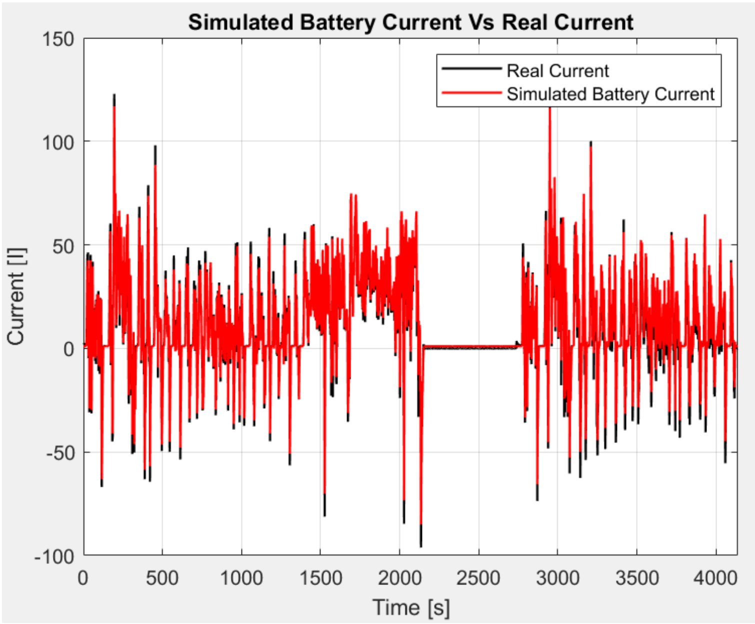

Figure A.38: Driving Cycle: UDDS Ph 1+2, HWY Ph3, UDDS Ph 4+5 – Battery DC Current.

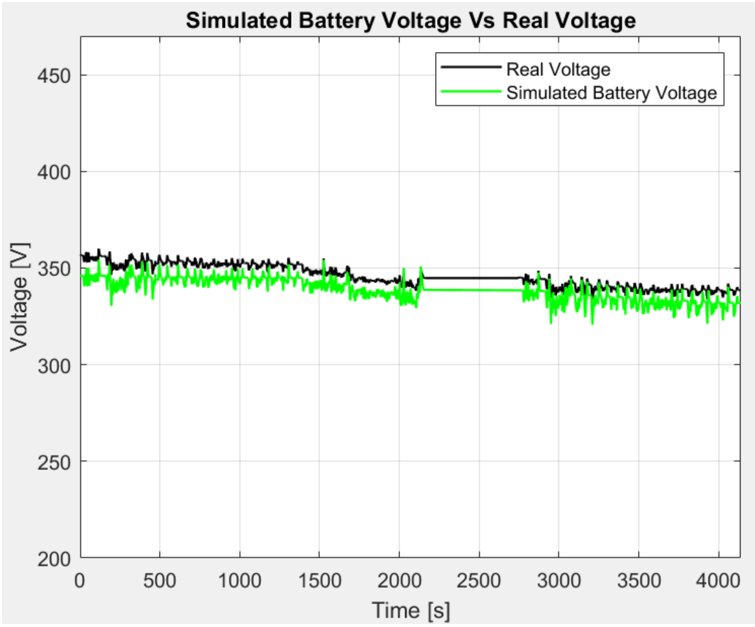

Figure A.39: Driving Cycle: UDDS Ph 1+2, HWY Ph3, UDDS Ph 4+5 – Battery Terminal Voltage.

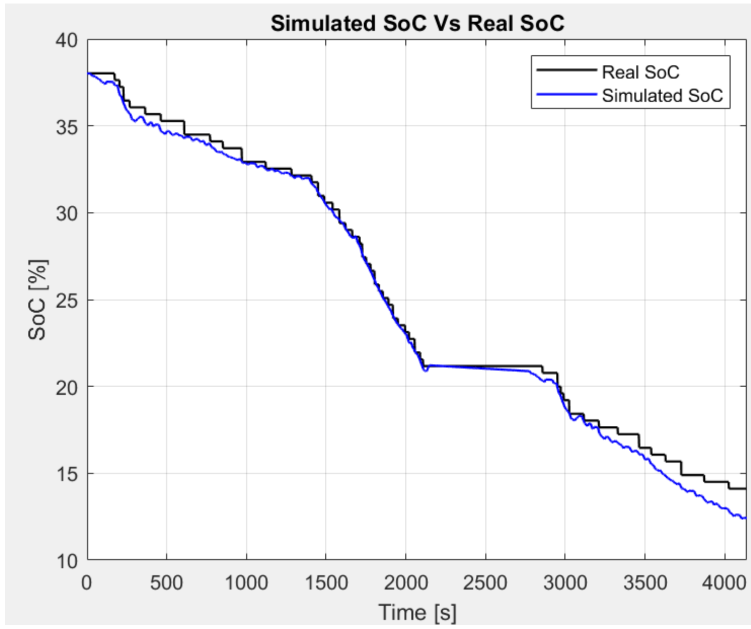

Figure A.40: Driving Cycle: UDDS Ph 1+2, HWY Ph3, UDDS Ph 4+5 – Battery SOC.

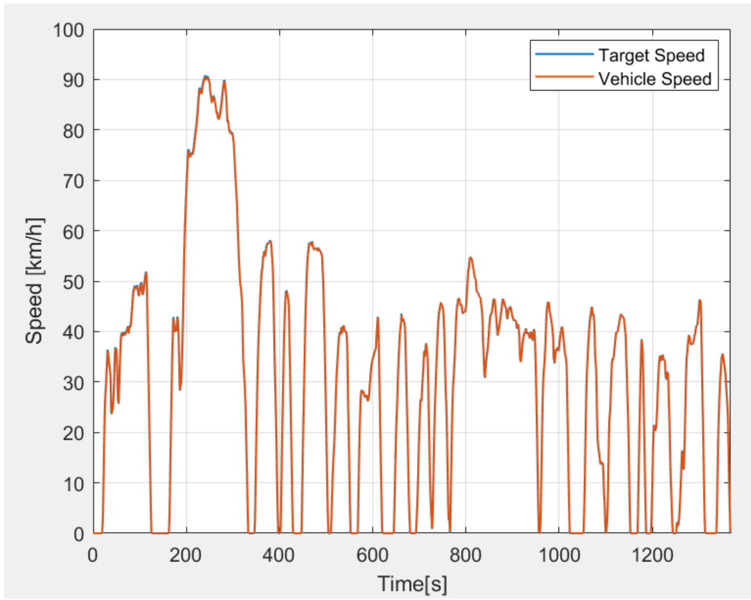

Figure A.41: Driving Cycle: UDDS Ph 1+2 - Vehicle Speed.

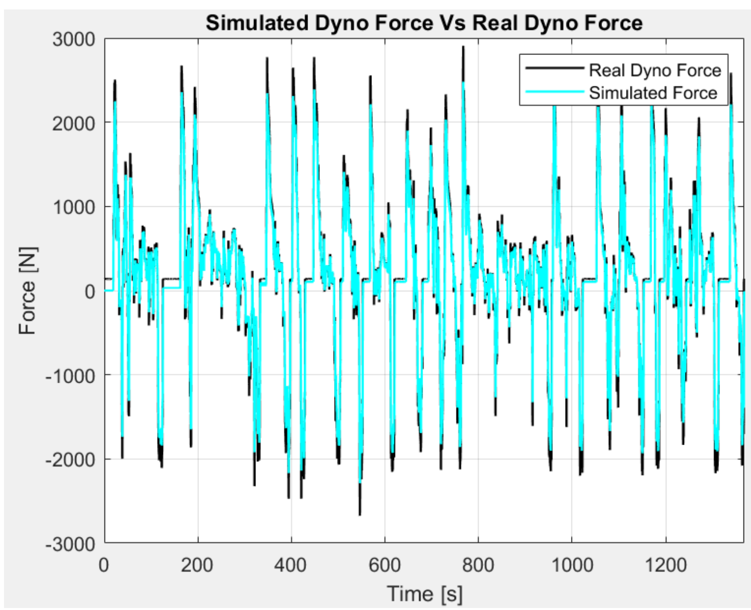

Figure A.42: Driving Cycle: UDDS Ph 1+2 - Tire Force.

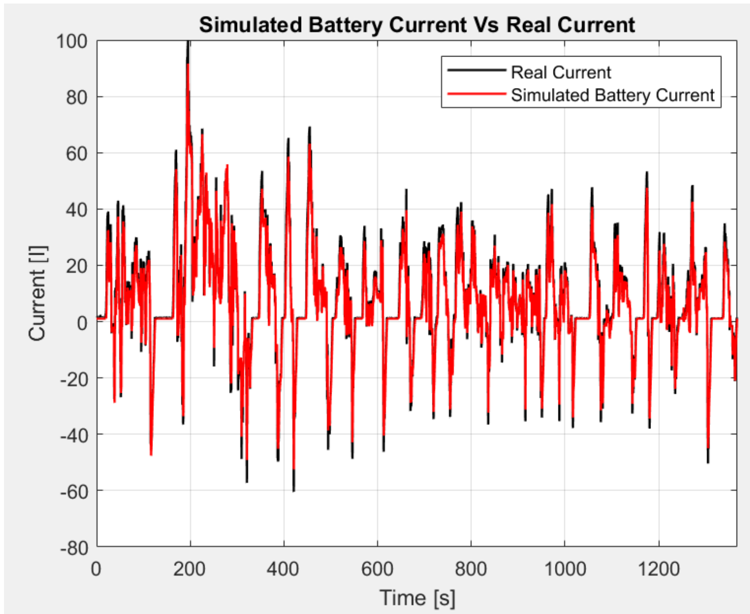

Figure A.43: Driving Cycle: UDDS Ph 1+2 - Battery DC Current.

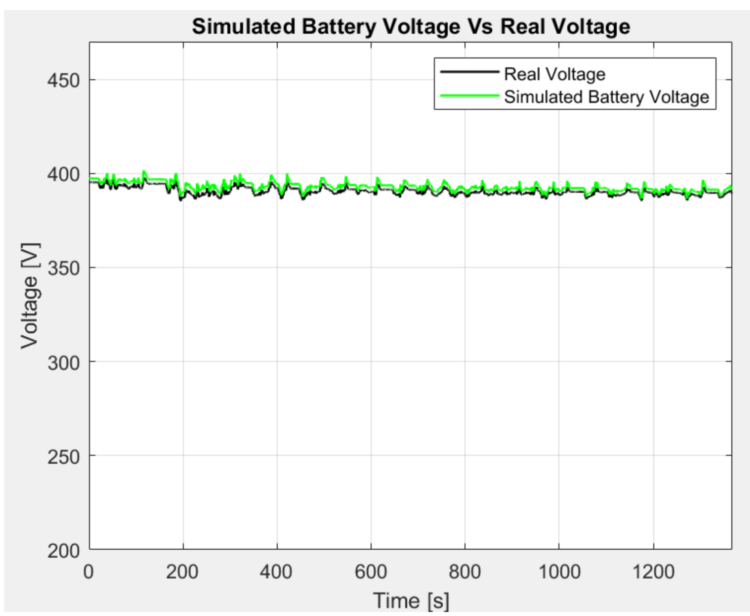

Figure A.44: Driving Cycle: UDDS Ph 1+2 - Battery Terminal Voltage.

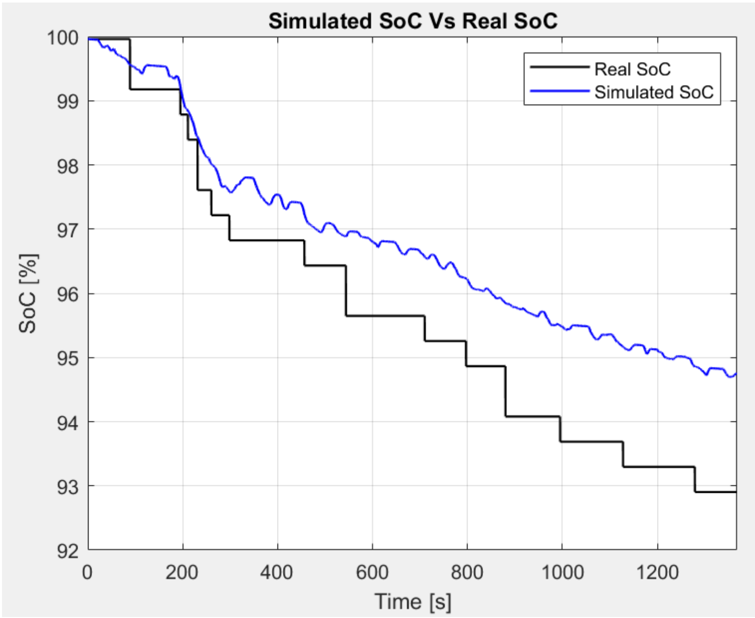

Figure A.45: Driving Cycle: UDDS Ph 1+2 - Battery SOC.

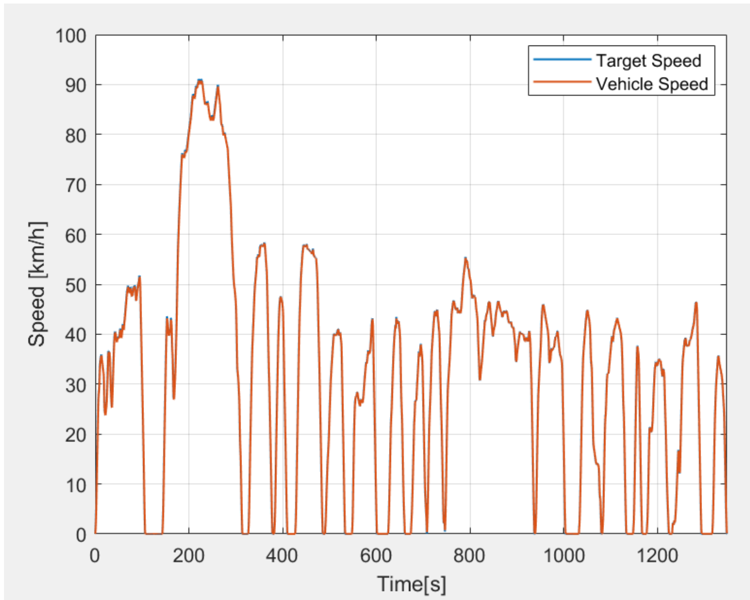

Figure A.46: Driving Cycle: UDDS Ph 4+5 - Vehicle Speed.

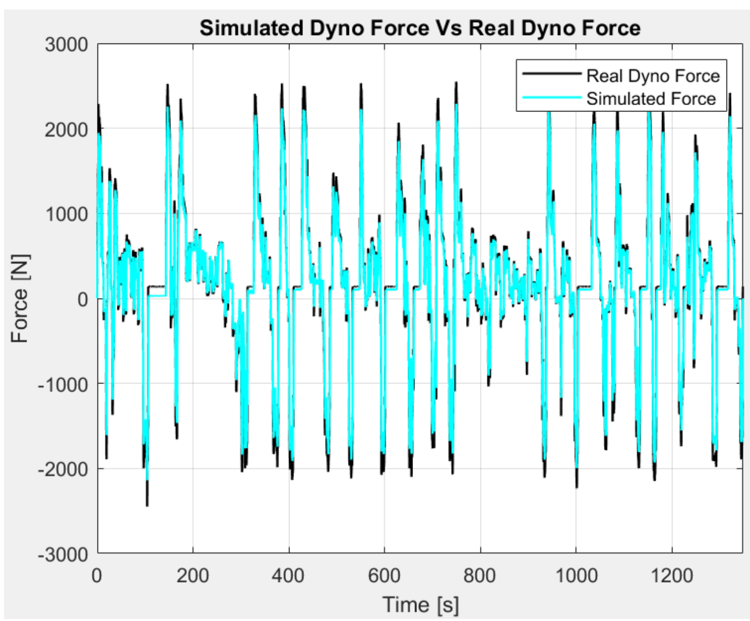

Figure A.47: Driving Cycle: UDDS Ph 4+5 - Tire Force.

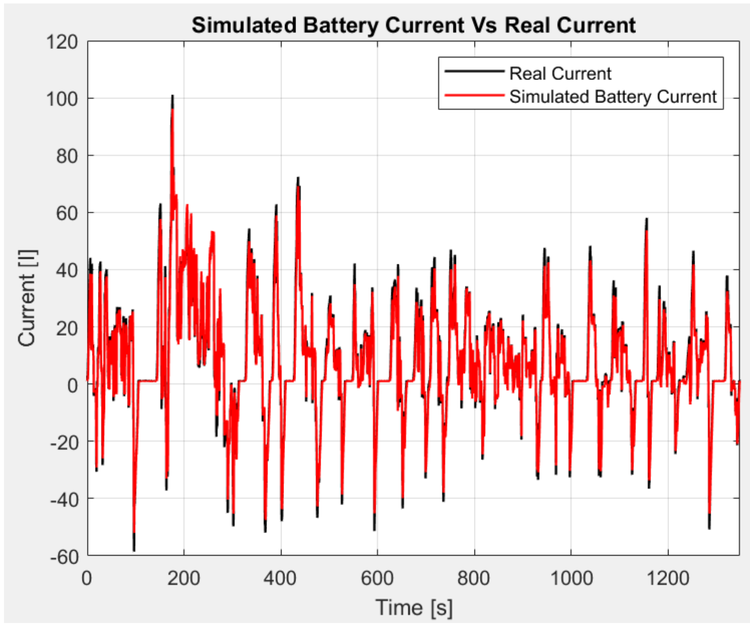

Figure A.48: Driving Cycle: UDDS Ph 4+5 - Battery DC Current.

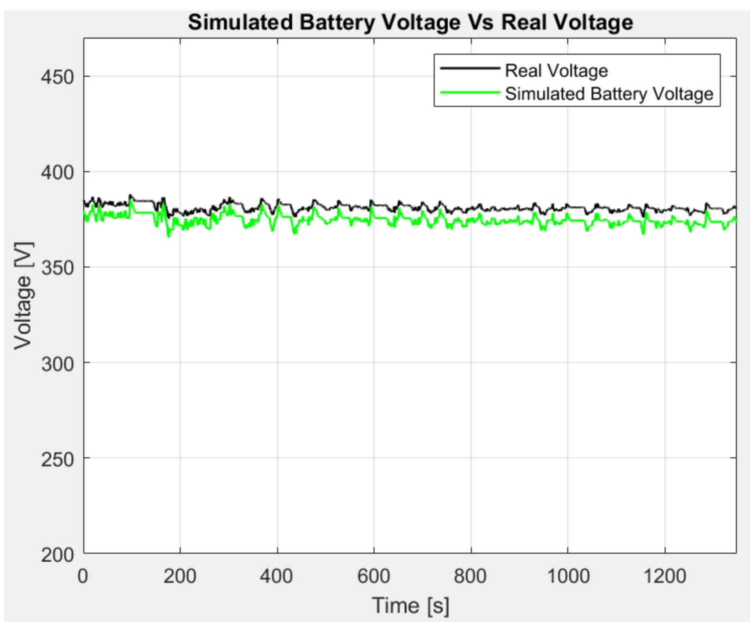

Figure A.49: Driving Cycle: UDDS Ph 4+5 - Battery Terminal Voltage.

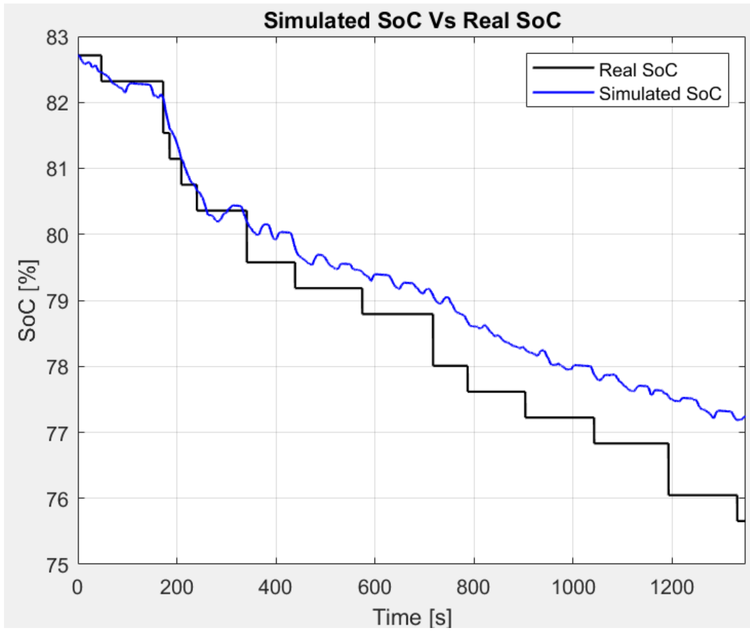

Figure A.50: Driving Cycle: UDDS Ph 4+5 - Battery SOC.

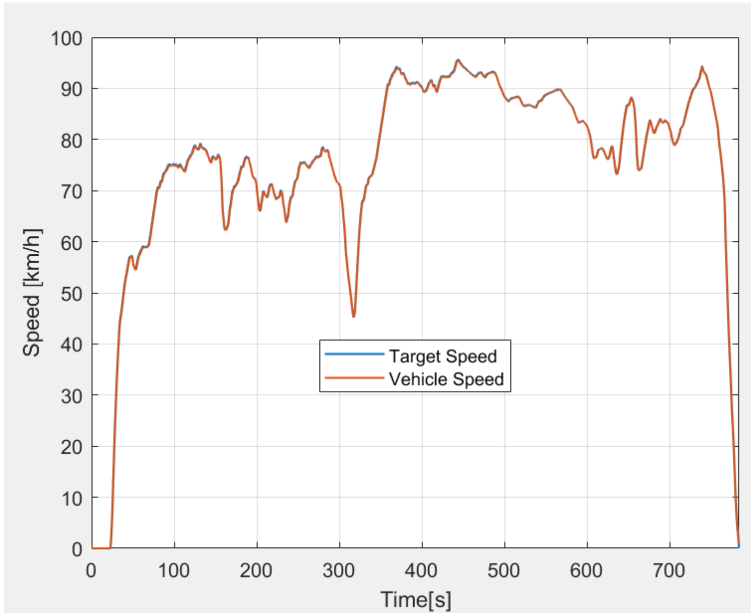

Figure A.51: Driving Cycle: HWY Ph3 - Vehicle Speed.

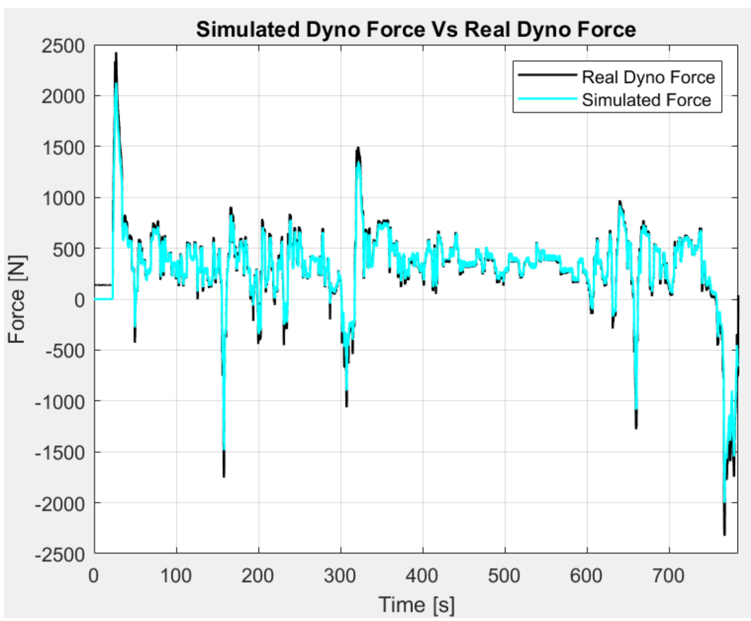

Figure A.52: Driving Cycle: HWY Ph3 - Tire Force.

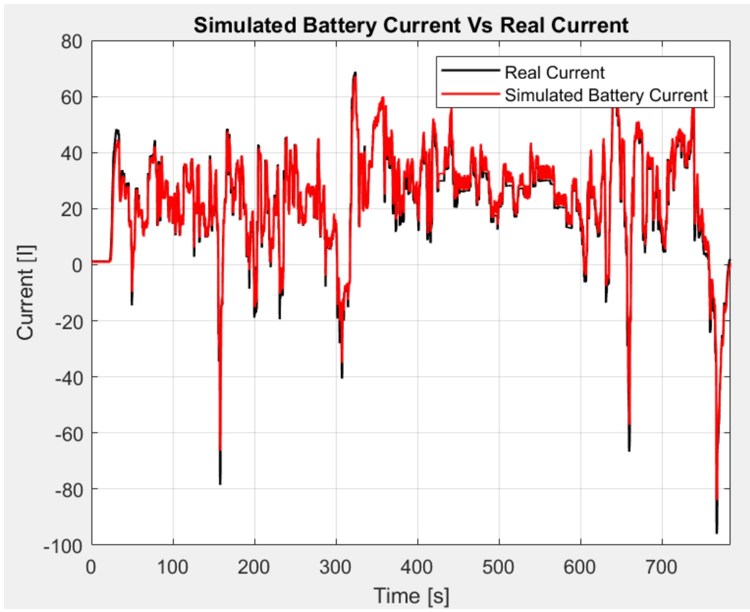

Figure A.53: Driving Cycle: HWY Ph3 - Battery DC Current.

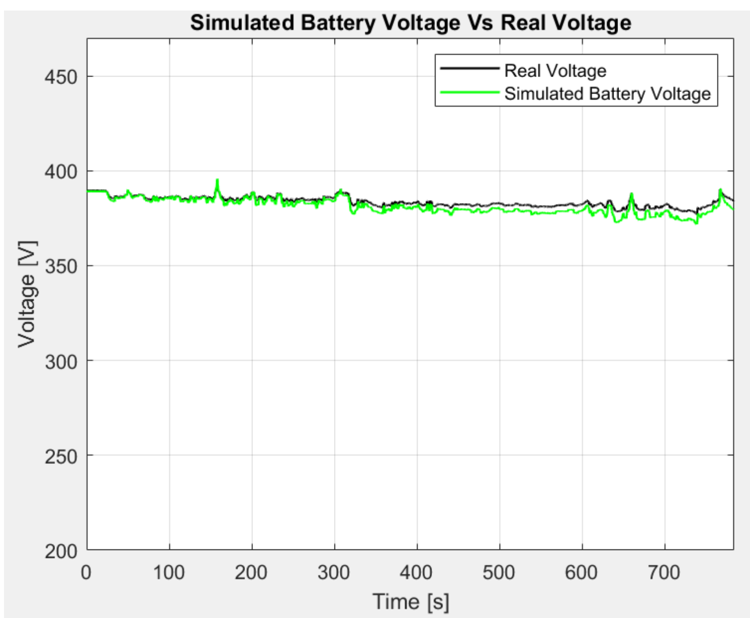

Figure A.54: Driving Cycle: HWY Ph3 - Battery Terminal Voltage.

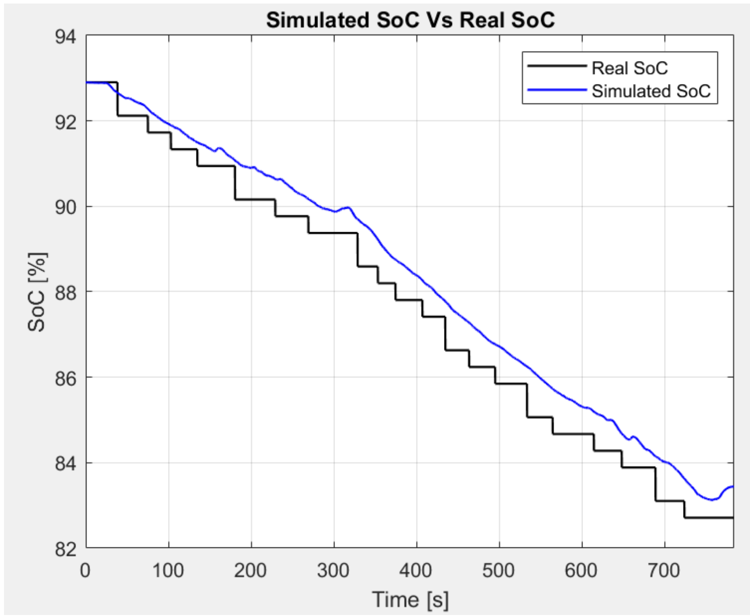

Figure A.55: Driving Cycle: HWY Ph3 - Battery SOC.

References

[1] J. Voelcker, "Green Car Reports," *Green Car Reports*, 2018. [Online]. Available: https://www.greencarreports.com/news/1065070_its-official-we-now-have-one-billion-vehicles-on-the-planet. [Accessed: 30-Sep-2018].

[2] Statista, "Statista," 2020. [Online]. Available: https://www.statista.com/statistics/200002/international-car-sales-since-1990/. [Accessed: 07-Apr-2020].

[3] "U.S. VEHICLE REGISTRATION STATISTICS," *Hedges & Company*, 2020. [Online]. Available: https://hedgescompany.com/automotive-market-research-statistics/auto-mailing-lists-and-marketing/. [Accessed: 10-Jun-2020].

[4] Z. Yang, "The ICCT - The International Council on Clean Air Transportation," 2018. [Online]. Available: https://theicct.org/sites/default/files/Global-Fuel-Economy-Policies-Overview_ICCT_ZYang_20032018.pdf. [Accessed: 11-Sep-2018].

[5] EPA, "Green House Gas Emissions," *EPA - United States Environmental Protection Agency, 2018*, 2018. .

[6] C. Le Quéré *et al.*, "Temporary reduction in daily global CO2 emissions during the COVID-19 forced confinement," *Nat. Clim. Chang.*, May 2020.

[7] J. Riswick, "Vehicle Types, Car Body Styles Explained," *Car and Driver*, 2019. [Online]. Available: https://www.caranddriver.com/shopping-

advice/g26100588/car-types/. [Accessed: 07-May-2020].

[8] A. Emadi, *Advanced Electric Drive Vehicles*. 2015.

[9] B. Bilgin *et al.*, “Making the Case for Electrified Transportation,” *IEEE Trans. Transp. Electrif.*, vol. 1, no. 1, 2015.

[10] D. G. L. Barroso, A. Emadi, and L. Bruck, “Driver-in-the-Loop Drivability and Energy Efficiency Analysis of Regenerative Braking Strategies for Electric Vehicles,” 2023.

[11] Argonne National Laboratory, “D3 2015 Chevrolet Spark EV,” *Transportation and Power Systems*, 2015. [Online]. Available: https://www.anl.gov/taps/d3-2015-chevrolet-spark-ev. [Accessed: 10-Jul-2019].

[12] W.-W. H. O. Organization, “What is a Pandemic?,” *World Health Organization*, 2010. [Online]. Available: https://www.who.int/csr/disease/swineflu/frequently_asked_questions/pandemic/en/. [Accessed: 01-Jun-2020].

[13] W.-W. H. O. Organization, “Alert & Response Operations,” *Emergencies preparedness, response*, 2007. [Online]. Available: https://www.who.int/csr/alertresponse/en/. [Accessed: 01-Jun-2020].

[14] W.-W. H. O. Organization, “The Who Pandemic Phases,” *Pandemic Influenza Preparedness and Response: A WHO Guidance Document.*, 2009. [Online]. Available: https://www.ncbi.nlm.nih.gov/books/NBK143061/. [Accessed: 01-Jun-2020].

[15] W.-W. H. O. Organization, "Considerations for quarantine of individuals in the context of containment for coronavirus disease (COVID-19)," 2020. [Online]. Available: Considerations for quarantine of individuals in the context of containment for coronavirus disease (COVID-19). [Accessed: 01-Jun-2020].

[16] International Monetary Fund - IMF, "World Economic Outlook, April 2020: The Great Lockdownd," Washington DC, 2020.

[17] J. Tollefson, "How the coronavirus pandemic slashed carbon emissions — in five graphs," *Nature*, May 2020.

[18] B. Metz, O. Davidson, P. Bosch, R. Dave, and L. Meyer, "Climate Change 2007 - Mitigation of Climate Change," New York, 2007.

[19] U.-U. Nations, "Climate Change," *United Nations - Global Issues*. [Online]. Available: https://www.un.org/en/sections/issues-depth/climate-change/. [Accessed: 01-Jun-2020].

[20] B. Hoffmann, "Air Pollution in Cities: Urban and Transport Planning Determinants and Health in Cities," in *Integrating Human Health into Urban and Transport Planning*, Cham: Springer International Publishing, 2019, pp. 425–441.

[21] G. Martinez, J. Spadaro, D. Chapizanis, V. Kendrovski, M. Kochubovski, and P. Mudu, "Health Impacts and Economic Costs of Air Pollution in the Metropolitan Area of Skopje," *Int. J. Environ. Res. Public Health*, vol. 15, no. 4, p. 626, Mar. 2018.

[22] P. M. Mannucci, S. Harari, and M. Franchini, "Novel evidence for a greater burden of ambient air pollution on cardiovascular disease," *Haematologica*, vol. 104, no. 12, pp. 2349–2357, Dec. 2019.

[23] J. Huang, X. Pan, X. Guo, and G. Li, "Health impact of China's Air Pollution Prevention and Control Action Plan: an analysis of national air quality monitoring and mortality data," *Lancet Planet. Heal.*, vol. 2, no. 7, pp. e313–e323, Jul. 2018.

[24] R. Bayat *et al.*, "Health impact and related cost of ambient air pollution in Tehran," *Environ. Res.*, vol. 176, p. 108547, Sep. 2019.

[25] D. E. Schraufnagel *et al.*, "Health Benefits of Air Pollution Reduction," *Ann. Am. Thorac. Soc.*, vol. 16, no. 12, pp. 1478–1487, Dec. 2019.

[26] W.-W. H. O. Organization, "Ambient (outdoor) air pollution," *WHO Health Topics*, 2018. [Online]. Available: https://www.who.int/news-room/fact-sheets/detail/ambient-(outdoor)-air-quality-and-health. [Accessed: 01-Jun-2020].

[27] S. C. Anenberg, P. Achakulwisut, M. Brauer, D. Moran, J. S. Apte, and D. K. Henze, "Particulate matter-attributable mortality and relationships with carbon dioxide in 250 urban areas worldwide," *Sci. Rep.*, vol. 9, no. 1, p. 11552, Dec. 2019.

[28] P. L. Kinney, "Interactions of Climate Change, Air Pollution, and Human Health," *Curr. Environ. Heal. Reports*, vol. 5, no. 1, pp. 179–186, Mar. 2018.

[29] U.-U. Nations, "Air pollution: The silent killer that claims 7 million lives

each year," *United Nations Human RIghts*, 2019. [Online]. Available: https://www.ohchr.org/en/NewsEvents/Pages/DisplayNews.aspx?NewsID=24248&LangID=E.

[30] J. Masters, "Coronavirus: How Are Countries Responding to the Economic Crisis?," *Council on Foreign Relations*, 2020. [Online]. Available: https://www.cfr.org/backgrounder/coronavirus-how-are-countries-responding-economic-crisis. [Accessed: 02-Jun-2020].

[31] S. Corbet and A. Charlton, "France Deploys $8.8 Billion to Rescue Car Industry and Boost Electric Vehicles," *TIME Magazine*, 2020. [Online]. Available: https://time.com/5842884/france-8-billion-electric-car-industry/. [Accessed: 07-Jun-2020].

[32] E. Newburger, "Here's how Biden's $2 trillion infrastructure plan addresses climate change," *Politcs - CNBC*, 2021. [Online]. Available: https://www.cnbc.com/2021/03/31/biden-infrastructure-plan-spending-on-climate-change-clean-energy.html. [Accessed: 16-Jun-2021].

[33] D. W. Dockery *et al.*, "An Association between Air Pollution and Mortality in Six U.S. Cities," *N. Engl. J. Med.*, vol. 329, no. 24, pp. 1753–1759, Dec. 1993.

[34] R. D. Brook *et al.*, "Particulate Matter Air Pollution and Cardiovascular Disease," *Circulation*, vol. 121, no. 21, pp. 2331–2378, Jun. 2010.

[35] L. T. M. Luong *et al.*, "Particulate air pollution in Ho Chi Minh city and risk of hospital admission for acute lower respiratory infection (ALRI) among

young children," *Environ. Pollut.*, vol. 257, p. 113424, Feb. 2020.

[36] D. Phung *et al.*, "Air pollution and risk of respiratory and cardiovascular hospitalizations in the most populous city in Vietnam," *Sci. Total Environ.*, vol. 557–558, pp. 322–330, Jul. 2016.

[37] H. Boogaard, K. Walker, and A. J. Cohen, "Air pollution: the emergence of a major global health risk factor," *Int. Health*, vol. 11, no. 6, pp. 417–421, Nov. 2019.

[38] A. Hansell *et al.*, "Historic air pollution exposure and long-term mortality risks in England and Wales: prospective longitudinal cohort study," *Thorax*, vol. 71, no. 4, pp. 330–338, Apr. 2016.

[39] J. K. Vanos, C. Hebbern, and S. Cakmak, "Risk assessment for cardiovascular and respiratory mortality due to air pollution and synoptic meteorology in 10 Canadian cities," *Environ. Pollut.*, vol. 185, pp. 322–332, Feb. 2014.

[40] Y. Cui *et al.*, "Air pollution and case fatality of SARS in the People's Republic of China: an ecologic study," *Environ. Heal.*, vol. 2, no. 1, p. 15, Dec. 2003.

[41] J. Yang *et al.*, "Prevalence of comorbidities and its effects in patients infected with SARS-CoV-2: a systematic review and meta-analysis," *Int. J. Infect. Dis.*, vol. 94, pp. 91–95, May 2020.

[42] I. Gerrentsen, "How air pollution exacerbates Covid-19," *Future Planet - BBC*, 2020. [Online]. Available:

https://www.bbc.com/future/article/20200427-how-air-pollution-exacerbates-covid-19. [Accessed: 07-Jun-2020].

[43] X. Wu, R. C. Nethery, M. B. Sabath, D. Braun, and F. Dominici, “Air pollution and COVID-19 mortality in the United States: Strengths and limitations of an ecological regression analysis,” *Sci. Adv.*, vol. 6, no. 45, Nov. 2020.

[44] N. Ali and F. Islam, “The Effects of Air Pollution on COVID-19 Infection and Mortality—A Review on Recent Evidence,” *Front. Public Heal.*, vol. 8, Nov. 2020.

[45] J. Lelieveld, J. S. Evans, M. Fnais, D. Giannadaki, and A. Pozzer, “The contribution of outdoor air pollution sources to premature mortality on a global scale,” *Nature*, vol. 525, no. 7569, pp. 367–371, Sep. 2015.

[46] J. Lelieveld, A. Pozzer, U. Pöschl, M. Fnais, A. Haines, and T. Münzel, “Loss of life expectancy from air pollution compared to other risk factors: a worldwide perspective,” *Cardiovasc. Res.*, Mar. 2020.

[47] L. Pimpin *et al.*, “Estimating the costs of air pollution to the National Health Service and social care: An assessment and forecast up to 2035,” *PLOS Med.*, vol. 15, no. 7, p. e1002602, Jul. 2018.

[48] W.-W. H. O. Organization and O. -, “Economic cost of the health impact of air pollution in Europe,” Copenhagen, Denmark, 2015.

[49] The World Bank and O. N. Accounts, “Global GDP Data,” *The World Bank Data Base*. [Online]. Available:

https://data.worldbank.org/indicator/NY.GDP.MKTP.CD. [Accessed: 08-Jun-2020].

[50] E. Coe, K. Enomoto, P. Finn, and J. Stenson, “Understanding the hidden costs of COVID-19’s potential impact on US healthcare,” *Mckinsey - Healthcare systems & Services*, 2020. [Online]. Available: https://www.mckinsey.com/industries/healthcare-systems-and-services/our-insights/understanding-the-hidden-costs-of-covid-19s-potential-impact-on-us-healthcare. [Accessed: 31-Oct-2020].

[51] Worldometer, “COVID-19 CORONAVIRUS PANDEMIC,” *Worldometer*, 2021. [Online]. Available: https://www.worldometers.info/coronavirus/. [Accessed: 31-Oct-2021].

[52] V. Masson-Delmotte, H.-O. Portner, J. Skea, P. Zhai, D. ROberts, and P. Shukla, “Special Report: Global Warming of 1.5C,” 2019.

[53] K. Levin, “According to New IPCC Report, the World Is on Track to Exceed its ‘Carbon Budget’ in 12 Years,” *World Resources Institute*, 2018. [Online]. Available: https://www.wri.org/blog/2018/10/according-new-ipcc-report-world-track-exceed-its-carbon-budget-12-years. [Accessed: 05-Jun-2020].

[54] T. Roxburgh *et al.*, “Global Futures report: Assessing the Global Economic Impacts of the Environemntal Change to Support Policy-Making,” 2020.

[55] Editorial, “Coronavirus response: a focus on containment is still apt,” *Nature*, vol. 579, no. 7797, pp. 7–7, Mar. 2020.

[56] E. Gibney, “Whose coronavirus strategy worked best? Scientists hunt most

effective policies,” *Nature*, vol. 581, no. 7806, pp. 15–16, May 2020.

[57] Z. Liu *et al.*, “COVID-19 causes record decline in global CO2 emissions,” Apr. 2020.

[58] International Energy Agency (IEA), “Global Energy Review 2020: The Impacts of the COVID 19 crisis on global energy demand and CO2 emissions,” 2020.

[59] International Energy Agency (IEA), “COVID-19 Impact on Eletricty Demand,” *IEA - International Energy Assossiation*, 2021. [Online]. Available: https://www.iea.org/reports/covid-19-impact-on-electricity. [Accessed: 21-Oct-2021].

[60] D. Mahler, N. Yonzan, C. Lakner, R. A. Castadena, and H. Wu, “Updated estimates of the impact of COVID-19 on global poverty: Turning the corner on the pandemic in 2021?,” *Data Blog, World Bank*, 2021. [Online]. Available: https://blogs.worldbank.org/opendata/updated-estimates-impact-covid-19-global-poverty-turning-corner-pandemic-2021. [Accessed: 16-Nov-2021].

[61] D. Maljer, C. Lakner, R. A. Aguilar, and H. Wu, “The impact of COVID-19 (Coronavirus) on global poverty: Why Sub-Saharan Africa might be the region hardest hit,” *WorldBank.org*, 2020. [Online]. Available: https://blogs.worldbank.org/opendata/impact-covid-19-coronavirus-global-poverty-why-sub-saharan-africa-might-be-region-hardest. [Accessed: 08-Jun-2020].

[62] G. Iacurci, "Unemployment is nearing Great Depression levels. Here's how the eras are similar — and different," *Personal Finance - CNBC*, 2020. [Online]. Available: https://www.cnbc.com/2020/05/19/unemployment-today-vs-the-great-depression-how-do-the-eras-compare.html. [Accessed: 08-Jun-2020].

[63] R. J. Millar *et al.*, "Emission budgets and pathways consistent with limiting warming to 1.5 °C," *Nat. Geosci.*, vol. 10, no. 10, pp. 741–747, Oct. 2017.

[64] K. Riahi *et al.*, "Locked into Copenhagen pledges — Implications of short-term emission targets for the cost and feasibility of long-term climate goals," *Technol. Forecast. Soc. Change*, vol. 90, pp. 8–23, Jan. 2015.

[65] IQAir, "COVID-19 Air Quality," 2020.

[66] T. Barboza, "L.A. coronavirus clean air streak has already come to an end. Here's why," *Los Angeles Times*, 2020. [Online]. Available: https://www.latimes.com/environment/story/2020-04-28/coronavirus-la-air-quality-improved-pandemic-dont-expect-it-to-last. [Accessed: 09-Jun-2020].

[67] R. Zhang, Y. Zhang, H. Lin, X. Feng, T.-M. Fu, and Y. Wang, "NOx Emission Reduction and Recovery during COVID-19 in East China," *Atmosphere (Basel).*, vol. 11, no. 4, p. 433, Apr. 2020.

[68] R. Bao and A. Zhang, "Does lockdown reduce air pollution? Evidence from 44 cities in northern China," *Sci. Total Environ.*, vol. 731, p. 139052, Aug. 2020.

[69] L. Y. K. Nakada and R. C. Urban, “COVID-19 pandemic: Impacts on the air quality during the partial lockdown in São Paulo state, Brazil,” *Sci. Total Environ.*, vol. 730, p. 139087, Aug. 2020.

[70] A. Rappeport and J. Smialek, “I.M.F. Predicts Worst Downturn Since the Great Depression,” *The New York Times*, 2020. [Online]. Available: https://www.nytimes.com/2020/04/14/us/politics/coronavirus-economy-recession-depression.html. [Accessed: 01-Jun-2020].

[71] International Monetary Fund - IMF, “RECOVERY DURING A PANDEMIC,” *WORLD ECONOMIC OUTLOOK OCTOBER 2021*, 2021. [Online]. Available: https://www.imf.org/en/Publications/WEO/Issues/2021/10/12/world-economic-outlook-october-2021. [Accessed: 31-Oct-2021].

[72] G. P. Peters, G. Marland, C. Le Quéré, T. Boden, J. G. Canadell, and M. R. Raupach, “Rapid growth in CO2 emissions after the 2008–2009 global financial crisis,” *Nat. Clim. Chang.*, vol. 2, no. 1, pp. 2–4, Jan. 2012.

[73] R. L. Murray, “The Future,” in *Nuclear Energy*, Elsevier, 2009, pp. 473–497.

[74] H. Lindquist, “The Journey of Reinventing the European Electricity Landscape—Challenges and Pioneers,” in *Renewable Energy Integration*, Elsevier, 2014, pp. 3–12.

[75] H. Ritchie and M. Roser, “Energy,” *Our World Data - University of Oxford*, 2015. [Online]. Available: https://ourworldindata.org/energy. [Accessed:

06-Jun-2020].

[76] T. Vujović, Z. Petković, M. Pavlović, and S. Jović, "Economic growth based in carbon dioxide emission intensity," *Phys. A Stat. Mech. its Appl.*, vol. 506, pp. 179–185, Sep. 2018.

[77] K. Feng, S. J. Davis, L. Sun, and K. Hubacek, "Drivers of the US CO2 emissions 1997–2013," *Nat. Commun.*, vol. 6, no. 1, p. 7714, Nov. 2015.

[78] International Energy Agency (IEA), "https://www.iea.org/reports/global-energy-review-2021/co2-emissions," *Global Energy Review 2021*, 2021. [Online]. Available: https://www.iea.org/reports/global-energy-review-2021/co2-emissions. [Accessed: 16-Nov-2021].

[79] C. Le Quéré *et al.*, "Drivers of declining CO2 emissions in 18 developed economies," *Nat. Clim. Chang.*, vol. 9, no. 3, pp. 213–217, Mar. 2019.

[80] IMF, "POLICY RESPONSES TO COVID-19," 2020. [Online]. Available: https://www.imf.org/en/Topics/imf-and-covid19/Policy-Responses-to-COVID-19#A. [Accessed: 26-Jun-2020].

[81] B. A. Emadi, "By Ali Emadi," *Transportation (Amst).*, no. august, 2011.

[82] B. P. J. Ansell and K. S. Haran, "Electrified Airplanes," pp. 18–26, 2020.

[83] R. Domínguez, A. J. Conejo, and M. Carrión, "Toward fully renewable electric energy systems," *IEEE Trans. Power Syst.*, vol. 30, no. 1, pp. 316–326, 2015.

[84] OCDE, *Investing in Climate, Investing in Growth*. OECD, 2017.

[85] A. Pfeiffer, R. Millar, C. Hepburn, and E. Beinhocker, "The '2°C capital

stock' for electricity generation: Committed cumulative carbon emissions from the electricity generation sector and the transition to a green economy," *Appl. Energy*, vol. 179, pp. 1395–1408, Oct. 2016.

[86] I. Wagner, "Statista," 2020. [Online]. Available: https://www.statista.com/statistics/257660/passenger-car-sales-in-selected-countries/. [Accessed: 09-Apr-2020].

[87] S. C. Davis and R. G. Boundy, *Transportation Energy Data Book*, 38th ed. Oak Ridge, Tennessee: U.S. Department of Energy, 2020.

[88] U. S. D. of Energy, "Energy Efficient Technologies," 2020. [Online]. Available: https://www.fueleconomy.gov/feg/tech_adv.shtml. [Accessed: 10-Jun-2020].

[89] *Cost, Effectiveness, and Deployment of Fuel Economy Technologies for Light-Duty Vehicles*. Washington, D.C.: National Academies Press, 2015.

[90] EPA, "Automotive Trends Report," 2018. .

[91] A. Emadi, *Advanced Electric Drive Vehicles*. Boca Raton, Florida: CRC Press LLC, 2014.

[92] A. Emadi, "Transportation 2.0," *IEEE Power Energy Mag.*, vol. 9, no. 4, pp. 18–29, Jul. 2011.

[93] Z. Q. Zhu and D. Howe, "Electrical Machines and Drives for Electric, Hybrid, and Fuel Cell Vehicles," *Proc. IEEE*, vol. 95, no. 4, pp. 746–765, Apr. 2007.

[94] W. Xu, J. Zhu, Y. Guo, S. Wang, Y. Wang, and Z. Shi, "Survey on electrical

machines in electrical vehicles," in *2009 International Conference on Applied Superconductivity and Electromagnetic Devices*, 2009, pp. 167–170.

[95] F. Un-Noor, S. Padmanaban, L. Mihet-Popa, M. Mollah, and E. Hossain, "A Comprehensive Study of Key Electric Vehicle (EV) Components, Technologies, Challenges, Impacts, and Future Direction of Development," *Energies*, vol. 10, no. 8, p. 1217, Aug. 2017.

[96] R. Balaji and E. M. Mockensturm, "Dynamic analysis of a front-end accessory drive with a decoupler/isolator," *Int. J. Veh. Des.*, vol. 39, no. 3, p. 208, 2005.

[97] D. A. Crolla and B. Mashadi, *VEHICLE POWERTRAIN SYSTEMS*. United Kingdom, 2012.

[98] D. Robinette and M. Powell, "Optimizing 12 Volt Start - Stop for Conventional Powertrains," *SAE Int. J. Engines*, vol. 4, no. 1, pp. 837–849, 2011.

[99] Y. S. Jo, L. Bromberg, and J. Heywood, "Optimal Use of Ethanol in Dual Fuel Applications: Effects of Engine Downsizing, Spark Retard, and Compression Ratio on Fuel Economy," *SAE Int. J. Engines*, vol. 9, no. 2, pp. 1087–1101, 2016.

[100] T. N. Patro and D. A. LaRue, "Alternate Fueled Powertrain – An Insight into Its Combustion Related NVH Issues," *J. Passeng. CARS*, vol. 108, no. 6, pp. 2802–2814, 1999.

[101] J. Zhao, “Research and application of over-expansion cycle (Atkinson and Miller) engines – A review,” *Appl. Energy*, vol. 185, pp. 300–319, Jan. 2017.

[102] A. Emaddi, *Handbook of Automotive Power Eletronics and Motor Drives*. 2005.

[103] Y. Cheng, R. Trigui, C. Espanet, A. Bouscayrol, and S. Cui, “Specifications and Design of a PM Electric Variable Transmission for Toyota Prius II,” *IEEE Trans. Veh. Technol.*, vol. 60, no. 9, pp. 4106–4114, Nov. 2011.

[104] Y. Sato, S. Ishikawa, T. Okubo, M. Abe, and K. Tamai, “Development of High Response Motor and Inverter System for the Nissan LEAF Electric Vehicle,” in *SAE 2011 World Congress & Exhibition*, 2011, p. 8.

[105] F. Momen, K. Rahman, and Y. Son, “Electrical Propulsion System Design of Chevrolet Bolt Battery Electric Vehicle,” *IEEE Trans. Ind. Appl.*, vol. 55, no. 1, pp. 376–384, Jan. 2019.

[106] G. Sieklucki, “An Investigation into the Induction Motor of Tesla Model S Vehicle,” in *2018 International Symposium on Electrical Machines (SME)*, 2018, pp. 1–6.

[107] K. T. Chau, “Overview of Electric Vehicle Machines - From Tesla to Tesla, and Beyond,” in *2016 International Conference of Asian Union of Magnetics Societies (ICAUMS)*, 2016, pp. 1–6.

[108] B. Bilgin, A. Emadi, and M. Krishnamurthy, “Comprehensive Evaluation of the Dynamic Performance of a 6/10 SRM for Traction Application in PHEVs,” *IEEE Trans. Ind. Electron.*, vol. 60, no. 7, pp. 2564–2575, Jul.

2013.

[109] B. Bilgin *et al.*, “Making The Case for Switched Reluctance Motors for Propulsion Applications,” *IEEE Trans. Veh. Technol.*, pp. 1–1, 2020.

[110] J. W. Jiang, B. Bilgin, B. Howey, and A. Emadi, “Design optimization of switched reluctance machine using genetic algorithm,” in *2015 IEEE International Electric Machines & Drives Conference (IEMDC)*, 2015, pp. 1671–1677.

[111] H. Li, E. Fairall, B. Bilgin, and A. Emadi, “Performance evaluation of a high-speed high-power switched reluctance motor drive,” in *2015 IEEE Applied Power Electronics Conference and Exposition (APEC)*, 2015, pp. 1337–1342.

[112] D. F. Valencia, R. Tarvirdilu-Asl, C. Garcia, J. Rodriguez, and A. Emadi, “Vision, Challenges, and Future Trends of Model Predictive Control in Switched Reluctance Motor Drives,” *IEEE Access*, vol. 9, pp. 69926–69937, 2021.

[113] D. Yu, X. Y. Huang, Y. T. Fang, and J. Zhang, “Design and comparison of interior permanent magnet synchronous traction motors for high speed railway applications,” in *2017 IEEE Workshop on Electrical Machines Design, Control and Diagnosis (WEMDCD)*, 2017, pp. 58–62.

[114] B. Bilgin *et al.*, “Making the Case for Electrified Transportation,” *IEEE Trans. Transp. Electrif.*, vol. 1, no. 1, pp. 4–17, Jun. 2015.

[115] A. Ramezani, M. Ghiasi, M. Dehghani, T. Niknam, P. Siano, and H. H.

Alhelou, “Reduction of Ripple Toothed Torque in the Internal Permanent Magnet Electric Motor by Creating Optimal Combination of Holes in the Rotor Surface Considering Harmonic Effects,” *IEEE Access*, vol. 8, pp. 215107–215124, 2020.

[116] Haizhong Ye, Y. Yang, and A. Emadi, “Traction inverters in hybrid electric vehicles,” in *2012 IEEE Transportation Electrification Conference and Expo (ITEC)*, 2012, pp. 1–6.

[117] J. Reimers, L. Dorn-Gomba, C. Mak, and A. Emadi, “Automotive Traction Inverters: Current Status and Future Trends,” *IEEE Trans. Veh. Technol.*, vol. 68, no. 4, pp. 3337–3350, Apr. 2019.

[118] K. Asano, Y. Inaguma, H. Ohtani, E. Sato, M. Okamura, and S. Sasaki, “High Performance Motor Drive Technologies for Hybrid Vehicles,” in *2007 Power Conversion Conference - Nagoya*, 2007, pp. 1584–1589.

[119] H. Chen and B. Gao, *Non Linear Estimation and Control of Automotive Drivetrains*. 2014.

[120] J. D. Halderman, *Automatic Transmission and Transaxles*, 7th ed. Boston: Pearson, 2017.

[121] G. Wu and Z. Dong, “Design, analysis and modeling of a novel hybrid powertrain system based on hybridized automated manual transmission,” *Mech. Syst. Signal Process.*, vol. 93, pp. 688–705, Sep. 2017.

[122] F. Vacca *et al.*, “On the Energy Efficiency of Dual Clutch Transmissions and Automated Manual Transmissions,” *Energies*, vol. 10, no. 10, p. 1562, Oct.

2017.

[123] A. Seedam, P. Jaisuk, P. Jirawattana, and T. Radpukdee, “Engine Map and Optimal Operation Path Construction for an Engine-CVT Powertrain System,” *Appl. Mech. Mater.*, vol. 564, pp. 42–47, Jun. 2014.

[124] D. A. Crolla, *Automotive engineering: powertrain, chasis system and vehicle body*, no. 1. 2009.

[125] *Bosch Automotive Handbook*, 10th ed. Robert Bosch, 2018.

[126] H. Kim and S. Jung, “Battery hybridization for achieving both high power and high energy densities,” *Int. J. Energy Res.*, vol. 42, no. 14, pp. 4383–4394, Nov. 2018.

[127] Y. Chung and M. S. Kim, “Thermal analysis and pack level design of battery thermal management system with liquid cooling for electric vehicles,” *Energy Convers. Manag.*, vol. 196, pp. 105–116, Sep. 2019.

[128] S. Arora, W. Shen, and A. Kapoor, “Review of mechanical design and strategic placement technique of a robust battery pack for electric vehicles,” *Renew. Sustain. Energy Rev.*, vol. 60, pp. 1319–1331, Jul. 2016.

[129] W. Du, N. Xue, A. Gupta, A. M. Sastry, J. R. R. A. Martins, and W. Shyy, “Optimization of LiMn2O4 electrode properties in a gradient- and surrogate-based framework,” *Acta Mech. Sin.*, vol. 29, no. 3, pp. 335–347, Jun. 2013.

[130] J. Wen, D. Zhao, and C. Zhang, “An overview of electricity powered vehicles: Lithium-ion battery energy storage density and energy conversion efficiency,” *Renew. Energy*, vol. 162, pp. 1629–1648, Dec. 2020.

[131] S. M. N. Hasan, M. N. Anwar, M. Teimorzadeh, and D. P. Tasky, “Features and challenges for Auxiliary Power Module (APM) design for hybrid/electric vehicle applications,” in *2011 IEEE Vehicle Power and Propulsion Conference*, 2011, pp. 1–6.

[132] A. Khaligh and M. D’Antonio, “Global Trends in High-Power On-Board Chargers for Electric Vehicles,” *IEEE Trans. Veh. Technol.*, vol. 68, no. 4, pp. 3306–3324, Apr. 2019.

[133] A. Lajunen, Y. Yang, and A. Emadi, “Recent Developments in Thermal Management of Electrified Powertrains,” *IEEE Trans. Veh. Technol.*, vol. 67, no. 12, pp. 11486–11499, Dec. 2018.

[134] A. Lajunen, Y. Yang, and A. Emadi, “Review of cabin thermal management for electrified passenger vehicles,” *IEEE Trans. Veh. Technol.*, pp. 1–1, 2020.

[135] S. G. Wirasingha and A. Emadi, “Pihef: Plug-in hybrid electric factor,” *IEEE Trans. Veh. Technol.*, vol. 60, no. 3, pp. 1279–1284, 2011.

[136] S. G. Wirasingha and A. Emadi, “Pihef: Plug-In Hybrid Electric Factor,” *IEEE Trans. Veh. Technol.*, vol. 60, no. 3, pp. 1279–1284, Mar. 2011.

[137] T. Johnson, “Vehicular Emissions in Review,” *SAE Int. J. Engines*, vol. 7, no. 3, pp. 2014-01–1491, Apr. 2014.

[138] Z. Han, Y. Hu, P. Sun, and H. Chen, “Model predictive control of diesel engine start-stop control in an HEV,” in *2017 36th Chinese Control Conference (CCC)*, 2017, pp. 9590–9595.

[139] S. Nazari, J. Siegel, and A. Stefanopoulou, “Optimal Energy Management for a Mild Hybrid Vehicle With Electric and Hybrid Engine Boosting Systems,” *IEEE Trans. Veh. Technol.*, vol. 68, no. 4, pp. 3386–3399, Apr. 2019.

[140] M. Lv, Z. Chen, Y. Yang, and J. Bi, “Regenerative braking control strategy for a hybrid electric vehicle with rear axle electric drive,” in *2017 Chinese Automation Congress (CAC)*, 2017, pp. 521–525.

[141] X. Wang, Y. Tian, Z. Zhu, C. Li, Q. Wei, and Z. Cheng, “The Parameters Matching and Simulation of the Series-parallel Hybrid Powertrain,” in *2019 IEEE 4th Advanced Information Technology, Electronic and Automation Control Conference (IAEAC)*, 2019, pp. 1758–1762.

[142] Z. Zhao and X. Tang, “Control of e-CVT to EV Mode Transition on Braking Deceleration Condition for a Compound Power-Split Hybrid Electrical Vehicle,” *IEEE Access*, vol. 7, pp. 111954–111967, 2019.

[143] Gou Jinfang, Wang Lifang, Liao Chenglin, Zhang Junzhi, and Yue Xiaowei, “The coordinated control of motor regenerative braking torques defined by accelerator pedal and brake pedal of electric vehicle,” in *2012 IEEE Vehicle Power and Propulsion Conference*, 2012, pp. 119–123.

[144] B. Mashadi and S. A. M. Emadi, “Dual-Mode Power-Split Transmission for Hybrid Electric Vehicles,” *IEEE Trans. Veh. Technol.*, vol. 59, no. 7, pp. 3223–3232, Sep. 2010.

[145] A. Sorniotti, “Torque Gap Filler for Automated Manual Transmissions:

Principles for the Development of the Control Algorithm," *SAE Int. J. Engines*, vol. 2, no. 1, pp. 2009-01–0952, Apr. 2009.

[146] M. Awadallah, P. Tawadros, P. Walker, and N. Zhang, "Comparative fuel economy, cost and emissions analysis of a novel mild hybrid and conventional vehicles," *Proc. Inst. Mech. Eng. Part D J. Automob. Eng.*, vol. 232, no. 13, pp. 1846–1862, Nov. 2018.

[147] G. T. Fattic, J. E. Walters, and F. S. Gunawan, "Cold Starting Performance of a 42-Volt Integrated Starter Generator System," 2002.

[148] P. Griefnow, J. Andert, and D. Jolovic, "Next-Generation Low-Voltage Power Nets Impacts of Advanced Stop/Start and Sailing Functionalities," *SAE Int. J. Fuels Lubr.*, vol. 10, no. 2, pp. 2017-01–0896, Mar. 2017.

[149] N. Mueller, S. Strauss, S. Tumback, G.-C. Goh, and A. Christ, "Next Generation Engine Start/Stop Systems: 'Free-Wheeling,'" *SAE Int. J. Engines*, vol. 4, no. 1, pp. 2011-01–0712, Apr. 2011.

[150] H. Yang, A. Smith, S. Swales, and J. Maguire, "Development of Two-Mode Hybrid Powertrain with Enhanced EV Capability," *SAE Int. J. Engines*, vol. 4, no. 1, pp. 2011-01–0883, Apr. 2011.

[151] N. Kim, E. Rask, and A. Rousseau, "Control Analysis under Different Driving Conditions for Peugeot 3008 Hybrid 4," *SAE Int. J. Altern. Powertrains*, vol. 3, no. 1, pp. 2014-01–1818, Apr. 2014.

[152] J. Wu, B. Ma, H. Li, and J. Liu, "Creeping control strategy for Direct Shift Gearbox based on the investigation of temperature variation of the wet multi-

plate clutch," *Proc. Inst. Mech. Eng. Part D J. Automob. Eng.*, vol. 233, no. 14, pp. 3857–3870, Dec. 2019.

[153] B. Hu *et al.*, "Progress and recent trends in 48 V hybridisation and e-boosting technology on passenger vehicles – a review," *Proc. Inst. Mech. Eng. Part D J. Automob. Eng.*, vol. 232, no. 11, pp. 1543–1561, Sep. 2018.

[154] M. Vignati, E. Sabbioni, D. Tarsitano, and F. Cheli, "Electric powertrain layouts analysis for controlling vehicle lateral dynamics with torque vectoring," in *2017 International Conference of Electrical and Electronic Technologies for Automotive*, 2017, pp. 1–5.

[155] U. S. D. of Energy, "Compare Side-by-Side," *Fueleconomy.gov the official U.S. government source for fuel economy information*, 2020. [Online]. Available: https://www.fueleconomy.gov/feg/Find.do?action=sbs&id=41943&id=41893. [Accessed: 11-Jun-2020].

[156] N. Kim, A. Moawad, N. Shidore, and A. Rousseau, "Fuel Consumption and Cost Potential of Different Plug-In Hybrid Vehicle Architectures," *SAE Int. J. Altern. Powertrains*, vol. 4, no. 1, pp. 2015-01–1160, Apr. 2015.

[157] E. D. Tate, M. O. Harpster, and P. J. Savagian, "The Electrification of the Automobile: From Conventional Hybrid, to Plug-in Hybrids, to Extended-Range Electric Vehicles," *SAE Int. J. Passeng. Cars - Electron. Electr. Syst.*, vol. 1, no. 1, pp. 2008-01–0458, Apr. 2008.

[158] "Peugeot 208 features new generation of 3-cylinder gasoline and Stop &

Start System (e-HDi) diesel engines," *Green Car Congress*, 2012. [Online]. Available: https://www.greencarcongress.com/2012/01/208-20120116.html. [Accessed: 11-Jun-2020].

[159] "Fiat 500 Hybrid e Panda Hybrid chegam a Portugal em março," *Fleet M*, 2020. [Online]. Available: http://fleetmagazine.pt/2020/01/13/fiat-500-hybrid-e-panda-hybrid-chegam-a-portugal-em-marco/. [Accessed: 11-Jun-2020].

[160] "Continental Technology Powers Jeep® Wrangler's New eTorque Mild-Hybrid System," *Continental Press Release*, 2019. [Online]. Available: https://www.continental.com/en/press/press-releases/2019-01-16-jeep-157550. [Accessed: 11-Jun-2020].

[161] "Mercedes-AMG GLE 53 performance SUV is a 48V mild hybrid," *Green Car Congress*, 2019. [Online]. Available: https://www.greencarcongress.com/2019/02/20190228-gle53.html. [Accessed: 11-Jun-2020].

[162] "Toyota Previews Generation III 2010 Prius Hybrid," *Green Car Congress*, 2009. [Online]. Available: https://www.greencarcongress.com/2009/03/toyota-previews.html. [Accessed: 11-Jun-2020].

[163] A. Ingram, "New Peugeot 3008 Hybrid4 2020 review," *Auto Press - Road Tests*, 2020. [Online]. Available: https://www.autoexpress.co.uk/peugeot/3008/108871/new-peugeot-3008-

hybrid4-2020-review. [Accessed: 11-Jun-2020].

[164] Halvorson, "Plugging in Pacifica Hybrid: City drive review of its 32-mile electric range," *Green Car Reports*, 2020. [Online]. Available: https://www.greencarreports.com/news/1123904_plugging-in-pacifica-hybrid-city-drive-review-of-its-32-mile-electric-range. [Accessed: 15-Jun-2020].

[165] S. Edelstein, "2021 BMW X5 plug-in hybrid SUV: More power, more than double the electric range," *Green Car Reports*, 2020. [Online]. Available: https://www.greencarreports.com/news/1128450_2021-bmw-x5-plug-in-hybrid-suv-more-power-more-than-double-the-electric-range. [Accessed: 15-Jun-2020].

[166] A. Ingram, "Chevrolet Voltt: Range-Extended Electric Car Ultimate Guide," *Green Car Reports*, 2014. [Online]. Available: https://www.greencarreports.com/news/1072137_chevrolet-volt-range-extended-electric-car-ultimate-guide. [Accessed: 15-Jun-2020].

[167] J. Voelcker, "BMW i3 REx range extender: owner assesses pros and cons of limited-power engine," *Green Car Reports*, 2016. [Online]. Available: https://www.greencarreports.com/news/1105823_bmw-i3-rex-range-extender-owner-assesses-pros-and-cons-of-limited-power-engine. [Accessed: 15-Jun-2020].

[168] Top Gear, "The Top Gear car review: Jaguar I-Pace," *BBC - Top Gear News*. [Online]. Available: https://www.topgear.com/car-reviews/jaguar/i-pace.

[Accessed: 15-Jun-2020].

[169] B. Halvorson, "2019 Audi E-tron road-trip review: Wait, range ratings aren`t everything?," *Green Car Reports*, 2019. [Online]. Available: https://www.greencarreports.com/news/1123243_2019-audi-e-tron-road-trip-review-wait-range-ratings-arent-everything. [Accessed: 15-Jun-2020].

[170] U. S. D. of Energy, "Fuel Economy Guide," 2019.

[171] John McIlroy, "Long-term test review: BMW i3 Range Extender," *Auto Express Long-term tests*, 2016. [Online]. Available: https://www.autoexpress.co.uk/bmw/i3/88777/long-term-test-review-bmw-i3-range-extender. [Accessed: 29-Sep-2021].

[172] Steve Cropley, "Fisker Karma 2011-2012 review," *Autocar - car reviews*, 2012. [Online]. Available: https://www.autocar.co.uk/car-review/fisker/karma-2011-2012. [Accessed: 29-Sep-2021].

[173] J. Groves and B. Miller, "Range Rover P400e PHEV hybrid review: dual-power waft," *Car Reviews*, 2019. [Online]. Available: https://www.carmagazine.co.uk/car-reviews/land-rover/range-rover-phev-plug-in-hybrid-2018-review/. [Accessed: 29-Sep-2021].

[174] William Walker, "2020 Lincoln Aviator Grand Touring First Drive: Plug-In Hybrid Power Takes on World," *Motor Trend*, 2020. [Online]. Available: https://www.motortrend.com/reviews/2020-lincoln-aviator-grand-touring-first-drive-review/. [Accessed: 29-Sep-2021].

[175] A. Nedelea, "2021 BMW 530e xDrive Review: Best Midsize Luxury Plug-

In Sedan?," *Inside EVs*, 2021. [Online]. Available: https://insideevs.com/reviews/489809/bmw-530e-road-test-review/. [Accessed: 29-Sep-2021].

[176] "Hyundai Ioniq review - Impressive specs and the choice of hybrid, PHEV and EV models make the Ioniq a serious rival for the Toyota Prius," *Auto Express IN-DEPTH REVIEWS*, 2021. [Online]. Available: https://www.autoexpress.co.uk/hyundai/ioniq. [Accessed: 29-Sep-2021].

[177] Auto Express, "Kia Niro review - The Kia Niro crossover comes in hybrid, plug-in and full electric guises," *Auto Express IN-DEPTH REVIEWS*, 2021. [Online]. Available: https://www.autoexpress.co.uk/kia/niro.

[178] S. Errity, "Jeep Compass plug-in hybrid headed for UK," *Driving Electric*, 2021. [Online]. Available: https://www.drivingelectric.com/jeep/compass. [Accessed: 29-Sep-2021].

[179] L. Sethuraman and M. Haris, "Hubload — causes, effects and mitigation measures on a P0 electrical machine in a typical mild hybrid electric vehicle powertrain," in *2017 IEEE Transportation Electrification Conference (ITEC-India)*, 2017, pp. 1–5.

[180] Zhou Yafu and Chang Cheng, "Study on the powertrain for ISG mild hybrid electric vehicle," in *2008 IEEE Vehicle Power and Propulsion Conference*, 2008, pp. 1–5.

[181] J. Rossi and C. Cavallino, "Modular P2-P3 Dedicated Hybrid Transmission for 48V and HV applications," in *2017 International Conference of*

Electrical and Electronic Technologies for Automotive, 2017, pp. 1–4.

[182] P. Biswas, "Adapting SUV AWD powertrain to P0/P2/P4 hybrid EV architecture: Integrative packaging and capability study," in *2017 IEEE Transportation Electrification Conference (ITEC-India)*, 2017, pp. 1–5.

[183] Y. Yang and A. Emadi, "Integrated electro-mechanical transmission systems in hybrid electric vehicles," in *2011 IEEE Vehicle Power and Propulsion Conference*, 2011, pp. 1–6.

[184] Y. Yang, K. A. Ali, J. Roeleveld, and A. Emadi, "State-of-the-art electrified powertrains - hybrid, plug-in, and electric vehicles," *Int. J. Powertrains*, vol. 5, no. 1, p. 1, 2016.

[185] B. P. Liu and F. Weslati, "Single input and single-output hybrid systemo Title," 9188201.

[186] A. Biswas and A. Emadi, "Energy Management Systems for Electrified Powertrains: State-of-the-Art Review and Future Trends," *IEEE Trans. Veh. Technol.*, vol. 68, no. 7, pp. 6453–6467, Jul. 2019.

[187] P. G. Anselma *et al.*, "Accelerated Sizing of a Power Split Electrified Powertrain," 2020.

[188] G. M. Candido and P. C. Kaminski, "The addition of Design for Armoring as an engineering methodology in the development of premium civilian vehicles," 2021.

[189] Z. Yang, "Overview of Global Fuel Economy Policies," *The International Council on Clean Air Transportation*, 2018. [Online]. Available:

https://theicct.org/sites/default/files/Global-Fuel-Economy-Policies-Overview_ICCT_ZYang_20032018.pdf. [Accessed: 11-Sep-2018].

[190] Trevor M. Letcher, *Future Energy*. Elsevier, 2020.

[191] D. Carrington, "Electric cars are already cheaper to own and run, says study," *The Guardian - Electric, Hybrid and low-emission cars*, 2019. [Online]. Available: https://www.theguardian.com/environment/2019/feb/12/electric-cars-already-cheaper-own-run-study. [Accessed: 07-May-2020].

[192] E. Commision, "Electrification of the Transport System," Brussels, Belgium, 2017.

[193] R. Aarenstrup, *Managing Model-Based Design*. Natick, MA: The Math Works, Inc, 2015.

[194] W. van Harselaar, T. Hofman, and M. Brouwer, "Automated Dynamic Modeling of Arbitrary Hybrid and Electric Drivetrain Topologies," *IEEE Trans. Veh. Technol.*, vol. 67, no. 8, pp. 6921–6934, Aug. 2018.

[195] R. Robinson and S. Tummalapalli, "Plugging into the future: Electrifying the global automotive industry," *Deloitte Insights*, 2018. [Online]. Available: https://www2.deloitte.com/us/en/insights/industry/automotive/vehicle-electrification-global-automotive-industry.html. [Accessed: 07-May-2020].

[196] M. White, "Making electrification a reality for the automotive industry," *The Manufacturer*, 2019. [Online]. Available: https://www.themanufacturer.com/articles/making-electrification-a-reality-for-the-automotive-industry/. [Accessed: 07-May-2020].

[197] R. Sanchez and A. Heene, *A Focused Issue on Competence Perspectives on New Industry Dynamics*. Bingley: Emerald Group Publishing, 2012.

[198] F. A. Forcellini and H. Rozenfeld, *Gestão de Desenvolvimento de Produtos - Uma Referência para a Melhoria do Processo*, 1st ed. Sao Paulo, Brasil: Editora Saraiva, 2012.

[199] D. W. Gao, C. Mi, and A. Emadi, "Modeling and Simulation of Electric and Hybrid Vehicles," *Proc. IEEE*, vol. 95, no. 4, pp. 729–745, Apr. 2007.

[200] Argone, "Energy Systems D3 2015 Chevrolet Spark EV," *Energy System Subdivision*, 2015. [Online]. Available: https://www.anl.gov/es/energy-systems-d3-2015-chevrolet-spark-ev.

[201] C. C. Chan, A. Bouscayrol, and K. Chen, "Electric, hybrid, and fuel-cell vehicles: Architectures and modeling," *IEEE Trans. Veh. Technol.*, vol. 59, no. 2, pp. 589–598, 2010.

[202] E. Alpaslan *et al.*, "A review on fuel cell electric vehicle powertrain modeling and simulation," *Energy Sources, Part A Recover. Util. Environ. Eff.*, pp. 1–37, Nov. 2021.

[203] A. M. Madni and M. Sievers, "Model-based systems engineering: Motivation, current status, and research opportunities," *Syst. Eng.*, vol. 21, no. 3, pp. 172–190, May 2018.

[204] A. Taoudi, J. Gandy, V. Hudson, C. Luo, and R. Follett, "Model Based Design and Verification of Automated Driving Features Using XIL Simulation Platforms," 2022.

[205] L. Bruck, B. Haycock, and A. Emadi, “A Review of Driving Simulation Technology and Applications,” *IEEE Open J. Veh. Technol.*, vol. 2, pp. 1–16, 2021.

[206] L. Bruck, A. Emadi, and K. P. Divakarla, “A review of the relevance of driving condition mapping and vehicle simulation for energy management system design,” *Int. J. Powertrains*, vol. 8, no. 3, pp. 224–251, 2019.

[207] L. Eriksson and L. Nielsen, *Modeling and Control of Engines and Drivelines*. Chichester, UK: John Wiley & Sons, Ltd, 2014.

[208] F. A. Bender, M. Kaszynski, and O. Sawodny, “Drive Cycle Prediction and Energy Management Optimization for Hybrid Hydraulic Vehicles,” *IEEE Trans. Veh. Technol.*, vol. 62, no. 8, pp. 3581–3592, Oct. 2013.

[209] L. Eriksson and L. Nielsen, *Modeling and Control of Engines and Drivelines*. Wiley, 2014.

[210] F. Assadian, G. Mohan, and S. Longo, “Comparative analysis of forward-facing models vs backward-facing models in powertrain component sizing,” in *Hybrid and Electric Vehicles Conference 2013 (HEVC 2013)*, 2013, pp. 10.7-10.7.

[211] R. Ahmed, M. El Sayed, I. Arasaratnam, Jimi Tjong, and S. Habibi, “Reduced-Order Electrochemical Model Parameters Identification and SOC Estimation for Healthy and Aged Li-Ion Batteries Part I: Parameterization Model Development for Healthy Batteries,” *IEEE J. Emerg. Sel. Top. Power Electron.*, vol. 2, no. 3, pp. 659–677, Sep. 2014.

[212] "Static Modeling," in *Software Modeling and Design*, Cambridge University Press, 2011, pp. 94–114.

[213] T. D. Gillespie, *Fundamentals of Vehicle Dynamics*. Warrendale, PA: SAE International, 1992.

[214] K. Rahman, S. Jurkovic, S. Hawkins, S. Tarnowsky, and P. Savagian, "Propulsion System Design of a Battery Electric Vehicle," *IEEE Electrif. Mag.*, vol. 2, no. 2, pp. 14–24, Jun. 2014.

[215] I. Baccouche, S. Jemmali, B. Manai, N. Omar, and N. Amara, "Improved OCV Model of a Li-Ion NMC Battery for Online SOC Estimation Using the Extended Kalman Filter," *Energies*, vol. 10, no. 6, p. 764, May 2017.

[216] International Energy Agency (IEA), "Global EV Outlook 2022 - Securing supplies for an electric future," 2022.

[217] W. Liu, H. Qi, X. Liu, and Y. Wang, "Evaluation of regenerative braking based on single-pedal control for electric vehicles," *Front. Mech. Eng.*, vol. 15, no. 1, pp. 166–179, Mar. 2020.

[218] D. Zhu and E. Pritchard, "NCSU Year Three Final Technical Report," 2014.

[219] D. G. Barroso, Y. Yang, F. A. Machado, and A. Emadi, "Electrified Automotive Propulsion Systems: State-of-the-Art Review," *IEEE Trans. Transp. Electrif.*, vol. 8, no. 2, pp. 2898–2914, Jun. 2022.

[220] S.-D. Lee and S.-L. Kim, "Characterization and Development of the Ideal Pedal Force, Pedal Travel, and Response Time in the Brake System for the Translation of the Voice of the Customer to Engineering Specifications,"

Proc. Inst. Mech. Eng. Part D J. Automob. Eng., vol. 224, no. 11, pp. 1433–1450, Nov. 2010.

[221] B. J. Varock, "Benchmarking of Regenerative Braking for a Fully Electric Car," 2011.

[222] E. Louback, F. Machado, L. Bruck, P. J. Kollmeyer, and A. Emadi, "Real-Time Performance and Driveability Analysis of a Clutchless Multi-Speed Gearbox for Battery Electric Vehicle Applications," in *2022 IEEE Transportation Electrification Conference & Expo (ITEC)*, 2022, pp. 1041–1046.

[223] F. Schockenhoff, H. Nehse, and M. Lienkamp, "Maneuver-Based Objectification of User Comfort Affecting Aspects of Driving Style of Autonomous Vehicle Concepts," *Appl. Sci.*, vol. 10, no. 11, p. 3946, Jun. 2020.

[224] H. Bellem, T. Schönenberg, J. F. Krems, and M. Schrauf, "Objective metrics of comfort: Developing a driving style for highly automated vehicles," *Transp. Res. Part F Traffic Psychol. Behav.*, vol. 41, pp. 45–54, Aug. 2016.

[225] D. Ossendorff, C. Heusch, L. Tatas, M. K. Wick, and G. Birmes, "Objectified Drivability Analysis and Evaluation of Deceleration Maneuvers for Electric Vehicles," *SAE Int. J. Engines*, vol. 14, no. 3, pp. 03-14-03–0023, Feb. 2021.

[226] International Energy Agency (IEA), "Trends in Electric Heavy-duty vehicles," *Global EV Outlook 2023*. [Online]. Available:

https://www.iea.org/reports/global-ev-outlook-2023/trends-in-electric-heavy-duty-vehicles. [Accessed: 05-Sep-2023].

[227] McKinsey & Co, "Preparing the World for Zero-Emission Trucks," *Mckinsey Center for Future Mobility*. [Online]. Available: https://www.mckinsey.com/industries/automotive-and-assembly/our-insights/preparing-the-world-for-zero-emission-trucks. [Accessed: 05-Sep-2023].

[228] D. Barroso, L. Bruck, and A. Emadi, "Light-Commercial Electric Vehicle Design: Total Cost of Ownership Assessment," in *2023 IEEE Transportation Electrification Conference & Expo (ITEC)*, 2023, pp. 1–9.

[229] R. Charette N., "How Software is Eating the Car," *IEEE Spectrum*, Jun-2021.

[230] Bosch Mobility, "The Software Defined Vehicle," *Mobility Topics*, 2022. [Online]. Available: https://www.bosch-mobility.com/en/mobility-topics/software-defined-vehicle/?gclid=Cj0KCQjwxuCnBhDLARIsAB-cq1ovwR5vW_rLJar51PLVLqI6BUZkBzjYlIPT2HPHFxSe3wZzeXS9LQgaAgVQEALw_wcB. [Accessed: 06-Sep-2023].

[231] O. Burkacky, J. Deichmann, M. Kellner, P. Keuntje, and J. Werra, "Rewiring car electronics and software architecture for the 'Roaring 2020s,'" *Mckinsey - Future Mobility*, 2021. .

[232] Y. Zhao, J. Hou, C. Wang, L. Chen, and Q. Sun, "Design of vehicle control research and development platform for a pure electric vehicle," *Adv. Mech.*

Eng., vol. 11, no. 2, p. 168781401982642, Feb. 2019.

[233] A. Goyal and A. Thakur, "An Overview of Drive by Wire Technology for Automobiles," in *2019 International Conference on Automation, Computational and Technology Management (ICACTM)*, 2019, pp. 108–110.

[234] Y. Zhao, J. Hou, C. Wang, L. Chen, and Q. Sun, "Design of vehicle control research and development platform for a pure electric vehicle.," *Adv. Mech. Eng.*, vol. 11, no. 2, p. 17, 2019.

[235] Z. Yongqiang, Z. Xin, L. Jiashi, H. Haitao, M. Teng, and Z. Chunyu, "A research on evaluation and development of single-pedal function for electric vehicle based on PID," *J. Phys. Conf. Ser.*, vol. 1605, no. 1, p. 012109, Aug. 2020.

[236] F. Sugimoto *et al.*, "Effects of one-pedal automobile operation on the driver's emotional state and cognitive workload," *Appl. Ergon.*, vol. 88, p. 103179, Oct. 2020.

[237] M. U. Cuma, Ç. D. Ünal, and M. M. Savrun, "Design and implementation of algorithms for one pedal driving in electric buses," *Eng. Sci. Technol. an Int. J.*, vol. 24, no. 1, pp. 138–144, Feb. 2021.

[238] J. J. P. Van Boekel, I. J. . Besselink, and H. Nijmeijer, "Design and realization of a One-Pedal-Driving algorithm for the TU/e Lupo EL," *World Electr. Veh. J.*, vol. 7, no. 2, pp. 226–237, Jun. 2015.

[239] H. H. Wen, W. Chen, and J. Hui, "A single-pedal regenerative braking

control strategy of accelerator pedal for electric vehicles based on adaptive fuzzy control algorithm," *Energy Procedia*, vol. 152, pp. 624–629, Oct. 2018.

[240] N. Kidambi, R. L. Harne, Y. Fujii, G. M. Pietron, and K. W. Wang, "Methods in Vehicle Mass and Road Grade Estimation," *SAE Int. J. Passeng. Cars - Mech. Syst.*, vol. 7, no. 3, pp. 2014-01–0111, Apr. 2014.

[241] M. Hu, W. Gao, Y. Zeng, H. Li, and Z. Yu, "Vehicle Mass and Road Grade Estimation Based on Adaptive Forgetting Factor RLS and EKF Algorithm," in *2020 5th International Conference on Power and Renewable Energy (ICPRE)*, 2020, pp. 342–346.

[242] Z. Yu, X. Hou, B. Leng, and Y. Huang, "Mass estimation method for intelligent vehicles based on fusion of machine learning and vehicle dynamic model," *Auton. Intell. Syst.*, vol. 2, no. 1, p. 4, Dec. 2022.

[243] K. M. Jensen, I. F. Santos, L. K. H. Clemmensen, S. Theodorsen, and H. J. P. Corstens, "Mass estimation of ground vehicles based on longitudinal dynamics using loosely coupled integrated navigation system and CAN-bus data with model parameter estimation," *Mech. Syst. Signal Process.*, vol. 171, p. 108925, May 2022.

[244] N. Lin, C. Zong, and S. Shi, "The Method of Mass Estimation Considering System Error in Vehicle Longitudinal Dynamics," *Energies*, vol. 12, no. 1, p. 52, Dec. 2018.

[245] T. Ghotikar, "Estimation of Vehicle Mass and Road Grade," Clemson

University, 2008.

[246] P. C. Young, *Recursive estimation and time-series analysis: an introduction*. Springer science & business media, 2012.